SYNTHESIS, PHOTOPHYSICS, AND APPLICATON OF FLUORESCENT PROTEIN CHROMOPHORE ANALOGS

A Dissertation
Presented to
The Academic Faculty

by

Anthony Baldridge

In Partial Fulfillment
of the Requirements for the Degree
Doctor of Philosophy in the
School of Chemistry and Biochemistry

Georgia Institute of Technology
August 2011

SYNTHESIS, PHOTOPHYSICS, AND APPLICATON OF FLUORESCENT PROTEIN CHROMOPHORE ANALOGS

Approved by:

Dr. Laren M. Tolbert Advisor
School of Chemistry and Biochemistry
Georgia Institute of Technology

Dr. Christoph J. Fahrni
School of Chemistry and Biochemistry
Georgia Institute of Technology

Dr. Stefan France
School of Chemistry and Biochemistry
Georgia Institute of Technology

Dr. Mohan Srinivasarao
School of Materials Science and Engineering
Georgia Institute of Technology

Dr. Charles Liotta
School of Chemistry and Biochemistry
Georgia Institute of Technology

Date Approved: May 4, 2011

ACKNOWLEDGEMENTS

I want to thank the multitude of people who came together to make this dissertation and my studies at the Georgia Institute of Technology possible. First off, I want to thank my advisor, Dr. Laren Tolbert for providing me a research group and project that came to fruition as this dissertation. Laren's generosity along the way has allowed me to develop this research as well as explore other options and ventures outside of chemistry. I also want to thank the research scientists, Dr. Kyril Solntsev and Dr. Janusz Kowalik as well as the members of the Tolbert group who have helped me along the way with invaluable discussions. Additional thanks goes to the graduate colleagues, Dr. Kathy Woody, Nick Haase, Chip Humphries, Anna Duraj-Thatte, Arren Washington, Brandon Polander, Lauren Polander, Juan Vargas, James Black and Shampa Sumpa, who throughout my studies at Georgia Tech have contributed to the research within this dissertation in both direct and indirect ways.

As with many things in life, the motivation, determination, and assistance to achieve a goal are not possible without the support of one's family. I would like to thank my mom (Nina Collins), my dad (Tony Baldridge), my sister (Lindsey Baldridge), and my grandparents (Lena R. Earley and the late George M. Earley, Sr.) as well as my extended family and stepfather (Leon Collins) who throughout my academic career have supported me to strive and continue to push for the greatest goal regardless of what it is. Words do little justice to convey my eternal gratitude toward my family and without their unwavering support; it is assured that I would have not reached this stage in my academic career.

During my studies at Georgia Tech I was fortunate to receive a number of opportunities outside of the typical graduate experience. I want to thank the Center for Organic Photonics and Electronics (COPE) for inducting me as a COPE Fellow during

my third year of graduate studies and providing me a travel grant to present research. I would also like to extend thanks to the Center for the Enhancement of Teaching and Learning especially Dr. Donna Llewellyn, Dr. Marion Usselman, Dr. Lydia Soliel, and Dr. Karen Head for awarding me a STEP Fellowship and a Georgia Tech Teaching Fellowship during my second and third years of graduate studies. Finally, I would like to thank the School of Chemistry and Biochemistry, Georgia Tech, and the Georgia Tech Foundation for the award of a Presidential Fellowship to aid financially in my studies here at Georgia Tech. These fellowships and the experiences that compliment them have significantly shaped my graduate life and career as well as the skills I have accumulated through my graduate tenure.

Noted within all the chapters, I would also like to thank the many collaborators who have helped propel this work to newer heights by providing the specialized knowledge to expand this research. While some of these collaborations did not reach the stage of a manuscript, each worked to add to contribute to the knowledge of AMI chromophores. These individuals and their research groups include: Dr. V. Ramamurthy, Dr. Pance Naumov, Dr. Stephen Meech, Dr. Young-Tae Chang, Dr. Bahareh Azizi, Dr. Mohan Srinivasarao, Dr. Andy Cooper, Dr. Sean Higgins, Dr. Dipaktar Sen Dr. Bruce Armitage, Dr. Peter Ford, Dr. Suzanne Fery Forgues, and Dr. Christiano Vlapplani.

I also want to offer my sincerest thanks to those who came together to make this dissertation a realization and offer an apology for those that I failed to mention within this acknowledgements section.

TABLE OF CONTENTS

LIST OF TABLES

LIST OF FIGURES

LIST OF SYMBOLS

Φ	Emission Quantum Yield
λ	Wavelength
ε	Molar Extinction Coefficient
A	Absorbance
c	Cis Isomer
t	Trans Isomer
o	Ortho substitution
m	Meta substitution
p	Para substitution
S_1	First Excited State
S_0	Ground State
μ	Trans Isomer
k_d	Ortho substitution
m	Meta substitution
F_{sat}	Formation constant-saturation
Å	Angstroms
E	Cis isomer
Z	Trans isomer
M	Molar (molarity)
pK_a	Acidity constant
h	Hour
W	Watt
g	Gram

L	Liter
I	Intensity
I_o	Initial Intensity

LIST OF ABBREVIATIONS

AMI	Arylideneimidazolidinone
fs	Femtosecond
GFP	Green Fluorescent Protein
Gly	Glycine
HOMO	Highest Occupied Molecular Orbital
HSA	Human Serum Albumin
HT	Hula Twist
IC	Internal Conversion
IR	Infared
LUMO	Lowest Unoccupied Molecular Orbital
nm	Nanometers
OA	Octa Acid
OBF	One Bond Flip
ps	Picosecond
RFP	Red Fluorescent Protein
Ser	Serine
Trp	Tryptophan
Tyr	Tyrosine
UV/Vis	Ultraviolet/Visible
wt-GFP	Wild-type Green Fluorescent Protein
PXR	Pregnane X Receptor
ER	Estrogen Receptor

Eq	Equivalent
MHz	Mega hertzs
AFM	Atomic Force Microscopy
EtOH	Ethanol
DMSO	Dimethylsufloxide
DFT	Density Functional Theory
Me	Methyl
Et	Ethyl
Pr	Propyl
Bu	Butyl
Pn	Pentyl

SUMMARY

The Green Fluorescent Protein has gained significant attention and the 2008 Nobel Prize as a non-invasive fluorescent marker that has revolutionized molecular biology. Within the 11-stranded β-barrel of the protein is protectively housed an arylideneimidazolidinone (AMI) chromophore formed via a post-translational cyclization that is responsible for the fluorescent properties of the protein. Following removal from the protective β-barrel, the chromophore exhibits remarkably different spectroscopic properties with a 10^4 diminished emission quantum yield. This observation has been attributed to torsional motions that allow for rapid internal conversion. These motions are a function of the structure of the AMI chromophore where cis/trans isomerization can occur about the benzylidene double bond as well as the formal single aryl bond. From this, the question arises: if these torsional motions are inhibited, can the fluorescence of the chromophore be restored?

In order to study these chromophores, AMI's were synthesized with a variety of functional groups. Synthesis of these chromophores is afforded through a 2+3 cycloaddition providing a combinatorial synthetic protocol contrary to the commonly cited synthetic procedure of the Erlenmeyer azalactone synthesis. The combinatorial cycloaddition provides tolerance for a myriad of functional groups and the relative synthetic ease has readily allowed for the synthesis of hundreds of AMIs to date. With an arsenal of AMI chromophores a number of studies can be accomplished researching the photophysical questions surrounding these chromophores.

It is rationalized that inhibition of conformational freedom should provide for the restoration of the emission quantum yield. This study was undertaken through the transformation of the AMI chromophore to a bidentate ligand where upon metal binding torsional motions are inhibited. This was further explored through the encapsulation of hydrophobic chromophores within octa acid cavitands that provide a restrictive environment similar to what is found within the β-barrel. Results from these studies show the topological effects experienced by these chromophores and how restrictive environments provide for an enhancement in the emission quantum yield.

Using the encapsulation studies as motivation additional studies were motivated to use these compounds as fluorescent probes. Collaborating with Dr. Young-Tae Chang, these chromophores can be screened against a myriad of analytes to determine interactions through emission response in an efficient fashion. This led to the use of these chromophores, and coupled with rational design, as a human serum albumin probe. Further collaborative studies show that these chromophores can be used as agonists for nuclear receptors where binding the ligand binding domain provides for a restrictive environment as well as a fluorescent probe.

In addition to these interesting applications, the photochemistry of specific chromophores shows an interesting photochemical reaction of dimerization resulting in mechanical motion. Synthetic modifications also allow for these chromophores to act as liquid crystalline materials. As shown from this summary the chromophore of GFP characterized as an AMI chromophore show interesting properties and applications as well as great potential in a number of fields.

CHAPTER 1

INTRODUCTION AND OVERVIEW

Motivation and Dissertation Overview

As multiple literature sources have shown, a great amount of interest surrounds GFP and the chromophore responsible for its fluorescent properties. Simply put, GFP has revolutionized molecular biology by providing a non-evasive, post-translational biological marker that can be added to various systems without the use of co-factors to study various biological processes and interactions. From a spectroscopic standpoint GFP has favorable spectral characteristics as well as an astounding quantum yield, contributing even more to its expansive use. Noting these characteristics, removal of the chromophore from the protein system responsible for these spectral features does not produce similar results. Upon removal from the protective β-barrel, the chromophore of GFP becomes essentially non-fluorescent showing sharp contrast to the Φ=0.79 noted within the protein. At the center of these studies lies the question: what mechanism is responsible for this phenomenon attributed to rapid internal conversion experienced by the chromophore? With this in mind another question that becomes significant is: can the emission properties be restored or altered without the β-barrel? As highlighted below, this consequence arises from the non-radiative decay pathways that quench the fluorescence. Modifications to this system allow for the idea that hindering or stopping these radiationless pathways could restore a portion or the entire emission quantum yield noted with the natural protein. This restoration could provide important information toward the mechanisms noted with GFP allowing for the engineering of superior or spectroscopically different proteins. Additionally, the chromophore could be used

without the protein eliminating the variable of steric bulk that the 238-amino acid residue protein presents to a system, especially with kinetics studies.

Motivation for the work has evolved with additional data. Initially, the idea of hindering cis/trans isomerization through complexation to a metal cation provided for early studies into the various deactivation pathways. This idea was a function of the notion that hindering both the single aryl bond rotation as well as the formal double rotation should provide a restoration of the emission quantum yield. Following work with Dr. V. Ramamurthy's group, the importance of the rotation about the single aryl bond became a significant contributor to the overall photophysical picture through the idea that inclusion within cavities restored a significant, but not the entire, portion of the emission quantum yield. Results from this work provided a foundation into the inclusion of these chromophores into various environments whereby inclusion "turns-on" the chromophores from a non-fluorescent ($\Phi \sim 10^{-4}$) to ($\Phi \sim 10^{-2}$).

For any and all of the studies highlighted, synthesis of model chromophores is a necessity. From the high demand of a myriad of chromophores with differing substitution patterns, an efficient synthesis tolerant of various functional groups is also a necessity. Motivation to develop a synthetic protocol that is more robust as well as less-time intensive as the Erlenmeyer azalactone synthesis is of vital importance.

Overview

Taking into account the knowledge and challenges presented within this introductory portion, a number of projects were undertaken to answer some of the key questions and obstacles surrounding studies involving the GFP chromophore. These studies are highlighted within this work and an overview of the chapters as well as the work contained within includes:

Chapter 2

Chapter 2 reports synthetic progress of various fluorescent protein chromophores, termed AMIs, for arylidenemethylimidazolinones, using a new method for synthesis via a

2+3 cycloaddition. This combinatorial synthetic protocol has allowed for the efficient synthesis of hundreds of different AMIs unnoted in the literature up to this point. The compounds and synthetic protocol highlighted in this chapter will provide the molecules used for studies in subsequent chapters (Copyright by Georg Thieme Verlag Stuttgart).

Chapter 3

Chapter 3 reports the modification of the *para*-hydroxy AMI derivative with a 2-pyridyl moiety allowing the creation of bidentate ligand capable of binding metal cations. Upon binding, a 100-fold emission enhancement is noted for Zn^{2+} showing the possibility of hindering torsional motions within AMI chromophores and the implication of such (Copyright of the Royal Chemistry Society, 2010).

Chapter 4

Chapter 4 reports an interesting photochemical mechanism within the solid state of specific AMI derivatives. Upon irradiation, certain AMIs undergo a dimerization reaction based upon their crystal packing pattern. Additionally, polymorphs, meaning different forms of crystals within the same sample, were noted for the *meta*-hydroxy AMI analog (Copyright of the American Chemical Society).

Chapter 5

Chapter 5 reports the results upon encapsulation of AMIs within supramolecular hosts, in this case octa acid cavitands and cholate salt aggregates. The consequences of this study are significant in that upon inclusion, rotation about the single aryl bond is hindered but irradiation still produces the trans isomer within these hosts. This data shows the significance of the single bond toward internal conversion while at the same time provides a proof of concept for use as these AMI chromophores as small molecule probes (Copyright of the American Chemical Society).

Chapter 6

Chapter 6 highlights a combinatorial screening method to test the photophysical consequence of the interaction of various AMI derivatives with biologically relevant

analytes. These screening results can readily be used toward the discovery of small molecule probes using the AMI core as a structural motif (Copyright of the American Chemical Society).

Chapter 7

Chapter 7 discusses the interaction of various AMI chromophore analogs with nuclear receptors, primarily the estrogen receptor α and the pregnane X receptor. Chromophores were discovered to interact with nuclear receptors through modeling calculations as well as combinatorial screening of the wild type nuclear receptors. Initial results show these specific AMI chromophores readily interact as antagonists for the nuclear receptors presented.

Chapter 8

Chapter 8 highlights a successful outcome of the screening process discussed within chapter 6. Initial results showed a dramatic interaction with specific AMIs and human serum albumin (HSA). Using rational design of the chromophores a new probe for HSA was realized showing great sensitivity and selectivity toward HSA compared to other homologous and competing analytes within an aqueous environment (Copyright of the American Chemical Society).

Chapter 9

Chapter 9 discusses some preliminary work toward the use of AMI chromophores as liquid crystals. The general structural motif of an electron-withdrawing group, realized through the imidazolinone heterocycle, coupled with use of a biphenyl substitution commonly noted in commercial liquid crystals, allows for the creation of liquid crystal candidates. Preliminary results of this study are presented.

Chapter 10

Chapter 10 highlights some general conclusions of this work and provides some ideas concerning future work that arises from the success and published results of this dissertation.

Overview of the GFP Chromophore

Housed within the 11-stranded β-barrel, the arylideneimidazolidinone (AMI) chromophore of the green fluorescent protein (GFP), the component responsible for the green fluorescence, has drawn significant attention for its interesting photophysical and photochemical properties both within the natural protein and upon denaturation. Formation of the chromophore *p*-hydroxybenzylideneimidazolidinone (*p*-HOBDI) in the green fluorescent protein (GFP) of the jellyfish *Aequorea victoria*[2] occurs via a post-translational autocatalytic cyclization followed by autoxidation within a tripeptide unit

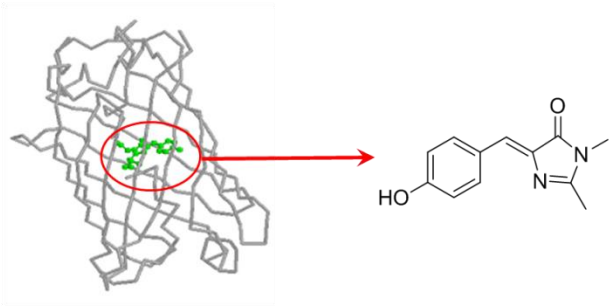

(Ser-65, Tyr-66, Gly-67) of the polypeptide sequence consisting of 238 amino acids (see

Figure 1.1. Green fluorescent protein β-barrel showing chromophore (p-HOBDI) encapsulated within the structure.

Figure 1.2).[3] X-ray diffraction studies reveal that the chromophore is protectively housed and covalently anchored along a coaxial helix threaded through the center of an 11-stranded β-barrel that secludes it from the aqueous solvent surrounding the protein.[4,5] Additional non-covalent coupling of the chromophore to the protein backbone is facilitated via an extended hydrogen-bonded network.[6]

Studies involving the chromophore devoid of the protective β-barrel reveal significantly different behavior. These studies are made possible through the synthesis of the chromophore carried out using Tonge's modification[7] of the Niwa synthesis,[8] often referred to as the Erlenmeyer azalactone synthesis. Additionally, as highlighted within

this work, other synthetic protocols are available including a Knoevenagel condensation and a 2+3 cycloaddition.

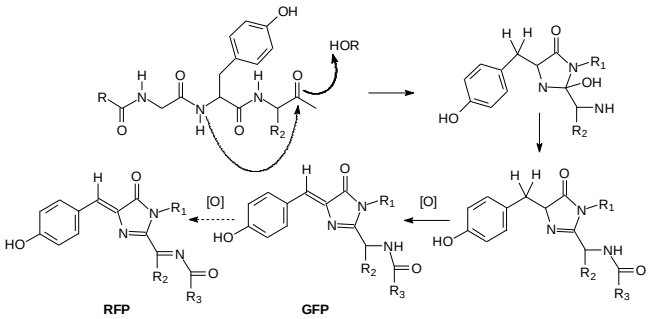

Figure 1.2. Autocatalytic cyclization and subsequent oxidation to yield GFP and additional oxidation to yield RFP.

Chapter 2 provides an overview of these synthetic protocols for AMI chromophores as well as the advances made within our laboratory regarding the 2+3 cycloaddition that have allowed the synthesis of hundreds of new chromophores.

Additional fluorescent protein chromophores

All proteins with visible light fluorescence isolated to date contain an AMI chromophore. Since the discovery of GFP, multiple other fluorescent proteins have been noted either in nature or through protein modifications. A general overview of these proteins provided in Figure 1.3[9] shows the structural modifications between the different classes of chromophores including a substitution of the Tyr-66 residue of GFP for a Trp or His residue in the cases of the blue and cyan fluorescent proteins, respectively. Contrary to a sequence substitution, the yellow fluorescent protein is achieved through the placement of an additional Tyr residue within close proximity of the chromophore allowing for π-π stacking interactions that bathochromically shift the spectral characteristics. Missing from this table is the red fluorescent protein whose chromophore occurs via an additional post-translational modification. This is achieved through an additional oxidation step, as highlighted in Figure 1.2, of the C-terminus of the imidazolinone ring resulting in an extension of the conjugation thus allowing for a 40-50 nm bathochromic shift.

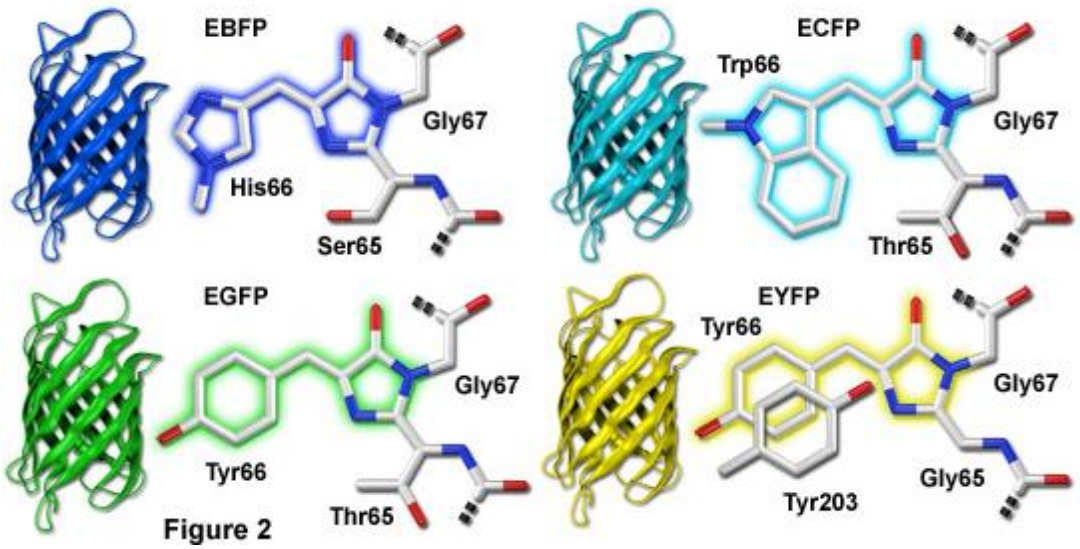

Figure 1.3. Variety of fluorescent proteins exhibiting different spectroscopic properties with their respective chromophores.

Photophysics of the GFP Chromophore

Following removal from the protective β-barrel, the GFP chromophore exhibits several spectral changes including a 10^4 decrease in emission quantum yield. Stark differences between the bound chromophore compared to the natural chromophore allude to complex photophysical mechanisms. Within wild-type GFP (wt-GFP) the chromophore exhibits two forms with absorbance bands at 398 nm and 477 nm corresponding to the neutral form and the anionic form, respectively and an emission band at 508 nm. Upon denaturation, a hypsochromic shift is noted with an absorbance band at 370 nm and an emission band at 440 nm. The mechanism of radiationless decay has been established as internal conversion, promoted by motion along a volume conserving mechanism, perhaps invoking a "hula twist",[10] nearly barrierless coordinate, which is disputed within the literature in favor of a phenyl rotation.[11] These various torsional motions are depicted in Figure 1.4, but one of the most significant consequences gained is that within the restrictive β-barrel these torsional motions are prohibited providing strong circumstantial support of the mechanism of radiationless decay. These motions of the chromophore have great implications within the protein as well. Fluorescent proteins are characterized

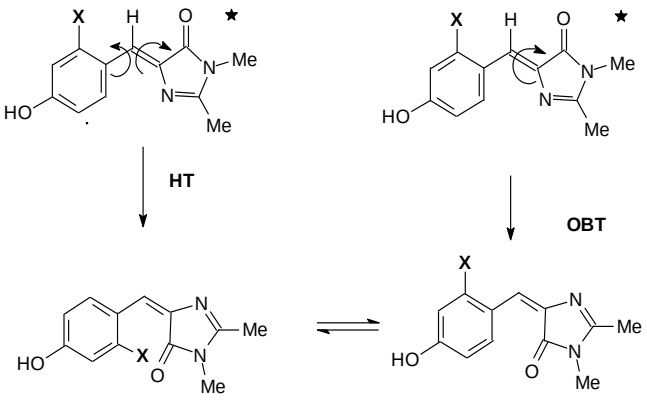

Figure 1.4. Torsional motions of the GFP chromophore showing the hula twist vs. one-bond twist.

by "blinking", which is the temporary conversion to a non-fluorescent form, which has been variously attributed to triplet formation,[12] proton transfer,[13] or cis/trans isomerization, for which the *trans* form is non-fluorescent. Strong support for cis/trans isomerization as the origin of blinking is provided by the behavior of kindling fluorescent proteins,[14] which, upon irradiation into the long-wavelength band, are "kindled" to the fluorescent form. The idea of cis/trans isomerization will prove to be a significant issue within the multiple projects highlighted throughout this dissertation. The next section highlights this important photophysical mechanism of the GFP chromophore.

Cis/trans isomerization

One of the main arguments in favor of rapid internal conversion of the chromophore is cis/trans isomerization. These studies expand to address a key unresolved issue in the photophysics of fluorescent proteins at to whether the cis/trans isomerization is responsible for the blinking phenomenon, which, in addition to isomerization, has been attributed to protonation and to triplet formation. The work of many groups including the Tolbert group,[15] suggests that formal isomerization from the resting cis form to the trans form resulting from the decay of the twisted intermediate to the trans hypersurface, must be permitted. This phenomenon has been the subject of

several studies[16] and corresponds in unexceptional ways to the mechanisms of other AMI chromophores.

Within the literature, the mechanism of photoisomerization has been the subject of several studies, but the mechanism of the thermal reverse isomerization is more problematic. The blinking phenomenon requires that isomerization, if involved, be thermally reversible. The results we have observed are consistent with the addition/elimination mechanism shown as Path b in Figure 1.5.[17] Although a plausible mechanism, literature precedents are fairly rare.

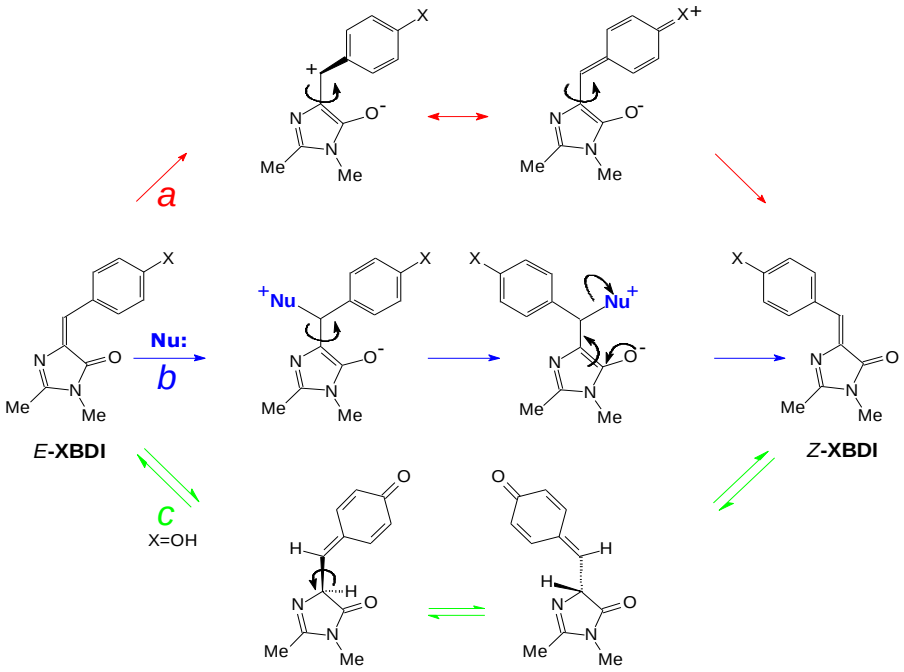

Figure 1.5. Proposed pathways for the ground-state *E*-XBDI to *Z*-XBDI isomerization showing (a) Direct (traditional); (b) Addition/elimination mechanism; (c) Isomerization by tautomerization.

An extensive body of work highlighting the mechanism of cis/trans isomerization within AMI chromophores exists within the literature. A variety of ultrafast optical techniques have been employed to study the photophysics and photochemistry of GFP chromophores. Using time-resolved infrared spectroscopy (TRIR) spectroscopy, a bleaching of the carbonyl band at 1696 cm^{-1}, and a new band at 1746–1780 cm^{-1} was noted for HOBDI. [18,19] Interestingly, the decay rate of this band coincides with the

fluorescence lifetime, which allows for the conclusion that this new band is the excited-state carbonyl stretch and some twisting about the formal double bond is occurring. The orientation of the transition moment of the IR-active carbonyl stretching vibration of HOBDI relative to that of the electronic transition dipole moment indicates that the C=O vibration acts in a "spectator mode" for the relative orientation of the phenolate and imidazolindinone groups, which allows the derivation of an effective near complete twisting around the ethylenic bridging bond upon electronic excitation of HOBDI providing indirect evidence of cis/trans isomerization. In addition to this work, Tolbert and coworkers demonstrated a direct relation between the degree of HOBDI twisting and the rate of deactivation by comparing the decays of HOBDI and 2,6-dimethyl-HOBDI.[20] In the latter the highly twisted structure with a 45° DFT-calculated dihedral angle between the phenyl and imidazolinone planes resulted in an unprecedented short S_1 lifetime (110 fs for anion) as compared to 530 fs for HOBDI anion in ethanol. In an attempt to decouple the two possible rotational coordinates involving the free rotation about the single aryl bond and the cis/trans isomerization about the formal double bond, a locked derivative of *m*-MeOBDI was synthesized (Figure 1.6).

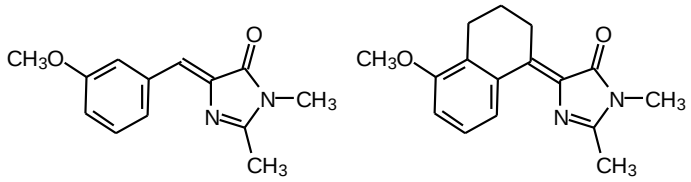

Figure 1.6. Depiction of "unlocked" (left) and "locked" (right) *Z m*-MeOBDI.

Interestingly, a counterintuitive result that the locked *m*-MeOBDI decays much faster than the unlocked one, with lifetimes of 260 fs and 1.4 ps[21] in methanol, respectively was observed. Single-crystal X-ray measurements demonstrate a dihedral angle increase from 3.90° for the unlocked[22] to 6.24° for the locked *m*-MeOBDI. These results demonstrate that the rotation around the double bond is indeed a major coordinate leading to the

conical intersection point; however, the twisted ground-state geometry appears to place the Franck-Condon state closer to conical intersection.

While the mechanism of cis/trans isomerization remains a debate both for the free chromophore as well as the sequestered chromophore, recent work within our groups have alluded to the importance of additional modes of deactivation as well as the presence of cis/trans isomerization. Highlighted within the multiple chapters of this dissertation, work within the Tolbert group has shown that inclusion/encapsulation of these AMI chromophores leads to fluorescence turn-on but fails to prevent cis/trans isomerization form occurring leading to the emission deactivation commonly noted in the studies presented above.

Terminology and Methodology

General overview of photophysics

The interaction of a molecule with light can lead to a number of processes. These processes can lead to the chemical modification of a molecule defined as photochemistry or to a change the energetics of a molecule without a modification to the chemical structure of a molecule defined as photophysics. Throughout this dissertation, references will be made to the photophysics of GFP chromophore analogs thus providing motivation for an overview of photophysical processes presented here.

The absorption of a photon of light by a molecule can initiate a number of different atomic movements. Molecules that contain a specific arrangement of atoms and/or functional groups that absorb light within the UV/Vis range are termed chromophores. Prior to interaction with light, molecules are said to be in the ground state. That is, the electronic structure obeys quantum mechanical calculations including Hund's rule, Pauli's exclusion principle, and Aufbau's principle. Within this context, the valence electrons located at the highest energy level occupy a molecular orbital termed the HOMO or highest occupied molecular orbital. By default the next molecular orbital

is termed the LUMO or lowest unoccupied molecular orbital. A number of simple and complex actions can occur following the absorption of a photon of light by a molecule. A comprehensive visual depiction of photophysical processes is given by the Jablonski diagram provided as Figure 1.7.[23]

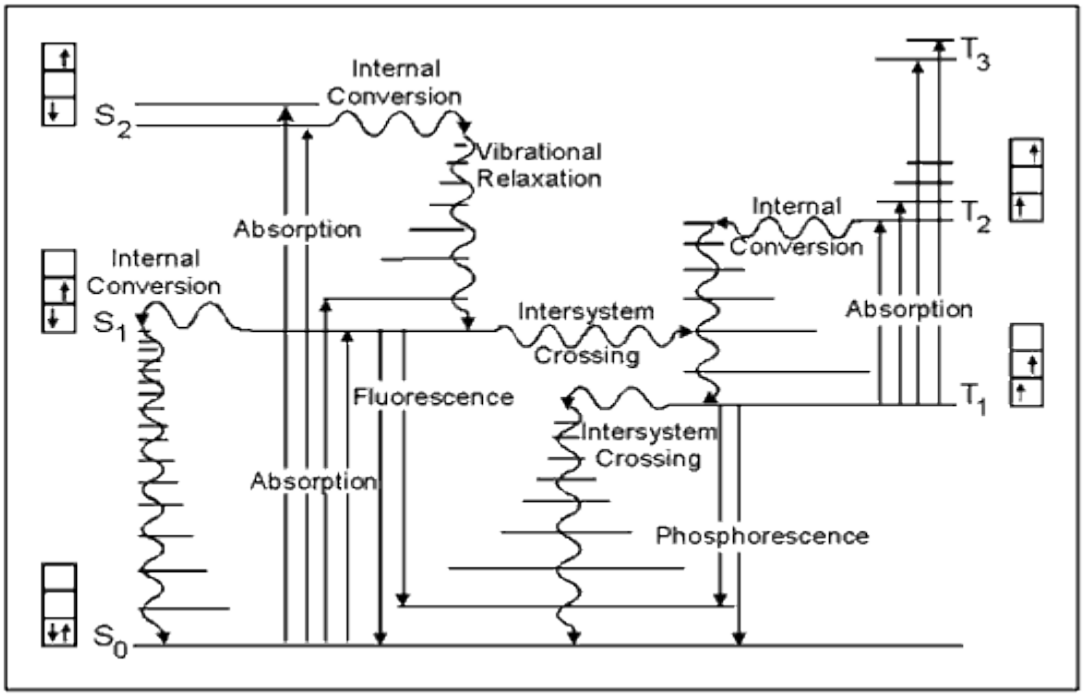

Figure 1.7. Jablonski diagram depicting range of photophysical process for a chromophore.

Within the Jablonski diagram, states describing the molecular orbitals are given as singlet -S_n- (meaning electrons within orbitals have opposite spins) and triplets -T_n- (meaning electrons within orbitals have the same spin). Upon absorbing a photon, a molecule is promoted from the S_0 state to a higher state most commonly S_1. A chromophore will only absorb light that brings about a single electronic transition, termed as the Stark-Einstein law. This has an exception in multi-photon absorption studies where special conditions allow for this law to be relaxed. Following the absorption of light and promotion to a higher energy state, which occurs on a very fast time-scale, the molecule is considered to be in the excited state. Promotion to higher energy states other

than the first singlet excited state (S_1) does occur but movement from higher energy states (S_2, S_3, etc.) to S_1 is extremely fast. This vibrational relaxation occurs so fast and provides the observation that all photochemistry and general photophysical studies are done with respect to the S_1 state, termed Kasha's rule. An additional consequence of the speed of electronic transitions lies in the fact that the lines as well as the depicted energy levels are vertical. This arises from the fact that these processes occur on such small time scales that nuclear motions do not occur thus the initial and final states of the chromophore remain the same.

Principles of light absorption

The interaction of a molecule with light is governed by the type and arrangement of atoms within a molecule, especially functional groups. Common functional groups including alkenes, conjugated alkenes, carbonyls, and aromatic compounds all readily absorb light in the UV/Vis range. Taking note of these examples it is observed that molecules containing pi-bonds as a rule of thumb make excellent candidates for chromophores. This does not go to say that single bonds do not absorb light, in fact they readily absorb light at <200nm, but these wavelengths are out of the typical UV/Vis range thus providing some complications in their use. Since absorbance of light is a process, a way to measure it and its efficiency is a necessity. This process is done using a spectrophotometer whereby incident light of a certain wavelength is introduced to a sample and the amount of light transmitted through the sample is measured Figure 1.8. This process will be elaborated upon further in the following section within this introduction. The amount of light transmitted through a sample is inversely proportional to the amount of light absorbed by the sample thus providing the absorption spectrum.

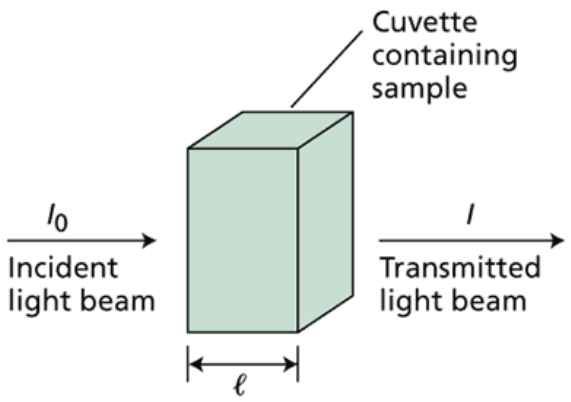

Figure 1.8. Typical schematic of absorption measuring process.

To measure the efficiency at which a chromophore absorbs light, the employment of the Beer-Lambert Law, primarily the molar extinction coefficient (ε), is necessary. The Beer-Lambert Law is given by:

$$\log\left[\frac{Io}{I}\right] = A = \varepsilon bc$$

where *Io* is the intensity of the incident light, *I* the intensity of the transmitted light, *A* is the absorbance of the sample, ε is the molar extinction coefficient ($M^{-1}cm^{-1}$), b is the path length (typically 1 cm) that the light travels through the sample, and *c* is the concentration of the sample in molarity. Compounds are often characterized by their molar absorbtivity, used interchangeably with molar extinction coefficient. From this, absorbance provides some fundamental characteristics of molecules. The principle of absorbance of visible light is one that has great implications within chemistry and leads to significant processes afterward including the important concept of fluorescence.

Fluorescence and other photophysical processes occurring after absorption

Following the absorbance of light, a number of photophysical processes can follow as highlighted in the Jablonski diagram. One of the most significant processes is termed fluorescence, which is the emission of a photon of light following the absorption of a photon. If a compound emits light following absorption of light it is termed a fluorophore. While this process is intuitively expected from the diagram, many

additional processes compete with fluorescence and can result in a chromophore not emitting light. These processes that do not produce light are termed non-radiative decay processes and can take many forms.

Fluorescence as shown can readily be measured using a spectrofluorometer. Following the gathering of absorption data, a molecule can be promoted to the excited state and the subsequent relaxation to the ground state can be measured as a fluorescence spectrum commonly called an emission spectrum since fluorescence is not guaranteed. An example spectrum is provided in Figure 1.9.[23]

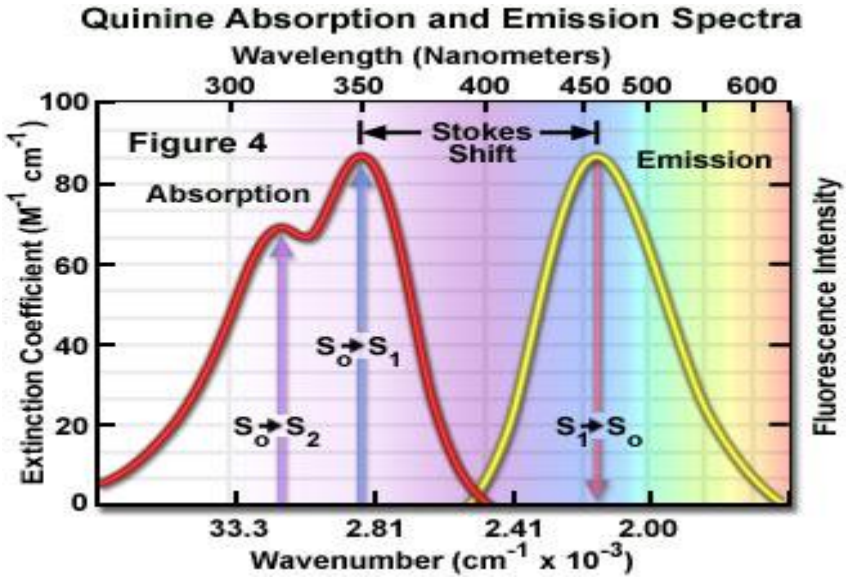

Figure 1.9. Example absorbance and emission spectrum of quinine.

A couple of spectral features to take into account arise from Figure 1.9. First, the energy maximum of emission is less than that of absorbance. This is a direct result of the non-radiative processes that occur that are in direct competition with fluorescence hence lowering the overall energy for fluorescence. The term given for the difference between the absorbance maxima and the emission maxima of the same transition (in this and most cases the transitions involving S_0 and S_1) is called the Stokes shift. Since fluorescence is a process that is readily measured, it becomes a necessity to measure its efficiency. The

overall efficiency of fluorescence is measured as the fluorescence quantum yield given by:

$$\Phi = \frac{number\ of\ photon\ emitted}{number\ of\ photons\ absorbed}$$

This calculation is readily achieved by the comparison of a given fluorophore with a known standard providing for an emission quantum yield. Mathematically, a quantum yield of 1.00 implies the same numbers of photons were emitted as absorbed. This is not readily the case given the competing process often found in flurophores, thus quantum yields are commonly reported as decimal values between 0 and 1. For general reference, the rate of fluorescence is a fast process, occurring on the order of 10^{-8} to 10^{-5} sec. Fluorescence lifetimes are measured through instrumentation involving "pumping" a molecule into the excited state and using a detector to measure the amount of time between pumping and emission. An important consequence of fluorescence lifetimes is achieved that relates lifetime to rate constants. That relationship is defined as:

$$^{1}/_{k_f} = \tau_f$$

where k_f is the rate constant of fluorescence and τ_f is the fluorescence lifetime.

A short overview of processes that readily compete with fluorescence is needed. Within the Jablonski diagram, note that three other main processes can occur: internal conversion, intersystem crossing, and phosphorescence. Internal conversion occurs within the same multiplicity (meaning singlet and triplet) and is noted when relaxation occurs from a higher state to a lower state. This readily competes with fluorescence since internal conversion from S_1 to S_0 can occur without the necessary emission of a photon. This is commonly associated with another energy releasing pathway including molecular movements (vibrations) or heat. This represents one of the key competitors of photon emission. Additionally, intersystem crossing can occur which involves the conversion of the electron from the singlet state to the triplet state requiring a spin-flip of the electron. Following conversion to the triplet state, the molecule can relax to the ground state via

phosphorescence. This process is much lengthier than emission from S_1 to S_0 at times achieving rates of minutes! It is important to note that multiple other processes can readily compete with fluorescence. These processes can include quenching which is due to the excited molecule's interaction with another molecule causing a radiationless relaxation of the excited molecule. Additional energy transfer can also occur and the interested reader is referred to the source cited for this section as well as a plethora of other sources that exist on these topics.

General overview of steady-state spectroscopy

The gathering of an absorbance spectrum or emission spectrum is an example of steady-state spectroscopy. Absorption spectroscopy makes use of a spectrophotometer given as a simple schematic in Figure 1.10.

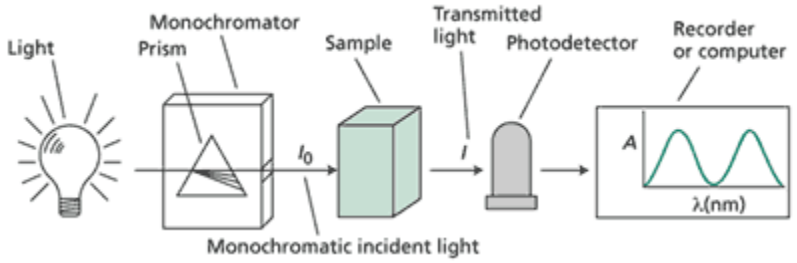

Figure 1.10. Simplified schematic of a spectrophotometer.

where incident light is generated by either a tungsten lamp (visible light) or a deuterium lamp (UV light) and passed through a monochrometer to determine the wavelengths of light that are absorbed by the sample (chromophore). This result is processed by the detector and given as an absorbance spectrum (highlighted earlier). For the purposes of this research, absorption spectra were recorded on a Perkin-Elmer Lambda 19 UV/Vis/NIR spectrophotometer.

The gathering of an emission spectrum shares some commonalities to the spectrophotometer. Emission spectra are taken using a spectrofluorometer given as the simple schematic in Figure 1.11.[24]

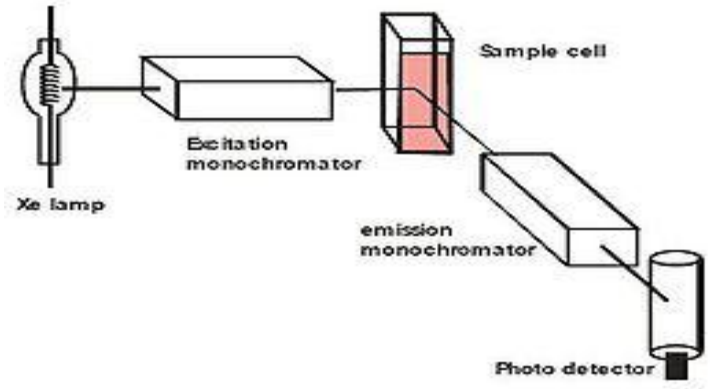

Figure 1.11. Simplified schematic of a spectrofluorometer.

Light is produced from a lamp source and passed through a monochrometer. Detection of light is done at 90^{o} after being subjected to a photomultiplier tube that produces the radiation measured by the detector providing an emission spectrum. For the purposes of this research, emission spectra were recorded using a Horiba Jobin Yvon Flurolog spectrofluorometer. Data from the spectrofluorometer was corrected using the correction file provided for the given light source and conditions.

References

[1] Tolbert, L.M.; Baldridge, A.; Kowalik, J.; Solntsev, K. Acc. Chem. Res. *Submitted.*

[2] Zimmer, M. *Chem. Rev.* **2002**, *102*, 759-781.

[3] (a) Tsien, R. Y. The Green Fluorescent Protein. *Annu. Rev. Biochem.* **1998**, *67*, 509-544. (b) Cubitt, A. B.; Heim, R.; Adams, S. R.; Boyd, A. E.; Gross, L. A.; Tsien, R. Y. *Trends Biochem. Sci.* **1995**, *20*, 448-455.

[4] Ormö, M.; Cubitt, A. B.; Kallio, K.; Gross, L. A.; Tsien, R. Y.; Remington, S. J. *Science* **1996**, *273*, 1392-1395.

[5] (a) Yang, F.; Moss, L. G.; Phillips, G. N. J. *Nature Biotech.* **1996**, *14*, 1246-1251. (b) Suhling, K.; Siegel, J.; Phillips, D.; French, P. M. W.; Leveque-Fort, S.; Webb, S. E. D.; Davis, D. M. *Biophys. J.* **2002**, *83*, 3589-3595.

[6] Brejc, K.; Sixma, T. K.; Kitts, P. A.; Kain, S. R.; Tsien, R. Y.; Ormö, M.; Remington, S. J. *Proc. Natl. Acad. Sci. U.S.A.* **1997**, *94*, 2306-2311.

[7] He, X.; Bell, A. F.; Tonge, P. J. *FEBS Lett.* **2003**, *549*, 35-38.

[8] Kojima, S.; Ohkawa, H.; Hirano, T.; Maki, S.; Niwa, H.; Ohashi, M.; Inouye, S.; Tsuji, F. I. *Tetrahedron Lett.* **1998**, *39*, 5239-5242.

[9] http://www.olympusfluoview.com/applications/fpcolorpalette.html

[10] Liu, R. S. H. *Acc. Chem. Res.* **2001**, *34*, 555-562.

[11] Martin, M. E.; Negri, F.; Olivucci, M. *J. Am. Chem. Soc.* **2004**, *126*, 5452-5464.

[12] (a) Habuchi, S.; Ando, R.; Dedecker, P.; Verheijen, W.; Mizuno, H.; Miyawaki, A.; Hofkens, J. *Proc. Natl. Acad. Sci. USA* **2005**, *102*, 9511-9516. (b) Jimenez-Banzo, A.; Nonell, S.; Hofkens, J.; Flors, C. *Biophys. J.* **2008**, *94*, 168-172.

[13] (a) Haupts, U.; Maiti, S.; Schwille, P.; Webb, W. W. *Proc. Natl. Acad. Sci. USA* **1998**, *95*, 13573-13578. (b) Liu, Y.; Kim, H. –R.; Heikal, A. A. *J. Phys. Chem. B* **2006**, *110*, 24138-24146.

[14] (a) Chudakov, D. M.; Feofanov, A. V.; Mudrik, N. N.; Lukyanov, S.; Lukyanov, K. A. *J. Biol. Chem.* **2003**, *278*, 7215-7219. (b) Quillin, M. L.; Anstrom, D. M.; Shu, X.; O'Leary, S.; Kallio, K.; Chudakov, D. M.; Remington, S. J. *Biochemistry* **2005**, *44*, 5774-5787. (c) Henderson, J. N.; Remington, S. J. *Physiol*. **2006**, *21*, 162-170.

[15] Maddalo, S. L.; Zimmer, M. *Photochem. Photobiol*. **2006**, *82*, 367-372.

[16] (a) Toniolo, A.; Olsen, S.; Manohar, L.; Martínez, T. J. *Faraday Discuss*. **2004**, *127*, 149-163. (b) Gepshtein, R., Huppert, D.; Agmon, N. *J. Phys. Chem. B* **2006**, *110*, 4434-4442. (c) Altoe, P.; Bernardi, F.; Garavelli, M.; Orlandi, G.; Negri, F. *J. Am. Chem. Soc*. **2005**, *127*, 3952-3963.

[17] Dong, J.; Abulwerdi, F.; Baldridge, A.; Kowalik, J.; Solntsev, K. M.; Tolbert, L. M. *J. Am. Chem. Soc*. **2008**, *130*, 14096-14098.

[18] Usman, A.; Mohammed, O. F.; Nibbering, E. T. J.; Dong, J.; Solntsev, K. M.; Tolbert, L. M. *J. Am. Chem. Soc.* **2005**, *127*, 11214-11215.

[19] Stoner-Ma, D.; Jaye, A. A.; Matousek, P.; Towrie, M.; Meech, S.R.; Tonge, P.J. *J. Am. Chem. Soc.* **2005**, *127*, 2864-2865.

[20] Conyard, J.; Kondo, M.; Heisler, I.; Baldridge, A.; Tolbert, L. M.; Solntsev, K. M.; Meech, S. R. *J. Phys. Chem. B* **2011** Doi:10.1021/jp111593x.

[21] Solntsev, K. M.; Poizat, O.; Dong, J.; Rehault, J.; Lou, Y.; Burda, C.; Tolbert, L. M. *J. Phys. Chem. B* **2008**, *112*, 2700-2711.

[22] Naumov, P.; Kowalik, J.; Solntsev, K. M.; Baldridge, A.; Moon, J. S.; Kranz, C.; Tolbert, L. M. *J. Am. Chem. Soc.* **2010**, *132*, 5845-5857.

[23] http://www.photobiology.info/Photochem.html.

[24] http://www.thefullwiki.org/Fluorescence_spectroscopy.

CHAPTER 2

SYNTHESIS OF NOVEL FLUORESCENT PROTEIN CHROMOPHORE ANALOGS

Introduction

The chromophore of the green fluorescent protein (GFP) has gained significant attention in the literature due to its unusual photophysical and photochemical properties.[2] Denaturation of the protein β-barrel leads to a loss in emission quantum yield, and numerous studies have sought to regain that brightness by incorporation into rings[3,4] or restriction in hydrophobic capsules.[5] In order to study the mechanisms by which these phenomena arise, convenient access to a wide spectrum of substituted arylideneimidazolinones (AMI) is required. Thus a high-yield, functional group-tolerant methodology adaptable to a combinatorial approach is motivated in order to provide materials to study this interesting class of molecules.

The Plöchl-Erlenmeyer synthesis,[6] an over a century old classic reaction in organic chemistry provides access to AMI's[7] and continues to dominate the literature concerning the synthesis of GFP chromophores as well as supplement more recent methods[8] (Figure 2.1).

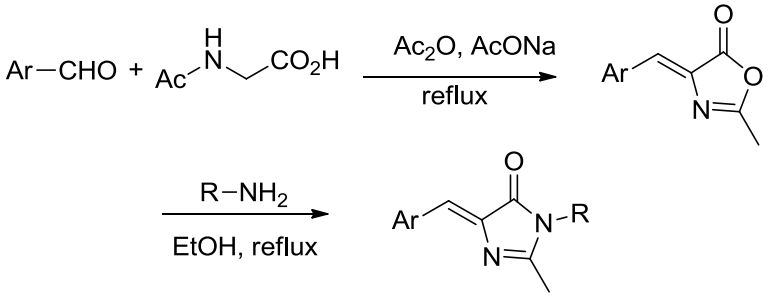

Figure 2.1. Synthetic scheme of the Erlenmeyer azalactone synthesis.

This two-step methodology requires initial preparation of an arylideneoxazolone followed by reaction with amines to yield respective imidazolinones and continues to dominate the synthesis of GFP chromophores as well as supplement more recent methods.[9] Alternative methods include the *de novo* formation of the imidazolinone ring[10]

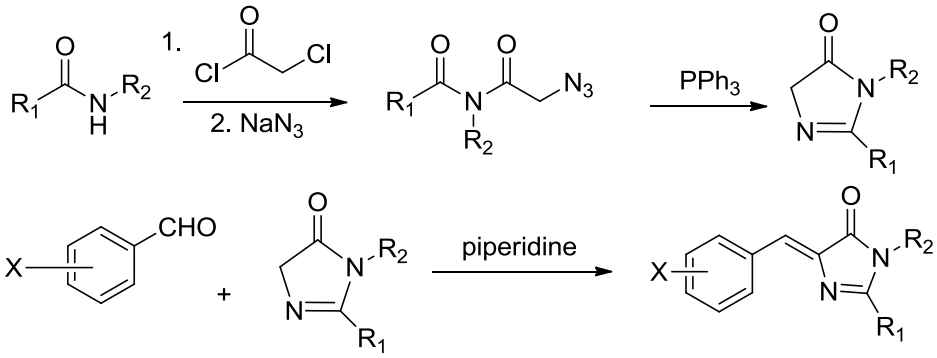

Figure 2.2. Synthetic scheme of the modified Knoevenagel condensation for AMI synthesis.

or interconversions of imidazolinones.[11] A recent excellent review of the former has appeared.[12]

Despite this progress, the need for reliable, quick and convenient access to a variety of substituted imidazolinones with varying substitution patterns remains, since such chromophores are of increasing interest in other disciplines,[13] including biosciences and medicine.[14] Such synthetic methods must provide efficiency, directness and a diversity of functional groups. We have found that the methodology proposed by Bazureau *et al*, a very clever adaptation of earlier chemistry developed by Grigg et al.[15] and other authors, is most adaptable for our purposes. In this paper we expand upon that synthesis to provide a general approach to arbitrary substituted AMIs.

Imines of α-aminoacid esters owe their synthetic versatility to easy equilibration (self-enolization) to a bipolar nitrogen ylide via facile 1,2 prototropic shift. The resulting stabilized imine ylide is an adaptable component of a 2+3 cycloaddition leading to an assortment of heterocycles, including arylideneimidazolinones.[16] The required iminoglycine methyl ester is readily produced from the reaction of ethyl acetimidate

hydrochloride with glycine methyl ester hydrochloride (Figure 2.3). The accompanying Schiff base, acting as a dipolarophile, is conveniently synthesized in high yields by a condensation of aromatic aldehydes and primary amines (Figure 2.3). In the resulting 4-arylideneimidazolin-5-one, the Schiff base provides the aromatic substituent as well as the amide nitrogen of the imidazolinone with its substituent, while the other reagent, (1-ethoxyethylideneamino) acetate, common for all reactions, contributes all other atoms in

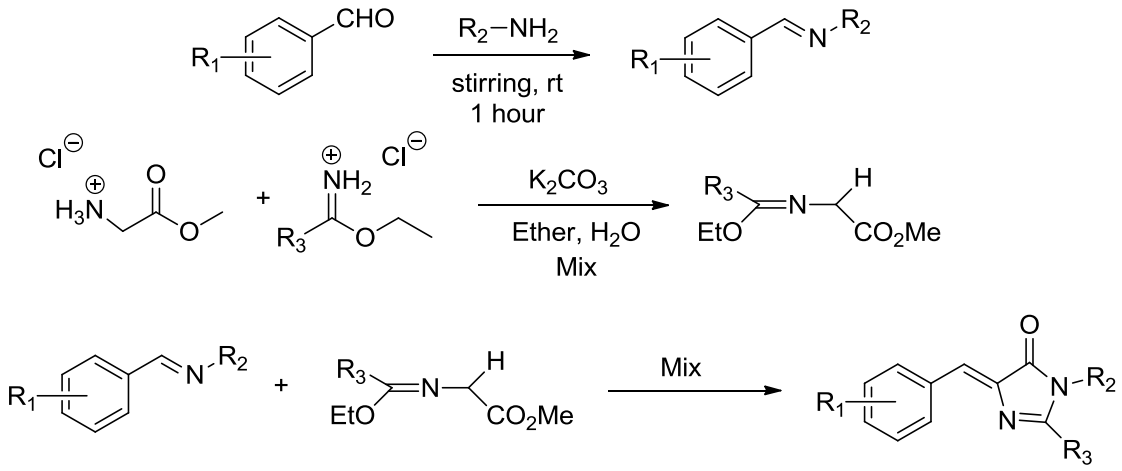

Figure 2.3. Synthetic scheme of the 2+3 cycloaddition.

the imidazolinone ring (Figure 2.3). Since both aromatic aldehydes and aliphatic amines are commercially available, and the synthetic method is tolerant of functional groups, it is readily adaptable and provides convenient access to a variety of substituted imidazolinones.

The synthesis is carried out by mixing 1 equiv of the corresponding Schiff base with 1.1 equiv of the imidate. In cases where the Schiff base contains acidic groups, a spontaneous reaction takes place with considerable generation of heat. The exothermic nature of this reaction is not as sizable when acidic groups are absent. For better control of the reaction, minimal amounts of ethanol were used as solvent. Magnetic stirring overnight under ambient conditions generally resulted in precipitation of a pure reaction

product. In cases where no solid was obtained, the reaction product was isolated and purified by column chromatography.

Through a different synthetic protocol, Lukyanov, et.al. proposed the functionalization of the C-terminus of the imidazolinone through the allylic oxidation of

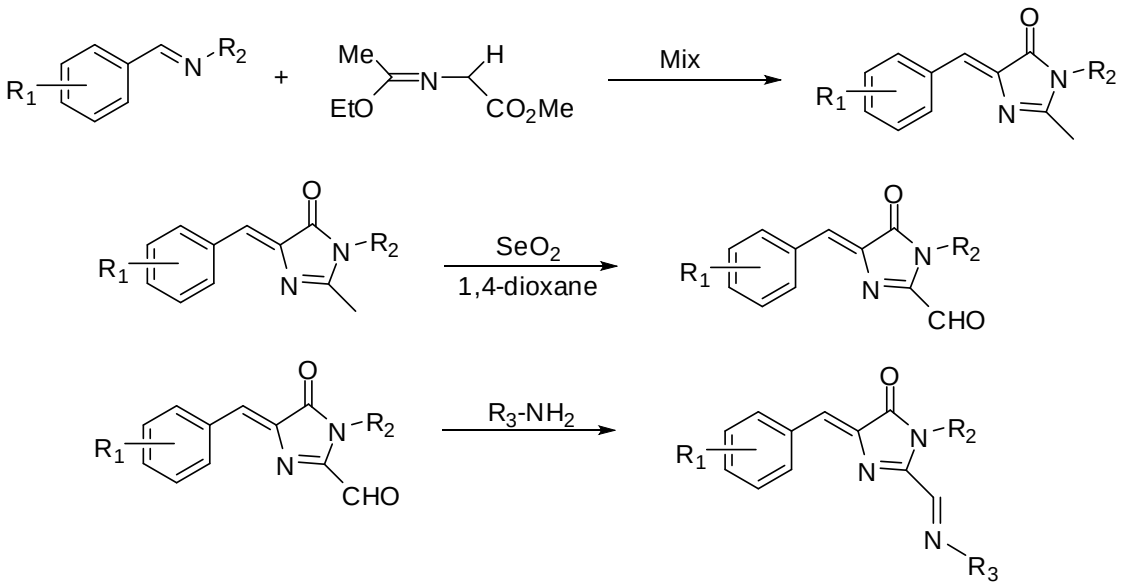

Figure 2.4. Synthetic scheme of 2+3 cycloaddition employing a SeO2 oxidation to allow for additional combinatorial substitution.

the methyl group to an aldehyde proving significant reactivity as a consequence of the aldehyde group. This oxidation is accomplished using SeO_2. Coupled with the imine chemistry extensively used in the 2+3 cycloaddition, a variety of substituted imidazolinones can be readily synthesized in quantitative yields. It is also significant to note that the synthesized analogs mimic the chromophore of the red fluorescent protein due to the extended conjugation provided by the imine bond.

Extension of the 2+3 cycloaddition can be realized through the reaction of aromatic ketones with primary amines under similar conditions. These reactions are not as well documented within the literature and require modified conditions compared to the condensation of the aldehydes with the primary amines due to sterics of the aromatic amines. Synthesis of the ketimines is accomplished in fair to excellent yields using

molecular sieves within the reaction as well as $TiCl_4$ in some cases as a catalyst. The

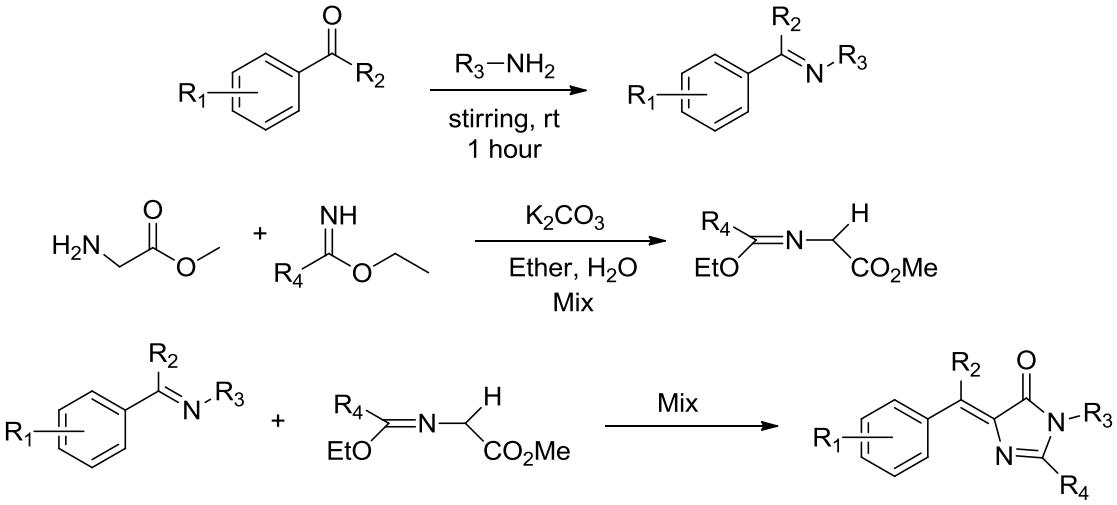

Figure 2.5. Synthetic scheme of AMI's using aromatic ketones providing bridging methine substitution.

ketimine products can subsequently be reacted with the synthesized imidate to form the imidazolinone final product (Figure 2.4). It is important to note that this represents the first time that a substitution on the bridging methine carbon, whose substitution is determined by the aromatic carbonyl compound initially used. The synthetic breadth of this substitution is somewhat limited compared to the aldehyde imine synthesis route resulting from a significantly fewer number of aromatic ketones available through commercial sources. The use of this new synthetic protocol coupled with all previous protocols allows for the full functionalization of the arylideneimidazolidinone.

Experimental Protocols

General Experimental

Melting points were measured on an Electrothermal melting appoint apparatus and are uncorrected. 1H NMR spectra were determined with a Varian Mercury Vx 300 spectrometer operating at 300 MHz (1H) and at 75 MHz (13C), in appropriate solvents, as indicated within the text. Chemical shifts were referenced to TMS. Low-resolution

MS spectra (EI 70 eV) were measured on a Micromass AutoSpec spectrometer. Elemental analyses were performed by the Atlantic Microlab, Inc., Norcross, Georgia (USA). TLC studies were carried out on Analtech Uniplate Silica Gel GF plates. Column chromatography was performed using Sorbent Technologies 40-63 υM standard grade silica gel. The organic solvents and reagents used to synthesize the compounds were used as received from commercial sources without further purification.

Imine synthesis

Synthesis of the various Schiff bases was carried out according to the literature by combining the given aromatic aldehyde (1 mmol) with the corresponding amine (1.1 mmol). In cases where the aldehyde or amine was solid, ~3mL of EtOH was used to solubilize the reagents. The reaction was allowed to stir under ambient conditions for 12 hours. In cases where a precipitate was noted, the product was isolated by filtration and washed with ~2mL of cold EtOH to afford pure product. In cases where both reagents were initially liquids, the solvents and excess amine were removed *in vacuo*. All Schiff base reactions gave at or near quantitative yields.[17]

Imidate synthesis

Synthesis of the imidate was carried out according to the literature.[18] Potassium carbonate (50 mmol) and methyl glycinate hydrochloride (50 mmol) were suspended in 125 mL of ether followed by addition of 20 mL of water then addition of ethyl acetimidate hydrochloride (50 mmol). The mixture was shaken for 6 min followed by decanting of the ether. An additional 75 mL portion of ether was added and the mixture shaken for 6 min and ether decanted. The two ether portions were dried over anhydrous $MgSO_4$. The ether was removed *in vacuo* to afford 4.30 g (yield: 54%) of the pure imidate as confirmed by NMR.

Imidazolinone synthesis

The required aromatic Schiff base (1 mmol) was combined with the imidate (1.1 mmol) in ~1 mL of absolute EtOH and allowed to stir in a capped vial overnight under

ambient conditions (Figure 2.3). In cases where the Schiff base was solid additional EtOH was used to solubilize the reactants. In some cases, as indicated in Table 2.3, the precipitated product was filtered and washed sequentially with ~2mL Et_2O and ~1mL EtOH to yield pure product. In the cases where precipitation did not occur at room temperature, the reaction mixture was placed at 0 ^oC for 1-4 days allowing precipitation to occur. Following this, the product was filtered and washed sequentially with ~2mL cold Et_2O and ~1mL cold EtOH. If precipitation did not occur by either method, flash column chromatography on silica gel was carried out using $CHCl_3$ as the elution solvent. Characterization of all purified imidazolinones is provided in Appendix A.

Allylic Oxidation

The imidazolinone product (1eq) was dissolved in anhydrous dioxane (50 mL) followed by addition of selenium dioxide (1.2 equiv). The suspension was stirred under reflux for 1 h followed by carefully decanting the red solid from the mixture while hot. The solution was concentrated in vacuo and the crude product was purified using column chromatography (silica gel).[19]

Results

Combinatorial approaches, as alluded to in the introduction, were exploited on the phenyl substitution as well as the N-terminus of the imidazolinone. This is readily realized through the combinatorial reaction of the corresponding aldehyde with a given primary amine forming the imine precursor for the final 2+3 cycloaddition step. Due to the quantitative nature and general synthetic robustness of the imine synthesis, as highlighted in the literature, an overarching combinatorial approach was adopted with the imine synthesis providing large quantities of starting materials for the cyclization step. To expedite this process and in collaboration with Dr. Andy Cooper at the University of Liverpool in Liverpool, England, robotics were used to combinatorially react 32 aldehydes with 16 amines yielding 512 different imines. With all starting materials

considered, there are greater than 1,000 different combinations of imines that can be synthesized for use with this synthesis. Table 2.1 lists the available aromatic aldehydes and primary amines currently available within the Tolbert laboratory and highlights the compounds sent to Liverpool for combinatorial synthesis. It is important to note that others on the list were excluded from the list due to high cost coupled with difficultly in shipment to international locations. If either of these were the case, the compounds were excluded from the robotic combinatorial synthesis.

Table 2.1. Available aromatic aldehydes and primary amines for use in combinatorial imine synthesis.

Ar components

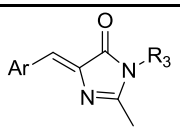

4-Me	2-OMe	2-OH	2-Br	2-OH, 4-$N(Et)_2$	4-$N(Et)_2$	2,4-Me
3-Me	1-naphthyl	3-OH	4-NO_2	3,5-t-Bu, 4-OH	4-CN	2-quinoline
2-Me	2-naphthyl	4-OH	3-NO_2	2-OH, 3-OEt	2-CF_3	4-i-Pr
4-OMe	4-t-Bu	2,3-OMe	4-CO_2H	2,6-Me, 4-OH	3-CF_3	4-i-Bu
3-OMe	Indole	2,5-OMe	2-F	2,4,5-OMe	4-CF_3	2,6-Me
2-Et	3-Et	4-Et	benzyl	2-imidazole	3-F	
4-Cl	3-Cl	2-Cl	4-Br	2-OH, 4-OMe	4-OBz	
2,4-Cl	3,4-Me	2,4-OH	3,4-OH	Me_4-Tetralin	4-$N(Me)_2$	
4-OAc	3,5-Me	4-F	3-Br	3,5-Me, 4-OH		

R_3 components

Me	Et	n-Pr	i-Pr	n-Bu	n-hexyl	n-heptyl
n-octyl	C_2H_4OH	C_3H_6OH	$C_3H_6CO_2H$	$C_5H_{10}CO_2H$	$C_{10}H_{20}CO_2H$	$C_4H_8CO_2H$
n-dodecyl	$C_3H_6N(Me)_2$	Thiazole	2-phenol	Benzyl		

Synthesis of the AMIs using the 2+3 cycloaddition provided a robust synthesis that yielded products with a myriad of functional groups located on both the phenyl ring

as well as the nitrogen of the imidazolinone ring. Compounds synthesized to the date of this dissertation are summarized in Table 2.2 with characterization data of these compounds provided in Appendix A.

Table 2.2. Imidazolinone library of compounds synthesized to date of dissertation publication. (sym indicates a "di-imidazolinone" where two compounds are joined by a methylene linker).

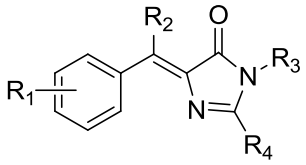

#	R_1	R_2	R_3	R_4	#	R_1	R_2	R_3	R_4
1	4-Me	H	Me	Me	**89**	3,5-Me 4-OH	H	Me	Me
2	3-OMe	H	Me	Me	**90**	3-F	H	Me	Me
3	3-OH	H	Me	Me	**91**	3-OH	H	C_3CO_2H	Me
4	2,3-OMe	H	Me	Me	**92**	$4\text{-}OC_{12}H_{25}$	H	Me	Me
5	$4\text{-}NO_2$	H	Me	Me	**93**	4-OMe	H	Me	Me
6	2,5-OMe	H	Me	Me	**94**	2-OMe	H	Me	Me
7	3,5-t-Bu 4-OH	H	Me	Me	**95**	4-OMe	H	n-Pr	Me
8	$4\text{-}CO_2H$	H	Me	Me	**96**	4-Cl	H	n-Pr	Me
9	$4\text{-}N(Me)_2$	H	Me	Me	**97**	4-Br	H	Me	Me
10	2-F	H	Me	Me	**98**	2-OMe	H	n-Pr	Me
11	4-OBz	H	Me	Me	**99**	2-Br	H	Me	Me
12	2,4,5-OMe	H	Me	Me	**100**	$4\text{-}PhC_8H_{17}$	H	Me	Me
13	2-pyridyl-4-OH	H	Me	Me	**101**	4-Br	H	n-Pr	Me
14	4-OH	H	Me	Me	**102**	2-Br	H	n-Pr	Me
15	2-Me	H	Me	Me	**103**	3-F	H	n-Pr	Me
16	4-CN	H	Me	Me	**104**	3-Cl	H	Me	Me
17	$4\text{-}N(Et)_2$	H	Me	Me	**105**	3-OMe	H	n-Pr	Me
18	4-OH	H	n-Pr	Me	**106**	Benzyl	H	n-Pr	Me
19	4-OH	H	n-Pn	Me	**107**	3-OH	H	C_3CO_2H	Me

20	4-OH	H	n-Bu	Me	**108**	Benzyl	H	C_3CO_2H	Me
21	4-Me	H	n-Pr	Me	**109**	4-PhC_5H_{11}	H	Me	Me
22	4-$N(Me)_2$	H	n-Pr	Me	**110**	4-*i*-Pr	H	Me	Me

Table 2.3. Continued

23	4-OH	H	C_3CO_2H	Me	**111**	3,4-Me	H	Me	Me
24	4-OH	H	C_5CO_2H	Me	**112**	2-OH 4-$N(Et)_2$	H	n-Pn	Me
25	1-naphthyl	H	Me	Me	**113**	2-OH 4-$N(Et)_2$	H	n-heptyl	Me
26	4-Et	H	Me	Me	**114**	2-OH 4-$N(Et)_2$	H	n-Pr	Me
27	3-Me	H	Me	Me	**115**	4-$N(Et)_2$	H	n-hexyl	Me
28	2,4-Me	H	Me	Me	**116**	2-OH 4-$N(Et)_2$	H	n-hexyl	Me
29	2-quinoline	H	Me	Me	**117**	2-OH	H	n-Pr	Me
30	2,5-Me	H	Me	Me	**118**	3-Cl	H	n-Pr	Me
31	1-naphthyl	H	Et	Me	**119**	2-OH 4-$N(Et)_2$	H	Dodecyl	Me
32	4-*i*-Pr	H	n-Pr	Me	**120**	2-OH 4-$N(Et)_2$	H	Octyl	Me
33	4-$N(Me)_2$	H	n-Bu	Me	**121**	4-*i*-Bu	H	C_3CO_2H	Me
34	2-CF_3	H	Me	Me	**122**	4-*i*-Bu	H	n-heptyl	Me
35	2-naphthyl	H	Me	Me	**123**	3,4-Me	H	C_3CO_2H	Me
36	4-$N(Et)_2$	H	*i*-Pr	Me	**124**	3-pyridyl	H	Me	Me
37	4-OH	H	EtOH	Me	**125**	3-Br	H	n-Pr	Me
38	4-OH	H	$CH_2(CF2)_7$ CF_3	Me	**126**	2,4-Cl	H	Me	Me
39	4-Et	H	n-Pr	Me	**127**	2-OH	H	Me	Me
40	2-Et	H	Me	Me	**128**	3-Br	H	Me	Me
41	2-Me	H	n-Pr	Me	**129**	4-PhC_3H_7	H	Me	Me
42	2-Me	H	CH_2CF_3	Me	**130**	3,5-t-Bu 4-OH	H	n-Pr	Me

43	4-OH	H	PrOH	Me	**131**	3,5-t-Bu 4-OH	H	n-Pn	Me
44	2-Et	H	n-Pr	Me	**132**	3,5-t-Bu 4-OH	H	n-hexyl	Me
45	3-NO_2	H	Me	Me	**133**	4-OMe	H	EtOH	Me

Table 2.4. Continued

46	4-$N(Et)_2$	H	n-Pr	Me	**134**	3,4-OMe	H	n-Pr	Me
47	2,6-Me	H	Me	Me	**135**	2-OH 3-OEt	H	2-phenol	Me
48	4-*i*-Pr	H	Me	Me	**136**	4-OH	H	$C_2N(Me)_2$	Me
49	4-*t*-Bu	H	Me	Me	**137**	3-OH	H	$C_2N(Me)_2$	Me
50	3-indole	H	Me	Me	**138**	2-OH	Me	Me	Me
51	2-F	H	n-Pr	Me	**139**	4-$N(Et)_2$	H	C_2-sym	Me
52	4-$N(Me)_2$	H	*i*-Pr	Me	**140**	Benzyl	H	$C_2N(Me)_2$	Me
53	4-tetralin	H	Me	Me	**141**	3,5-t-Bu 4-OH	H	EtOH	Me
54	2-Me	H	Et	Me	**142**	2-OH 4-OMe	H	n-Pr	Me
55	4-$N(Et)_2$	H	n-Pn	Me	**143**	2,4-Cl	H	n-Pr	Me
56	Benzyl	H	Me	Me	**144**	4-$N(Et)_2$	H	C_4-sym	Me
57	2-OH 3-OEt	H	Me	Me	**145**	2-OH 4-OMe	H	Me	Me
58	4-F	H	Me	Me	**146**	Piperonal	H	Me	Me
59	2-OH 4-$N(Et)_2$	H	Me	Me	**147**	2-CF_3	H	n-Pr	Me
60	2-imidazole	H	Me	Me	**148**	4-OH	H	Allyl	Me
61	2-Et	H	Et	Me	**149**	2,5-OMe	H	n-Pr	Me
62	3-Me	H	n-Pr	Me	**150**	4-$N(Me)_2$	H	PrOH	Me
63	2-Me	H	n-Bu	Me	**151**	3-OH 4-Br	H	Me	Me
64	2-Me	H	n-Pn	Me	**152**	4-OH	H	2-heptyl	Me
65	2-Me	H	*i*-Pr	Me	**153**	4-Ph	H	Me	Me
66	3-OMe 4-OH	H	C_3CO_2H	Me	**154**	4-OMe	H	Allyl	Me

67	4-Me	H	Et	Me	**155**	2-OH 4-OMe	H	PrOH	Me
68	2,3-OMe	H	C_3CO_2H	Me	**156**	4-$N(Me)_2$	H	2-heptyl	Me
69	4-$N(Et)_2$	H	C_3CO_2H	Me	**157**	4-OC_4H_9	H	Me	Me

Table 2.5. Continued

70	4-Cl	H	Me	Me	**158**	4-$N(Me)_2$	H	$C_3N(Me)_2$	Me
71	3-CF_3	H	n-Pr	Me	**159**	4-$N(Me)_2$	H	C_2CN	Me
72	4-CF_3	H	Me	Me	**160**	2-OH 4-$N(Et)_2$	H	C2-sym	Me
73	4-OH	H	$C_3N(Me)_2$	Me	**161**	4-Me	H	C_2H_4CN	Me
74	3-CF_3	H	Me	Me	**162**	2-Indole	H	n-Pn	Me
75	2,4-OH	H	C_3CO_2H	Me	**163**	3-OH	H	2-heptyl	Me
76	3,4-OH	H	C_3CO_2H	Me	**164**	3-OH	H	3-Pn	Me
77	2-Cl	H	Me	Me	**165**	2-Indole	H	$C_3N(Me)_2$	Me
78	2-Cl	H	n-Pr	Me	**166**	4-$N(Me)_2$	H	EtOH	Me
79	4-CF_3	H	n-Pr	Me	**167**	4-$N(Et)_2$	H	C_6-sym	Me
80	3,5-Me	H	Me	Me	**168**	2-Indole	H	n-Pr	Me
81	4-tetralin	H	C_3CO_2H	Me	**169**	3-OH	H	2-heptyl	Me
82	Benzyl	H	C_3CO_2H	Me	**170**	4-CN	H	PrOH	Me
83	2-OH 4-$N(Et)_2$	H	C_3CO_2H	Me	**171**	4-OBu	H	n-Pn	Me
84	4-$N(Me)_2$	H	C_3CO_2H	Me	**172**	4-OH	H	3-Pn	Me
85	4-OC_6H_{13}	H	Me	Me	**173**	4-OH	H	CH_2CF_3	Me
86	2,6-Me 4-OH	H	Me	Me	**174**	4-$N(Me)_2$	H	Allyl	Me
87	3,5-*t*-Bu 4-OH	H	Benzyl	Me	**175**	4-OH	H	C_2H_4CN	Me
88	4-OH	H	Benzyl	Me					

It is important to note that the compound numbers provided Table 2.2 will be used throughout this thesis to identify compounds unless a coding system of compounds is

developed as a consequence of the publication respective of each chapter or unless otherwise noted in the introductory paragraph. Additionally, full characterization data for the above compounds including ^{1}H NMR, ^{13}C NMR, mass spectrometry, and melting points is provided in the appendix verifying the purity of these compounds.

Table 2.3. Yields of synthesized compounds following respective purification methods where ([a]) indicates precipitation with overnight stirring, ([b]) indicates precipitation at 0 ^{o}C, and ([c]) indicates purified by column chromatography.

#	Yield %	#	Yield %	#	Yield %
1	81 [a]	**31**	90 [a]	**61**	60 [b]
2	54 [a]	**32**	70 [b]	**62**	72 [a]
3	79 [a]	**33**	30 [b]	**63**	91 [c]
4	72 [a]	**34**	50 [a]	**64**	59 [c]
5	99 [a]	**35**	69 [a]	**65**	63 [c]
6	96 [a]	**36**	62 [a]	**66**	20 [a]
7	46 [a]	**37**	67 [a]	**67**	50 b
8	65 [a]	**38**	30 [a]	**68**	85 b
9	64 [a]	**39**	63 [b]	**69**	70 [a]
10	67 [a]	**40**	59 [a]	**70**	71 [a]
11	64 [a]	**41**	72 [b]	**71**	35 b
12	80 [a]	**42**	38 [b]	**72**	76 [a]
13	50 a	**43**	30 [b]	**73**	84 b
14	69 [a]	**44**	60 [b]	**74**	59 a
15	49 [a]	**45**	75 [a]	**75**	79 a
16	96 [a]	**46**	72 [a]	**76**	75 a
17	49 [a]	**47**	45 [a]	**77**	25 a
18	50 [a]	**48**	66 [b]	**78**	20 a
19	44 [a]	**49**	66 [a]	**79**	43 [b]
20	46 [a]	**50**	71 [a]	**80**	63 a
21	84 [a]	**51**	40 [a]	**81**	96 a
22	48 [b]	**52**	46 [b]	**82**	80 a
23	74 [a]	**53**	42 [a]	**83**	70 a
24	78 b	**54**	57 [b]	**84**	94 a
25	95 [a]	**55**	50 [b]	**85**	70 c
26	55 [a]	**56**	64 [a]	**86**	51 a
27	70 [a]	**57**	95 [a]	**87**	89 a
28	70 [a]	**58**	60 [a]	**88**	67 a
29	75 [a]	**59**	85 [a]	**89**	66 a
30	55 [a]	**60**	37 [a]	**90**	60 [b]

In addition to the robust nature of the synthesis, the yields were good to very good, which made the process amenable to a combinatorial approach. The reaction outcomes and yields are noted in Table 2.3. The purification method of each of the compounds is also noted in Table 2.3, showing that with the combinatorial approach that is adopted using this synthetic protocol, the ease of purification vial washing and/or simple extraction is coupled with this overall synthetic ease.

Conclusions

As shown, the 2+3 cycloaddition can readily be used to synthesize a variety of substituted AMI's in good to excellent yields. Prior to the application of the 2+3 cycloaddition synthetic protocol, synthesis of fluorescent protein chromophores was commonly accomplished through the Erlenmeyer azalactone synthesis. This synthesis, while versatile in terms of available compounds, requires harsh conditions as well as purification via column chromatography not providing for a combinatorial approach to be adopted. Contrary to the Erlenmeyer azalactone synthesis, as well as other synthetic protocols, the combinatorial approach of imine chemistry that can be extended from aromatic aldehydes to include aromatic ketones provides thousands of starting materials for cyclization and the overall synthetic breadth of the cycloaddition presents possibilities to synthesize AMI's for a range of studies in a very efficient manner. Even with the wide synthetic applicability of the cycloaddition, a number of factors exist that limit its use. The main deficiency of the cycloaddition is the lack of synthetic ease to readily functionalize the R4 position of the imidazolinone resulting from the sparse commercial availability of available imidates used to make the amino imidate. While this presents a real challenge, the cycloaddition can be used to provide a wide range of synthetic options and allow the study of these chromophores from the substitution of the R_1, R_2, and R_3. The remainder of this dissertation details the applications and advanced studies these

compounds are being used to study as well as the possibility of these compounds to be used in a number of different applications.

References

[1] Baldridge, A.; Kowalik, J.; Tolbert, L.M. *Synthesis* **2010**, *14, 2424-2436.*

[2] Tonge, P.J.; Meech, S.R. *J. Photochemistry and Photobiology, A* **2009**, 205 (1), 1-11.

[3] Wu, L. Burgess, K. *J. Am. Chem. Soc.* **2008**, *130*, 4089-4096.

[4] Chen, K.-Yu. Cheng, Y.-M. Lai, C.-H. Hsu, C.-C. Ho, M.-L. Lee, G.-H. Chou, P.-T. *J. Am. Chem. Soc.* **2007**, *129*, 4534-4535.

[5] Baldridge, A.; Samanta, S. R.; Jayaraj, N.; Ramamurthy, V.; Tolbert, L. M. *J. Am. Chem. Soc.*, **2010**, *132*, 1498-1499.

[6] Even though Emil Erlenmeyer is customarily credited with this discovery (*Lieb. Ann. Chem*. **1893**, *275*, 1), an earlier report on the reaction of hippuric acid with benzaldehyde and acetic anhydride actually came from J. Plöchl, (*Ber*. **1883**, *16*, 2815-2825). The correct, azalactone structure of the reaction product came later, Erlenmeyer, E. *Ber*. **1900**, *33*, 2036; W. Kropp and H. Decker *Ber*. **1909**, *42*, 1184-1192).

[7] (a) Williams, D.L.; Ronzio, A.R. *J. Am. Chem. Soc.* **1946**, *68*, 647-649; (b) Islam, A.M.; Khalil, A.M.; Abd El-Gawad, I.I. *Aust. J. Chem.* **1973**, *26*, 827; (c) Badr, M.Z.; El-Sherief, H.A.H.; Tadros, M.E. *Bull. Chem. Soc. Jpn.* **1982**, *55*, 2267-2270; (d) Islam, A.M.; Khalil, A.M.; El-Houseni, M.S. *Aust. J. Chem.* **1973**, *26*, 1701-1704.

[8] (a) He, X.; Bell, A.F.; Tonge, P.J. *Org. Lett*. **2002**, *4*, 1523-1526. (b) Chen, K-Y.; Cheng, Y-M.; Lai, C-H.; Hsu, C-C.; Ho, M-L. ; Lee, G-H. ; Chou, P-T. *J. Am. Chem. Soc.* **2007**, *129*, 4534-4535.

[9] Kojima, S.; Okhawa, H.; Hirano, T.; Maki, S.; Niwa, H.; Ohashi, M.; Inouye, S.; Tsui, F.I. *Tetrahedron Lett.* **1998**, 5239-5242.

[10] (a) Kawasaki, A.; Maekawa, K.; Kubo, K.; Igarashi, T.; Sakurai, T. *Tetrahedron* **2004**, *60*, 9517-9524. (b) Wu, L.; Burgess, K. *J. Am. Chem. Soc.* **2008**, *130*, 4089-4096. (c) Lerestif, J.M.; Bazureau, J.P.; Hamelin, J, *Tetrahedron Lett*. **1993**, 4639-4642. (d) Devasia, G. *Tetrahedron Lett.* **1976**, 571-572. (e) Niwa, H.; Inouye, S.; Hirano, T.; Matsuno, T.; Kojima, S.; Kubota, M.; Ohashi, M.; Tsui, F.I. *Proc. Natl. Acad, Sci. USA*, **1996**, *93*, 13617-13622. (f) Oumouch, S.; Bourotte, M.; Schmitt, M.; Bourguignon, J-J. *Synthesis* **2005**, 25-27.

[11] (a) Bhattacharjya, G.; Agasti, S.S.; Ramanathan, G. *ARKIVOC* **2006** (x) 152-161. (b) Yampolsky, I.V; Kislukhin, A.A.; Armatov, T.T.; Shcherbo, D.; Potapov, V.K.; Lukyanov, S.; Lukyanov, K.A. *Bioorg. Chem.* **2008**, *36*, 96-104.

[12] P. E. Ivashkin, I. V. Yampolsky, and K. A. Lukyanov, *Russ. J. Bioorg. Chem.*, **2009**, *35*, 652–669.

[13] (a) Bahadur, L.; Srivastava, P. *Semicond. Sci. Technol.* **2004**, *19*, 531-536. (b) Jain, V.; Rajbongshi, B.K.; Mallajosyula, A.T.; Bhattacharjya, G.; Iyer, S.S.K.; Ramanathan, G. *Solar Energy Mater. Solar Cells*, **2008**, *92*, 1043-1046.

[14] (a) Nienhaus, G.U.; Wiedenmann, J. *ChemPhysChem*. **2009**, *10*, 1369-1379. (b) Ribchester, R.R. *Current Opinion in Pharmacology* **2009**, *9*, 297-305 (c) Bizzarri, R.; Serresi, M.; Luin, S.; Beltram, F. *Anal Bioanal Chem* **2009**, *393*, 1107–1122. (d) Muller-Taubenberger, A.; Anderson, K.I. *Appl. Microbiol. Biotech.* **2007**, *77*, 1-12. (e) Hoffman, R.M. *Nature* **2005**, *5*, 796-806.

[15] Grigg, R.; Kemp, J.; Sheldrick, G.; Trotter, J. *J.C.S. Chem. Commun.* **1978**, 109-111.

[16] (a) Clark, S.J. In "Nitrogen, Oxygen and Sulfur Ylide Chemistry", Clark, S.J. Ed.; Oxford University Press, **2002**, 1-98. (b) Escolano, C.; Duque, M.D.; Vazques, S. *Curr. Org. Chem.* **2007**, *11*, 741-772.

[17] Mangeney, P.; Tejero, T.; Alexakis, A.; Grosjean, F.; Normant, J. *Synthesis* **1988**, 255-257.

[18] (a) Cornforth, J.W.; Cornforth, R.H. *J. Chem. Soc.* **1947**, 96-102. (b) Lerestif, J.M.; Perrocheau, J.; Tonnard, F.; Bazureau, J-P.; Hamelin, J. *Tetrahedron* **1995**, *51*, 6757-6774.

[19] Ivashkin, P. E.; Yampolsky, I. V.; Lukyanov, K. A. *Russ. J. Bioorg. Chem*. **2009**, *35*, 652-669.

CHAPTER 3

UNDERSTANDING THE PHOTOPHYSICS OF FLUORESCENT PROTEIN CHROMOPHORES: INHIBITION OF TWISTING USING METAL COMPLEXATION

Introduction

One of the remarkable features of the Green Fluorescent Protein (**GFP**) is that when the chromophore is removed from the β-barrel by denaturation or by independent synthesis (*p*-hydroxybenzylideneimidazolinone, p-HBDI, Figure 3.1), the fluorescence is almost abolished. This extraordinary 10^4 decrease in fluorescence intensity is noteworthy even among structurally analogous chromophores, e.g., *trans*-stilbene, which show considerable emission quenching in solution associated with an internal conversion mechanism induced by twisting in the excited state, similar to a *Z/E* isomerization pathway. This phenomenon has been put to use in imaging, for instance in stilbene-modified antibodies that exhibit increased fluorescence upon binding,[2] and Katzenellenbogen's use of a stilbene-like analog of diethylstilbestrol,[3] to image estrogen receptors.[4] In this case, the rigidity of the aliphatic rings maintains a higher emission quantum yield as compared to the linear chromophore. Li et al. have used the inhibition of twisting in styryl chromophores as an assay for amyloid plaques.[5] In a similar fashion, Prodhomme et al.[6] and Armitage et al.[7] have developed thiazole orange and related fluorophores as convenient site-specific assays for RNA and DNA through intercalative inhibition of double-bond isomerizations. Such observations provide motivation for the use of the **GFP** chromophore to act as probes. Following these motivations, the idea arises that metal complexation could serve one

pathway to such inhibition.

The nitrogen lone pair of the imidazolidinone provides a basic moiety for interaction with the adjacent ring. One possibility for inhibition of twisting has been

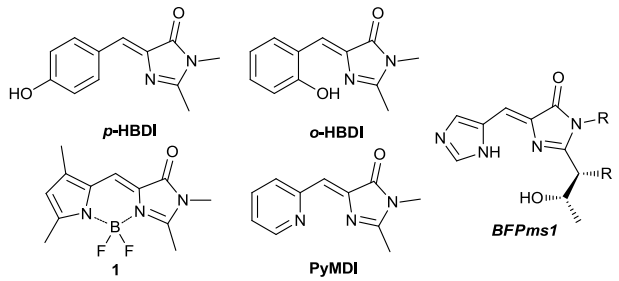

Figure 3.1. GFP synthetic chromophores and the chromophoric moiety of the BFP variant *BFPms1*.[10] For the latter only three out of five binding sites are shown.

reported by Chen et al. through intramolecular hydrogen bonding using, *o*-hydroxybenzylideneimidazolinone (o-HBDI) such that the adjacent hydroxyl group forms a weak hydrogen bond, and further allows for intramolecular excited-state proton transfer.[8] An alternate approach developed by Wu and Burgess involves the use of another Lewis acid, a BF_2 group, to restrain twisting.[9] In this study, the aryl moiety is replaced with by a pyrrole (structure 1, Fig. 3.1), and the conformation becomes irreversibly fixed. In a very elegant way Barondeau et al. synthesized the Blue Fluorescent Protein mutant *BFPms1* (Fig. 3.1) and demonstrated Zn(II) binding by its chromophore.[10] X-ray data revealed the 5-coordinate Zn(II) cite that included the bidentate chromophore, Thr65 and Glu222 moieties, and the water molecule. However, Zn(II) binding increased fluorescence intensity only 2-fold. It was reasoned that replacement of the benzyl moiety in p-HBDI by a 2-pyridyl moiety would provide a bidentate ligand which, upon complexation should result in a fluorescence "turn on", but in a reversible fashion.

Experimental Protocols

Synthesis of PyMDI

The title compound (**PyMDI**) was conveniently obtained in a 76% yield via a Knoevenagel-type condensation of 2-pyridinecarbaldehyde with 1,2-dimethyl-1*H*-imidazol-5(4*H*)-one.[11] The reaction was catalyzed using 3-butyl-1,2-dimethyl-1*H*-imidazol-3-ium hydroxide, a recently developed ionic liquid with literature precedence for use with aldol condensation reactions[12], Michael additions[13] and Knoevenagel condensations.[14] It is critical that the reaction product, (*Z*)-1,2-dimethyl-4-(pyridin-2-ylmethylene)-1*H*-imidazol-5(4*H*)-one immediately be purified, flushed with nitrogen, and stored at 0^{o}C in the dark. For purification, column chromatography on alumina was used with ethyl acetate as the eluent.

Results

The requisite 2-pyridylmethylene-dimethylimidazolinone (**PyMDI**, Fig. 3.1) was conveniently obtained in a 76% yield via a Knoevenagel-type condensation of 2-pyridinecarbaldehyde with 1,2-dimethyl-1*H*-imidazol-5(4*H*)-one.[15] The reaction was catalyzed with 3-butyl-1,2-dimethyl-1*H*-imidazol-3-ium hydroxide, a recently developed ionic liquid with literatature precedence for use with aldol condensation reactions (Fig. 3.2).[16]

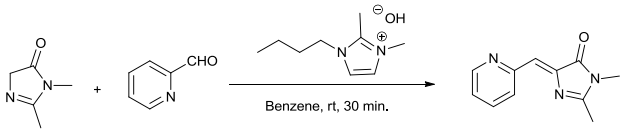

Figure 3.2. Synthetic scheme of **PyMDI.**

The chromophore was readily soluble in methanol/water mixtures at concentrations suitable for fluorimetric analysis. In methanol/water (1/1 vol) solutions, absorption/emission maxima were 344/440 nm. In the absence of metals, the chromophore was very weakly fluorescent (Φ_f<0.001) presumably due to internal conversion caused by *Z/E* photoisomerization.[17,18] This phenomenon is common for the wide array of synthetic analogs of fluorescent proteins chromophores.[19] Upon

treatment of 10^{-5} M solutions of **PyMDI** with a variety of metal salts, either no fluorescene response was observed, the weak fluorescence was quenched, or the fluorescence was significantly enhanced.

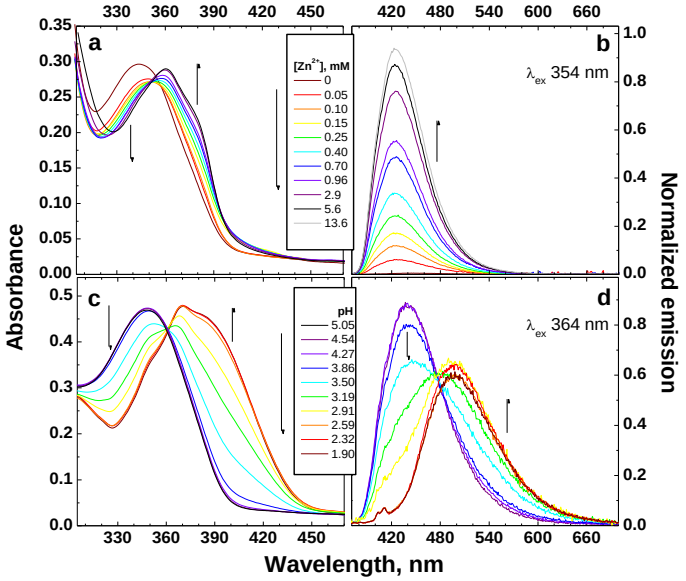

Figure 3.3. Absorption and fluorescence spectra of **PyMDI** in the presence of various concentrations of Zn(II) and hydrogen ions in methanol/water (1/1 vol) solutions.

The increase in fluorescence was particularly dramatic in the presence of Zn(II) salts ($Zn(NO_3)_2 \cdot 6H_2O$ was used, see Fig. 3.3) reaching 150-fold at saturation in the presence of 15 mM zinc ions. A similiar but less dramatic response was noted for Cd(II) salts as well. Analysis of Zn(II) binding using the Job plot and Benesi-Hildebrand methods resulted in a 1:1 metal/ligand stochiometry,[16] with an **Zn-PyMDI** formation constant (K_f) of 1900 M^{-1}, the absorption/emission maxima of the complex were 360/424 nm,with a lifetime of 1.3 ns.

Stoichiometry of Zn(II) binding to PyMDI in solution.

The stoichiometry of complexation in solution was determined using a Job plot according to method described in Ref [20]. Referring to Fig. 3.4, the maximum occurs at a mole fraction of 0.5, implying a 1:1 complex. Given a 1:1 stoichiometry, a Benesi-Hildebrand plot can be created to determine the binding constant of the

complex. It should be noted that Benesi-Hildebrand plots are only applicable to 1:1 complexes. The Benesi-Hildebrand equation for fluorescence spectroscopy is given by:[21] $1/(I-I_0) = 1/(I_1-I_0) + 1/(K_f (I_1-I_0))$ x $1/[Zn^{2+}]$ where I_0 is the emission intensity of

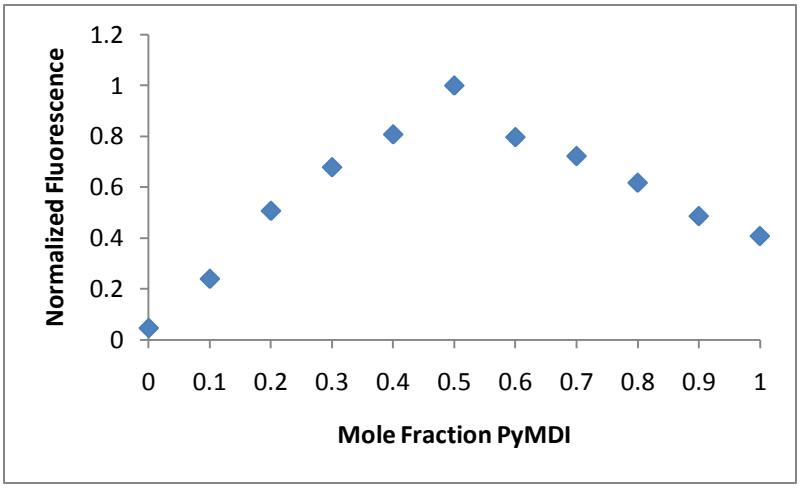

Figure 3.4. Job plot of PyMDI with Zn^{2+} showing 1:1 binding.

a free ligand, and **PyMDI** is the emission intensity of the complex at some Zn(II) concentration. Additionally, it is noted that the Benesi-Hildebrand plot confirms the assumptions made from the Job plot with respect to the 1:1 stoichiometric

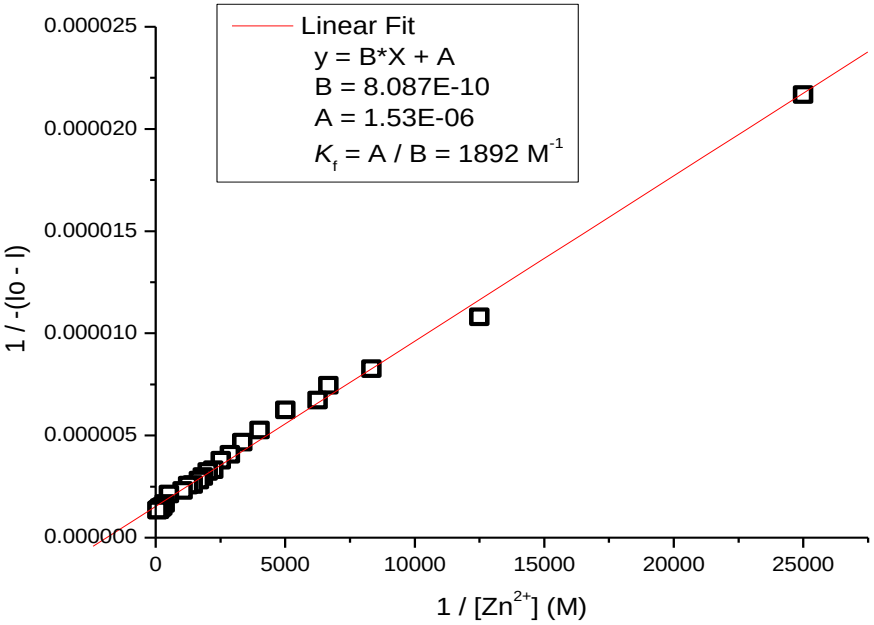

Figure 3.5. Benesi-Hildebrand plot for titration of **PyMDI** with Zn^{2+} in solution.

relationship. The Benesi-Hildebrand plot in Fig. 3.5 (shown below) yields an R^2 = 0.997 and gives a binding constant for Zn(PyMDI) of 1892 M^{-1}.

Metal cation binding

The response to Zn (II) and Cd (II), and to a smaller extent Pb(II), is consistent with the Irving-Williams order[22] (see Fig. 3.6). This order is derived from the K_f of the M^{2+} ions of the 3d transition metals that show an increase in log K_f values across the periodic row regardless of the ligand. The general case is that an increase in stability correlates with ionic radius, suggesting an electrostatic effect.[23]

Both Cd(II) and Zn(II), as d^{10}-s^0 metals, have no mechanism for facile spin-orbit coupling. In contrast, both Fe(III) and Cu(II), as high-spin metals, readily

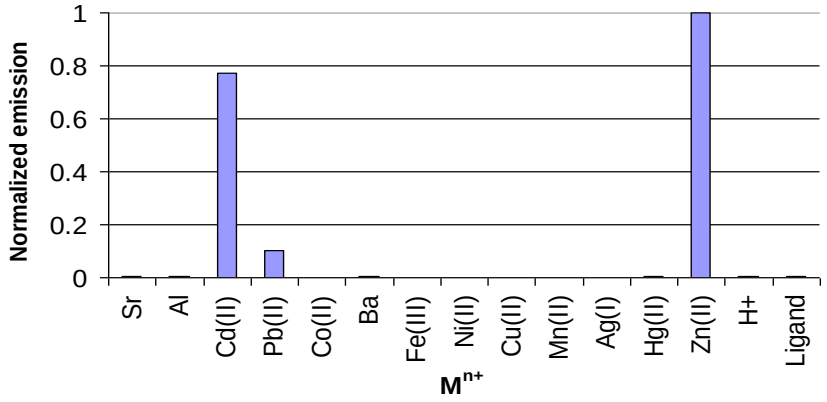

Figure 3.6. Fluorescence response of **PyMDI** in 15 mM methanol/water (1/1 vol) solutions of protons and various salts.

facilitate rapid internal conversion, while the other metals have relatively little effect. Unfortunately, the salts of Cu(I), which is isoelectronic to Cd(II) and Zn(II), had very poor solubility in water and aqueous methanol, thus no reliable data could be obtained for cuprous salt solutions.

From its structure, **PyMDI** is readily classified as a fluorescent ligand. Such compounds are marked by an aromatic or heterocyclic ring with functional groups that can act as metal-chelating sites. These sites can function as both the binding and signaling site within the sensor. Numerous examples of this class of ligands exist and

include bipyridyls, hydroxyquinolines, and Schiff bases, with many of these acting as bidentate ligands. In a review by Rurack,[24] it is noted that ligands within this classification have high selectivity toward Zn^{2+} or Hg^{2+} depending upon a number of factors, especially the binding site and functional groups present. The selectivity toward Zn^{2+} for a number of ligands within this class is also attributed to the Irving-Williams order. The marked decrease in fluorescence intensity of Cd(II) and Pb(II) compared to Zn(II) can be rationalized by the heavy-atom effect.[25] It is important to note that similar fluorescent responses were noted by Fahrni et al. with respect to Zn(II) and Cd(II), which provided a fluorescence turn-on of benzimidazole derivatives for use as ratiometric probes.[26] The dissociation constant of **Zn-PyMDI** complex ($K_d = 1/K_f$) is more than two orders of magnitude smaller that in Zn(II) complexes with bipyridyl and phenanthroline derivatives.[27]

Crystallography of complex

By combining a stoichiometric amounts of **PyMDI** and $Zn(NO_3)_2 \cdot (H_2O)_6$ in methanol, it was possible to isolated a crystalline product whose X-ray structure is represented in Fig. 3.7. Curiously, this slightly deformed hexacoordinated bidentate complex involves *two* **PyMDI** molecules coordinated with zinc virtually orthogonally with a nitrate ion chelating zinc via its two oxygen atoms. There is no solvent (or water) present in the coordination sphere of zinc. Instead, a single molecule of methanol and two nitarte ions for charge compensation are found in the unit cell, composed of two **Zn-PyMDI** complex molecules which are placed outside the coordination sphere of zinc ions. We attribute the double coordination to the higher concentrations of ligand obtained under crystallizing conditions.

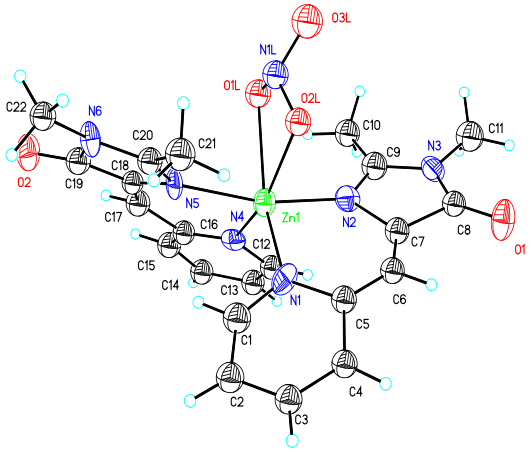

Figure 3.7. Molecular structure of **PyMDI** zinc complex. ORTEP image with 35 % probability ellipsoids.

pH studies

Both metallo- and prototropic responces of **PyMDI** were studied. Upon pH decrease from 6 to 1, the bathochromic shifts of both absorption and emission maxima were observed resulting in the formation of a monocation with absorption/emission maxima at 370/497 nm. Most probably the pyridine moiety of **PyMDI** is protonated first since the observed pK_a is very close to that of some 2-vinylpyridines.[28] Lowering the pH of solutions of **PyMDI** did *not* yield an increase in the fluorescence intensity, which would be expected if the hydrogen bridged the two nitrogens and hindered cis/trans isomerizations, as noted for Zn(II) and Cd(II), or the mechanism of fluorescence quenching would be based on the photoinduced electron transfer. Titration curves derived from the absorption and the emission spectra were identical within experimental errors and resulted in a pK_a of 3.3.[16] Such similiarity demonstrates an absence of an enhanced *adiabatic* photobasicity for **PyMDI**. We also have checked the dependence of **PyMDI** fluorescence on water concentration in methanol/water mixtures. In all cases only the emission from the neutral species was observed.[16] Its intensity decreased as the water concentration increased, due to an unestablished quenching mechanism. The chemical structure of **PyMDI** assumes no acid-base transitions at pH > 6. Nevertheless, upon pH increase from 6 to 10, a

hypsochromic shift of the absorption maximum as well as strong fluorescence quenching was observed.[16] These spectral evolutions were irreversible and are attributed to hydrolysis of the imidazolidinone ring.

It is also worthy to note an amazing similarity between the pK_a and pK_d values! Such a relationship between the basicity of ligands and stability of chelates is a known phenomenon and was observed for several Zn complexes with bidentate ligands.[27] We have checked the stability of the **Zn-PyMDI** complex at different pH. Upon a pH decrease the fluorescence was quenched, and the absorbance peak transformed from that of **Zn-PyMDI** into the monocation **H-PyMDI**.[16] This observation demonstrates rather weak pH-stability of the complex.

Conclusions

The observations noted within this work show the importance of inhibition of conformational freedom toward the EQY of AMI chromophore derivatives. While a two-order of magnitude enhancement was achieved it is noted that additional photophysical mechanisms as well as a twisted complex do not allow for complete restoration of the EQY. The sensitivity of **PyMDI** to Zn in methanol/water is remarkable, given that no attempt was made to optimize the association constant. The use of additional complexing ligands, or, alternatively, unnatural amino acids such as azaphenylalanine to create zinc-sensitive derivatives of the green fluorescent protein, promises great potential in the optimization of sensors bases upon inhibition of the cis/trans (or *Z/E*) isomerizations of such chromophores. A similar, but indirect approach, has been developed recently by Mizuno et al.[29] The **GFP**-based protein was demonstrated to fold into the trimeric coil (rigid β-barrel) structure only in the presence of different metal ions. As a result, the embedded fluorophore lost its flexibility and regained fluorescence. Similarly, Fierke developed a Zn sensor with pM sensitivity based upon the known affinity of carbonic anhydrase for Zn.[30] A wide

variety of Zn-sensing proteins[31] may serve as a molecular background for the ligand structure optimization. Whether increased Zn sensitivity can be produced within such optimization is the subject of current research.

References

[1] Baldridge, A.; Solntsev, K.M.; Song, C.; Tanioka, T.; Kowalik, J.; Hardcastle, K.; Tolbert, L.M. *Chem. Comm.* **2010**, *46(31)*, 5686-5688.

[2] (a) A. Simeonov, et al. *Science* 2000, **290**, 307-313. But see also (b) E. W. Debler, G. F. Kaufmann, M. M. Meijler, A. Heine, J. M. Mee, G. Pljevaljcic, A. J. Di Bilio, P. G. Schultz, D. P. Millar, K. D. Janda, I. A. Wilson, H. B. Gray and R. A. Lerner, *Science* 2008, **319**, 1232-1235.

[3] T. D. Doyle, W. R. Benson, and N. Filipescu, N. *J. Am. Chem. Soc*. 1976, **98**, 3262-3267.

[4] (a) R. J. Miksicek and J. A. Katzenellenbogen, *NATO ASI Ser., A: Life Sci*. 1996, **286**, 213-219. (b) Y. Dobrydneva, R. L. Williams, J. A. Katzenellenbogen, P. H. Ratz and P. F. Blackmore, *Thromb. Res*. 2003, **110**, 23-31.

[5] Q. Li, J. Min, Y.-H. Ahn, J. Namm, E. M. Kim, R. Lui, H. Y. Kim, Y. Ji, H. Wu, T. Winsniewski and Y.-T. Chang, *ChemBioChem* 2007, **8**, 1679-1687.

[6] S. Prodhomme, J. P. Demaret, S. Vinogradov, U. Asseline, L. Morin-Allory and P. Vigny, *J. Photochem. Photobiol. B* 1999, **53**, 60–69.

[7] (a) B. A. Armitage and P. B. Berget, *Science* **2008**, *319*, 1195-1196. (b) G. L. Silva, V. Ediz, D. Yaron and B. A. Armitage, *J. Am. Chem. Soc*. 2007, **129**, 5710-5718. (c) T. P. Constantin, G. L. Silva, K. L. Robertson, T. P. Hamilton, K. Fague, A. S. Waggoner and B. A. Armitage, *Org. Lett.* 2008, **10**, 1561-1564.

[8] K.-Yu. Chen, Y.-M. Cheng, C.-H. Lai, C.-C. Hsu, M.-L. Ho, G.-H. Lee and P.-T. Chou, *J. Am. Chem. Soc.* 2007, **129**, 4534-4535.

[9] L. Wu and K. Burgess, *J. Am. Chem. Soc.* 2008, **130**, 4089-4096.

[10] D. P. Barondeau, C. J. Kassmann, J. A. Tainer and E. D. Getzoff, *J. Am. Chem. Soc*. 2002, **124**, 3522-3524.

[11] The 1,2-dimethyl-1*H*-imidazol-5(4H)-one was synthesized according to Wu, L.; Burgess, K. *J. Am. Chem. Soc.* **2008**, *130*, 4089-4096.

[12] Mehnert, C.P.; Dispenziere, N.C.; Cook, R.A. *Chem. Commun.* **2002**, 1610-1611.

[13] Ranu, B.C.; Banerjee, S. *Org. Lett.* **2005**, *7*, 3049-3052.

[14] Ranu, B.C.; Jana, R. *Eur. J. Org. Chem.* **2006**, 3767-3770.

[15] The 1,2-dimethyl-1*H*-imidazol-5(4H)-one was synthesized according to Ref. 8.

[16] Details noted in experimental section.

[17] N. M. Webber, K. L. Litvinenko and S. R. Meech, *J. Phys. Chem. B* 2001, **105**, 8036–8039.

[18] The fluorescence quantum yield was about one order of magnitude larger than that of *p*-HBDI. An analysis of the prototropic behavior and ultrafast kinetics involving possible *diabatic* photoinduced proton transfer will be reported in a full paper.

[19] (a) K. M. Solntsev, O. Poizat, J. Dong, J.; Rehault, Y. Lou, C. Burda and L. M. Tolbert, *J. Phys. Chem. B* 2008, **112**, 2700-2711. (b) S. R. Meech, *Chem. Soc. Rev*. 2009, **38**, 2922-2934. (c) I. Petkova, G. Dobrikov, N. Banerji, G. Duvanel, R. Perez, V. Dimitrov, P. Nikolov and E. Vauthey, *J. Phys. Chem. A* 2010, **114**, 10–20.

[20] MacCarthy, P. *Anal*. *Chem*. **1978**, *50*, 2165-2166.

[21] Galan, M.; Carmona, C.; Guardado, P.; Munoz, M.A.; Balon, M. *J. Photochem. Photobiol. A* **2002**, *147*, 103-108.

[22] H. Irving and D. H. Mellor, *J. Chem. Soc.* 1962, 5222-5237.

[23] D. F. Shriver and P. Atkins, *Inorganic Chemistry: 4th ed.* Freeman and Co., New York, 2006.

[24] K. Rurack, *Spectrochim. Acta A* 2001, **57**, 2161-2195.

[25] A. W. Varnes, R. B. Dodson and E. L. Wehry, *J. Am. Chem. Soc.* 1972, **94**, 946-950.

[26] M. M. Henary, Y. Wu and C. Fahrni, *Chem. Eur. J.* 2004, **10**, 3015-3025.

[27] (a) M. Calvin and K. W. Wilson, *J. Am. Chem. Soc*. 1945, **67**, 2003-2007. (b) M. Yasuda, K. Sone and K. Yamasaki, *J. Phys. Chem*. 1956, **60**, 1667-1668.

[28] A. Ballistreri, L. Gregoli, G. Musumarra and A. Spalletti, *Tetrahedron* 1998, **54**, 9721-9730.

[29] T. Mizuno, K. Murao, Y. Tanabe, M. Oda and T. Tanaka, *J. Am. Chem. Soc.* 2007, **129**, 11378-11383.

[30] R. A. Bozym, R. B. Thompson, A. K. Stoddard and C. A. Fierke, *ACS Chem. Biol.* 2006, **1**, 103-111.

[31] Maret, W. and Li, Y. *Chem. Rev*. 2009, **109**, 4682–4707.

CHAPTER 4

PHOTOCHEMISTRY OF GREEN FLUORESCENT-LIKE PROTEIN CHROMOPHORES IN THE SOLID STATE

This work was carried out in collaboration with the laboratory of Dr. Pance Naumov at the Department of Material and Life Science, Graduate School of Engineering at Osaka University in Japan. All compounds were synthesized, characterized, and optical characterized within the Tolbert lab while all the crystallographic data and experiments were done in the Naumov laboratory. Data analysis and manuscript composition was equally shared.

Introduction

Fluorescence from the green fluorescent chromophore (GFP) and its derivatives is characterized by a complex ensemble of photophysical phenomena which allow the fluorescence to occur with high quantum yield only within the confines of the protective β-barrel, which inhibits otherwise facile decay pathways. In other environments, including other proteins, fluorescence is in competition with a host of decay pathways, which have been explored by independent synthesis of the chromophores and examination of the photophysics in solution,[2] at low temperature,[3] in the gas-phase,[4] at high pressure,[5] in host-guest complexes,[6] and in the solid state.[7] Of these environments, the environment most analogous to the β-barrel is arguably the solid state. A consistent theme to these studies has been the intervention of twisting modes, both involving the formal double bond and leading to double-bond isomerization and/or the single bond between that bond and the aryl group. Notwithstanding the strong role of the β-barrel in

providing a strong restoring force, preventing both facile internal conversion via twisting and double-bond [*trans* (*E*) → *cis* (*Z*)] isomerization, proteins which undergo such isomerization ("photoswitching proteins")[8] are now increasingly evident. Concerns about such restraining forces have led to widespread acceptance of the volume-conserving "hula twist",[9] which incorporates simultaneous twisting about dihedral angles τ and φ in the excited-state. This "least-motion" scenario, in order to maintain both aromatic rings in plane, would produce an initial conformer with any *ortho* or *meta* substituents in a *syn* relationship,[10] as opposed to the *anti* relationship in the "one-bond flip" process (see Scheme 1). Thus we have undertaken a study of such isomerization in the solid state, using derivatives which perturb crystal packing in rationalizable ways. As a result of these investigations, we now report a variety of direct photochemical consequences from the crystal packing, including a remarkable photomechanical effect of the benzylidenedimethylimidazolinone (BDI) chromophores, and additional insight into the possible intervention of the hula twist.

We began these studies with derivatives of the parent chromophore, *p*-hydroxybenzylidenedimethylimidazolinone (**4-HOBDI**).[7] We found that fluorescence "turn-on" occurred in the solid-state for *O*-alkyl derivatives which were almost completely non-fluorescent in solutions. Steady-state and time-resolved emission spectroscopy, as well as X-ray diffraction analysis, revealed the nature of complex emission in the crystals, including the fluorescence of monomers and aggregates. The size of *O*-alkyl substituents played a dramatic role in color tuning of crystalline luminescence. With the increase of alkyl group from methyl to hexyl to dodecyl, the interaction between the aromatic molecules in the lattice became weaker, resulting in a

hypsochromic shift in the apparent emission from the crystals. No emission was observed from the unsubstituted hydroxyl derivative, which, unlike the others, was characterized by hydrogen bonding between phenolic OH and the imidazolone carbonyl group. However, none of these molecules exhibited any permanent photochemistry in the solid state, nor could *para* substituents distinguish between the one-bond flip and hula twist processes. In order to further characterize their photophysics, therefore, we undertook a study of molecules for which substituents at the *ortho* and *meta* positions would provide additional stereochemical tags, allowing us to establish whether aryl rotation, at least, was a component of the solid-state chemistry and thus provide direct insight into the hula twist mechanism.

Experimental Section

Photolysis and product analysis

A sample of **3-HOBDI** (ca. 80 mg) was spread thin between glass plates and exposed to irradiation from a Hanovia Hg lamp for 1.5 h followed by flipping the plate and continuing irradiation for another 1.5 h. The powder was collected and acetone was used to remove the remaining starting material (4 times). The remaining white solid was allowed to dry on the frit funnel and used for spectroscopy. The yield was ~ 50% (no attempts were made to maximizing the yield of the product).

Spectroscopy

Ultraviolet-visible absorption spectra were recorded on a Perkin Elmer Lambda19 spectrophotometer. Measurements of solid-state photoluminescence were carried out using the front face emission scan mode on a Jobin-Yvon FluoroLog-3 spectrofluorimeter. The entrance/exit slits of the monochromators were adjusted to the

proper fluorescence intensity of each sample. Crystalline powder samples were placed between the quartz plates. Fluorescence lifetimes were measured using an Edinburgh Instruments time-correlated single photon counting (TCSPC) system. In this measurement, two picosecond excitation pulses diode lasers (LDH-P-C-375 and LDH-P-C470) with different wavelengths (372 nm and 478 nm) were used as excitation light sources. The detection system consisted of a high speed MicroChannel Plate PhotoMultiplier Tube (MCP-PMT, Hamamatsu R3809U-50) and TCSPC electronics.

Atomic force microscopy

In order to more fully characterize the nature of the phototransformation of the **3-HOBDI** crystals, we examined the AFM images of the crystals before and after irradiation. The AFM imaging was completed on a single crystal of **3-HOBDI**-A. For imaging, the crystal was mounted flat on its largest surface using carbon tape on silicon wafer in such a way that part of the crystal was immobilized on the tape while the remaining part was not attached, which allowed for unrestricted movement (a schematic of this assembly is shown in Figure 4.1). The crystal mounting process was done with limited ambient light; however ambient light was not entirely eliminated. From this, preexisting conditions cannot be rigorously excluded. The crystal was irradiated using a Pyrex-filtered Hanovia medium pressure 450 W Hg lamp for 15 minutes and subjected to AFM analysis. Both segments of the crystal (attached and non-attached) were analyzed. Atomic force microscopy imaging was performed with a model 5500 AFM from Agilent Technologies (Chandler, AZ). The 5500 AFM operates in a "top-down" configuration with the AFM probe mounted on the piezo-scanner for imaging of the sample surface. The AFM was placed in a vibration isolation chamber (Agilent Technologies, Chandler,

AZ), and additionally in a Faraday cage in order to reduce environmental vibration and electromagnetic noise. AFM images were post-processed with the PicoScan 5.3.3 software (Agilent Technologies, Chandler, AZ) for tilt correction or flattening of the image background. For the imaging, Dynamic mode AFM technique was employed. In this technique, the cantilever is oscillated at a certain resonant frequency and amplitude damping as a result of repulsive tip-sample interaction is monitored. This reduces frictional forces at the sample surface due to the intermittent contact of the tip.

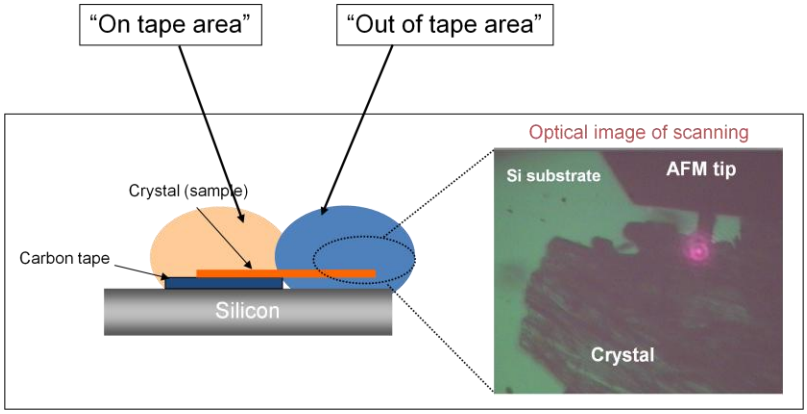

Figure 4.1. Schematic of the setup for AFM analysis of **3-HOBDI**-A (left) and optical image of the scanning (right).

Polymorph screening and X-ray diffraction

Extensive screening of the BDIs from fifteen common organic solvents was undertaken to check the existence of polymorphs and solvates. The identity of the crystals from different batches was checked by comparison of the cell parameters obtained from limited number of reflections. The samples for X-ray diffraction analysis were prepared by slow evaporation from hexane or ethanol solutions, which always afforded samples of best crystallinity. Except for **3-HOBDI**-A, which always crystallized as very slender long crystals, all BDIs appear as large prismatic or blocky crystals. If exposed to room light for a week, some of the crystals (most notably, **3-HOBDI**-A and **2-FBDI**) tend to deform

and turn opaque. Therefore, all recrystallized samples were manipulated and stored in the dark (see below), under faint light or red safelight (λ > 660 nm), including the X-ray measurements.

The X-ray diffraction data were collected in ω-scan mode at room temperature with APEX2 diffractometer (Bruker AXS),[39] using MoKα X-rays obtained from a rotating anode source, a confocal multilayer X-ray mirror as monochromator and CCD area detector. The integrated and scaled[39] data were empirically corrected for absorption effects with SADABS.[40] The structures were solved by using direct methods[41] and refined on F_{obs} with SHELXL.[42] All non-hydrogen atoms were assigned anisotropic displacement parameters. The aromatic protons were set as riding bodies, and the methyl hydrogen atoms were placed at calculated positions, with their rotational angles refined from the electron density. The protons in the hydroxyl groups were kept at calculated distances, but their rotation angles were refined. The crystals of **3-HOBDI**-A are extremely slender (the one used for X-ray diffraction was thick only 10 μm) and tend to curve slightly during the crystallization process (see Figure 4.4), even when it is conducted in dark and at lowered temperature, which is why the structure could be refined only to R_1 = 7.14%. Although not optimal, this accuracy was considered sufficient for the purpose of analysis of the molecular structure and intermolecular interactions topology. The photoreaction of **3-HOBDI**-A is a homogeneous solid-state process,[43] and proceeds simultaneously with the bending throughout any part of the crystals that had been exposed to UV light. Therefore, although that the resulting crystal still diffracted as one component, its diffraction pattern was inevitably distorted, which ultimately prevented us from structure determination of the product. The gradual distortion of the

diffraction picture was an expected consequence of the continuous progression of the reaction throughout the crystal, although the crystal integrity was preserved. The crystals of **2-FBDI** were refined from a twinned crystal; the twinning was explicitly accounted for in the refinement. Both methyl groups at the imidazole ring of **3-MOBDI** are rotationally disordered, and thus they were included in the model with two positions of equal occupancy. The structure of the partially reacted **3-HOBDI**-C was refined by using several limitations, including constraints (± 0.2 Å) on the C8′—N12′ (1.400 Å), N10′—C9′ (1.340 Å) and C9′—O16′ (1.250 Å) bonds. Soft restraint was applied to keep the imidazolone ring atoms of the product flat, and two pairs of atoms were restrained to have similar displacement parameters. The effect on the changes in the crystal color observed by UV irradiation depended on the sample (**2,5-DMBDI** and **4-HOBDI** turn yellow, while **2-FBDI** turns opaque). The attempts to resolve the structure of the photoinduced dimer created in single crystals of the BDIs were not successful, because the crystallinity specimens decreased upon exposure to UV light, as it became evident from the diffraction pattern of **2,5-DMBDI**.

Results

Synthesis, characterization and crystallization

Over fifteen BDI chromophores were synthesized according to our previously published protocols.[2d,4b,7] The crystal structures of six representative compounds were determined by single crystal X-ray diffraction (Figure 4.3). One of these, **3-HOBDI**, produced four polymorphs, three of which were completely structurally characterized and are labeled A, B, and C.[11] Form A (**3-HOBDI-**A) has the most distinctive crystal structure, with crystal

packing characterized by linear chains of molecules connected by strong hydrogen bonds between the phenolic OH and adjacent imidazolone carbonyls. Photoisomerization of such a supramolecular structure, if done in a single-crystal-to-single-crystal fashion, should favor the intervention of a hula twist in order to maintain the hydrogen-bonding network. We were gratified and surprised to see, not just a photochemical transformation, but a dramatic photomechanical effect, with rod-like crystals bending upon exposure at angles up to more than 90^{o} without breaking.

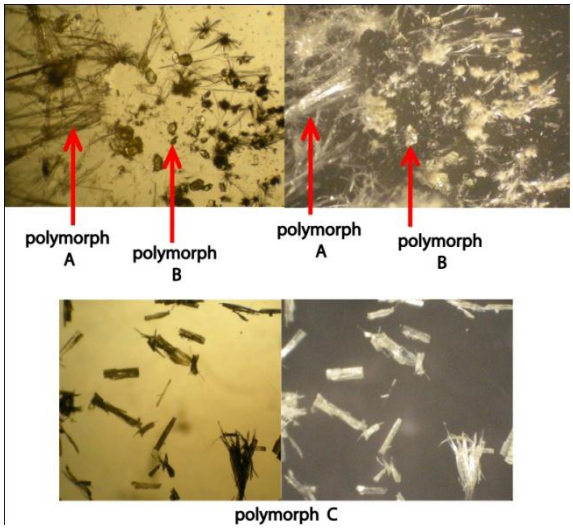

Figure 4.2. Micrographs of crystals of the three polymorphs of 3-HOBDI recorded in transmission and in reflection mode.

Of the remaining crystals, four (the other two polymorphs of **3-HOBDI**, **2-FBDI** and **2,5-DMBDI**, see Chart 1) underwent photoreactions with complete conversion to stable products within minutes, in yields sufficient for NMR characterization. Notably, such photoreactions were accompanied by readily observable photobleaching of the yellow crystals, a phenomenon we had observed occasionally but not previously investigated.

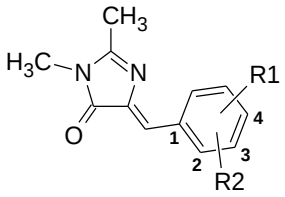

R1	R2	Label	#(CCDC)
3-OH	H	**3-HOBDI**-A[a]	CCDC #761072
3-OCH_3	H	**3-MOBDI**	CCDC #761075
2-F	H	**2-FBDI**	CCDC #761068
2-CH_3	H	**2-MeBDI**	CCDC #761069
2-CH_3	5-CH_3	**2,5-DMBDI**	CCDC #761071
2-CH_3	4-CH_3	**2,4-DMBDI**	CCDC #761070

[a]Polymorphs: CCDC #761073 (form B), CCDC #761074 (form C)

Figure 4.3. Chemical structures and Cambridge Structure Database reference numbers of the respective crystallographic data of the six model GFP fluorophores.

Photomechanical effects in 3-HOBDI-A crystals

A 0.70 × 0.04 × 0.01 mm single crystal of **3-HOBDI**-A was mounted at one end on a glass rod with epoxy adhesive (Araldite) and exposed to very weak (< 1 $mW \cdot cm^{-2}$), unfocused, heat-filtered UV light (λ_{max} = 365 nm, with minor contribution from the 313 nm line) from a 250 W medium-pressure Hg lamp (SP-7, Ushio). On flashing by UV light (0.1 s), the slender, long crystals of **3-HOBDI**-A underwent a dramatic deformation: the crystals *bent* along their longest axis to > 90^o without breaking (see Figure 4.4 and Movie S1 in the SI). As shown in panels b–d of Figure 4.4, because the crystal curved only during excitation, the angle at the curvature could be controlled by varying the exposure time. At weak excitation power density, the crystal bending ceased in absence of excitation. After more than a minute of continuous or discontinuous irradiation, the crystal had curved more than 90^o, before it started to twist due to bending along the second largest axis, until a fracture appeared at the kink and normal to the longest axis (see panels f–g in Figure 4.4). If flashed or continuously irradiated with stronger UV light (> 5 $mW \cdot cm^{-2}$), non-fixed crystals showed a readily observable photosalient effect: they jumped a few millimeters as a result of acute lattice distortion. This photomechanical effect was observed during a few seconds even after the excitation had been terminated,

probably due to latent release of the accumulated structural stress in the crystal lattice. The deformation was plastic, so that the original shape of the crystals was not restored, even after they had been aged in the dark. None of the crystals of the other compounds exhibited similar photomechanical behavior, but thicker crystals of **3-HOBDI**-B, **3-HOBDI**-C, **2-FBDI** and **2,5-DMBDI**, as well as of the 4-hydroxy derivative, **4-HOBDI** (analogous to the real GFP emitter), tended to crack perpendicular to the longest axis after long-term exposure to UV light.

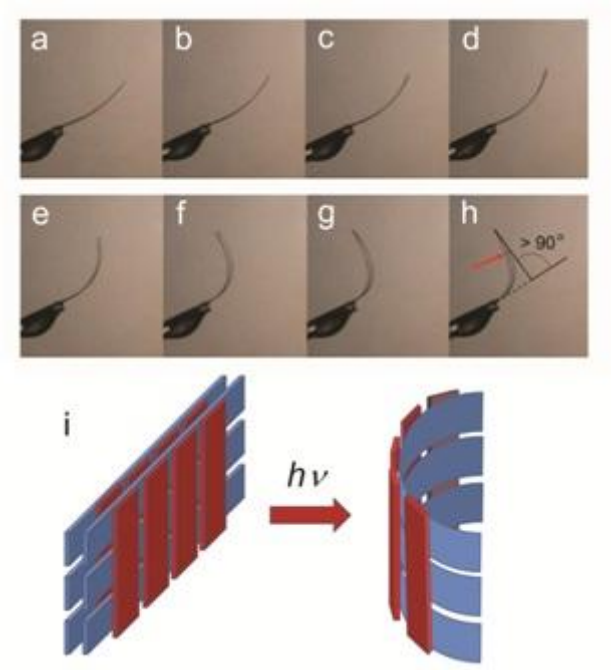

Figure 4.4. (a–h) Photomechanical effects of the single crystal of **3-HOBDI** exposed to unfocused weak UV light (left) and (i) schematic of the suggested mechanism. The panels b–h show the deformation caused by consecutive exposure (each of b–d corresponds to consecutive 0.1-s flash). Comparison of the panels f and g shows the twisting of the crystal that appears as a result of bending along the smaller axis, after the maximal bending has been reached along the longest axis (the fracture is arrowed in panel h). The perpendicular hydrogen-bonded tapes in the structure are represented schematically in panel i by red and blue ribbons.

UV irradiation (< 300 nm, Pyrex-filtered medium pressure 450 W Hg lamp) led to complete quenching of the weak emission of **3-HOBDI**-A at λ^{em} = 440 nm. Upon several

30 s-exposures to weak polychromatic UV light (250 W Hg lamp), the IR spectra of powders of **3-HOBDI** (all three structurally characterized polymorphs), **2-FBDI**, **2,5-DMBDI** and **4-HOBDI** dispersed in KBr showed drastic changes due to gradual and complete conversion to photostable products (Figure 4.5), while the other three compounds remained nonreactive. Most characteristic were the blueshifts of the ν(CO) and of ν(OH) modes (in the case of 3-**HOBDI** and **4-HOBDI**): typically, for **3-HOBDI**-A the respective values were $\Delta\tilde{\nu}$ = 17 and 125 cm^{-1}. The reaction of **2-FBDI**

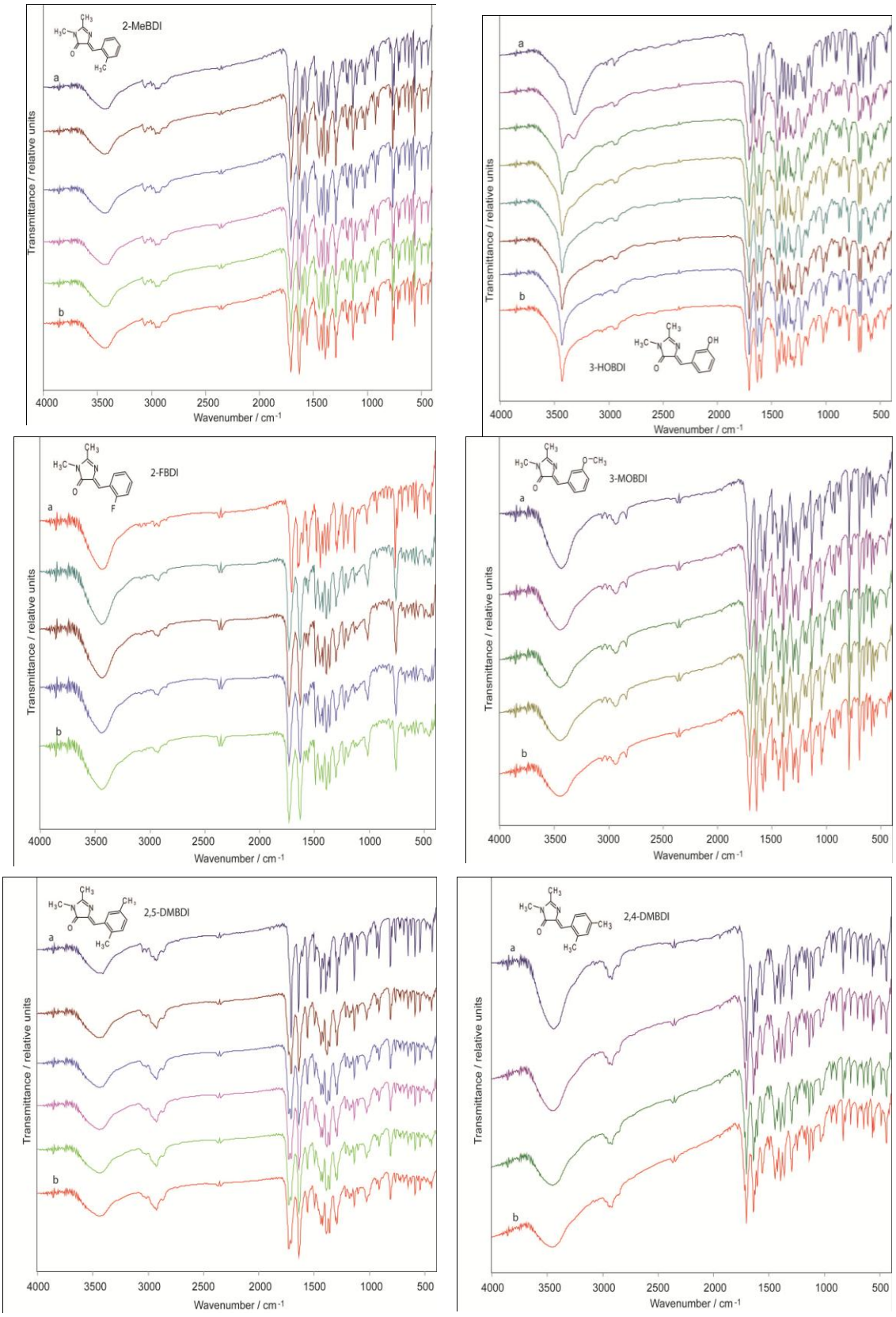

Figure 4.5. Effects of UV excitation on the IR spectrum of the six compounds tested. The irradiation time increases going down the spectrum with (a) representing t = 0 s.

and **2,5-DMBDI** was more rapid relative to **3-HOBDI** and was completed within a minute. The photoreactivity was confirmed by ^{1}H NMR spectra recorded in solid state and in solution, and could be also visually observed as bleaching of excited powdered samples. The reaction product from **3-HOBDI** was purified by removing the soluble starting material with multiple acetone washes. The NMR spectra clearly showed differences between the starting material and the product. Most pronounced was the loss of the vinyl double bond, along with appearance of a new two-proton singlet at 4.4 ppm. The signals due to the imidazolone ring were present and slightly shifted from their positions in the starting material. There was no change in the total number of protons in the product compared to the starting material. The ^{13}C NMR spectrum indicated a total disappearance of the vinyl carbon atoms, and showed the presence of the imidazolone carbon atoms in addition to the appearance of two new signals, at approximately 53 ppm and 73 ppm. The total number of distinct carbon atoms remained the same as in the starting material. The mass spectrum of the pure product showed a molecular ion signal at 432 (M^+) and a fragmentation peak at 216 ($M^+/2$), which strongly suggested a dimer fragmenting in half across two C—C bonds. Symmetrical [2+2] photodimers of unsaturated compounds have been well characterized as containing either mirror symmetry (C_s) or two-fold symmetry ($C2$). In retrospect, we now recognize that several of these derivatives showed the presence of "impurities" in purified samples, a phenomenon we can now attribute to the photodimerization and which serves as a caution when handling such compounds in the solid state. On the basis of the NMR spectrum, we believe that the homodimer of **3-HOBDI** was the two-fold symmetric *trans,trans* species (see Scheme 3), although we must concede that we cannot exclude other symmetric

dimers. The remaining photoactive derivatives yielded analogous products, in all cases, again yielding, presumably, the *C*2-symmetric photodimer.[12]

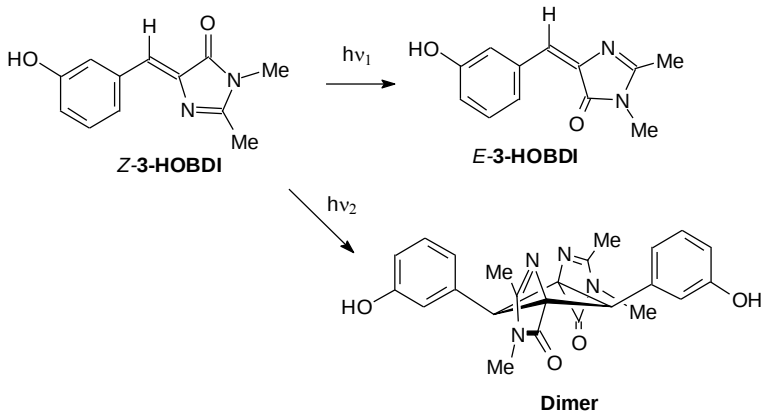

Figure 4.6. Products of irradiating **3-HOBDI** in solution and in the solid state.

Crystal Structures of the BDIs

Polymorph/solvate screening of the six BDIs in Chart 1 afforded four polymorphs of the *m*-hydroxy compound (**3-HOBDI**-A, -B, –C and -D), three of which were characterized, and a single form of each of the other compounds. None of the eight crystal structures characterized by X-ray diffraction analysis included solvent, as expected from the flatness of the BDI molecules and their close packing provided by the molecular stacking (Figure 4.7). The molecular shape varied from flat (the angle between the two rings is 1.52(11)^{o} in **2,4-DMBDI** and 1.74(2)^{o} in **2-FBDI**) to slightly bent (in the case of **3-HOBDI**-B, 8.49(27) and 8.90(24)^{o}, and **2,5-DMBDI**, 7.86(10)^{o}), so that some of the molecules appeared bow-shaped. The substituents at the phenyl ring did not appear to have significant effect on the intramolecular distances, so that the bridging double

bond (1.340(7) – 1.350(8) Å) and single bond (1.450(2) – 1.462(7) Å) remained essentially constant over all electron-donor and acceptor substituents. Although the free rotation of the phenyl ring around its axis indicates that both *syn* and *anti* isomers can exist for each of the non-symmetrically substituted compounds, in all cases where the phenyl ring is substituted with a group which is devoid of acidic proton (**2-MeBDI**, **2-FBDI**, **3-MOBDI**, **2,5-DMBDI**, **2,4-DMBDI**), the proximate (*ortho* or *meta*) phenyl substituent in the crystals is juxtaposed *anti* in respect to the *ortho*-nitrogen of the imidazole ring. The preferred *anti* orientation is determined by the fact that it leaves the

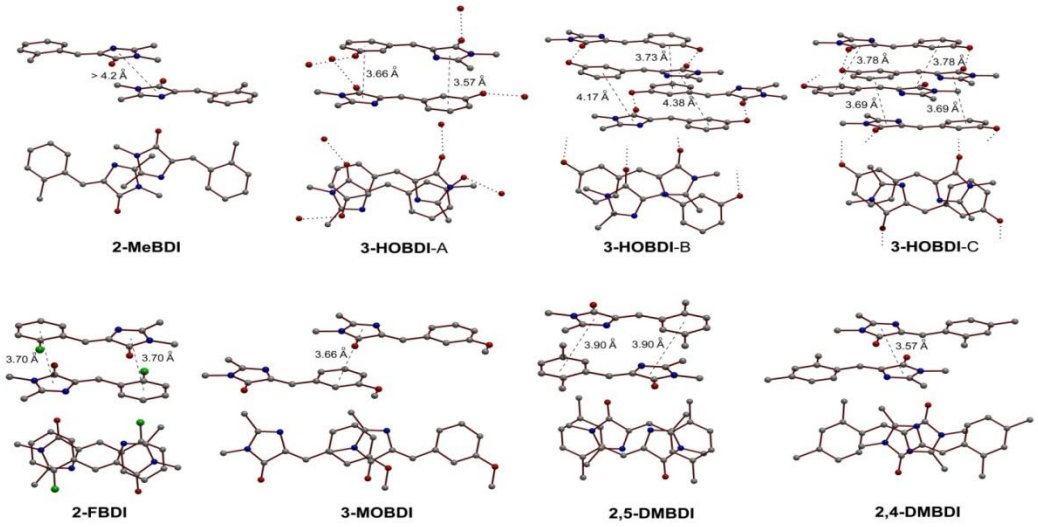

Figure 4.7. Packing in the crystals of the BDIs showing the relevant center-to-center distances (in Ångströms, rounded to ± 0.01 Å for clarity) and the relative molecular orientation. From the hydrogen bonds, only the strong O—H···O bonds in the three forms of the 3-hydroxyl derivative (**3-HOBDI**) are shown.

substituents to point outwards, turning them accessible for other intermolecular interactions.

To our knowledge, **3-HOBDI** is the only BDI-type molecule that has been crystallized as more than one polymorph (Figure 4.2). At ambient conditions, the majority of sample crystallized as form **3-HOBDI**-A, presumably the thermodynamically

most stable structure. Occasionally, a small amount of **3-HOBDI**-B was obtained concomitantly with **3-HOBDI**-A. In a few trials, pure batches of the third form, **3-HOBDI**-C, were obtained. At a molecular level, most apparent factors for the existence of stable polymorphs of **3-HOBDI** at room temperature and their absence in the case of other compounds, despite similar molecular shapes, is the combination of a very asymmetric structure of its nearly planar molecule with hydrogen bond donors (OH) and acceptors (CO and N) in both rings, and the rotational freedom around the C—Ph bond. The overall structure resembles that of the decamorphic compound ROY.[14] **3-HOBDI**-A is also the only crystal which contains one of the two structurally different molecules having its phenyl substituent (the hydroxyl group) *syn*-orientated with respect to the imidazolone ring. In contrast to form A, in **3-HOBDI**-B both crystallographic types of molecules are in the *anti* conformation, whereas in **3-HOBDI**-C there is only one *anti* molecule (Figure 4.2). In the three polymorphs, these two conformations exist as three different hydrogen bonding patterns: infinite polymeric head-to-tail hydrogen bonded chains of either *anti* or *syn* molecules similar to **4-HOBDI** in **3-HOBDI**-A,[7] and head-to-tail hydrogen bonded dimers in **3-HOBDI**-B and **3-HOBDI**-C. The all-*syn* and all-*anti* chains in the crystal of **3-HOBDI**-A are arranged into alternating sheets, each containing only molecules of identical stereochemistry, and the all-*syn* and all-*anti* chains from adjacent sheets are perpendicular to each other. Similar to **4-HOBDI**,[6] the double bonds in the crystals of **3-HOBDI**, **2-FBDI** and **2,5-DMBDI** are separated at distances < 4 Å, but only in form C of **3-HOBDI**, **2,5-DMBI** and in the non-stacked **3-MOBDI**, are they entirely parallel to each other (Figure 4.7 and Table 4.1).

Steady-state and time-resolved spectroscopy of BDIs

To examine whether the emission properties of the solid-state BDI chromophores were stacking-mode specific, which might have implications for the GFP photochemistry, we used our previous approach,[7] where we correlated the spectral features of **4-HOBDI** and its ethers in the solid-state with their crystal packing properties leading to fine tuning of monomer-excimer emission. The two-dimensional excitation-emission spectra recorded from solid sample are shown in Figure 4.8. The variety of offset stacking geometries that we observe here for different substituents (Figure 4.8) provides grounds for more quantitative consideration of the relative importance of aggregation- and stacking-induced modulation of the emission energy.

In polar basic solvent (DMSO)[13] all six compounds demonstrated amazingly similar absorption and emission spectra (Table 4.1), showing very weak spectral dependence on the nature of the phenyl ring substituents. Minor bathochromic shifts of **3-HOBDI** emission maxima and broadening of the spectrum can be explained by the known solvatochromic behavior of phenols in basic solvents.[14] The fluorescence decays of **2-MOBDI**, **2,4-DMBDI** and **2,5-DMBDI** were faster than 10 ps, the time resolution of our TCSPC instrument. However, the fluorescence lifetimes of **3-MOBDI**, **2-FBDI** and **3-HOBDI** were considerably longer (as reported earlier for the latter compound),[15] and therefore they could be measured using TCSPC. Spectral and kinetic data of all compounds are summarized in Table 1.

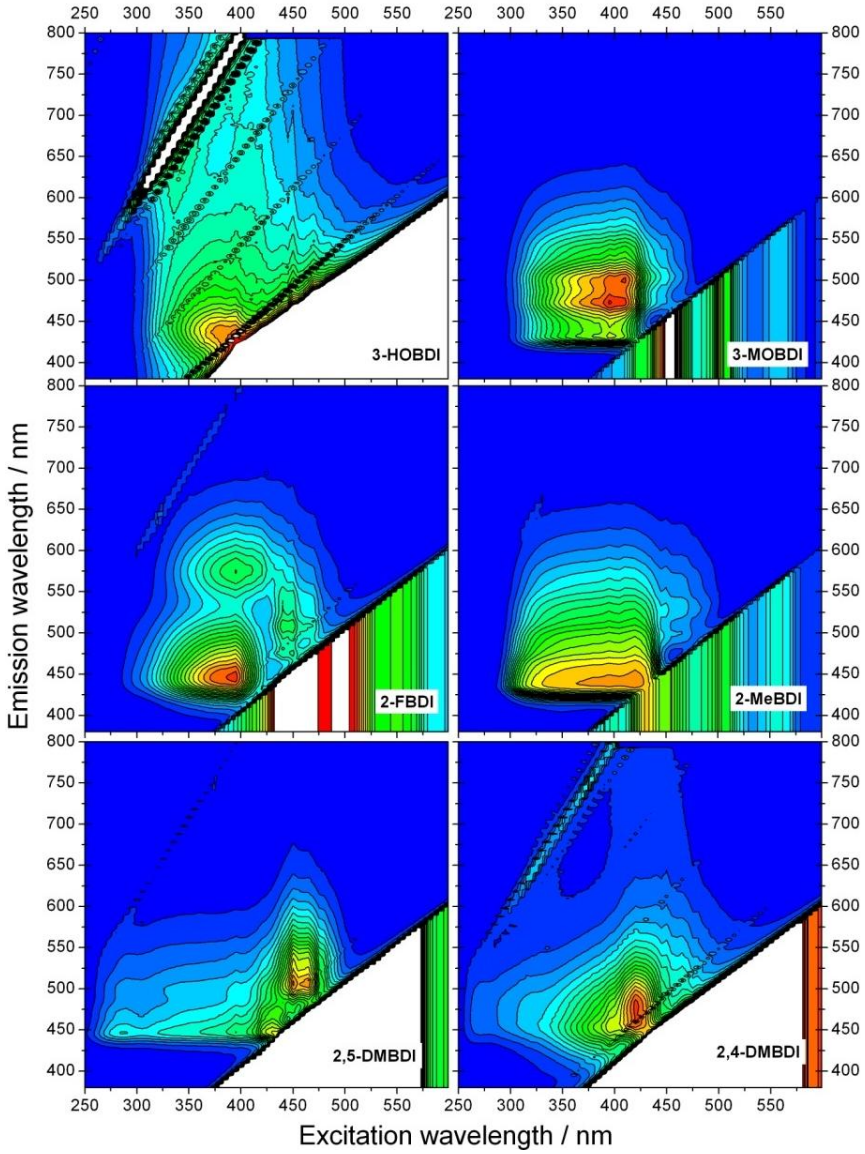

Figure 4.8. Excitation-emission contour profiles of the solid GFP model chromophores. The intensity increased from blue to red regions.

X-ray photodiffraction analysis of 3-HOBDI-C

During handling of the BDI crystals, we noticed that some of the crystals which have not been protected from the fluorescent room light, gradually turned opaque during period of several weeks, even without prior exposure to UV light. Most of the samples

developed visible cracks perpendicular to their longest axis, and some also became curved (for micrographs of the curved crystals of **2-FBDI**, see Figure 4.10). Intrigued by the reason for the apparent sensitivity of the BDI samples to visible light, we approached X-ray diffraction analysis of the opaque crystals which had been stored in air at room light for several weeks, performing all further experimental procedures (including the diffraction data collection) under red safelight (λ > 660 nm). The reacted crystals from most of the samples were of insufficient diffraction quality, due to partial disintegration and/or deformation.

Table 4.1. Selected structural and spectroscopic parameters of the benzylidenedimethylimidazolinones (BDIs). [a] nanometers

ID	*d* / Å	B.P.	React	λ_{max}^{abs} (DMSO	λ_{max}^{em} (DMSO) [a]	λ_{max}^{ex} (solid)	λ_{max}^{em} (solid) [a]	τ
2-MeBDI	6.892	Y	N	363	429	395	440	0.99 ns (445 nm)
3-HOBDI-A	3.649, 3.555	N	Y	366	436	390	440	ultrafast (440 nm)
	4.005,	N						100 ps
3-HOBDI-B	3.871, 3.556	N	Y			-	-	-
3-HOBDI-C	3.574	Y	Y			-	-	-
2-FBDI	3.848	Y	Y	363	433	390	459, 570	ultrafast (450 nm)
	3.716	Y				450	500	2.7 ns
3-MOBDI	6.964	Y	N	365	432	?	450	130 ps
2,5-DMBDI	3.783	Y	Y	368	429	?	450	ultrafast (450 nm)
	5.483	Y					~550	1.56 ns, 3.56 ns
2,4-DMBDI	4.078, 4.526	Y	N	366	429	430	470	1.0 ns, 4.1 ns (biexp.)
4-HOBDI	3.705, 3.585	N	Y					ultrafast (440 nm)

only in the case of **3-HOBDI**-C, for which the crystal shape remained the least deformed, could we succeed in selecting several well-diffracting opaque specimens which remained compact for analysis with X-ray diffraction.

The X-ray photodiffraction analysis of a reacted **3-HOBDI**-C crystal, where the **3-HOBDI** molecule is in its *Z* configuration (*Z*-**3-HOBDI**), revealed that the crystal symmetry was preserved. However, the difference Fourier electron density map (F_{obs}–F_{calc}) clearly showed new peaks around the imidazolone ring from a secondary, product species with a population that refined to 12.9% (Figure 4.9).[18] In the structure of the crystal refined as a two-component mixture,[19] the carbonyl group of the product, which due to the symmetric methyl substitution represented a useful marker of the orientation of the imidazolone ring, was flipped to the opposite side of the ring relative to the double bond (Figure 4.9). The residual peaks corresponding to the methyl groups and the nitrogen atoms were also significantly and simultaneously shifted, so that the imidazolone ring of the product represented slightly offset mirror image of that of the reactant, which appeared as an increased angle at the bridging carbon atom. Except for somewhat increased thermal ellipsoids, no significant movements could be detected for the phenyl carbon atoms, so that the phenyl ring was retained at nearly identical position as in the reactant. It should be noted that the product molecule, with the τ-flipped imidazolone ring and *E* configuration (*E*-**3-HOBDI**), was the only detectable product; particularly, no evidence of a dimeric product (that is, peaks corresponding to cyclobutane atoms which were usually detected in [2 + 2] photodimerization reactions)[12] could be observed. This result clearly showed that the τ-one-bond-flipped isomer *E*-**3-**

HOBDI was the main product of this slow photoreaction in the crystal exposed to visible light.

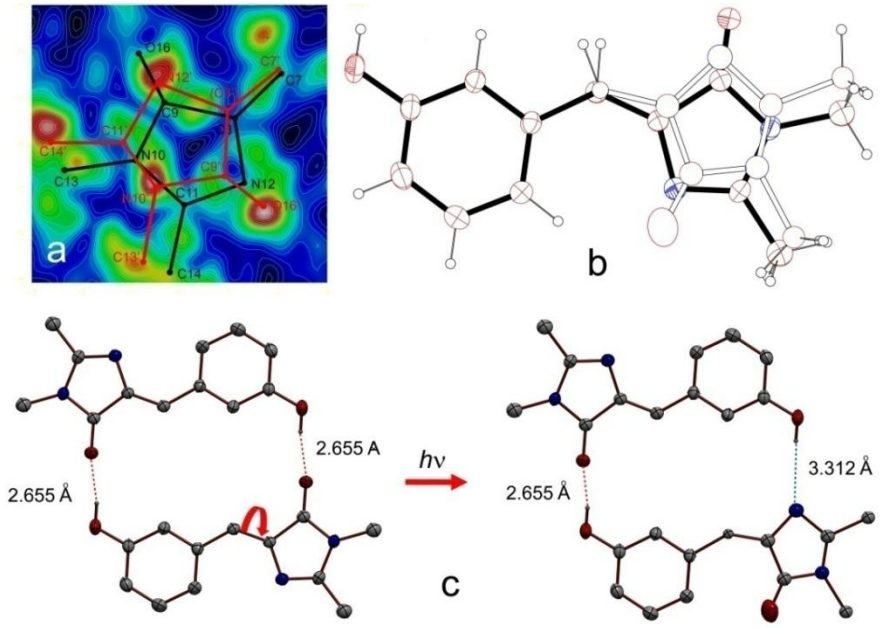

Figure 4.9. (a) Slice of the residual electron density (F_{obs}–F_{calc}) through the imidazolinone. (b) ORTEP-style plot of 3-HOBDI. (c) Changes in hydrogen bonding following a one-bond flip.

The electron density increased from deep blue (negative) to white (positive) regions. The parent (*Z*-**3-HOBDI**) and product conformations (*E*-**3-HOBDI**) are represented as black and red sticks, respectively. Note that the structure of *E*-**3-HOBDI** is drawn through the *projections* of the observed maximum peaks onto the ring plane of *Z*-**3-HOBDI**, which appears as offset of the difference peak maxima from the atomic positions of *E*-**3-HOBDI**. A ORTEP-style plot of the disordered molecule of **3-HOBDI** in the crystals of form C exposed to visible light is shown in figure 4.10 where the major (*Z*-**3-HOBDI**, 87.1%) and minor (*E*-**3-HOBDI**, 12.9%) components are represented as full and empty ellipsoids/bonds, respectively. Changes in the hydrogen bonding pattern occurring upon single τ one bond flip in the dimers of **3-HOBDI**-C and respective O···O or O···N distances are noted in figure 4.10 item C. All but the hydroxyl hydrogen atoms

are omitted for clarity. The hydrogen-bonded dimers in the unreacted crystal (left) and in the reacted crystal (one molecule in *Z*-**3-HOBDI** conformation and the other in *E*-**3-HOBDI** conformation, right) are shown.

Discussion

General Overview of Results

Spatial and temporal *in vivo* monitoring of the GFP-tagged proteins, for example, by the double-labeling FRET method,[16] requires excitation of the chromophore. In the low-energy region, the wild-type GFP absorbs at 397 nm (A band) and 475 nm (B band), corresponding to the neutral molecule and the conjugate base of the emitter, respectively, and excitation of both bands results in the green emission of the ion at 508 nm. Low-energy excitation with light of moderate powers induces reversible changes and isomerization of the protein structure via a Förster cycle.[17] However, at higher energies and increased light density, complex reactions leading to irreversible changes of the protein structures may occur, typically, decarboxylation of the proximate glutamate residue.[18] Such denaturation processes can be important for analytical methods which require high input powers due to low signal for detection, such as single-molecule spectroscopy[19] or fluorescence correlation spectroscopy.[20] The primary processes triggering irreversible chemical reactions of the protein are believed to start at the chromophore itself, and thus complete understanding of the photochemistry from the higher-order transitions and the faith of low-energy excitations which do not contribute to the main reaction pathways is essential to the improvement of the analytical feasibility of the GFP-like proteins. Such irreversible processes in model GFP systems and

particularly, the allosteric-like response from the chromophore environment, however, have not been investigated yet.

By having access to a large variety of chromophores of similar electronic structure but varied crystal packing, we have a unique opportunity to examine how crystal packing influences their varied behavior, from photophysics to photodimerization to photoisomerization. On the one hand, the presence of a double bond in close proximity to another leads to efficient cycloaddition, a phenomenon that has been extensively studied in the cinnamate literature.[21] When such proximity is accompanied by an extensive hydrogen-bonded network, the bond contraction produced by dimerization can lead to a surprising photomechanical effect. On the other hand, when such proximity is absent, dimerization is extinguished and isomerization can take place. We now consider each of these phenomena in turn.

Effect of crystal packing on the emission spectra of BDIs

We find that the crystal packing of the BDIs strongly affects their fluorescence properties in the solid state, and it is reproduced well in the two-dimensional excitation-emission spectra (Figure 4.10). In the crystal of **2-MeBDI**, where the molecules are offset and isolated from each other (the distance between the double bonds is 6.892 Å), and they interact only by weak C—H···O hydrogen bonds (d(C···O) = 3.425 Å), the excitation energy remains localized within individual molecules. The emission from the singlet excited state, with λ_{max}^{ex} = 395 nm, appears as a single strong peak with λ_{max}^{em} = 440 nm, along with the existence of a single major emitting species. As reported previously,[7] this band is slightly red-shifted by the environment effects relative to the emission in solution (431 nm). The decay times are weakly dependent on the wavelength

and range from 0.99 ns (445 nm) to 1.37 ns (490 nm). Contrary to the isolated emission observed from **2-MeBDI**, in the structure of **3-HOBDI**-A**,** where the molecules exist as hydrogen bonded chains (d(O—H···O)$_{syn\text{-}syn}$ = 2.754 Å, d(O—H···O)$_{anti\text{-}anti}$ = 2.682 Å), the cooperative effects from the intermolecular interactions are expected to affect significantly the emission intensity and the time-decay profile from the individual molecules. Accordingly, only a weak emission with one major emission peak with λ_{max}^{ex} = 390 nm and λ_{max}^{em} = 440 nm is observed. At all wavelengths, the decays of the emission are non-monoexponential and ultrafast, the major amplitude with a contribution of > 98% weight corresponding to a species that decays within 10 ps, which remains below the detection limit. Similar efficient fluorescence quenching in the solid state was observed previously for **4-HOBDI**.[7]

Although each of **2-FBDI** and **3-MOBDI** contains a single structural type of the respective molecule, they exhibit at least two emission centers, which are separated better in the case of **2-FBDI**. For **2-FBDI**, the stronger emitter is excited at λ_{max}^{ex} = 390 nm and emits at two wavelengths, $\lambda_{max,1}^{em}$ = 450 nm and $\lambda_{max,1}^{em}$ = 570 nm. The second emitter, excited at λ_{max}^{ex} = 450 nm, exhibits wider energy distribution and emits at $\lambda_{max,1}^{em}$ = 500 nm. At 595 nm, the lifetime of the second component is 2.7 ns. The two emissions of **3-MOBDI** are strongly overlapped. The species emitting at $\lambda_{max,1}^{em}$ = 450 nm decays at 130 ps, while the one $\lambda_{max,1}^{em}$ = 500 nm, with rise time of 240 ps, follows a biexponential decay law, with component lifetimes of 1.5 and 10.6 ns and an amplitude ratio of 12:1. Unlike **2-MeBDI** and **3-HOBDI**, the molecules of **2-FBDI** and **3-MOBDI** are not completely isolated and they are not included in extensive hydrogen bonding. Instead, in both cases two molecules are stacked with each other with at least one half of their

skeleton (Figure 4.10). **2-FBDI** forms antiparallel dimers, where both the phenyl and the imidazolone rings of one molecule are stacked with the imidazolone and phenyl ring from its molecular counterpart. In the structure of **3-MOBDI**, the molecules are displaced relative to each other, so that only one half of the molecule forms stack with the neighbor molecule (that is, the phenyl ring is stacked with an imidazolone ring). The emission of the individual molecules in such case will be affected by the proximity of the molecules by activation of excimer transitions, which could explain the complicated pattern observed in the kinetics of their emission spectra.

Photomechanical effects in crystalline BDIs

Mechanical effects in photomechanically active materials[22] and thermosalient crystals[23] (the latter occasionally also referred to as "jumping crystals"), such as the one described here for **3-HOBDI**, are extremely rare solid-state phenomena and are considered important for the design of actuators, as well as for conversion of the light or kinetic energy into mechanical work. In particular, photomechanical effects in the solid state present an opportunity for photoactuators in several photoactive systems. A large number of these have relied upon cis/trans isomerization of azobenzene as the structural perturbation, with a clever recent example.[22c] More commonly, such effects have been developed for azobenzene-containing polymers,[24] although examples using [2 + 2][25] and [4 + 4] [22a,22b] cycloadditions have been also reported. **3-HOBDI-**A presents a startling example for which a unique polymorph presents a special deactivation pathway.

The very low excitation power, uniform excitation of the crystal, high melting point, short exposure time and absence of photomechanical effects in the other compounds (even when the crystal shape is similar to that of **3-HOBDI-**A, such as is the

case with **2-FBDI**) all indicate that the photoinduced effects observed for **3-HOBDI**-A are not due to heating or partial (surface) melting, but to the photochemical reaction which was evidenced by IR (Figures 4.5) and NMR spectroscopy for bulk samples. The two-dimensional excitation-emission profiles (Figure 5) show that contrary to the other compounds, the fluorescence of **3-HOBDI** is quenched in the solid state. This observation may indicate deexcitation through non-radiative pathways due to strong intermolecular interactions (hydrogen bonding) or by means of photochemical reaction from the excited state.

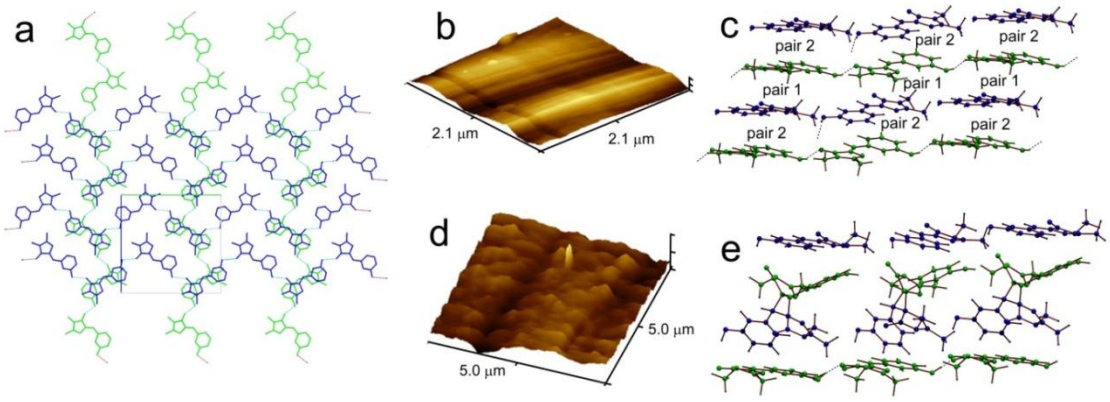

Figure 4.10. (a) Sheets of hydrogen bonded chains of *syn* (green) and *anti* (blue) **3-HOBDI** molecules in the crystal of **3-HOBDI**-A. (b) and (d): AFM images of the crystal surface before and after UV irradiation, showing the UV-induced changes of the crystal surface morphology. (c) and (e): packing of the crisscrossed layers of *syn*-**3-HOBDI** (green) and *anti*-**3-HOBDI** (blue) in the unreacted crystal (c) and in a model structure in which the closer pairs are dimerized, considering the usual geometry of the central cyclobutane ring.

The main reason behind the different photochemical properties and the appearance of dramatic photomechanical effects of **3-HOBDI**-A, which are not observed for the other forms of **3-HOBDI** and the other compounds in this group, are the strongly anisotropic packing interactions. As explained above, the structure of **3-HOBDI**-A is composed of alternating and perpendicular to each other layered two-dimensional sheets

of all-*syn* hydrogen-bonded strings parallel to the *c*-axis and all-anti zigzag strings parallel to the *b*-axis (see Figures 4.10 and Figure 4.11).

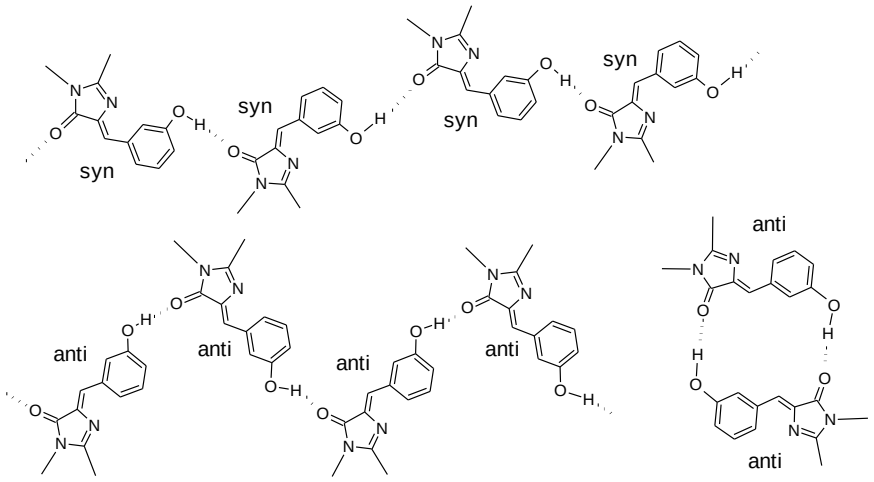

Figure 4.11. Polymeric (A, B) and dimeric (C) hydrogen bonding patterns observed in the three characterized polymorphs of **3-HOBDI**

Larger bunches of the coaxial molecular strings in **3-HOBDI**-A are observed by AFM spectroscopy as ridges in the surface of non-irradiated crystal (Figure 4.11b). The surface of the crystal is relatively smooth with a roughness of 2.6–6.4 nm. From these dimensions, the surface of the crystal appeared fluted, reminiscent of a grating, with large ridges approximately 1 μm apart. Individual structures consist of smaller, parallel string substructures, with some layering close to the top of the features also being apparent. This arrangement is reminiscent of cylinders placed side-by-side. The molecules within the chains are held together by strong intermolecular O—H···O hydrogen bonds, whereas the stacked sheets are crisscrossed and interact with each other through weak π—π interactions. Unlike forms B and C, for which the strong interactions in the crystal are confined within the doubly hydrogen bonded head-to-tail *anti* dimers (Chart 2), the infinite chains of strong hydrogen bonds in **3-HOBDI**-A provide notable strength and flexibility within the sheets, and could act as basis for one-dimensional transfer of

cooperative effects within the crystal. Being glued by much weaker interactions, the shear-free, individual sheets have larger freedom to slide on the top of each other, which is related to the unusual elasticity of the crystals of form A during the bending.

Pairs of any two symmetrically non-equivalent molecules from the adjacent perpendicular strings (colored green and blue in Figure 4.10a), which are stacked in antiparallel displaced fashion, define two types of alternating C---C separations, with nearly identical inter-bond dihedrals: molecular pair 1 (3.648 and 3.555 Å, angle: 56.9^{o}) and molecular pair 2 (4.005 and 4.176 Å, angle 57.3^{o}). According to the topochemical criteria,[13] it is expected that all bonds of the first, closer pair, are photoreactive. Although there might be competition for dimerization between the two pairs, the notable difference in the double bond separations at virtually identical relative orientations of the double bonds indicates that the dimerization of the double bonds within the pair of closer bonds (bond pair 1) is preferred and largely prevents subsequent reaction between the bonds of the more distant bonds (bond pair 2). Coincidentally, such dimerization leads to a *trans,trans* symmetric dimer which is the most stable according to semiempirical calculations. Therefore, most of the molecules from one sheet selectively form dimers with their counterpart molecules from the other sheet rather than from different sheets, that is, the dimers are almost exclusively formed between molecular pairs 1 but not between molecular pairs 2, as shown in Figures 4.10. Due to the bending of the individual reacting molecules and the inclination of the phenyl rings upon the cyclobutane ring formation, the molecules of the dimerized sheets become devoid of the π—π interactions with molecules from the adjacent dimerized (or still monomeric) sheets, thus resulting in "pairing" of the originally equidistant sheets and subsequent separation of the resulting

sheet pairs. The disappearance of the π—π interactions, which served as weak "glue" between the paired sheets, increases their mobility in respect to each other, so that small perturbations such as local heating or defects are expected to cause significant and cooperative sliding of the sheets of dimers relative to each other. This photomechanical effect, which is macroscopically observed as bending of **3-HOBDI**-A crystals, is induced by dimerization, and it is shear-driven at a molecular level. Moreover, because the original strings are composed of different types of molecules (*syn* and *anti* along the *c* and *b* axes, respectively), the preference for sliding along the two directions are different, which corresponds well with the subsequent bending along the second longest axis that ultimately results in twisting motion. Apparently, after maximum strain has been achieved by sliding of the paired layers in one direction, the sliding in the second direction becomes dominant to the point where the mechanical strain overweighs the cooperative forces and a macroscopic crack appears on the crystal perpendicular to its longest axis Figure 4.10. This mechanism is consistent with the absence of observable photomechanical effect in forms **3-HOBDI**-B and **3-HOBDI**-C, where the *anti* molecules form head-to-tail bonded dimers, despite the fact that both forms are photochemically active (IR spectroscopy). Although the dimerization in forms B and C occurs, the crystals do not bend, but instead they tend to crack normal to the longest axis. Similar disintegration is observed for the other photoreactive compounds (**2-FBDI** and **2,5-DMBDI**).

As exemplified with the *syn* chains in the mechanism shown in Figure 4.11, the formation of dimers inevitably results in disruption of the intermolecular hydrogen bonds by separation of the hydroxyl (donor) and keto (acceptor) groups from each other, which

is confirmed by the large blue shift (125 cm^{-1}) of the ν(OH) mode observed in the IR spectra of completely photoreacted sample. The disruption of the hydrogen bonds along the strings and the notable shrinkage of the strings due to the bending of the component molecules (Figure 4.11) is expected to result in accumulation of mechanical stress along the strings. On a microscopic scale, this perturbation of large numbers of molecules along the initially straight strings has to be released, which would affect the macroscopic appearance of the crystal surface. Indeed, AFM images of UV-irradiated crystal (Figure 4.10) show that the crystal surface is visibly more disturbed, and the roughness has increased to 10–14 nm. The initially smooth parallel "waves" appear "chopped" and out-of-plane, giving the crystal surface a fish scale appearance—a consequence of crystal bending and mass redistribution. The image of the crystal which remained unattached to the basis is similar but the roughness, depending on area, is as low as 7 nm but as high as 43 nm.

Packing effects on the photoisomerization by one-bond-flip

In contrast to **3-HOBDI-**A, **3-HOBDI-**C allows us to test the influence of crystal packing on cis/trans isomerization. The hula twist has been accepted as a compelling rationale for chromophore isomerization in fluorescent proteins.[26] Nevertheless, considerable theoretical[27] and experimental[28] evidence exists that such a double motion pays considerable energetic penalties within the fluorescent protein barrel. Unfortunately, neither tyrosine nor phenylalanine, which form the aromatic rings of the largest group of protein chromophores, has a *meta* or *ortho* substituent to isolate the double twist. Either the tryptophan or histidine derivative ("cyan fluorescent protein") could plausibly test such motions.

Although the relevance of our observations to the protein itself can be argued, we note that when the aromatic ring is constrained by hydrogen bonding as in **3-HOBDI**-C, facile isomerization via one-bond rotation about the double bond occurs even within the solid state (Figure 4.9). From the X-ray diffraction analysis of partially photoreacted crystal, it is concluded that while dimers of the BDIs are obtained by high-energy excitation (365 nm; see the NMR, IR and MS results described above), in single crystals of **3-HOBDI**-C, prolonged exposure to low excitation energies in the visible region (ambient light) cause *Z*—*E* isomerization with τ one bond flip of the imidazolone ring. Similar dependence on the dimerization versus isomerization on the excitation energy was reported previously for solutions of 5-aryl- and 5-pyridylmethylenehydantoins.[29] Our result represents the first direct evidence of such processes occurring in crystals of pure BDI chromophore. Based on this observation, we conclude that conservation of volume is not a sufficient impediment to isomerization via a bond twist.

Closer analysis of the supramolecular structure in the **3-HOBDI**-C crystal reveals an important effect of the photoreaction, induced from the excited state, to the intermolecular interactions. Assuming a statistical distribution of the product molecules, the small conversion (12.9%) implies that, after imidazolone ring flipping, almost every reactive molecule rebinds to its non-reacted counterpart (Figure 4.9). Therefore, because the position of the phenyl half of the molecule is essentially preserved in the product, a weaker hydrogen bond O—H···N (3.312 Å) is substituted for a stronger hydrogen bond O—H···O (2.655 Å). This clearly thermodynamically disfavored process is only possible from excited state. Once created, however, the flipped product is stabilized by the newly formed hydrogen bond, which is why the product molecule accumulates to detectable

amount. This result may have implications for the one-bond flip mechanism suggested for the GFP chromophore.

The dimers in **3-HOBDI**-B and **3-HOBDI**-C are confined to a space of similar shape, and the two molecules within each dimer interact with hydrogen bonds of similar strength. Yet, only in the latter can flipping occur to a significant extent without interfering with the long-range crystalline order. This observation can be rationalized by inspection of the Hirshfeld surfaces[30] plotted around the respective monomers (Figure 4.12).

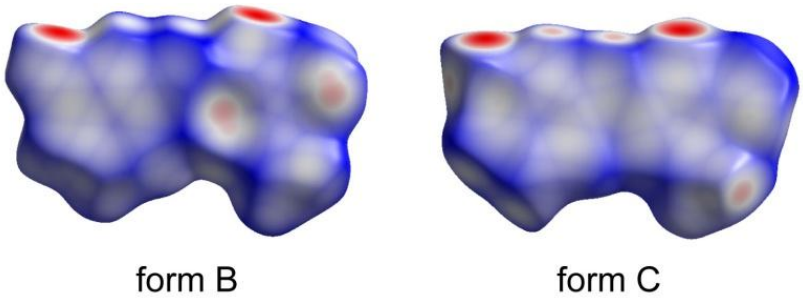

Figure 4.12. Hirshfeld surfaces (plotted as d_{norm}) of the molecules in forms B and C of 3-HOBDI.

The Hirshfeld surfaces[31] provide a convenient way to depict the molecular shape and to visualize the intermolecular interactions. They represent plots, which are obtained by partitioning the space in the crystal into regions where the contribution from the electron distribution of a sum of spherical atoms for the molecule exceeds the contribution from the corresponding sum over the crystal. From the red regions on the imidazolone ring in **3-HOBDI**-B it becomes apparent that it is sandwiched more tightly and interacts more strongly by the surrounding neighbor molecules. The imidazolone ring in **3-HOBDI**-C, on the other hand, interacts weakly and thus has larger freedom for flipping.

Conclusions

The spectroscopic and chemical properties of AMI chromophores within the solid state show great differences than those compared in solution. It has been common practice to consider the reactivity of molecules independent of their extended environment. With the advent of "supramolecular photochemistry", we now recognize that reactivity can be promoted or constrained by rigid environments. The systems studied here illustrate that when the "solvent" is the molecule itself, the disposition of such molecules within the solid state can have a profound influence, and different polymorphs can have totally different reactivities. The way in which structure determines crystal packing and thus reactivity in the solid state continues to be an elusive and important goal.

References

[1] Naumov, P.; Kowalik, J.; Solntsev, K.M.; Baldridge, A.; Moon, J-S; Kranz, C.; Tolbert, L.M. *J. Am. Chem. Soc.* **2010**, *132(16)*, 5845-5857.

[2] (a) Follenius-Wund, A.; Bourotte, M.; Schmitt, M.; Iyice, F.; Lami, H.; Bourguignon, J.-J.; Haiech, J. *Biophys. J.* **2003**, *85*, 1839–1850. (b) Yang, J.-S.; Huang, G.-J.; Liu, Y.-H.; Peng, S.-M. *Chem. Commun*. **2008**, 1344–1346. (c) Solntsev, K. M.; Poizat, O.; Dong, J.; Rehault, J.; Lou, Y.; Burda, C.; Tolbert, L. M. *J. Phys. Chem. B*. **2008**, *112*, 2700–2711. (d) Dong, J.; Abulwerdi, F.; Baldridge, A.; Kowalik, J.; Solntsev, K. M.; Tolbert, L. M. *J. Am. Chem. Soc.* **2008**, *130*, 14096–14098. (e) Vengris, M.; van Stokkum, I. H. M.; He, X.; Bell, A. F.; Tonge, P. J.; van Grondelle, R.; Larsen, D. S. *J. Phys. Chem*. **2004**, *A108*, 4587–4598. For reports on the ultrafast photophysics of the chromophore inside the protein, see: (g) Chattoraj, M.; King, B. A.; Bublitz, G. U.; Boxer, S. G. *Proc. Natl. Acad. Sci. USA* **1996**, *93*, 8362–8367. (h) Lossau, H.; Kummer, A.; Heinecke, R.; Pöllinger-Dammer, F.; Kompa, C.; Bieser, G.; Jonsson, T.; Silva, C. M.; Yang, M. M.; Youvan, D. C.; Michel-Beyerle, M. E. *Chem. Phys*. **1996**, *213*, 1–16. (i) Leiderman,

P.; Ben-Ziv, M.; Genosar, L.; Huppert, D.; Solntsev, K. M.; Tolbert, L. M. *J. Phys. Chem*. **2004**, *B108*, 8043–8053. (j) Meech, S. R. *Chem. Soc. Rev*. **2009**, *38*, 2922–2934. (j) van Thor, J. J. *Chem. Soc. Rev*. **2009**, *38*, 2935–2950. (k) Fang, C.; Frontiera, R. R.; Tran, R.; Mathies, R. A. *Nature* **2009**, *462*, 200–204.

[3] (a) Litvinenko, K. L.; Webber, N. M.; Meech, S. R. *J. Phys. Chem. A* **2003**, *107*, 2616–2623. (b) Stavrov, S. S.; Solntsev, K. M., Tolbert, L. M.; Huppert, D. *J. Am. Chem. Soc*. **2006**, *128*, 1540–1546.

[4] (a) Andersen, L. H.; Bochenkova, A. V. *Eur. Phys. J.* **2009**, *D51*, 5–14. (b) Rajput, J.; Rahbek, D. B.; Andersen, L. H.; Rocha-Rinza, T.; Christiansen, O.; Bravaya, K. B.; Erokhin, A. V.; Bochenkova, A. V.; Solntsev, K. M.; Dong, J.; Kowalik, J.; Tolbert, L. M.; Åxman Petersen, M.; Brøndsted Nielsen, M. *Phys. Chem. Chem. Phys*. **2009**, *11*, 9996–10002. (c) Forbes, M. W.; Jockusch, R. A. *J. Am. Chem. Soc*. **2009**, *131*, 17038–17039.

[5] Leiderman, P.; Huppert, D.; Remington, S. J.; Tolbert, L. M.; Solntsev, K. M. *Chem. Phys. Lett.* **2008,** *455*, 303–306.

[6] Baldridge, A.; Jayaraj, N.; Samanta, S. R.; Ramamurthy, V.; Tolbert, L. M. *J. Am. Chem. Soc.* **2010**, *132*, in press.

[7] Dong, J.; Solntsev, K. M.; Tolbert, L. M. *J. Am. Chem. Soc.* **2009**, *131*, 662–670.

[8] (a) "*Cis-trans Isomerization in Biochemistry*" (Ed.: C. Dugave), Wiley-VCH: Weinheim, 2006. (b) Henderson, J. N.; Ai, H.-w.; Campbell, R. E.; Remington, S. J., *Proc. Natl. Acad. Sci. USA* **2007,** *104*, 6672–6677. (c) Andresen, M.; Stiel, A. C.; Trowitzsch, S.; Weber, G.; Eggeling, C.; Wahl, M. C.; Hell, S. W.; Jakobs, S. *Proc. Natl. Acad. Sci. USA* **2007,** *104*, 13005–13009, S13005/13001-S13005/13005. (d) Stiel, A. C.; Trowitzsch, S.; Weber, G.; Andresen, M.; Eggeling, C.; Hell, S. W.; Jakobs, S.; Wahl, M. C. *Biochem. J.* **2 007,** *402*, 35–42. (e) Voliani, V.; Bizzarri, R.; Nifos, R.; Abbruzzetti, S.; Grandi, E.; Viappiani, C.; Beltram, F. *J. Phys. Chem*. **2008**, *B112*, 10714–10722. (f) Habuchi, S.; Ando, R.; Dedecker, P.; Verheijen, W.; Mizuno, H.; Miyawaki, A.; Hofkens, J. *Proc. Natl. Acad. USA* **2005**, *102*, 9511–9516. (g) Usman, A.; Masuhara, H.; Asahi, T. *J. Phys. Chem*. **2006**, *110*, 20085–20088.

[9] (a) Liu, R. S. H.; Yang, L.-Y.; Liu, J. *Photochem. Photobiol.* **2007**, *83*, 2–10. (b) Liu, R. S. H. *Acc. Chem. Res.* **2001**, *34*, 555–562.

[10] Imamoto, Y.; Kuroda, T.; Kataoka, M.; Shevyakov, S.; Krishnamoorthy, G.; Liu, R. S. H. *Angew. Chem., Int. Ed*. **2003**, *42*, 3630–3633.

[11] (a) Chung, J. W.; You, Y.; Huh, H. S.; An, B.-K.; Yoon, S.-J.; Kim, S. H.; Lee, S. W.; Park, S. Y. *J. Am. Chem. Soc*. **2009**, *131*, 8163–8172. (b) Yang, S.-Y.; Naumov, P. Fukuzumi, S. *J. Am. Chem. Soc*. **2009**, *131*, 7247–7249. (c) MacGillivray, L. R.; Papaefstathiou, G. S.; Friščić, T.; Hamilton, T. D.; Bučar, D.-K.; Chu, Q.; Varshney, D. B.; Georgiev, I. G. *Acc. Chem. Res.* **2008**, *41*, 280–291. (d) Georgiev, I. G.; MacGillivray, L. R. *Chem. Soc. Rev.* **2007**, *36*, 1239–1248. (e) Ajamian, A.; Gleason, J. L. *Angew. Chem., Int. Ed.* **2004**, *43*, 3754–3560. (f) Cozzi, P. G. *Chem. Soc. Rev.* **2004**, *33*, 410–421. (g) Cao, G.; Mallouk, T. E. *J. Solid State Chem.* **1991**, *94*, 59–71. (h) Sharma, C. V. K.; Panneerselvam, K.; Shimoni, L.; Katz, H.; Carrell, H. L.; Desiraju, G. R. *Chem. Mater.* **1994**, *6*, 1282–1292.

[12] (a) Bernstein, J. *Polymorphism in molecular crystals*, Oxford University Press: Oxford, 2002, pp. 170–176. (b) Price, C. P.; Grzesiak, A. L.; Matzger, A. J. *J. Am. Chem. Soc.*, **2005**, *127*, 5512–5517. (c) Chen, S.; Guzei, I. A.; Yu, L. *J. Am. Chem. Soc.*, **2005**, *127*, 9881–9885. (d) Chen, S.; Xi, H.; Yu, L. *J. Am. Chem. Soc.*, **2005**, *127*, 17439–17444.

[13] The absorption and emission spectra of **3-HOBDI** and **3-MOBDI** in various solvents have been reported earlier (see reference 1c).

[14] (a) Solntsev, K. M.; Huppert, D.; Tolbert, L. M.; Agmon, N. *J. Am. Chem. Soc.* **1998**, *120*, 7981–7982. (b) Solntsev, K. M.; Huppert, D.; Agmon, N. *J. Phys. Chem.* **1998**, *A102*, 9599–9606. (c) Dong, J.; Solntsev, K. M.; Tolbert, L. M. *J. Am. Chem. Soc*. **2006**, *128*, 12038–12039.

[15] Dong, J.; Solntsev, K. M.; Poizat, O.; Tolbert, L. M. *J. Am. Chem. Soc*. **2007**, *129*, 10084–10085.

[16] Lippincott-Schwartz, J.; Snapp, E.; Kenworthy, A. *Nat. Rev. Mol. Cell Biol*. **2001**, *2*, 444–456.

[17] Brejc, K.; Sixma, T. K.; Kitts, P. A.; Kain, S. R.; Tsien, R. Y.; Ormö, M.; Remington, S. J. *Proc. Nat. Acad. Sci. USA* **1997**, *94*, 2306–2311.

[18] (a) van Thor, J. J.; Gensch, T.; Hellingwerf, K. J.; Johnson, L. N. *Nat. Struct. Biol*. **2002**, *9*, 37–41. (b) Bell, A. F.; Stoner-Ma, D.; Wachter, R. M.; Tonge, P. J. *J. Am. Chem. Soc*. **2003**, *125*, 6919–6926.

[19] Dickson, R. M.; Cubitt, A. B.; Tsien, R. Y.; Moerner, W. E. *Nature* **1997**, *388*, 355–358.

[20] Haupts, U.; Maiti, S.; Schwille, P.; Webb, W. W. *Proc. Natl. Acad. Sci. USA* **1998**, *95*, 13573–13578.

[21] (a) Lewis, F. D.; Quillen, S. L.; Hale, P. D.; Oxman, J. D. *J. Am. Chem. Soc.* **1988**, *110*, 1261–1267. (b) Bertmer, M.; Nieuwendaal, R. C.; Barnes, A. B.; Hayes, S. E. *J. Phys. Chem.* **2006**, *B110*, 6270–6273.

[22] (a) Al-Kaysi, R. O.; Müller, A. M.; Bardeen, C. J. *J. Am. Chem. Soc*. **2006**, *128*, 15938–15939. (b) Al-Kaysi, R. O.; Bardeen, C. J. *Adv. Mater*. **2007**, *19*, 1276–1280. (c) Koshima, H.; Ojima, N.; Uchimoto, H. *J. Am. Chem. Soc*. **2009**, *131*, 6890–6891. (d) Barrett, C. J.; Mamiya, J.; Yager, K. G.; Ikeda, T. *Soft Matter* **2007**, *3*, 1249–1261. (e) Colombier, I.; Spagnoli, S.; Corval, A.; Baldeck, P. L.; Giraud, M.; Léaustic, A.; Yu, P. *Mol. Cryst. Liq. Cryst*. **2005**, *431*, 495–499. (f) Bubnov, M. P.; Nevodchikov, V. I.; Fukin, G. K.; Cherkasov, V. K.; Abakumov, G. A. *Inorg. Chem. Commun*. **2007**, *10*, 989–992. (g) Yamada, M.; Kondo, M.; Mamiya, J.; Yu, Y.; Kinoshita, M.; Barrett, C. J.; Ikeda, T. *Angew. Chem., Int. Ed*. **2008**, *47*, 4986–4988. (h) Kobatake, S.; Takami, S.; Muto, H.; Ishikawa, T.; Irie, M. *Nature* **2007**, *446*, 778–781.

[23] (a) Zamir, S.; Bernstein, J.; Greenwood, D. J. *Mol. Cryst. Liq. Cryst*. **1994**, *242*, 193–200. (b) Steiner, T.; Hinrichs, W.; Saenger, W. *Acta Cryst.* **1993**, *B49*, 708–718. (c) Kaftory, M.; Botoshansky, M.; Kapon, M.; Shteiman, V. *Acta Crystallogr*. **2001**, *B57*, 791–799. (d) Lieberman, H. F.; Davey, R. J.; Newsham, D. M. T. *Chem. Mater.* **2000,** *12*, 490–494. (e) Crottaz, O.; Kubel, F.; Schmid, H. *J. Mater. Chem*. **1997**, *7*, 143–146. (f) Corbett, J. M.; Dickman, M. H. *Acta Crystallogr.* **1996**, *C52*, 1851–1853. (g) Ding, J.; Herbst, R.; Praefcke, K.; Kohne, B.; Saenger, W. *Acta Crystallogr.* **1991**, *B47*, 739–742. (h) Gigg, J.; Gigg, R.; Payne, S.; Conant, R. *J. Chem. Soc., Perkin Trans. I* **1987**, 2411–2414. For remarkable recent studies of mechanical properties of molecular crystals, see: (i) Reddy, C. M.; Gundakaram, R. C.; Basavoju, S.; Kirchner, M. T.; Padmanabhan, K. A.; Desiraju. G. R. *Chem. Commun*. **2005**, 3945–3947. (j) Reddy, C. M.; Kirchner, M. T.; Gundakaram, R. C.; Padmanabhan, K. A.; Desiraju, G. R. *Chem.–Eur. J.* **2006**, *12*, 2222–2234. (k) Reddy, C. M.; Basavoju, S.; Desiraju, G. R. *Chem. Commun.* **2005**, 2439–2441.

[24] Zhang, C.; Zhao, X.; Chao, D.; Lu, X.; Chen, C.; Wang, C.; Zhang, W. *J. Appl. Polym. Sci.* **2009**, *113*, 1330–1334.

[25] He, J.; Zhao, Y.; Zhao, Y., *Soft Matter* **2009**, *5*, 308–310. (b) Lendlein, A.; Jiang, H.; Juenger, O.; Langer, R. *Nature (London)* **2005**, *434*, 879–882.

[26] (a) Maddalo, S. L.; Zimmer, M. *Photochem. Photobiol*. **2006**, *82*, 367–372. (b) Megley, C. M.; Dickson, L. A.; Maddalo, S. L.; Chandler, G. J.; Zimmer, M. *J. Phys. Chem.* **2009**, *B113*, 302–308.

[27] (a) Norton, J. E.; Houk, K. N. *Mol. Phys*. **2006**, *104*, 993–1008; (b) Martin, M. E.; Negri, F.; Olivucci, M. *J. Am. Chem. Soc*. **2004**, *126*, 5452–5464.

[28] (a) Saltiel, J.; Bremer, M. A.; Laohhasurayotin, S.; Krishna, T. S. R. *Angew. Chem., Int. Ed*. **2008**, *47*, 1237–1240. (b) Saltiel, J.; Krishna, T. S. R.; Turek, A. M. *J. Am. Chem. Soc*. **2005**, *127*, 6938–6939.

[29] Tan, S.-F.; Ang, K.-P.; How, G.-F. *J. Phys. Org. Chem*. **1991**, *4*, 707–713.

[30] Hirshfeld, F. L. *Theor. Chim. Acta* **1977**, *44*, 129–138.

[31] McKinnon, J. J.; Spackman, M. A. *Chem. Commun.* **2007**, 3814–3816. (b) McKinnon, J. J.; Mitchell, A. S.; Spackman, M. A. *Chem.–Eur. J*. **1998**, *4*, 2136–2141. (c) McKinnon, J. J.; Spackman, M. A.; Mitchell, A. S. *Acta Crystallogr.* **2004**, *B60*, 627–668.

CHAPTER 5

ENCAPSULATION OF GFP CHROMOPHORE ANALOGS IN SUPRAMOLECULAR HOSTS: OCTA ACIDS AND CHOLATE SALT AGGREGATES

Introduction to octa acid cavitands

The chromophore in the green fluorescent protein (GFP) exhibits a remarkable difference in emission quantum yield as a function of sequestration within the β-barrel. Upon denaturation, the fluorescence diminishes by four orders of magnitude, the result, presumably, of disruption of the restraining β-barrel.[4] The effect of sequestration has mostly been interpreted as inhibition of double bond twisting to a diradical state, although rotation about the formal single aromatic bond has been proposed.[5] The former effect is somewhat belied by both the fluorescence of some chromophores which also undergo cis/trans isomerization and by the relatively modest viscosity effect. Alternatively, a combination of the two twisting modes ("hula twist") has been speculated to account for a volume conserving process within the β-barrel (see Scheme 1).[6] We were therefore intrigued with the possibility of encapsulation of the chromophore within a deep cavity cavitand, the so-called "octa acid" (OA), which forms a hydrophobic capsule-like container, of dimensions 14 x 7 Å upon dimerization[7] and mimics the β-barrel. Following the initial results from the encapsulation studies using various alkyl-substituted AMI's the motivation arose to separate the influence of electronic and steric effects on the encapsulation phenomenon, which differ both in their steric volumes and the electronic effects, on the fluorescence turn-on.

The BMI chromophores were synthesized using previously described methods.[8] (see R_1 and R_2 in Table 1) and were exposed to buffered solutions of OA in D_2O. In all cases, complexation of the chromophores[9] was validated by the upfield NMR chemical shifts of the guests compared to CD_3CN solvent, corresponding to placement of protons within the shielding region of the aromatic cavity. As seen in our earlier studies,**Error! Bookmark not defined.**,[10] the alkyl derivatives experienced strong shielding of both aryl ring and *N*-alkyl groups within the cavity. Notably, CH_3CH_2- as an ortho substituent did not lead to a stable complex.

Experimental for octa acid studies

Stoichiometric titration

Titration of OA solution (1 mM solution of OA made in 10 mM borate buffer in D_2O) with GFP chromophore (in DMSO-d_6) was studied by ^1H NMR spectroscopy by gradual addition of guest (GFP chromophore) to the host solution. Titration showed that all of them form 1:2 capsular assemblies (G : H) with OA along with the up field shift of the guest's proton signal. The guest resonances were assigned based upon systematically comparing the variation in the structure of guest and also with the aid of 2D-NMR studies.

Emission studies

A 10^{-5} M solution of GFP chromophore was prepared in benzene and in 4×10^{-5} M solution of OA (G : H = 1 : 4, 10 mM borate buffer solution). Fluorescence spectra of these solutions were recorded (excitation 370 nm) and compared. For comparison of the fluorescence intensity the same excitation wavelength was used for each chromophore.

Quantum yield studies

Quantum yields were determined the by relative method by using quinine sulfate standard (λ_{ex} 349 nm, Φ_f = 0.54). In each case the absorbance of the given samples (in H_2O and in benzene) were matched to the standard (in 50 mM H_2SO_4) and maintained <

0.1. Quantum yields were calculated using equation below, where F represents the emission area and η is reflective index of the solvent.

$$\Phi_{sample} = \Phi_{reference} (F_{sample} / F_{reference}) (\eta_{sample} / \eta_{reference})^2$$

Photoisomerization Studies

Photoirradiation of 10-5 M solution of GFP chromophore in OA (H : G = 2:1, 2*10-5 M) and benzene was done a using 310 nm filter. Fluorescence measurements were taken after given increments of time to note the intensity change of the chromophore.

Photochemistry Studies

A 0.5 mM solution of GFP chromophore was prepared in CD_3CN and complex solution of these compounds were prepared in 1 mM octa acid solution (H:G = 2:1, 10 mM borate buffer solution of D_2O). These solutions were irradiated using a 310 nm filter. The relative time required to reach photo stationary state for conversion of cis isomer to trans isomer (T_{PSS}) and the ratio of two isomer was monitored by ^1H NMR.

Thermal Isomerization Studies

A solution of OA (1mM) and *cis* and *trans*-GFP were prepared in a 2:1 ratio. A 0.5 mM solution solution of the given GFP chromophore in CD_3CN was prepared. These solutions were irradiated using a 310 nm filter and additionally were separately heated at 60 ^oC in water bath. The relative ratios of the given isomers was monitored by ^1H NMR.

Encapsulation studies of alkylated AMIs within octa acids

General Overview of alkylated AMIs within octa acids

Using previously described methods, we synthesized a number of benzylidene-3-methylimidazolidinones ("BMIs") with alkyl groups on both the phenyl ring and C-2 (see Table 1) and exposed them to buffered solutions of OA in D_2O.[11] Complexation of the chromophores is associated with upfield chemical shifts, corresponding to placement of

protons within the shielding region of the hydrophobic (aromatic) cavity (see supplementary information). For reference spectra, acetonitrile-d_3 is used. As we anticipated from earlier studies, the *p*-methyl or *p*-ethyl derivatives exhibited strong

Table 5.1. Substitution pattern of BMIs incorporated in octa acid cavitand.

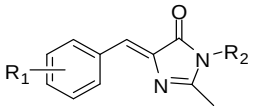

#	R_1	R_2	#	R_1	R_2
1	H	Me	**10**	2-Me	n-Bu
2	2-Me	Me	**11**	2-Me	n-Pent
3	3-Me	Me	**12**	3-Me	n-Pr
4	4-Et	Me	**13**	2-Et	n-Pr
5	2,5-Me	Me	**14**	4-Me	Et
6	4-Me	Me	**15**	4-Et	n-Pr
7	2-Et	Et	**16**	4-Me	n-Pr
8	2-Me	Et	**17**	2-Me	i-Pr
9	2-Me	n-Pr			

shielding of the alkyl groups within the cavity, as did the N-alkyl groups > ethyl (see below). In contrast, *m*- and *o*-alkyl groups were shielded less effectively, suggesting that the para groups anchor the aryl group effectively at one end of the capsule.

Examination of the effect of encapsulation on fluorescence led to relative quantum yields, relative to benzene solution, which were at variance with our expectations based upon anchoring of the aryl groups. Thus neither the *para*-alkyl group nor the *meta*- alkyl group was effective in ameliorating internal conversion. In contrast, the *ortho*-alkyl groups had a dramatic effect, increasing the emission intensity by ca. one order of magnitude.

GFP chromophores, as do certain GFP mutants, undergo relatively efficient cis/trans isomerization.[12] Thus we were intrigued by the possible effect of encapsulation on the photochemistry as well. Indeed, all of the chromophores, which were produced in their initial cis configuration, readily underwent isomerization in CH_3CN to reach a

photostationary state (PSS) with cis:trans ranging from ca. 40:60 to 60:40 (see Table 5.2). In contrast, irradiation in OA capsule produced, in most cases, PSS favoring the less stable trans isomer, reaching 95% trans in the case of **1** or **9** and 98% in the case of **11**.

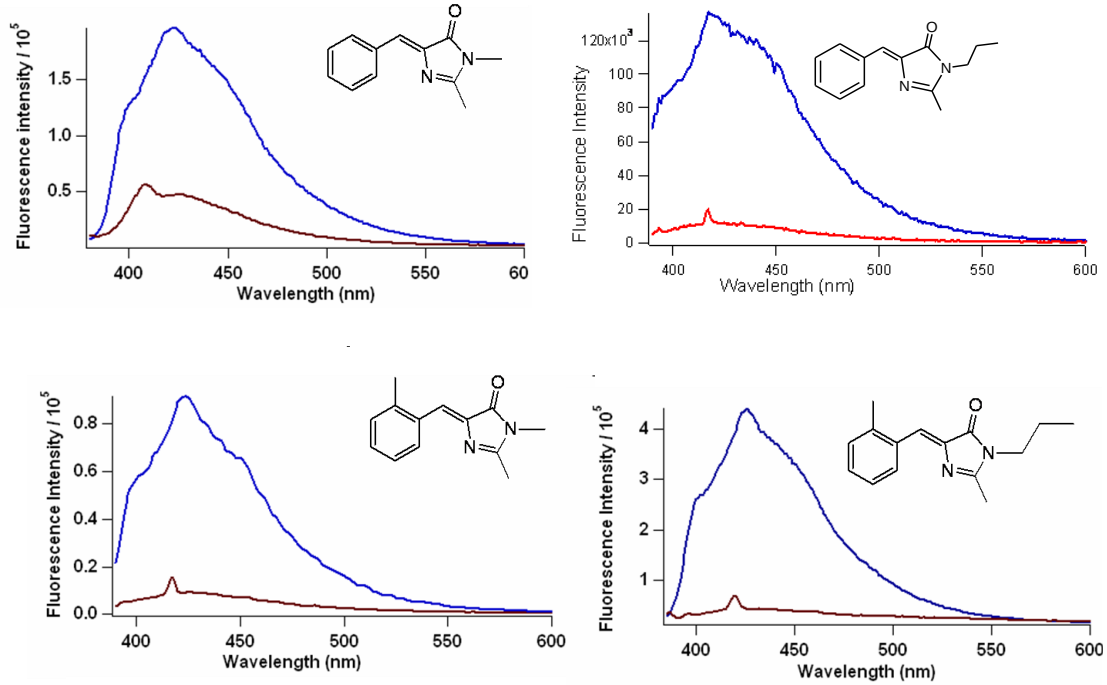

Figure 5.1. Representative emission spectra showing the response of o–Me substituted GFP chromophore and benzyl GFP chromophore (parent compound) in OA (blue) (H:G = 2:1) and in benzene (red). Excitation at 370 nm.

NMR Studies of alkylated AMIs within octa acids

The PSS favoring trans is rationalized by the more efficient sequestration of the two ends of the molecule in the more extended conformation. The OA causes the chemical shifts of the N-alkyl substituents in the cis isomer to be greatly shifted upfield as a result of placement within the shielding region of the aromatic rings. Upon conversion to the trans isomer, the *N*-alkyl protons are shifted downfield, while the C-2 methyl substituent is shifted upfield, reflecting a better fit when the imidazolinone ring is not anchored through the N-alkyl group.

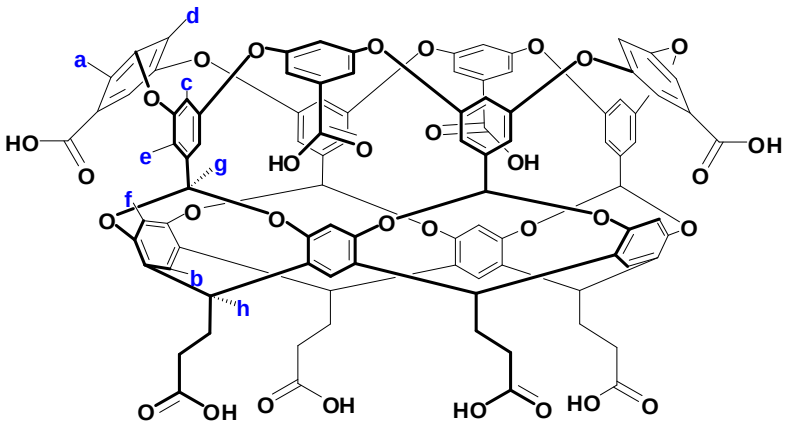

Figure 5.2. Various proton resonances of the host OA are designated as 'a-h'.

Table 5.2. Isomerization ratio,[a] T_{PSS}[b], and emission quantum yields within OA.
[a]monitored from ^{1}H NMR spectra. Irradiations were done by using a 310 nm cutoff filter.
[b]time required to reach PSS.

No.	OA (cavitand)		CD_3CN		Emission
	After irrad. (cis:trans)	T_{PSS} (min)	After irrad. (cis:trans)	T_{PSS} (min)	Φ_f (in OA) x10^{-3}
1	5 : 95	6	50:50	10	5.64
2	22:78	8	43:57	10	0.95
8	22:78	8	58:42	10	3.04
9	6:94	2	39:61	10	4.42
10	24:76	10	39:61	10	3.83
11	2:98	10	39:61	10	1.17

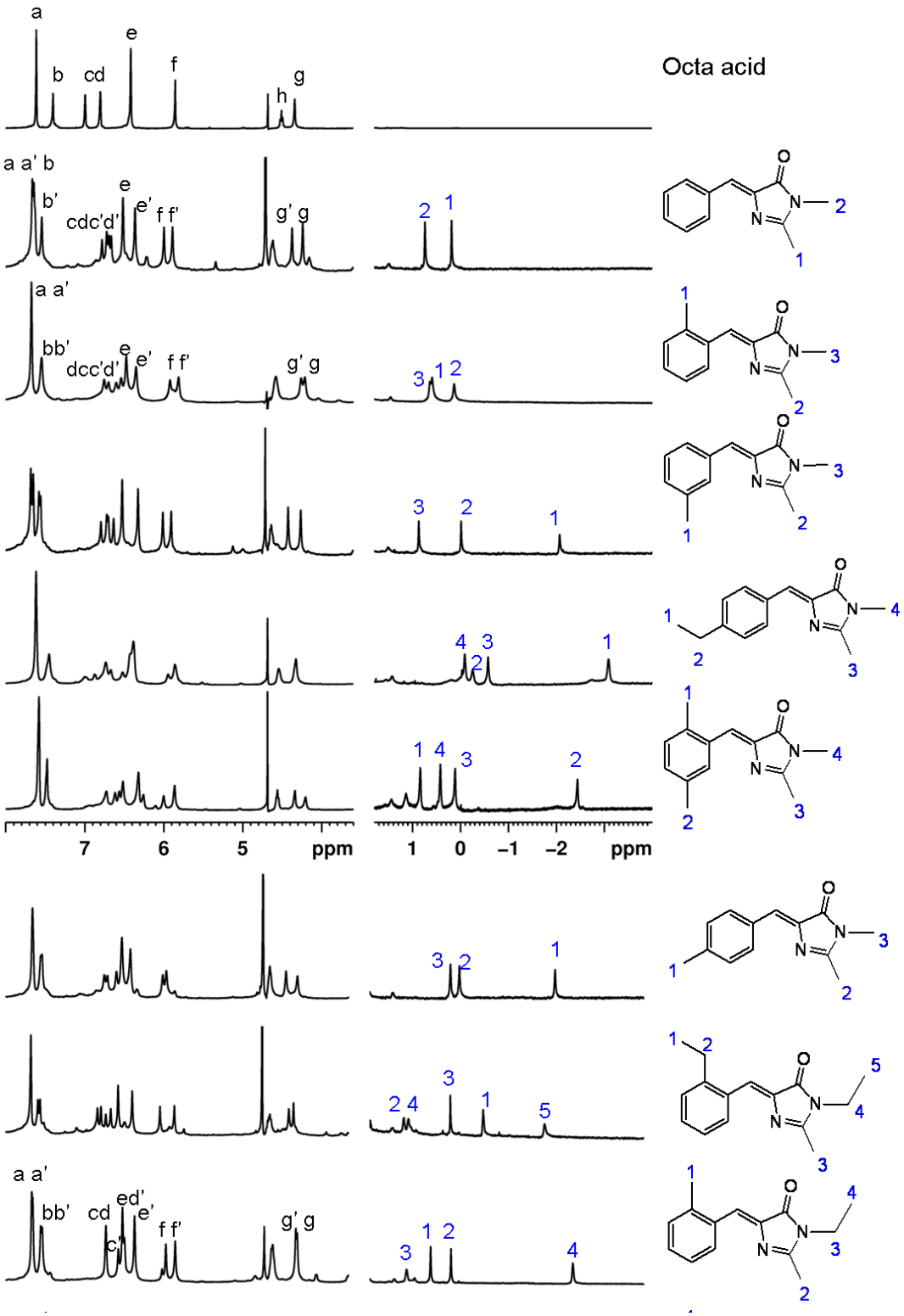
Octa acid
7
6
5
ppm
1
0
–1
–2
ppm

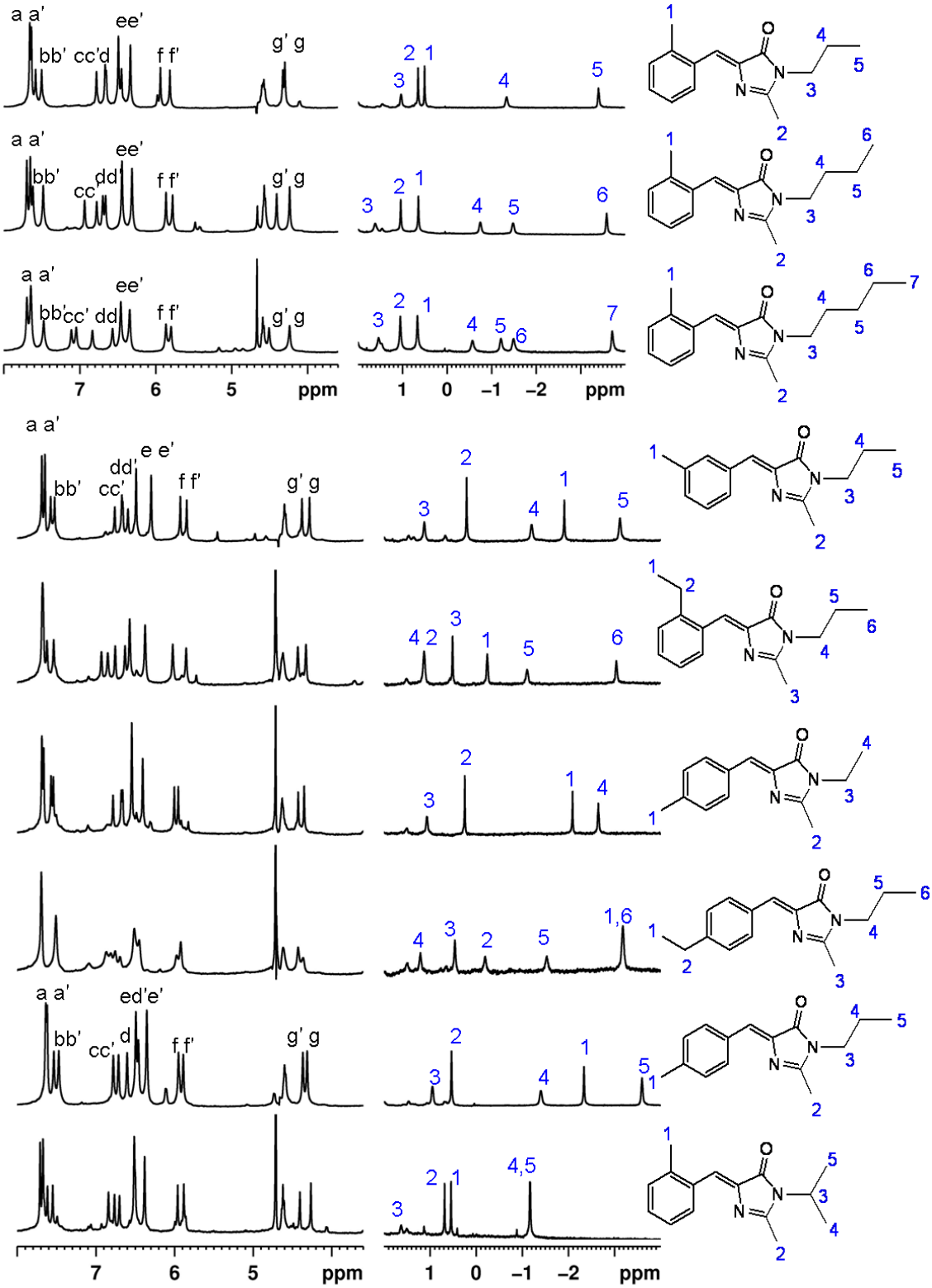

Figure 5.3. ^{1}H NMR (500 MHz) spectra of selected OA-complex of *cis*- isomer of GFP chromophores with OA (H:g = 2:1). [OA] = 1 mM in 10 mM buffer (D_2O).

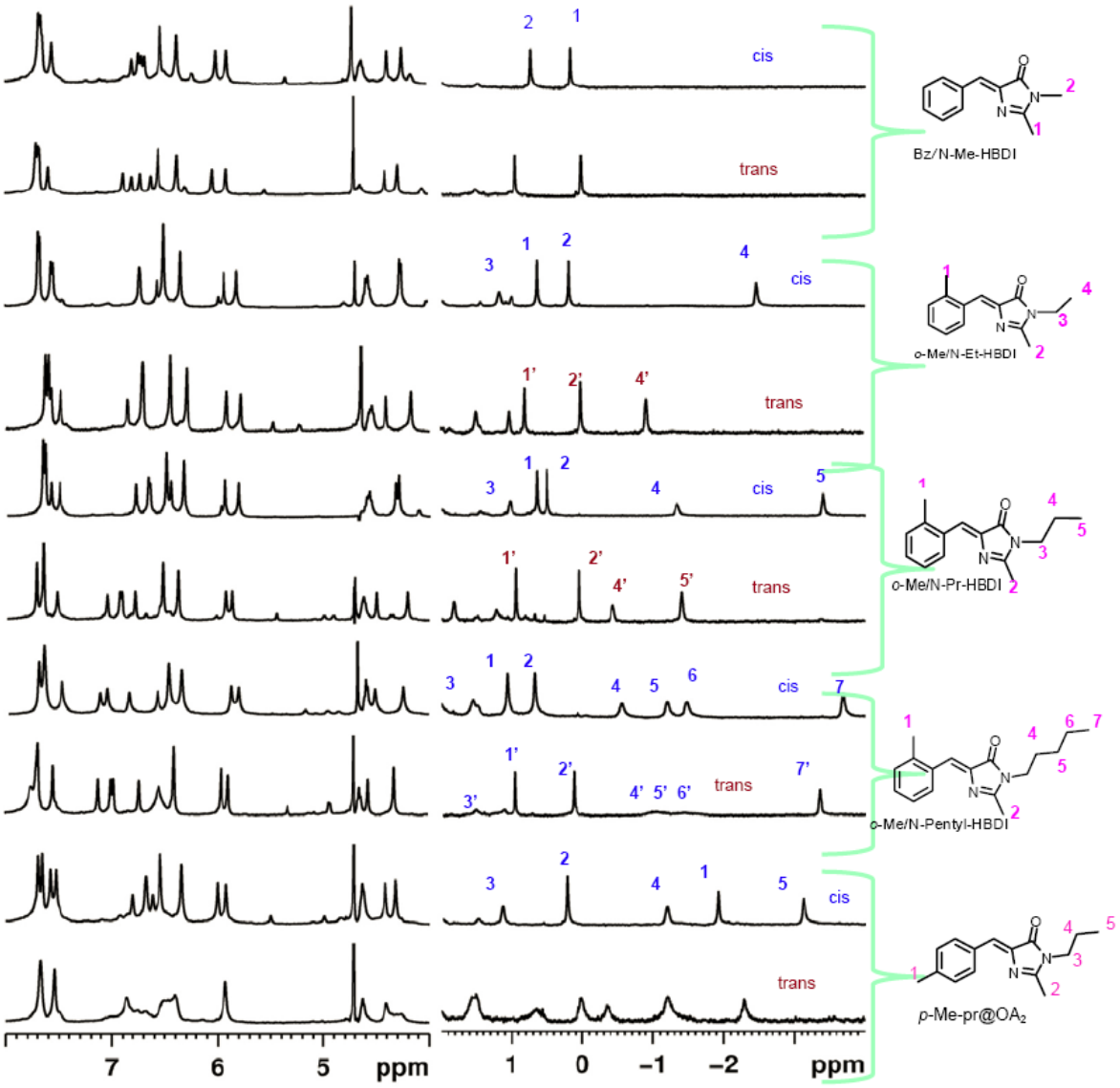

Figure 5.4. ^{1}H NMR spectra of selected OA-complex of cis and trans isomer of given GFP chromophores with OA (h:g = 2:1). Trans signals are denoted with a (‘).

This is further supported by the increasing trans isomer in the case of the o-Me derivative on progressing from methyl through pentyl on the imidazolidinone ring, which packs the molecule more tightly.

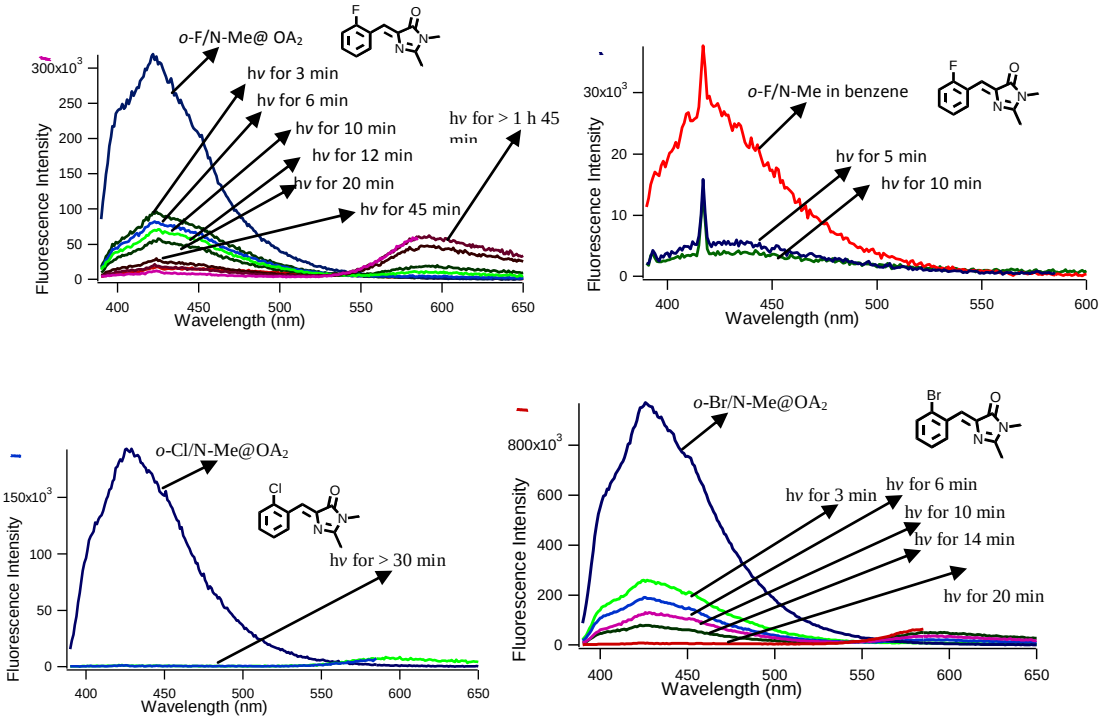

Figure 5.5. Fluorescence emission spectra of photoirradiation of GFP-chromophore in OA and benzeneusing 310 nm filter.

We note, parenthetically, that while the cis isomer is the most stable one in solution, encapsulation of the chromophore drives the photostationary state toward the trans isomer, reflecting the more favorable equilibrium for encapsulation of the trans. Similarly, the slow ground-state isomerization of the chromophore also drives formation of the trans isomer, which becomes the stable form in the presence of the octa acid.

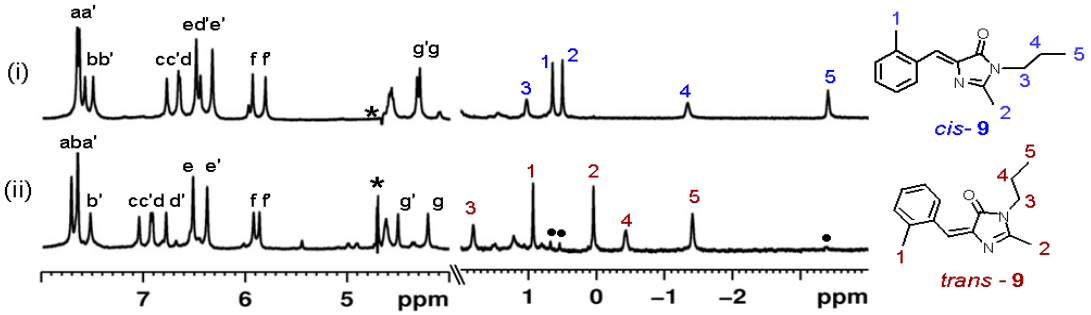

Figure 5.6. ^{1}H NMR (500 MHz, 10 mM sodium tetraborate in D_2O) spectra for the capsular assemblies of (i) *cis*-*o*-Me/N-Pr@OA_2 (9) and (ii) *trans*-*o*-Me/N-Pr@OA_2 (9). (Host resonances are represented as 'a-g'; '●' represents the ~5% of *cis*- isomer and '*' represents the residual water resonances).

Curiously, the propensity for cis/trans isomerization does not correlate readily with internal conversion efficiency. Isomerization of stilbene-like molecules, for instance, is generally associated with formation of a twisted-diradical state which quenches fluorescence.[13] In our case, the presence of an ortho substituent inhibits internal conversion without necessarily inhibiting isomerization. We are forced to conclude that, within the OA capsule, the ortho substituent prevents ready twisting around the single bond (motion φ). Thus when single-bond rotation is prevented, less efficient internal conversion allows either fluorescence or double-bond isomerization to take place. In solution, however, the combination of one-bond flip with efficient single-bond twisting allows both ready isomerization and efficient internal conversion. As we have observed, in the protein a low frequency motion is largely responsible for the loss of fine structure and contributes heavily to internal conversion.[14]

Finally, we note that, in cases where the cis form fluoresces, the PSS also fluoresces, although with an efficiency that requires a much lower quantum yield from the trans form. We note, parenthetically, that so-called switchable fluorescent proteins exhibit similar behavior,[6b,15] with fluorescence almost invariably occurring predominantly from the cis form.

Steric and electronic studies of encapsulated AMIs within octa acids

General Overview of steric/electronic studies of AMIs within octa acids

Following the success of encapsulation of alkylated AMIs, the necessity arose to determine the steric and electronic parameters relative to the substitution patterns. This motivation arose from the observation that ortho substitution gave the greatest emission quantum yield within the alkylated AMIs. To explore this motivation, the electronic and steric effects on excited-state decay by appealing to the fluorescence quantum yields Φ_f^X as a function of substituent X (R_1 and R_2) must be applied. Since $\Phi_f^X = k_f^X/k_{dt}^X$, where k_f^X is the rate constant for fluorescence and k_{dt}^X ($= k_f^X + k_{nr}^X$) is the rate constant for total decay and k_{nr}^X is the non-radiative decay rate constant, we obtain $\Phi^{Xrel} = \Phi_f^X/\Phi_f^H = (k_f^X/k_f^H)/(k_{dt}^X/k_{dt}^H)$. Making the somewhat less than rigorous assumption that the oscillator strengths are not greatly affected by weakly perturbing substituents, we conclude $k_f^X \approx k_f^H$ so that $\Phi^{Xrel} \approx k_{dt}^H/k_{dt}^X$. Strictly speaking, we are interested in non-radiative decay rates, k_{nr}^H/k_{nr}^X, but for relatively low Φ_f^X we can assume that total decay is dominated by internal conversion. Spectroscopic data used for these equations is provided in Table 5.3.

Substituent effects are classically a function of electronic and steric effects, represented by a Linear Free Energy (LFE) relationship (see Equation 1). Here σ is the Hammett substituent constant and ρ is the reaction constant, while χ is a steric constant and α is the related proportionality constant. Steric constants have been represented in a variety of ways, including the Charton ν constants[16] and A-values.[17] However, these generally do not capture the total volume of a substituent, but rather only its steric hindrance, which may be inappropriate for the effect within a confined space. For instance, a methoxy group has a larger volume but a smaller A-value than a methyl group because the nearest neighbor atom is smaller. Instead we deem it more appropriate to represent χ by the change in molecular volume, determined via DFT calculations, upon

Table 5.3. The quantum yield of chromophores in OA (G : H = 1 : 4) and in benzene.

#	Chromophore	Quantum yield		
		Φ_f (in OA) $\times 10^{-3}$	Φ_f (in Benzene)$\times 10^{-3}$	Φ_f (in OA) / Φ_f (in Benzene)
1	H/N-Me	3.3	1.4	2.4
2	*o*-F/N-Me	69.0	4.4	15.7
3	*m*-F/N-Me	125.5	8.8	14.2
4	*p*-F/N-Me	2.3	1.2	1.9
5	*o*-Cl/N-Me	78.0	5.6	13.9
6	*m*-Cl/N-Me	18.8	6.8	2.8
7	*o*-Br/N-Me	137.7	5.3	26.0
8	*m*-Br/N-Me	13.50	6.5	2.1
9	*p*-Br/N-Me	15.4	3.3	4.7
10	*o*-Me/N-Me	1.4	1.0	1.4
11	*m*-Me/N-Me	1.2	1.3	0.9
12	*p*-Me/N-Me	1.7	0.8	2.1
13	*o*-OMe/N-Me	2.3	1.1	2.0
14	*o*-OMe/N-Me	2.3	1.1	2.0
15	*p*-OMe/N-Me	1.0	0.6	1.7
16	*o*-CF_3/N-Me	435.6	38.8	11.2
17	*m*-CF_3/N-Me	75.5	13.1	5.8
18	H/N-Pr	14.7	1.4	11.3
19	*o*-Me/N-Et	3.2	1.3	2.5
20	*o*-Me/N-Pr	10.0	1.5	6.7
21	*o*-Me/N-Butyl	4.9	1.1	4.5
22	*o*-Me/N-Pentyl	2.2	1.2	1.8
23	*m*-Me/N-Pr	2.0	1.4	1.4
24	*p*-Me/N-Pr	2.3	0.9	2.6
25	*m*-F/N-Pr	215.6	8.8	24.5
26	*p*-F/N-Pr	7.3	1.8	4.1
27	*o*-Cl/N-Pr	163.4	5.6	29.1
28	*m*-Cl/N-Pr	20.0	5.8	3.4
29	*o*-Br/N-Pr	183.4	5.2	35.7
30	*m*-Br/N-Pr	7.6	7.1	1.1
31	*p*-Br/N-Pr	28.6	2.9	9.9
32	*o*-OMe/N-Pr	9.0	1.0	9.0
33	*m*-OMe/N-Pr	10.7	2.2	4.9
34	*p*-OMe/N-Pr	1.3	0.6	2.2
35	*o*-CF_3/N-Pr	146.0	41.3	3.5
36	*m*-CF_3/N-Pr	171.2	13.1	13.1

replacing hydrogen with the substituent on benzene in the case of R_1 and replacing the methyl group in toluene by the appropriate alkyl group in the case of R_2.

$$\log(\Phi^{Xrel}) = \log(k_{nr}{}^{X}/k_{nr}{}^{H}) = \sigma\cdot\rho + \alpha\cdot\chi \qquad 1$$

$$\log(\Phi^{Xrel}) \approx \log(k_{nr}{}^{X}/k_{nr}{}^{H}) = \sigma\cdot\rho + \alpha\cdot\chi_1 + \beta\cdot\chi_2 \qquad 2$$

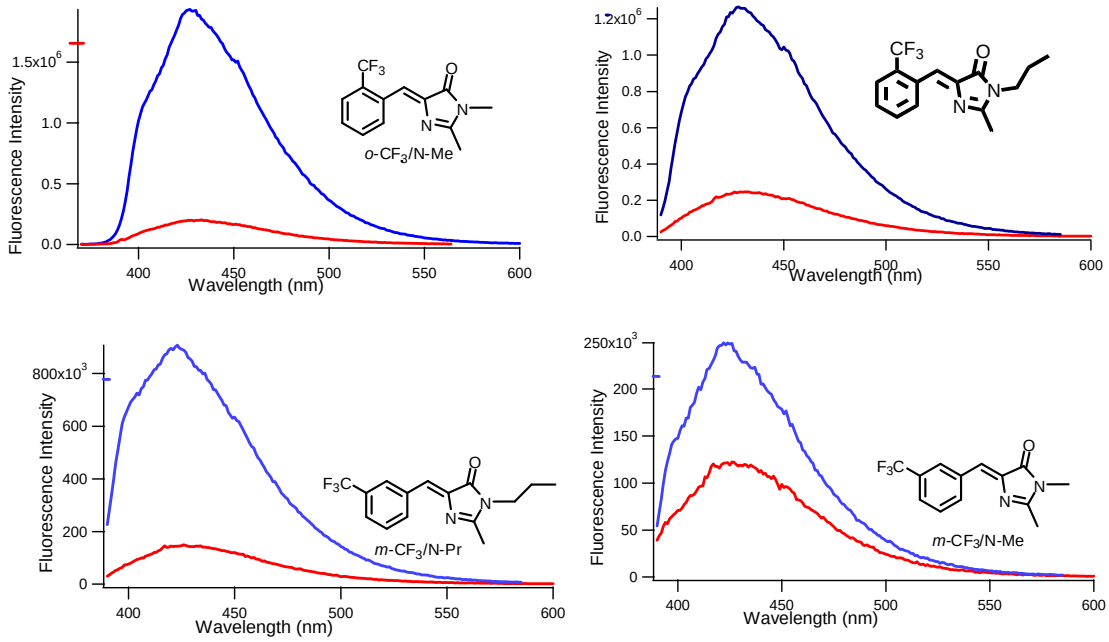

Figure 5.7. Representative emission response showing the spectra of $-CF_3$ substituted GFP chromophore in OA (blue) (H:G = 2:1) and in benzene (red). Excitation at 370 nm.

Use of the Hammett equation for excited-state processes has a somewhat checkered history, and there have been a number of substituent constants proposed for photochemical processes.[18] To determine the relationship between electronic (Hammet parameters) against emission of GFP encapsulated within octa acid cavitands, quantum yields of the GFP- chromophore analogs with a methyl substitution on the N-terminus of the imidazolinone with varying phenyl substitutions were measured in benzene and OA. The data for these experiments is presented in the below tables and tabulated within the chart that follows. The logarithmic value of the ratio of emission intensity of these chromophore with parent compound, unsubstituted benzyl derivative, was plotted with respect to the reported electronic effect (σ) of *meta* and *para* substituted group.

Table 5.4. Fluorescence quantum yield vs. σ in benzene (Hammatt's plot).

Chromophore	Quantum yield in benzene(QY) x 10^{-3}	σ [in X axis]	log (QY/1.4) [in Y axis]
H/N-Me	1.4	0	0
H/N-Pr	1.4	0	-0.0165
m-Me/N-Me	1.3	-0.069	-0.0203
m-Me/N-Pr	1.4	-0.069	-0.00972
p-Me/N-Me	0.8	-0.17	-0.2521
p-Me/N-Pr	0.9	-0.17	-0.20165
p-OMe/Me	0.6	-0.268	-0.3530
p-OMe/Pr	0.6	-0.268	-0.3607
m-OMe/Me	2.2	0.115	0.2049
m-OMe/Pr	2.2	0.115	0.1983
m-F/N-Me	8.8	0.337	0.7963
m-F/N-Pr	8.8	0.337	0.7974
p-F/N-Me	1.2	0.062	-0.0551
p-F/N-Pr	1.8	0.062	0.1203
m-Cl-Me	6.8	0.373	0.6864
m-Cl/N-Pr	5.8	0.373	0.6188
m-Br/Me	6.5	0.393	0.666391
m-Br/Pr	7.1	0.393	0.703942
p-Br/Me	3.3	0.232	0.3760
p-Br/Pr	2.9	0.232	0.3193
m-CF_3/N-Me	13.1	0.43	0.9711
m-CF_3/N-Pr	13.1	0.43	0.9734
p-CF_3/N-Me	23.6	0.54	1.2262

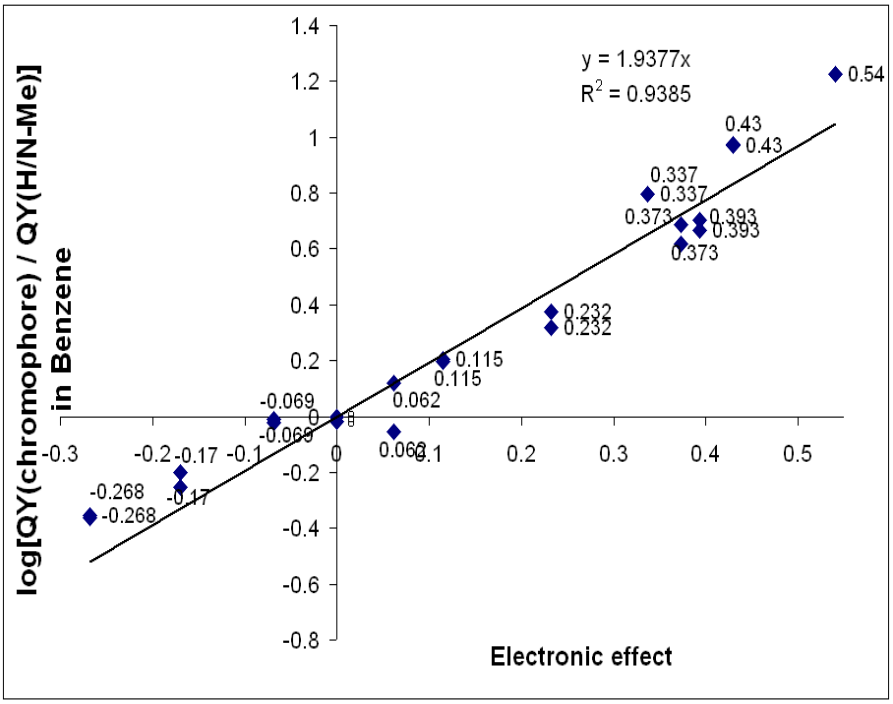

Figure 5.9. Hammett's plot of emission intensity vs. electronic effect (σ) in Benzene.

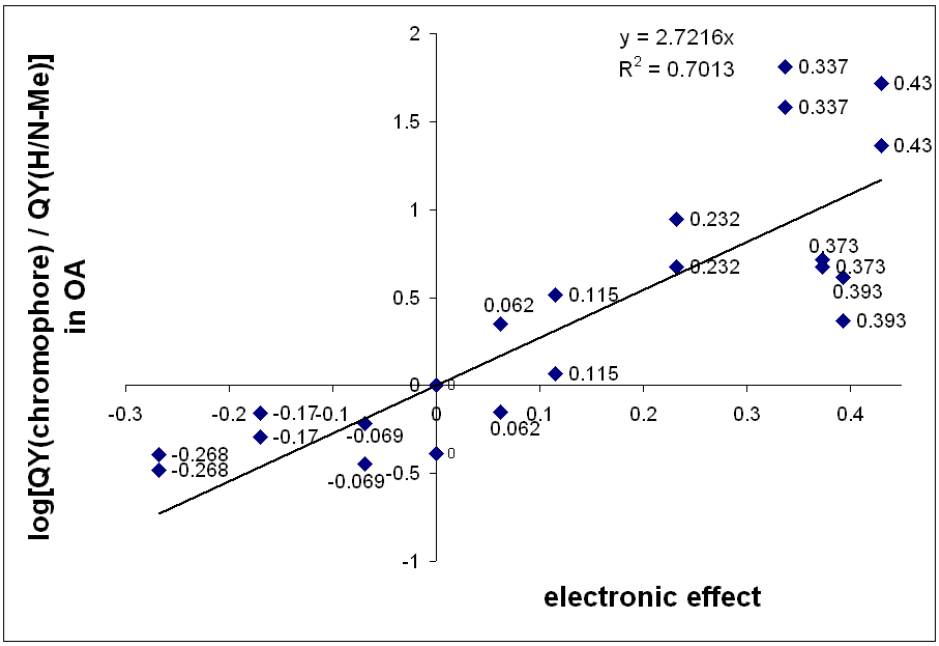

Figure 5.8. Hammett's plot of emission intensity vs. electronic effect (σ) in OA.

Table 5.5. Fluorescence quantum yield vs. σ in OA (Hammatt's plot).

Chromophore	Quantum yield in OA (QY)	σ [in X axis]	log (QY/3.3) [in Y axis]
H/N-Me	3.3	0	0
Bz/N-Pr	14.7	0	-0.38492
m-Me/N-Me	1.2	-0.069	-0.4457
m-Me/N-Pr	2.0	-0.069	-0.21826
p-Me/N-Me	1.7	-0.17	-0.2939
p-Me/N-Pr	2.3	-0.17	-0.15623
m-OMe/Me	3.8	0.115	0.06751
m-OMe/Pr	10.7	0.115	0.5156
p-OMe/Me	15.4	-0.268	-0.4825
p-OMe/Pr	28.6	-0.268	-0.3939
m-F/N-Me	125.5	0.337	1.58
m-F/N-Pr	215.6	0.337	1.81
p-F/N-Me	2.3	0.062	-0.149
p-F/N-Pr	7.3	0.062	0.3487
m-Cl-Me	18.8	0.373	0.7135
m-Cl/N-Pr	20.0	0.373	0.6721
m-Br/N-Me	7.6	0.393	0.36658
m-Br/N-Pr	13.5	0.393	0.616965
p-Br/Me	15.4	0.232	0.6729
p-Br/Pr	28.6	0.232	0.9424
m-CF_3/N-Me	75.5	0.43	1.3636
m-CF_3/N-Pr	171.2	0.43	1.719

The data clearly show that an excellent correlation exists for the chromophores within benzene but this relationship is somewhat muddled when the chromophores are encapsulated within octa acid. As is generally the case in LFEs, we appeal to the success of the method at reproducing data. Moreover, while LFEs are well developed for meta and para substituents, the use of **σ**-values for ortho substituents is fraught with problems, almost all of these have to do with dissecting electronic vs. steric effects.[19] Thus we

adopt the ortho **σ**-values developed by Tribble and Traynham, which are based upon the apparently sterically-independent chemical shifts of phenols.[20]

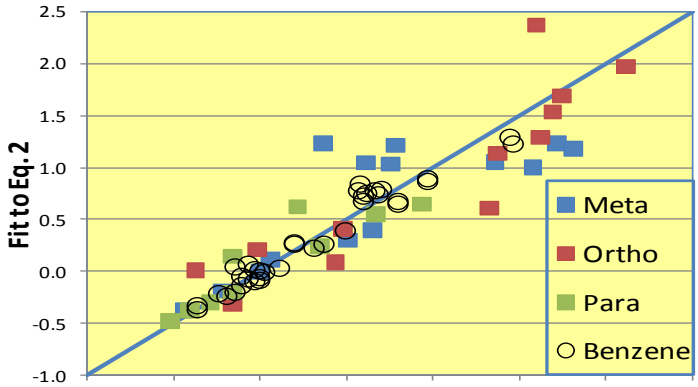

Figure 5.10. Fit of Equation 2 to experimental data.

Table 5.6. Relative contribution of electronic and volumetric factors.

	Host	ρ	α (R_1)	β (R_2)
Ortho	C_6H_6	1.17	0.011	-0.001
Weight		84.1%	15.1%	0.8%
Meta	C_6H_6	1.92	0.002	0.000
Weight		99.7%	0.3%	0.0%
Para	C_6H_6	1.17	-0.001	-0.001
Weight		98.5%	0.4%	1.1%
Ortho	OA	1.88	0.014	0.010
Weight		82.7%	9.1%	8.3%
Meta	OA	3.09	-0.009	0.005
Weight		90.4%	8.1%	1.6%
Para	OA	2.11	0.003	0.003
Weight		96.6%	1.7%	1.7%

Using benzene solvent as a proxy for the aromatic OA interior,[21] we perform a linear regression on Equation 2 for each of the ortho, meta, and para substituents, obtaining the correlation (open circles) shown in Figure 5.10. We now consider the interplay of the steric and electronic factors. Using the sum of the correlation factors $\Sigma_i(\sigma_i\rho_i)^2$, $\Sigma_i(\alpha_i\chi_{1i})^2$, and $\Sigma_i(\beta_i\chi_{2i})^2$, we can estimate the percent contribution to variance of

each factor (see Table 2). First, we consider the substituent effects in benzene. We note that the electronic effect of the substituent **σ** dominates the decay, and the effect of the ortho substituent is similar to that of the para, consistent with the usual ortho/para formalism. Second, the effect of the substituents is almost entirely electronic.

The one exception, of course, is the ortho substituent, where 15.1 % of the variance is due to the steric effect. Again, this is not surprising given the difficulty in dissecting steric from electronic effects in ortho substituents. Third, the N-alkyl substituent (R_2) has almost no effect, in agreement with little steric perturbation of the transition state. Finally, the **ρ**-value is positive and >1, indicating substantial negative charge transfer to the aryl ring in the transition state for decay. Since the excited-state can be represented by a diradical and is known to have significant negative charge transfer to the imidazolidinone ring, it is not surprising that internal conversion would reflect that reverse charge transfer. We now consider the effect of encapsulation. Unlike the results in benzene, the remote N-alkyl substituent has a significant effect (see Table 2), approaching that of the ortho substituent and decreasing in the order ortho>meta>para, as suggested by our previous results.**Error! Bookmark not defined.** Curiously, as we increase the volume in the series R_2 = Me, Et, Pr, Bu, and Pn (pentyl), keeping R_1 = Me, we see a linear increase, then a decrease, in the fluorescence enhancement (see Figure 5.11), reflecting, presumably, the effect of locking, and then overcrowding, the capsule. Parenthetically, we note that the Charton and A-values for propyl, butyl, pentyl are nearly identical,[16] validating our use of molecular volume. For this reason, we restrict our consideration to Me and Pr as *N*-alkyl groups but maintain the linearity with volume as the contribution to the LFE.

Comparing the steric effects for ortho, meta, and para, we see a decreasing steric effect for the phenyl substituent and a more dramatic decrease for the N-alkyl substituent. The "locking" effect we suggested earlier**Error! Bookmark not defined.** is seen more clearly,

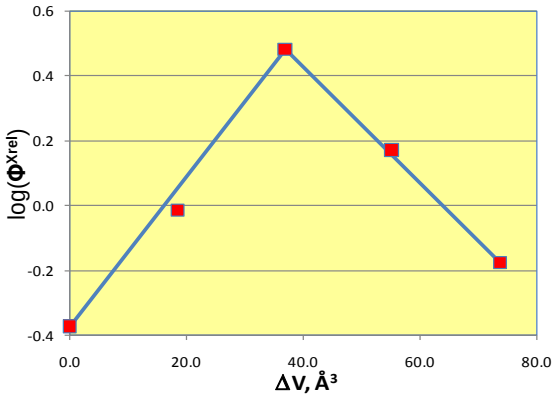

Figure 5.11. Effect of *N*-alkyl substituent.

with the ortho and meta substituents having a major steric effect while the para substituent, which cannot prevent aryl rotation, having less impact.

Finally, we consider the nature of the Hammett ρ-value in the capsule. With some variation for the ortho, meta, and para substituents, which presumably result from different sets of σ-values in each case, in all cases, we note that ρ(OA)>ρ(PhH). Thus internal conversion within the octa acid must require more charge transfer back to the ground state, resulting in the observed higher values for ρ within the octa acid than in benzene solution. This may reflect a larger amount of twist within the capsule than in benzene. Thus the role of the host molecule in rigidifying the chromophore is clearly demonstrated.

In other guest molecules, including biomolecules, we have observed analogous rigidification of FP chromophores which are dependent upon structure in analogous ways. We believe that such topological control of fluorescence represents a diverse method for creating molecular probes.

Introduction to cholate salt aggregates

Bile salts, including sodium cholate (NaCh), are amphiphilic molecules with a concave hydrophilic side and a convex hydrophobic side.[22] By forming aggregates in

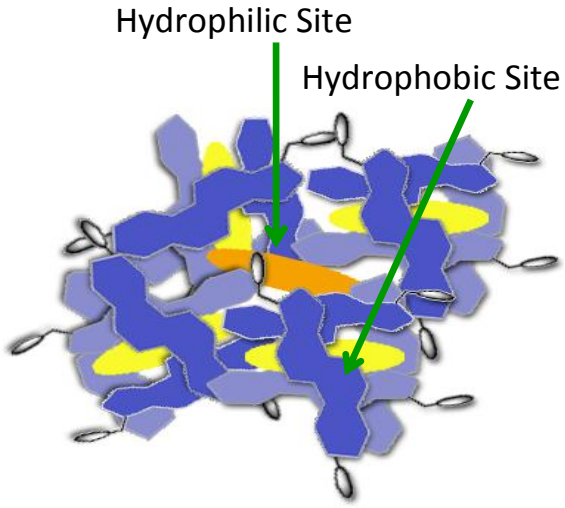

Figure 5.12. Idealized bile salt aggregate showing hydrophobic (yellow) and hydrophilic (orange) binding sites.

aqueous solution, these natural surfactants serve vital biological roles for the solubilization of cholesterol, lipids, and fat-soluble vitamins, and thus are involved in the transport and absorption of important biological molecules.[23] The aggregation of bile salts has been the focus of literature review.[24] A widely adopted model argues that at low concentrations, bile salt monomers aggregate to form single primary binding sites while at high concentrations further aggregation results in the formation of secondary binding sites (See Figure 5.12).[25] Additional models argue the formation of hydrogen bonds between monomer units[26] while a third model argues the interactions are not defined in that multiple interactions may interplay to the overall system.[27] A general classification of the binding sites is marked by their encapsulation of both hydrophobic molecules (hydrophobic site) and hydrophilic molecules (hydrophilic site).[28] Following our success with encapsulation of fluorescent protein chromophore (FP) analogs by synthetic hydrophobic and hydrophilic hosts, based upon substitution patterns,[29] we now report the

binding and turn-on of other analogs by bile salt aggregates, observations which may lead to new tools for studying trafficking in these important systems.

Experimental for cholate salt aggregate studies

Titration Experiments

A series of cholate solutions were prepared by dissolving given aliquots of a NaCh stock solution (400nM) in 0.2M NaCl aqueous solution. The solutions prepared contained a final NaCh concentration of: (0, 10, 20, 30, 40, 60, 75, 100, 125, 150, 175, 200) mM. To each of these solutions, 0.02mL of chromophore stock solution (5mM) was added and allowed to stir capped for 24hrs under ambient conditions. Absorbance and emission spectra of each solution was taken to determine the optimal NaCh concentration for other experimental conditions. These tests were repeated 3 times to ensure reproducibility.

Emission Quantum Yield Studies

Quantum yields were determined the by integrative method by using quinine sulfate standard (λ_{ex} 349 nm, Φ_f = 0.54). In each case the absorbance of the given samples (in 0.2M NaCl solution) were matched to the standard and maintained < 0.1. Quantum yields were calculated using the equation below, where I represents the emission area and η is reflective index of the solvent.

$$\Phi_{sample} = \Phi_{reference} (I_{sample} / I_{reference}) (\eta_{sample} / \eta_{reference})^2$$

Emission "turn-on" Ratio Experiments

For each chromophore, a 0.02mL aliquot of chromophore stock solution in MeOH (5mM) was added to 2.0 mL of a 75mM NaCh / 0.2M NaCl aqueous solution. Baseline fluorescence of studied chromophores was determined using a 0.02mL aliquot of chromophore stock solution in 0.2M NaCl aqueous solution. Both solutions were allowed to stir capped under ambient conditions for 24 hrs before measurement. Relative turn-on ratios were determined by dividing the corrected absolute peak intensity with and

without NaCh present. The reported values in Table 1 within the manuscript represent the average of 3 trials.

Isomerization Study

A 0.02mL aliquot of chromophore stock solution (5mM) was added to 2.0mL of a 75mM NaCh / 0.2M NaCl aqueous solution. The sample was irradiated at 310nm for the given time intervals followed immediately by collection of an emission spectrum.

For the NMR study, a chromophore solution was prepared in CD_3CN and added to a 75mM NaCh / 0.2M NaCl deuterated solution (prepared in D_2O). This solution was irradiated for 24 hrs and following at 310nm which was directly followed by collection of NMR spectrum.

Results of inclusion studies within cholate salt aggregates

AMIs were synthesized using previously described methods (see Table 5.6).[30] Substituents for the FP analogs were chosen based upon the hydrophobic/hydrophilic nature and their steric bulk. For all studies, 0.2 M NaCl aqueous solutions were used and were allowed to stir 24 hrs prior to measurement to allow equilibrium. Encapsulation of the chromophores into the binding sites was marked by a shift in the absorbance maximum compared to that of free chromophore in solution. The hydrophilic chromophores are included in the hydrophilic sites whose interaction with the chromophores is starkly different, thus allowing for significantly more non-radiative processes and lower quantum yields. Additionally, a wide variation in turn-on ratios is noted, with the hydrophobic chromophores most sensitive due to structural changes in the bile salt aggregation site structure upon inclusion. This phenomenon has been noted for bile salts.[4,31]

Table 5.7. FP Analogs and Spectroscopic Characteristics in bile salt aggregates. [a]Intensity(AMI+NaCh)/Intensity(AMI) at λ_{em}. AMI [10^{-5} M] and NaCh [75 mM] was used. [b] λ_{abs} 0.2 M NaCl / λ_{abs} 75 mM NaCh.

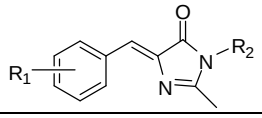

#	R_1	R_2	F/F_o [a]	λ_{abs} [b]	log P[32]
1	H	Me	19	347/352	1.25
2	4-Br	Me	96	353/360	2.06
3	2-CF_3	Me	157	340/354	2.10
4	3-CF_3	Me	75	346/357	2.12
5	4-CF_3	Me	122	348/359	2.15
6	4-OH	Me	2	372/383	0.77
7	2-Br	Me	57	348/359	2.01
8	2-Cl	Me	93	348/359	1.88
9	3-OH	Me	5	354/358	0.75
10	H	n-Pr	44	340/355	2.13
11	2-CF_3	n-Pr	212	340/355	2.98
12	4-OH	n-Pr	5	371/379	1.65
13	2-Cl	n-Pr	167	350/361	2.76

Titration of AMIs with NaCh shows an emission enhancement with increasing concentration, owing to the continuing formation of hydrophobic binding sites.[33]

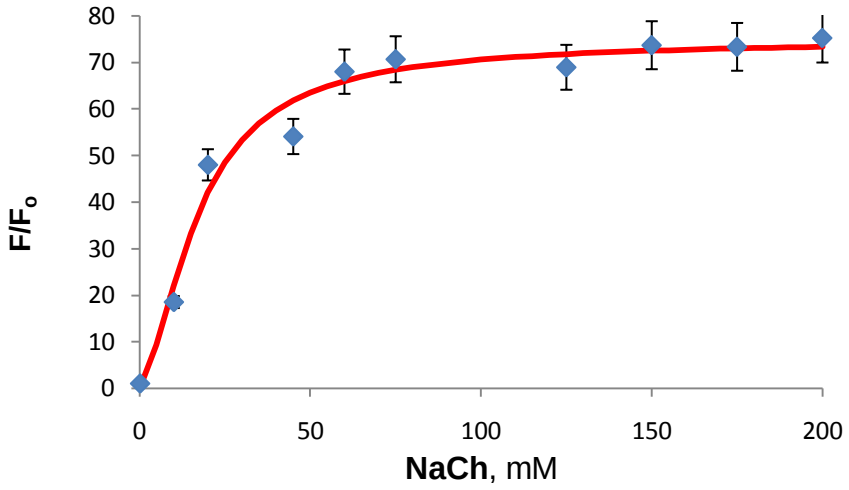

Figure 5.13. Titration of 11 with NaCh in 0.2 M NaCl

Figure 5.13 shows the fluorescence response with **11** where peak enhancement is achieved with increasing cholate concentration up to 75 mM. Using the response of **11** as

a standard, F/F_o ratios were calculated using 75 mM NaCh for all experiments. Support for the inclusion of hydrophobic chromophores into the hydrophobic sites is also shown through spectroscopic shifts in cyclohexane vs. water. Table 5.7 and Figure 5.14 show a distinct red shift in absorbance upon inclusion due to the change in polarity.

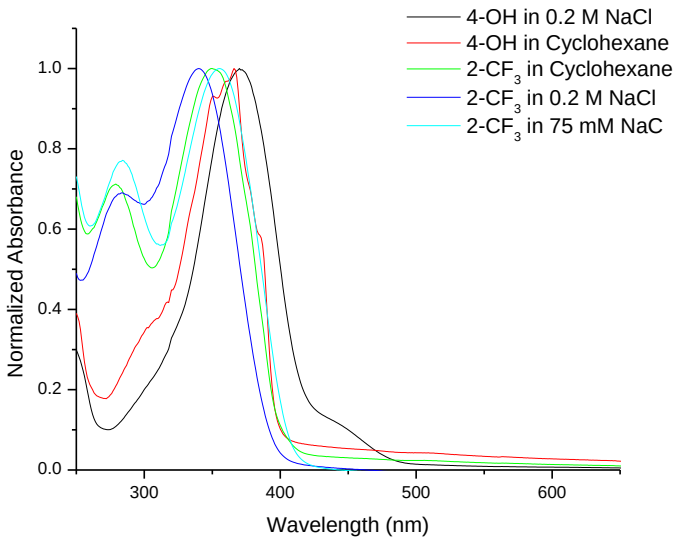

Figure 5.14. Absorbance spectra comparing **11** in NaCh and **11** in cyclohexane. Note that similar shifts are observed when encapsulated within NaCh and dissolved in cyclohexane owing to inclusion into primary aggregates.

An additional bathochromic shift of 7nm is observed compared to cyclohexane, perhaps due to planarization of the chromophore. This result is also rationalized through the higher F/F_o ratios achieved by the hydrophobic chromophores in 75 mM NaCh solution. The data in Figure 5.13 were fit to a two-site cooperative binding model[34] with two dissociation constants (K_d) of 74 mM and 2.0 mM and a saturation ratio of 73.

In solution, rapid deactivation (<1 ps) of FP chromophores is attributed to twisting in the excited state, leading to isomerization and taking the chromophores from the fluorescent cis (Z) isomer to the non-fluorescent (E) isomer.[35] Irradiation of **11** within cholate aggregates shows a quenching of fluorescence, consistent with the conversion of the initially planar cis isomer--the initial conformation of all AMIs--to the non-planar trans isomer.

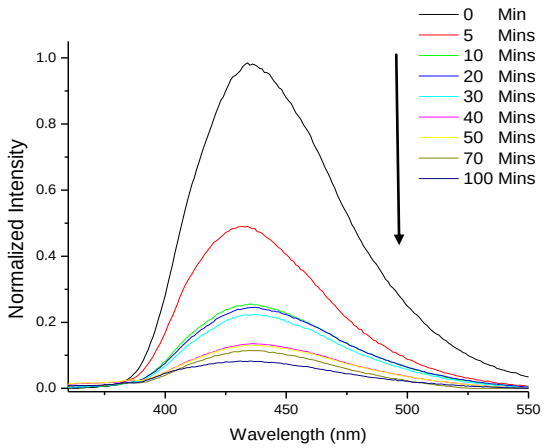

Figure 5.15. Irradiation of **11** in 75 mM NaCh.

This observation is further confirmed by NMR studies which show significant amounts of the trans product produced following irradiation with NaCh present. Additionally, this reinforces the significance of rotation about the formal single aromatic bond toward the overall photophysics of AMI's, since from Figure 5.15 we conclude that inclusion inhibits internal conversion (via blocking rotation about the formal single aromatic bond) but not isomerization, an observation reminiscent of previous work within our group documented in the literature[5].

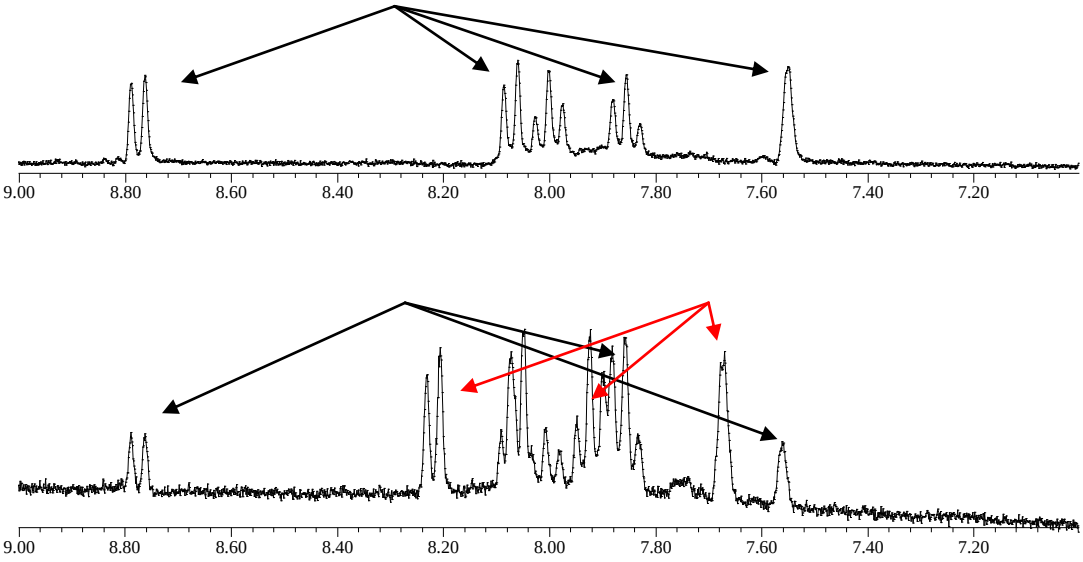

Figure 5.16. NMR spectra of **11** in 75mM NaCh (10% CD_3CN/90% D_2O) with no irradiation and 18 hrs of irradiation at 310 nm. Black arrows indicate cis isomers while red arrows represent trans isomers.

Hydrophobicity is generally indicated by octanol/water partition coefficients (log P values, Table 1) that can be estimated using computational means. While the hydrophobic/hydrophilic substituent of the chromophores dictates their general inclusion into hydrophobic and hydrophilic aggregation sites respectively, a plot of F/F_o vs. log P values (not shown) provides a good correlation of the emission response to the hydrophobic nature of each chromophore. It should be noted that for AMIs **3**, **4**, and **5**, with similar substitutions, the log P is ~2.10, but yields significantly different F/F_o values. This is consistent with the results of Amundson, et al., who showed that packing of NaCh monomers around hydrophobic aromatic guests depends upon the shape and dimensions of guests to provide optimal encapsulation efficiency. We surmise that, for **3** and **11**, the o-CF_3 group provides optimal characteristics, most likely obtaining an optimal packing of the monomer units[36] forming the adaptable aggregate cavity, while the n-Pr substituent provides additional hydrophobicity, yielding an even greater interaction and inhibiting deactivating torsional motions. We note parenthetically that a similar "ortho" effect holds

true in bile salts and in "octa acid" cavities,[29] again reinforcing the role of twisting about the single bond.

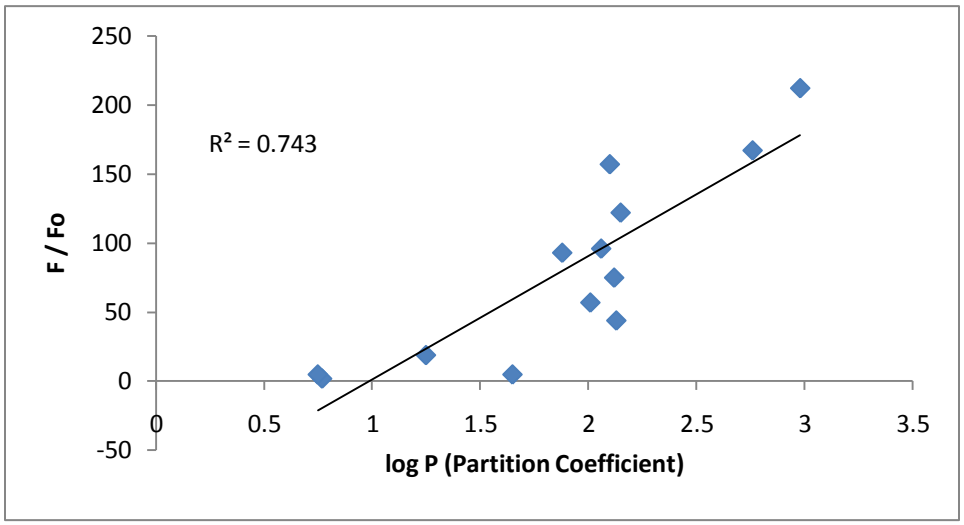

Figure 5.17. Log P values vs. F / Fo enhancement ratios of all compounds studied noting the correlation observed between emission enhancement and electronic parameters.

It is tempting to conclude that the two-site binding model obtained from the fit of Figure 5.13 represents the affinity for the two binding sites in the cholate aggregates. However, the equilibria for such complexes is extraordinarily complicated, and our data, because of the scatter in these slowly equilibrating systems, do not allow a definitive conclusion. Nevertheless, the use of such turn-on small fluorophores certainly provides an additional tool to study such complexation.

In summary, following encapsulation of FP chromophores, bile salts inhibit non-radiative decay processes and thus restore some of the EQY by mimicking β-barrel conditions. Encapsulation of hydrophobic chromophores is markedly different due to the guest interactions, which recently were shown to dictate the guest-aggregate system[37], with the bile salt aggregate resulting in planarization of the chromophore and a distinct EQY enhancement. The biological role of bile salts within the body allows them to act as delivery systems for biologically active aromatic compounds. Structure-activity

relationships of these compounds with macromolecular transporters can provide significant information allowing for the optimal design of compounds for both probes and medicinal purposes. Additionally, various biological processes and interactions involving bile salts remain mysterious. AMIs within this study allow us to develop fluorescent probes for bile salt aggregates to examine these interactions. Of specific note are the interactions of bile salts with nuclear receptors and other proteins, for which our group has developed fluorescent probes different from those highlighted in this manuscript.[38] It is instructive to note that in vivo, bile salts are mixed with lipids and behave differently than bile salts in solution.[39] With this, the interaction of the chromophores will be different; however the presence of restrictive aggregate sites should encapsulate the chromophores, yielding a fluorescence response and making these useful probes within these systems. This work shows that FP chromophores provide a convenient tool for studying the macromolecular environment of bile salts. These results demonstrate that the subtle interplay between the bile salt host and its guests is significant to the details of the encapsulation complex.

Conclusions

As noted from the octa acid and cholate salt aggregate studies, the inclusion of GFP chromophore analogs into supramolecular spaces results in a emission quantum yield enhancement. Irradiation studies show that this enhancement is a function of hindering the free rotation about the aryl-single bond.

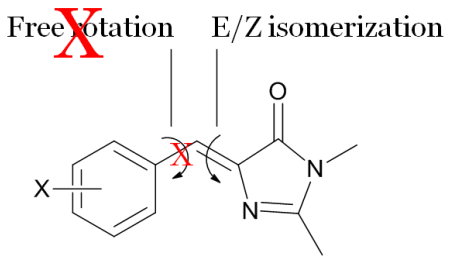

Figure 5.18. Depiction of photophysical processes within GFP chromophore analogs upon inclusion within supramolecular hosts.

In both studies cis/trans isomerization was noted in both cases leading to a quenching of fluorescence due to the conversion of the fluorescent cis isomer to the non-fluorescent trans isomer. Studies within the octa acid showed that this was even further accelerated due to the stabilizing of the trans isomer within the cavitand. Regardless of the consequence of irradiation, the results within this chapter show that inclusion within a host system provides a means to restore a portion of the emission quantum yield rendering these chromophores useful for application as fluorescent probes. Additionally, these results show the importance of the free rotation about the single aryl bond as a method of deactivation possibly contributing to the rapid internal conversion experienced by these chromophores outside of the protective β-barrel. The consequences of this chapter will be the foundation of multiple chapters within this dissertation that follow this one on the motivation that inclusion of these chromophores coverts these essentially non-fluorescent molecules into fluorescent ones providing the framework for molecular probes.

References

[1] Baldridge, A.; Samanta, S.R.; Jayaraj, N.; Ramamurthy, V.; Tolbert, L.M. *J. Am. Chem. Soc.* **2010**, *132(5)*, 1498-1499.

[2] Baldridge, A.; Samanta, S.R.; Jayaraj, N.; Ramamurthy, V.; Tolbert, L.M. *J. Am. Chem. Soc*. **2011,** *133*, 712-715.

[3] Baldridge, A.; Amador, A.; Tolbert, L.M. *Langmuir* ASAP.

[4] Enoki, S.; Saeki, K.; Maki, K.; Kuwajima, K. *Biochemistry* **2004**, *43*, 14238-14248.

[5] Martin, M. E.; Negri, F.; Olivucci, M. *J. Am. Chem. Soc.* **2004**, *126*, 5452-5464.

[6] (a) Liu, R. S. H. *Acc. Chem. Res.* **2001**, *34*, 555-562. (b) Maddalo, S. L.; Zimmer, M. *Photochem. Photobiol.* **2006**, *82*, 367-372.

[7] (a) Gibb, C. L. D.; Gibb, B. C. *J. Am. Chem. Soc.* **2004**, *126*, 11408-11409. (b) Jayaraj, N.; Zhao, Y.; Parthasarathy, A.; Porel, M.; Liu, R. S. H.; Ramamurthy, V. *Langmuir* **2009**, *25*, 10575-10586.

[8] Lerestif, J. M.; Perrocheau, J.; Tonnard, F.; Bazureau, J. P.; Hamelin, J. *Tetrahedron* **1995**, *51*, 6757-6774.

[9] Unfortunately, use of the more hydrophilic *p*-OH group (R_2=Me) precluded complexation.

[10] Parthasarathy, A.; Kannumalle, L. S.; Ramamurthy, V. *Org. Lett*., **2007**, *9*, 5059-5062.

[11] Baldridge, A.; Kowalik, J.; Tolbert, L.M. *Synthesis* **2010**, *14, 2424-2436.*

[12] (a) He, X.; Bell, A. F.; Tonge, P. J. *FEBS Lett.* **2003**, *549*, 35-38. (b) Henderson, J.N.; Ai, H.-W.; Campbell, R. E.; Remington, S. J. *Proc. Natl. Acad. Sci. USA* **2007**, *104***,** 6672-6677. (c) Andresen, M.; Stiel, A. C.; Trowitzsch, S.; Weber, G.; Eggeling, C.; Wahl, M. C.; Hell, S. W.; Jakobs, S. *Proc. Natl. Acad. Sci. USA* **2007**, *104***,** 13005-13009.

[13] (a) Waldeck, D. H. *Chem. Rev.* **1991**, *91*, 415-36 (b) Saltiel, J.; Waller, A S.; Sears, D. F., Jr *J. Am. Chem. Soc.***1993**, *115*, 2453-65.

[14] Stavrov, S. S.; Solntsev, K. M.; Tolbert, L. M.; Huppert, D. *J. Am. Chem. Soc.* **2006**, *128*, 1540-1546.

[15] (a) Stiel, A. C.; Trowitzsch, S.; Weber, G.; Andresen, M.; Eggeling, C.; Hell, S. W.; Jakobs, S.; Wahl, M. C. *Biochem J.* **2007**, *402*, 35-42. (b) Nam, K.-H.; Kwon, O. Y.; Sugiyama, K.; Lee, W.-H.; Kim, Y. K.; Song, H. K.; Kim, E. E.; Park, S.-Y.; Jeon, H.; Hwang, K. Y. *Biochem. Biophys. Res. Comm.* **2007**, *354*, 962-967.

[16] (a) Charton, M. *J. Am. Chem. Soc.* **1975**, *97*, 1552–1556. (b) Charton, M. *J. Org. Chem.* **1976**, *41*, 2217–2220.

[17] Eliel, E. L.; Wilen, S. H.; *Stereochemistry of Organic Compounds*, Wiley, 1993, p. 696.

[18] Cordes, T.; Schadendorf, T.; Priewisch, B.; Rueck-Braun, K.; Zinth, W. *J. Phys. Chem. A.* **2008**, *112(4)*, 581-588.

[19] Gustafson, J. L.; Sigman, M. S.; Miller, S. J. *Org. Lett*. **2010**, *12*, 2794-2797.

[20] Tribble, M. T.; Traynham. J. G. *J. Am. Chem. Soc.* **1969**, *91*, 379-388.

[21] Porel, M.; Jayaraj, N.; Kannumalle, L.S.; Maddipatla, M.V.S.N.; Parthasarathy, A.; Ramamurthy, V. *Langmuir* **2009**, *25*, 3473-3481.

[22] Small, D. M.; Penkett, S. A.; Chapman, D. *Biochim. Biophys. Acta* **1969**,*176*, 178–189.

[23] O'Connor, C. J.; Wallace, R. G. *Adv. Colloid Interface Sci.* **1985**, *22*, 1–111.

[24] Small, D.M.; Penkett, S.A.; Chapman, D. *Biochim Biophys. Acta* **1969**, 176, 178-189.

[25] Kawamura, H.; Murata, Y.; Yamaguchi, T.; Igimi, H.; Tanaka, M.; Sugihara, G.; Kratohvil, J. P. *J. Phys. Chem.* **1989**, *93*, 3321–3326.

[26] (a) Bonincontro, A.; Briganti, G.; D'Archivio, A.A.; Galantini, L.; Giglio, E. *J Phys. Chm. B* **1997**, 101, 10303-10309. (b) Bottari, E.; D'Archivio, A.A.; Festa, M.R.; Galantini, L.; Giglio, E. *Langmuir* **1999**, 15, 2996-2998.

[27] Matsuoka, L.; Moroi, Y. *Biochim, Biophys. Acta* **2002**, 1580, 189-199.

[28] (a) Amundson, L. L.; Li, R.; Bohne, C. *Langmuir* **2008**, 24, 8491-8500. (b) Kolehmainen, E. *J. Colloid Interface Sci.* **1985**, *105*, 273–277.

[29] (a) Baldridge, A.; Samanta, S. R.; Jayaraj, N.; Ramamurthy, V.; Tolbert, L. M. *J. Am. Chem. Soc.* **2010**, *132*(5), 1498-1499. (b) Baldridge, A.; Samanta, S. R.; Jayaraj, N.; Ramamurthy, V.; Tolbert, L. M. *J. Am. Chem. Soc.* **2010**, *132*(5), ASAP, **DOI:** 10.1021/ja1094606.

[30] (a) Lerestif, J. M.; Perrocheau, J.; Tonnard, F.; Bazureau, J. P.; Hamelin, J. *Tetrahedron* **1995**, *51*, 6757-6774. (b) Baldridge, A; Kowalik, J.; Tolbert, L.M. *Synthesis* **2010**, *14*, 2424-2436.

[31] Waissbluth, O.L.; Morales, M.C.; Bohne, C. *Photochem. Phtobio.* **2006**, 82, 1030-1038.

[32] Log P values were determined using Molinspiration.

[33] Shurtenberger, P.; Mazer, N.; Ka¨nzig, W. *J. Phys. Chem.* **1983**, *87*, 308-315.

[34] Dill, K.; Bromberg, S. *Molecular Driving Forces: Statistical Thermodynamics in Chemistry, Physics, Biology, and Nanoscience*. Garland Science Press, 2002.

[35] (a) He, X.; Bell, A. F.; Tonge, P. J. *FEBS Lett.* **2003**, *549*, 35-38. (b) Henderson, J.N.; Ai, H.-W.; Campbell, R. E.; Remington, S. J. *Proc. Natl. Acad. Sci. USA* **2007**, *104***,** 6672-6677. (c) Andresen, M.; Stiel, A. C.; Trowitzsch, S.; Weber, G.; Eggeling, C.; Wahl, M. C.; Hell, S. W.; Jakobs, S. *Proc. Natl. Acad. Sci. USA* **2007**, *104***,** 13005-13009.

[36] Li, G.; McGown, L.B. *J. Phys. Chem.* **1994**, *98*, 13711-13719.

[37] Li, R.; Carpentier, R.; Newell, E.D.; Olague, L.M.; Heafey, E.; Yihwa, C.; Bohne, C. *Langmuir* **2009**, 25, 13800-13808.

[38] Duraj-Thatte, A.; Baldridge, A.; Azizi, B.; Tolbert, L.M. *J. Med. Chem.*, Submitted.

[39] Trauner, M.; Boyer, J.L. *Physiol Rev.* **2003**, *83*, 633-671.

CHAPTER 6

FLUORESCENCE RESPONSE PROFILING OF THE GREEN FLUORESCENT PROTEIN CHROMOPHORE AND ITS DERIVATIVES.

This work was carried out in collaboration with the laboratory of Dr. Young-Tae Chang at the National University of Singapore. All compounds were synthesized within the Tolbert lab and emission data gathered at the Chang lab. Data analysis and manuscript composition were equally shared. For the purposes of maintaining the same terminology as found within publication, "BDI" is used throughout this chapter but refers to the same compounds as is found throughout this manuscript as "AMI".

Introduction

The green fluorescent protein (GFP) has attracted great attention as a fluorescent probe to study diverse problems in molecular biology.[2] Taking advantage of the autocatalytic cyclization and oxidation of three amino acid residues to form a natural chromophore (*p*-hydroxybenzylideneimidazolone, *p*-HBDI),[3] GFP generates a very effective and intense fluorescence signal. Nevertheless, investigation of the chromophore reveals distinct differences in fluorescent properties between wild type GFP (wt GFP) and the synthetic chromophore. The fluorescent quantum yield of the synthetic chromophore is much less and shows solvent and temperature dependence.[4] Studies suggest that the GFP β-barrel structure plays a critical role in protecting the chromophore and reducing conformational flexibility and thus diminishing the rate of radiationless decay. Within the rigid β-barrel structure, *p*-HBDI undergoes excited-state proton

transfer (ESPT)[5] from the chromophore to the adjacent residue, E222,[6] resulting in very efficient emission from the anionic form. To exploit the GFP chromophore as a sensor, this environment-sensitive fluorescence turn-on phenomenon is utilized in several bi-molecular fluorescence protein sensors.[7] However, the chromophore itself is rarely scrutinized to detect analyte molecules directly.

We envisioned that synthetic GFP chromophore derivatives have superior potential as small molecule fluorescent sensors, due to their desirable characteristics such as extremely low background in aqueous solution and high environmental sensitivity. Low background sensors are favorable in many applications due to their high signal-to-noise ratio.[8] Recently, the Burgess group has demonstrated that, by incorporating an *ortho*-aryl BF_2 group which complexes with the imidazolone nitrogen, the conformation of the chromophore can be frozen and the emission turned on.[9] Similarly, Chou has demonstrated that incorporation of an *ortho* hydroxyl group can turn on the emission through intramolecular hydrogen bonding, leading in the latter case to excited-state proton transfer.[10] We concluded that such fluorescent turn-on detection for target molecules could be attained by specific interactions between GFP chromophores and analyte molecules, which instead of freezing the conformation intrinsically through the structure of the chromophore, instead freezes the conformation after complexation with the analyte. Indeed, recently we observed that proper construction of a hydrophobic chromophore could increase the fluorescence response by a factor of 15.[11] Accordingly, it would be of interest to investigate the chromophore modes of interaction with endogenous biomolecules, despite most previous studies, which focused on the nature of chromophore within the β-barrel in wt GFP. In this paper, we report a systematic analysis of the fluorescence change of the GFP chromophore and its derivatives when applied for sensing of biologically relevant analytes.

In order to develop an effective fluorescent sensor, an important criterion that must be met is high selectivity for a target molecule. The selectivity of probes can be

evaluated by parallel comparison against a similar class of analytes. For example, Chang's group validated selectivity of their metal probes by carefully comparing various kinds of metal ions together with the target metal ions.[12] Many examples of diversity-oriented fluorescence sensors were discovered by *in vitro* fluorescence response assessments prior to their application in a biological system.[13,14] It is noteworthy that the fluorescence response profile against diverse analytes could provide ultimate selectivity information. While similar profiling approaches have been widely used in drug discovery,[15] their application to develop fluorescent sensors is still at an early stage.

The challenge of large-scale, quantitative investigation of fluorescence sensor development requires a practical high-throughput screening platform. For this, a microplate assay platform is chosen due to its unique advantages, such as simple adoption for any kind of analytes, flexible throughput control, and the homogeneous interaction between a sensor molecule and an analyte. To broaden the scope of fluorescent sensor discovery, we collected 10 classes of bio-analytes (total 94 individual analytes) for high-throughput *in vitro* screening and performed an assay in 384-well microplates. From the resulting profile, we identified fluorescent small molecule sensors for pH, human serum albumin (HSA), and total ribonucleic acid (RNA).

Experimental

General Experimental

All reagents were purchased from commercial sources and used without further purification. The solvents used for the spectroscopy experiments were of spectrophotometric grade. Spectroscopic properties of compounds and *in vitro* high-throughput screenings were performed on SpectraMax M2 plate reader (Molecular Devices Inc.). NMR spectra for the synthetic component were recorded using a Varian

Mercury spectrometer (300MHz) and processed using MestRe-C 2.3a. Mass spectroscopy data was completed by the Georgia Tech Mass Spectroscopy Center.

Materials and Methods

All the materials were obtained from commercial suppliers (Aldrich) and used without further purification. The solvents used for the spectroscopy experiments were of spectrophotometric grade. Spectroscopic properties of compounds and *in vitro* high-throughput screenings were performed on SpectraMax M2 plate reader (Molecular Devices Inc.).

Quantum Yield Measurements

Quantum yields were calculated by measuring the integrated emission area of the fluorescent spectra and comparing that value to the area measured for FITC in EtOH when excited at 489 nm ($\Phi_{FITC} = 0.93$). Quantum yields for the BDI compounds were then calculated using equation (1), where F represents the area of fluorescent emission, n is reflective index of the solvent, and Abs is absorbance at excitation wavelength selected for standards and samples.

$$\Phi_{flu}^{sample} = \Phi_{fl}^{reference}\left(\frac{F^{sample}}{F^{reference}}\right)\left(\frac{\eta^{sample}}{\eta^{reference}}\right)\left(\frac{Abs^{reference}}{Abs^{sample}}\right)$$

Determination of the dissociation constant

The fluorescent emission spectra with various concentrations of **BDI** compounds were measured on a SpectraMax M2 plate reader. The fluorescent titration curve was fitted to the standard equation using Graphpad Prism v5 software. The bound fraction (X) of fluorescent sensor at each concentration was determined using the equation:

$$X = \frac{F_c - F_o}{F_{sat} - F_o}$$

where F_c and F_o are the fluorescence intensities of a given concentration of **BDI** compounds with and without target analyte, respectively. F_{sat} is the fluorescence intensity at the same concentration of **BDI** compounds when fully bound with target analyte. F_{sat}

was determined by fluorescence titration at each concentration with a series concentration of analyte. The results were plotted according to a non-linear fitting curve equation (3)

$$F = F_o + (F_{sat} - F_o)([BDI]) / (K_D + [BDI])$$

where K_D is dissociation constant, [BDI] is concentration of **BDI** compound.

***In vitro* Fluorescence Screening**

BDI compounds (100 μM) were screened in 20 mM HEPES, pH 7.4. Fluorescence intensities were measured using a SpectraMax M2 plate reader in 384-well format. Excitation was provided at each compound's excitation range, and emission was obtained starting from at least 30 nm longer wavelengths from the excitation. All the analytes were tested at four serial concentrations depending on the endogenous concentration of the analyte (Table 6.1). Every analyte was prepared same day prior to the fluorescence experiment to minimize sample contamination. For detailed protocols refer to the supporting information.

Solubility test

A 1mg sample of the chromophore was added to 10 mM DMSO in a 1.5 ml microcentrifuge tube (note that if the molecule is not fully dissolved it is reported as "Solubility Problem in DMSO"). For the molecules fully soluble in 10 mM DMSO solution, 1μl of 1 mM DMSO solution was placed into a 0.5 ml microcentrifuge tube, and 99 μl of HEPES (20 mM, pH 7.4) was added to give 100 uM final concentration solution. In the event precipitation occurred upon adding the solution to the buffer a note of ("Solubility Problem in HEPES") was recorded, otherwise the compound was tested for emission response reproducibility.

Fluorescence spectrum reproducibility test.

Using the stock solutions prepared in the previous section, 1 μl of stock was placed into one well of transparent 96-well plate, and 99 μl of HEPES (20 mM, pH 7.4)

added to provide 100 μM final concentration solution. Successive dilutions of this stock solution were done to produce testing concentrations of 1 and 10 μM final concentration. These solutions and finished 96-well plates were placed into the plate reader for analysis.

***In vitro* fluorescence response screening.**

All analyte samples were prepared daily. The analyte solutions were placed into 4 separate deep-well pates according to the analyte map depends on the concentration (Figure 6.1). The initial Plate A was prepared followed by dilution from Plate A to give Plate B, C, D respectively (Plate A: the highest concentration, Plate B: 2nd highest concentration, Plate C: 3rd highest concentration, Plate D: the lowest concentration set). For testing 200 μl of 10 mM dye stock solution was titrated into a reservoir, and 3.8 ml of HEPES buffer added. The dye concentration for all experiments was 500 μM. Approximately 10 μl of 500 uM dye solution was transferred into each well of the plate. For combinatorial analysis, 40 μl of analyte solutions were transferred to designated positions of 384-plate using Precision™ Microplate Pipeting System (Biotek Inc.). The plates were incubated for 10 min at room temperature and the emission spectra measured.

Table 6.1. In vitro screening analyte molecules and their classes.

Analyte class	Individual analyte molecules [**concentrations**]
Control	Distilled water, HEPES (10 mM, pH 7.4)
Viscosity	Glycerol **[volume %: 25 %, 18.75 %, 12.5 %, 6.25 %]**
pH	pH 2, 3, 4, 5, 6, 7, 8, 9, 10, 11
Nucleotides and nucleosides	Adenosin, AMP, ADP, ATP, Cytidine, CMP, CDP, CTP, Guanosine, GMP, GDP, GTP, Uridine, UMP, UDP, UTP, Sodium phosphate, sodium pyrophosphate, Sodium triphosphate, cyclic AMP, cyclic GMP **[100 uM, 50 uM, 25 uM, 12.5 uM]**
Genetic macromolecules	single strand DNA (ssDNA) double strand DNA (dsDNA) transfer RNA (t-RNA) total RNA **[1mg/ml, 0.5mg/ml, 0.25mg/ml, 0.12mg/ml]**

Table 6.2. Continued

Peptides	HA tag (YPYDVPDYA) HA12CA5 tag (CYPYDVPDYA) His tag (HHHHHH) HisG tag (HHHHHG) VSV-G tag (YTDIEMNRLGK) V5 tag (CGKPIPNPLLGLDST) IQ tag (IQSPHFF) AP tag (KKKGPGGLNDIFEAQKIEWH) FLAG tag (DYKDDDK) cMyc tag (EQKLISEEDL)	**[100 μg/ml, 50 μg/ml, 25 μg/ml, 12.5 μg/ml]**
Protein	Human Immunoglobulin G (human IgG) Bovine Immunoglobulin G (bovine IgG) Human serum albumin (HSA) Bovine serum albumin (BSA) holo-Transferrin apo-Transferrin Insulin Histone Hemoglobin Ubiquitin Myoglobin Fibrinogen Cytochrome C	**[1mg/ml, 0.5mg/ml, 0.25mg/ml, 0.12mg/ml]**
Metal ions	NaCl, KCl, $MgCl_2$, $ZnCl_2$, $FeCl_2$, $CaCl_2$	**[5 mM, 1 mM, 200 μM, 40 μM]** **[100 μM, 20 μM, 4 μM, 0.8 μM]**
Oxido-reduction related molecules	Ascorbic acid DL-dithiothreitol (DTT) L-Glutathione reduced form (GSH) L-Glutathione oxidized form (GSSG) Nicotinamide adenine dinucleotide (NAD) Sodium hypochlorite (NaOCl) Potasium dioxide (KO_2) Hydrogen peroxide (H_2O_2) Iron (II) with hydrogen peroxide (Fe^{2+}+H_2O_2) 2,2-azobis(2-methylpropionamidine) dihydrochloride (AAPH)	**[5 mM, 1 mM, 200 μM, 40 μM]**
Pesticides	Bitertanol Buprofezin Carbaryl Diazinon Dimethoate Ethoprophos Hexythiazox Phosalone	**[10 μM, 5 μM, 2.5 μM, 1.2 μM]**
Miscellaneous molecules	Heparin Caffeine gamma-aminobutyric acid (GABA) Monosodium glutamate (MSG) Histamine, Dopamine Glucose, Glucose phosphate Fructose, Fructose phosphate	**[1 mg/ml, 200 μg/ml, 40 μg/ml, 8 μg/ml]** **[5 mg/ml, 1 mg/ml, 0.2 mg/ml, 40 μg/ml]** **[10 mM, 2 mM, 400 μM, 80 μM]**

The screening was done using a 96-well plate that was arranged using the analyte concentrations from Table 6.1 as shown in arrangement in Figure 6.1.

96-well plate	1	2	3	4	5	6	7	8	9	10	11	12
A	Adenosine	AMP Sodium	ADP Sodium	ATP Disodium	IgG (human)	IgG (bovine serum)	HA tag	HA 12CA5	pH 2	pH 3	pH 4	pH 5
B	Cytidine	CMP Sodium	CDP Sodium	CTP Sodium	HSA	BSA	His tag	HisG tag	pH 6	pH 7	pH 8	pH 9
C	Guanosine	GMP Sodium	GDP Sodium	GTP Sodium	Transferrin holo	Transferrin apo	VSV-G tag	V5 tag	pH 10	pH 11	HEPES 7.4	water
D	Uridine	UMP Disodium	UDP Sodium	UTP Sodium	Insulin	Histone	IQ tag	AP tag	GSH	GSSG	NAD	NADH
E	P Sodium	PP sodium	PPP sodium	CytoC bovine heart	Hemoglobin	Ubiquitin	FLAG	cMyc	Ascorbic acid	DTT	NaOCl	ROO-
F	cAMP	cGMP	bitertanol	Buprofezin	Myoglobin	Fibrinogen	Histamine	Dopamine	Heparin	KO2	H2O2	Fe2+ with H2O2
G	ss DNA	tRNA	Carbaryl	diazinon	Hexythia-zox	Phosalone	Caffeine	GABA	MSG	Na+	Mg2+	Fe2+
H	ds DNA	total RNA	dimethoate	Ethopro-phos	Glucose	Glucose 6 phosphate	Fructose	Fructose 6 phosphate	Glycerol	K+	Zn2+	Ca2+

Figure 6.1. Plate map of analyte stock solutions. NADH was excluded in this BDI study because fluorescence emission of NADH was overlapped with most of BDI compounds.

Results and Discussion

Design of BDI Compounds

The endogenous GFP chromophore contains two aromatic moieties, a *para*-hydroxy benzene and an imidazolinone ring linked by a methine group. Based on these building block structures, 41 benzylideneimidazolinone (**BDI**) derivatives were synthesized with substitution patterns highlighted in Table 6.2. Since a lot of benzaldehyde building blocks are commercially available, we could easily maximize structural diversity of R1 moiety. Each **BDI** compound shares a common core moiety, however each analog has distinct structures that may provide unique fluorescent turn-on

phenomena by interacting with target molecules. Synthesis of the **BDI**s was carried out by a 2 + 3 cycloaddition of the corresponding aromatic Schiff base with the imidate as highlighted in Chapter 2 of this thesis.[16]

Photophysical Properties in Solution

The spectroscopic properties of **BDI** compounds were examined and are summarized in Table 6.2. As previously reported, most **BDI** compounds show very low extinction coefficients and fluorescence quantum yields in ethanol. Each of these compounds absorbs in the visible range, with λ_{max} (abs) between 341 nm and 440 nm and has fluorescence emission ranging from 464 nm to 599 nm.

BDI compounds that consist of either 4-diethylamino (**BDI 24)** or 4-dimethylamino (**BDI 25, 33, 35)** exhibit significantly longer absorption max wavelength than other derivatives ($\Delta\lambda_{abs}$ = 71.7 nm between the mean absorbance wavelength of **BDI 24**, **25**, **33**, and **35** compared to other compounds). The notable red shift of the absorbance indicates the elongated "push-pull" electronic conjugation from the aminobenzyl group.

Table 6.2. Substiution patterns and spectroscopic properties of BDI compounds. [a]All data were measured in ethanol with the presence of 1% DMSO as co-solvent. The fluorescence quantum yield was determined using FITC as a standard (Φ_{fl} = 0.93 in 0.1 M NaOH).

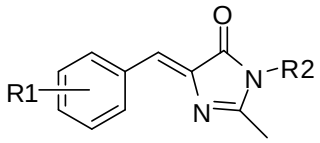

BDI #	R1	R2	λ_{abs} (nm)	λ_{em} (nm)	ε (M^{-1} cm^{-1})	ϕ
1	4-OH	Me	368	473	2,596	0.0060
2	4-OMe	Me	367	490	12,961	0.0018
3	4-OAc	Me	350	472	5,106	0.0045
4	4-CO_2H	Me	356	474	5,913	0.0085
5	4-OBz	Me	368	476	9,611	0.0020

Table 6.2. Continued

6	3,5-*t*-Bu/4-OH	Me	373	471	8,888	0.0021
7	3-OH	Me	365	469	1,857	0.0247
8	2-(N)/4-OH	Me	359	481	3,805	0.0485
9	4-Me	Me	348	471	7,105	0.0044
10	3-Me	Me	348	468	5,499	0.0050
11	2-Me	Me	349	472	5,630	0.0034
12	2,4-Me	Me	352	472	5,630	0.0036
13	2,5-Me	Me	357	478	4,360	0.0041
14	4-Et	Me	353	478	6,733	0.0032
15	2-CF_3	Me	341	490	3,826	0.0455
16	3-OMe	Me	355	510	9,501	0.0041
17	2,3-OMe	Me	352	579	6,251	0.0471
18	2,4,5-OMe	Me	413	527	5,894	0.0111
19	2,5-OMe	Me	396	548	3,799	0.3062
20	4-NO_2	Me	376	599	4,869	0.2008
21	4-Cl	Me	352	472	6,598	0.0060
22	2-F	Me	351	475	6,299	0.0096
23	4-CN	Me	361	475	5,498	0.2490
24	4-$N(Et)_2$	Me	438	527	12,817	0.0065
25	4-$N(Me)_2$	Me	430	527	13,529	0.0029
26	1-naphthyl	Me	374	476	2,247	0.2080
27	2-naphthyl	Me	369	483	9,026	0.0048
28	2-quinoline	Me	372	476	3,784	0.0971
29	1-naphthyl	Et	378	464	5,214	0.0039
30	4-OH	n-Pr	369	476	10,783	0.0018
31	4-Me	n-Pr	351	470	8,334	0.0034
32	4-*i*-Pr	n-Pr	353	509	6,434	0.0039
33	4-$N(Me)_2$	n-Pr	433	504	8,604	0.0739
34	4-OH	n-Bu	371	476	10,739	0.0018
35	4-$N(Me)_2$	n-Bu	440	505	10,063	0.0650
36	4-OH	n-Pentyl	371	503	9,031	0.0019
37	4-OH	$C_3H_6N(Me)_2$	372	471	4,867	0.0029
38	4-OH	$C_3H_6N(Me)_3$	369	472	4,091	0.0035
39	4-OH	n-$C_{11}H_{22}OH$	369	554	8,007	0.0020
40	4-OH	n-C_{16}	371	504	6,723	0.0020
41	3-OH	n-C_{16}	353	474	3,328	0.0112

High throughput *in vitro* fluorescence response profiling

Prior to experimentation, the solubility of all compounds was validated in 100 μM concentration of HEPES buffer (20 mM HEPES with 1% of the DMSO stock solution at

pH 7.4). Under these conditions, all 41 **BDI** compounds avoided precipitation, and the absorbance/fluorescence spectra exhibited reproducible peak shape in spite of their extremely weak extinction coefficients and low quantum yields.

To systematically investigate the fluorescence response profile of **BDI** compounds, 10 classes of analytes related to various biological processes were screened. The analyte classes were (i) pH standard solutions, (ii) viscous buffer solution, (iii) nucleotides and nucleosides, (iv) nucleic acids, (v) peptides, (vi) proteins, (vii) metal cations, (vii) oxidation-reduction related molecules, (viii) pesticides, and (ix) miscellaneous analytes, totaling 94 individual analyte molecules (Table 6.1). Each analyte was tested at four serial concentrations together with a given concentration of **BDI** compounds to determine the dose response dependence on their endogenous concentration or effective concentration, and these fluorescent emission intensities were compared with the value of chromophore itself in the buffer solution. Additionally, the entire concentration-response pattern was used for investigation of the selectivity among the different sets of analytes.

Fluorescence spectra were obtained using a monochromator-based fluorescence microplate reader not only to investigate emission spectra change, but also to increase throughput.[17] Excitation wavelengths of individual **BDI** molecules were determined based on their maximum wavelength of absorbance in 20 mM HEPES. It should be noted that maximum wavelength of excitation and emission used *in vitro* screening are different from the values in Table 6.1 due to the solvent effect. Fluorescence emission spectra were measured for all **BDI** compounds and 94 analytes at 4 concentrations. In order to facilitate the broad use of this data, a fluorescence response profile database was configured. Primary screening results of total spectra were stored in the database, and changes to the emission spectrum were visualized by a heat map method. A heat map is a graphical representation of fluorescence fold change using two color codes to simplify complexity of data. Green represents an increase of emission intensity, while red

represents a decrease in emission intensity. In this two-color profile, the fluorescence response pattern against 94 analytes could be easily evaluated. For instance, Figure 6.2 shows the *in vitro* fluorescence response profile of **BDI 8**, which showed strong pH dependence with a fluorescence increase in acidic media as well as showing a fluorescence increase in the presence of one metal cation and two miscellaneous analytes in a dose dependent manner. The concentration dependent response pattern is useful to evaluate the quality of an assay, and allows for the determination of dynamic ranges and sensitivity of probes.[18] For those analytes that showed remarked response, further experiments were pursued to determine the sensitivity for selective sensor application. The given profiles were analyzed for structure fluorescence response relationships.

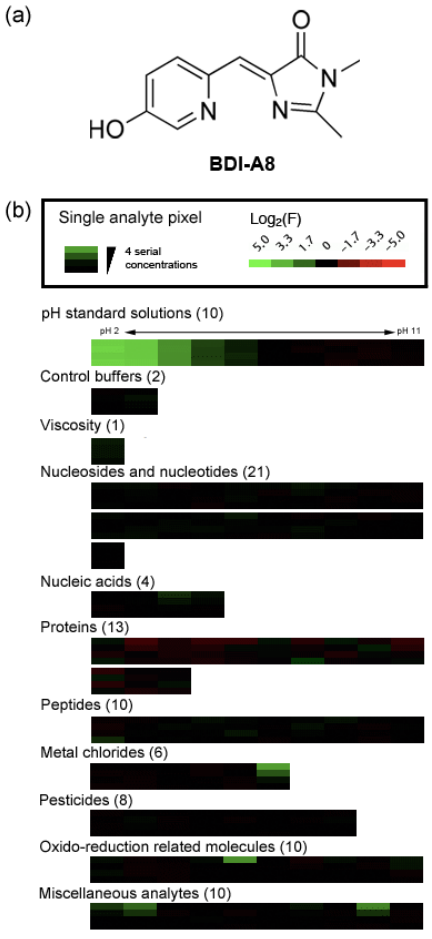

Figure 6.2. (a) Structure of BDI 8, and (B) *in vitro* fluorescence response profile of BDI 8. The number inside the parenthesis indicates the number of individual analytes. Green color represents fluorescence intensity increase, and red color represents fluorescence

decrease as denoted in the scale bar. Four serial concentrations were stacked in the same column in a dose dependent manner. Fluorescence intensity fold change was obtained at 520 nm (λ_{ex} = 370 nm). For detail decoding table, refer Figure 6.1.

Fluorescence response profile and structural relationship

The present profile allows for evaluation of the fluorescence intensity change of a given **BDI** compound with its structural building blocks. In pH profiles, all amino benzyl containing **BDI** compounds (**BDI 24** and **25**) revealed strong fluorescence quenching in acidic conditions, which most likely is induced by *N*-protonation (Figure 6.3, $\Phi_{pH=2}$ **BDI 24** = 0.002, $\Phi_{pH=7}$ **BDI 24** = 0.021). Compounds containing different functional groups in the *ortho* position showed a distinct pH dependent pattern. Four functional moieties were compared within a given series of equivalent R2 substitutions including compounds of: methyl (**BDI 11**, **12**, **13**), trifluoromethyl (**BDI 15**), fluoro- (**BDI 22**), and methoxy- (**BDI 17**, **18**, **19**), with fluorescence quenching in acidic solution observed for only *ortho*-methoxy compounds (Figure 6.5). Single atom substitution in the aromatic ring also induced dramatic changes in the fluorescence response patterns. The wt-GFP chromophore, **BDI 1**, showed slight emission enhancement in basic media, however, its pyridine derivative, **BDI 8**, exhibited a strong emission enhancement in acidic solution (Figure 6.2, $\Phi_{pH=2}$ **BDI 8** = 0.786, $\Phi_{pH=7}$ **BDI 8** =0.008). Likewise, we observed an emission decrease from the quinoline derivative (**BDI 28**), whereas the naphthalene derivative (**BDI 29**) showed minimal pH response (Figure 6.3).

Similar structural analysis could also be performed based on the structure of analytes. Within the miscellaneous analyte class, primary amines caused fluorescence enhancement at high concentration for most **BDI** compounds (Figure 6.3). Since the pH changes induced by two primary amines, dopamine and histamine, were already included in the pH profile, it is believed that **BDI** compounds share common interaction modes with those primary amines. Another notable response is the hydrophobic interaction with macromolecules. Many fluorescent small molecules, including 8-

aminonaphthalenesulfonamide or rosamine compounds, show non-specific fluorescence increase to hydrophobic proteins such as albumin.[14] Conversely, most **BDI** compounds

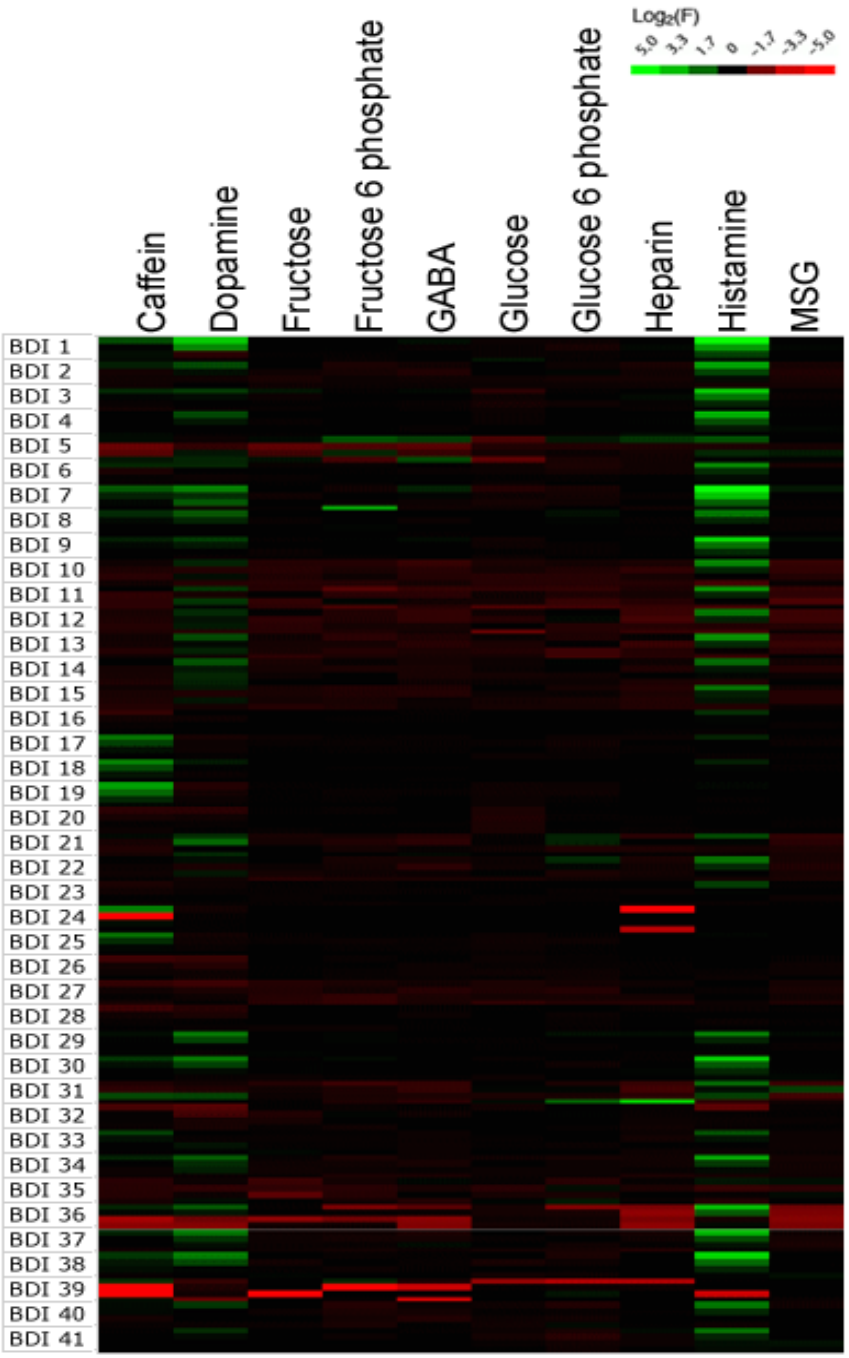

exhibited fluorescence quenching towards albumins. Considering the fluorescence enhancement in wt-GFP stimulated by rigidifying the chromophore structure, this profile implies that protein analytes do not have a common binding pocket for the **BDI** scaffold.

Figure 6.3. Heat map profile of mis s. Most BDI compounds exhibit fluorescence intensity increa at contain primary amine m**Figure 6.4**. Heat map profile of genetic macromolecule class.

The results of these analyses demonstrate that the profiles generated are useful to analyze the relationship between fluorescence responses and structural characteristics in both analytes and probes. With this general response pattern information, we further sought to discover selective fluorescence turn-on sensors.

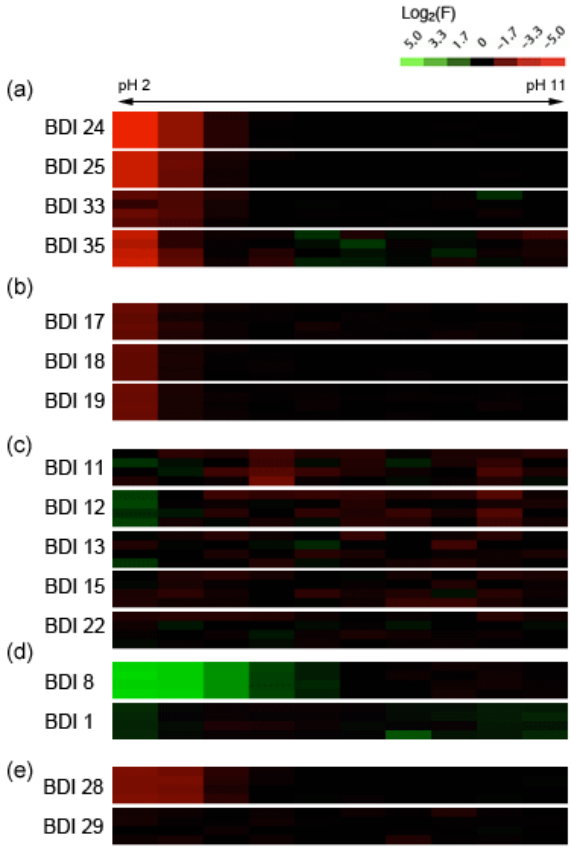

Figure 6.5. Heat map profiles of pH response from **BDI** compounds containing (a) *para*-amino benzyl, (b) *ortho*-methoxy moieties, and (c) other functional group in the *ortho* position. Fluorescence profile comparison between homocyclic and heterocyclic rings; (d) *p*-hydroxyl benzyl and *p*-hydroxyl pyridine derivatives, (e) naphthalene and quinoline derivatives.

Fluorescence sensor discovery from the profile

To be maximally useful, the fluorescence response profile should allow for the discovery of novel sensor molecules. Since we initially classified analytes in terms of the nature of the individual analyte, it was straightforward to compare fluorescence response

within the same class of analytes. In this study, we found two sensor molecules from separate analyte classes that warranted further investigation.

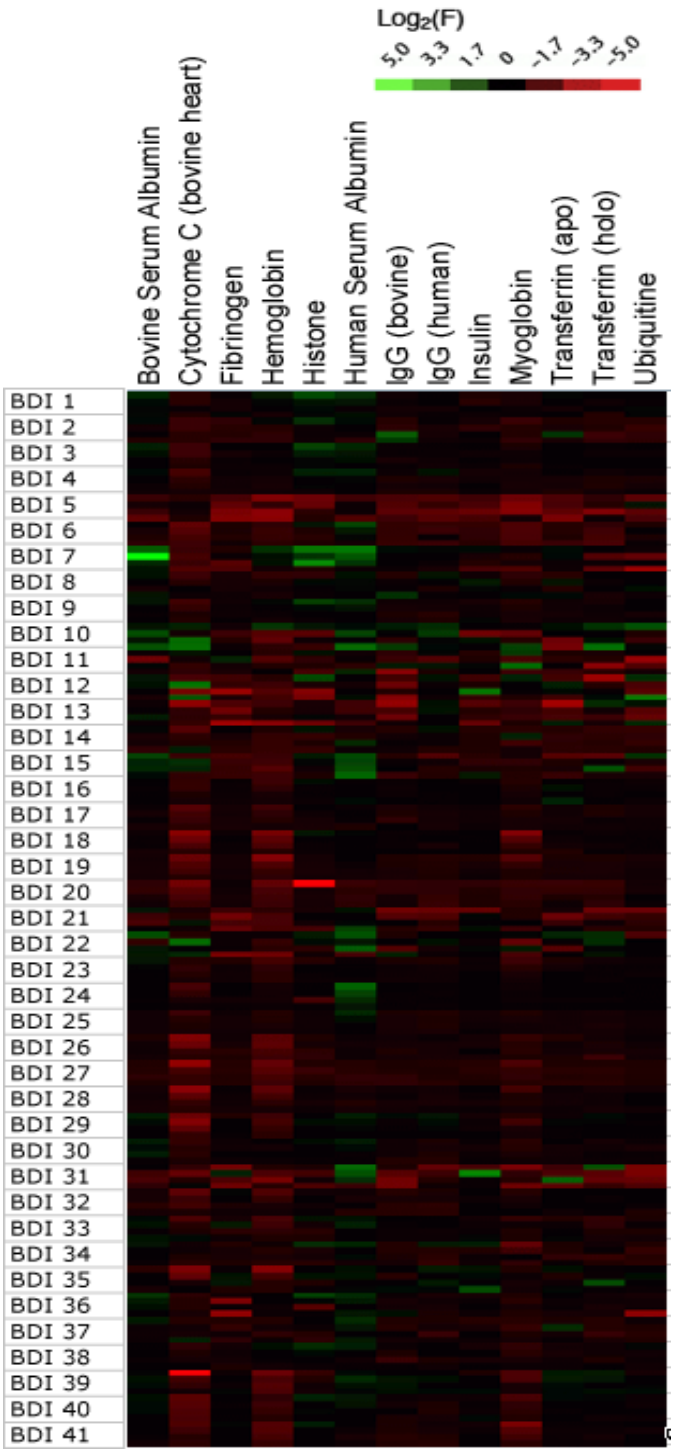

Figure 6.6. Heat map profile of protein class analytes. Most **BDI** compounds exhibit fluorescence intensity decrease trend.

RNA Sensors

Although fluorescence small molecule sensors for nucleic acid macromolecules have been extensively used for cell imaging and sequencing, the continued development of improved sensors that can distinguish different kinds of nucleic acids is currently of great interest.[19] Accordingly, 4 kinds of nucleic acids were collected as a primary screening analyte class to discover sensors that could discriminate double strand DNA (dsDNA), single strand DNA (ssDNA), RNA, and *t*-RNA. First of all, we found **BDI 37** and **BDI 38** exhibited an increase in fluorescence emission for all four kinds of nucleic acids from the primary screening (Figure 6.4). **BDI 38** contain a positively charged linker in the **BDI** derivatives, and it has strong Coulomb interaction with all negatively charged nucleic acids.

Primary hit compounds that enhanced emission in the presence of RNA compared to DNA were further tested to confirm primary profiles, and 3 **BDI** compounds revealed selectivity towards total RNA. Interestingly, all selected RNA sensors, **BDI 2**, **BDI 3**, and **BDI 5**, contain alkyloxy/aryloxy groups (-OR) at the *para* position in the R1 moiety. These findings suggest that the *para*-alkyloxy group plays a role in distinguishing RNAs over DNAs in **BDI** scaffolds. We also note that the *para*-alkoxy groups played a significant role in enhancing the fluorescence in the solid state.[18] Among the three primary hits, the *para*-methoxy group brought not only the highest fold change in fluorescence to total RNA, but also exceptionally low cross reactivity to other nucleic acids (Figure 6.7). When we tested these hit compounds toward different 16-mer RNA oligomers, they generally exhibited higher fluorescence increment towards “AU” rich oligomers (Figure 6.7). Although we observed a response trend against “AU” rich oligomers, it is still not clear which specific RNA sequences were necessary for selective recognition of each compound or how these compounds were interacting with total RNA mixture in solution. However, this example clearly shows that large-scale profiling could

identify novel modes of interaction between sensor molecule and analyte. Such studies are currently in progress.

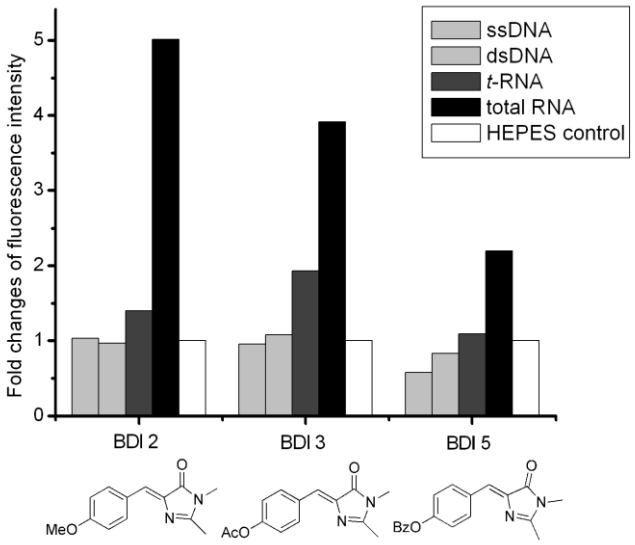

Figure 6.7. Fluorescence intensity fold changes of (a) BDI 2 at λ_{em} 512 nm, (b) BDI 3 and (c) BDI 5 at λ_{em} 532 nm against 4 nucleic acids at 1 mg/ml final concentrations in 20 mM HEPES (pH 7.4).

Human Serum Albumin Sensors

As mentioned earlier, most **BDI** compounds showed fluorescence quenching towards many proteins (Figure 6.6). Noticeable primary hit compounds were **BDI 24** and **BDI 25**. These two compounds, which contain a dialkylamino motif, showed clear emission enhancement to human serum albumin (HSA) in a dose dependent manner.

HSA is the most abundant protein in human blood plasma (60 % of total plasma protein) and is known to bind to diverse exogenous drug molecules by hydrophobic interactions.[20] Since **BDI 24** exhibited a greater fold increase, we further examined the bindings between HSA and **BDI 24**. In the presence of HSA, the maximum wavelength of fluorescence emission was blue-shifted from 530 nm to 515 nm, while the intensity increased by 10.4 fold (Figure 6.8). This hypsochromic shift can be caused by solvatochromism, the reduction of non-radiative decay, or the perturbation of electronic conjugation system through the binding with HSA. To further investigate the binding

properties of HSA and **BDI 24** quantitatively, various concentrations of **BDI 24** were titrated with HSA and a fractional saturation curve revealed a dissociation constant (K_d) of 3.57 μM (Figure 6.8). Results from this screening will provide the motivation to Chapter 8 in this dissertation.

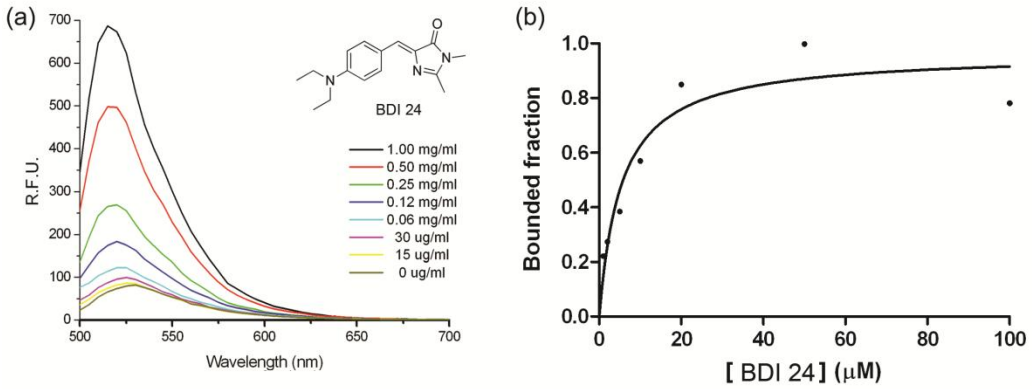

Figure 6.8. Fluorescence titration analysis for the binding of BDI 24 with HSA. (a) Fluorescence spectral change of BDI 24 (100 uM) upon addition of the HSA in 20 mM HEPES buffer (pH 7.4). (b) Fractional saturation curve of BDI 24 with HSA. Dissociation constant was measured. using 7.5 μM concentration HSA. Experimental K_d = 3.57 μM.

Conclusions

Although the sensitivities displayed here do not compare to others for the same proteins, they are based upon a limited initial set of chromophores. Nevertheless, this study represents the first example of small molecule fluorescence sensor discovery utilizing the green fluorescent protein chromophores by large-scale fluorescence profiling. We believe this profiling approach could accelerate the fluorescence sensor discovery process for other fluorescent scaffolds, since the diversity of the fluorophores introduced here represents a very small fraction of the potential structural space. In the current report, we have demonstrated the use of the fluorescence response pattern based sensor discovery utilizing the green fluorescent protein chromophore and its derivatives. 41 structurally related **BDI** compounds were synthesized and exploited for the generation of fluorescence response profiles towards 10 classes of analytes or a total of 94 individual biologically relevant analytes. From the large-scale fluorescence profile, the structural

moieties that induce specific pH response were identified as well as those showing a unique response pattern to specific analytes. Further experiments exhibited a selective fluorescence emission enhancement upon interaction between **BDI 24** with HSA (K_d = 3.57 μM) and **BDI 2** with total RNA, which showed a marked selectivity with a 5-fold emission increase. The use of more carefully focused recognition elements should increase the sensitivity and approach the on/off ratio of GFP itself. For instance, we now have increased the sensitivity to the hydrophobic "octa acid" by another factor of 10.[21] Further studies are currently in progress.

References

[1] Baldridge, A.; Lee, J.-S.;; Feng, S.; Yang, S. Q.; Kim, Y. K.; Tolbert, L. M.; Chang, Y.-T. *ACS Comb. Sci.* **2011**, *13(1)*, 32-38.

[2] Tsien, R. Y. *Annu. Rev. Biochem.* **1998**, *67*, 509-544.

[3] Heim, R.; Prasher, D. C.; Tsien, R. Y. *Proc. Natl. Acad. Sci. USA* **1994**, *91*, 12501-12504.

[4] (a) Mandal, D.; Tahara, T.; Meech, S. R. *J. Phys. Chem. B* **2004**, *108*, 1102-1108; (b) Kummer, A. D.; Kompa, C.; Niwa, H.; Hirano, T.; Kojima, S.; Michel-Beyerle, M. E. *J. Phys. Chem. B* **2002**, *106*, 7554-7559; (c) Webber, N. M.; Litvinenko, K. L.; Meech, S. R. *J. Phys. Chem. B* **2001**, *105*, 8036-8039.

[5] (a) Stoner-Ma, D.; Jaye, A. A.; Matousek, P.; Towrie, M.; Meech, S. R.; Tonge, P. J. *J. Am. Chem. Soc.* **2005**, *127*, 2864-2865; (b) Agmon, N. *Biophys. J.* **2005**, *88*, 2452-2461.

[6] Stoner-Ma, D.; Melief, E. H.; Nappa, J.; Ronayne, K. L.; Tonge, P. J.; Meech, S. R. *J. Phys. Chem. B* **2006**, *110*, 22009-22018.

[7] (a) Hu, C. D.; Chinenov, Y.; Kerppola, T. K. *Mol. Cell* **2002**, *9*, 789-798; (b) Hynes, T. R.; Tang, L.; Mervine, S. M.; Sabo, J. L.; Yost, E. A.; Devreotes, P. N.; Berlot, C. H. *J. Biol. Chem.* **2004**, *279*, 30279-30286; (c) Shaffer, J. M.; Hellwig, S.; Smithgall, T. E. *Biochemistry* **2009**, *48*, 4780-4788.

[8] Domaille, D. W.; Que, E. L.; Chang, C. J. *Nat. Chem. Biol.* **2008**, *4*, 507-507.

[9] Wu, L. X.; Burgess, K. *J. Am. Chem. Soc.* **2008**, *130*, 4089-4096.

[10] Chen, K. Y.; Cheng, Y. M.; Lai, C. H.; Hsu, C. C.; Ho, M. L.; Lee, G. H.; Chou, P. T. *J. Am. Chem. Soc.* **2007**, *129*, 4534-4535.

[11] Baldridge, A.; Samanta, S. R.; Jayaraj, N.; Ramamurthy, V.; Tolbert, L. M. *J. Am. Chem. Soc.* **2010**, *132*, 1498-1499.

[12] a) Yoon, S.; Miller, E. W.; He, Q.; Do, P. H.; Chang, C. J. *Angew. Chem. Int. Ed. Engl.* **2007**, *46*, 6658-6661; (b) He, Q.; Miller, E. W.; Wong, A. P.; Chang, C. J. *J. Am. Chem. Soc.* **2006**, *128*, 9316-9317; (c) Zeng, L.; Miller, E. W.; Pralle, A.; Isacoff, E. Y.; Chang, C. J. *J. Am. Chem. Soc.* **2006**, *128*, 10-11; (d) Yoon, S.; Albers, A. E.; Wong, A. P.; Chang, C. J. *J. Am. Chem. Soc.* **2005**, *127*, 16030-16031.

[13] (a) Lee, J. S.; Kim, Y. K.; Vendrell, M.; Chang, Y. T. *Mol. Biosyst.* **2009**, *5*, 411-421; (b) Wang, S.; Kim, Y. K.; Chang, Y. T. *J. Comb. Chem.* **2008**, *10*, 460-465; (c) Ahn, Y. H.; Lee, J. S.; Chang, Y. T. *J. Am. Chem. Soc.* **2007**, *129*, 4510-4511; (d) Li, Q.; Lee, J. S.; Ha, C.; Park, C. B.; Yang, G.; Gan, W. B.; Chang, Y. T. *Angew. Chem. Int. Ed. Engl.* **2004**, *43*, 6331-6335.

[14] Ahn, Y. H.; Lee, J. S.; Chang, Y. T. *J. Comb. Chem.* **2008**, *10*, 376-380.

[15] (a) Lamb, J. et al. *Science* **2006**, *313*, 1929-1935; (b) Paull, K. D.; Shoemaker, R. H.; Hodes, L.; Monks, A.; Scudiero, D. A.; Rubinstein, L.; Plowman, J.; Boyd, M. R. *J. Natl. Cancer Inst.* **1989**, *81*, 1088-1092; (c) Weinstein, J. N.; Kohn, K. W.; Grever, M. R.; Viswanadhan, V. N.; Rubinstein, L. V.; Monks, A. P.; Scudiero, D. A.; Welch, L.; Koutsoukos, A. D.; Chiausa, A. J.; *Science* **1992**, *258*, 447-451; (d) Hughes, T. R. et al. *Cell* **2000**, *102*, 109-126.

[16] (a) Dong, J.; Solntsev, K. M.; Poizat, O.; Tolbert, L. M. *J. Am. Chem. Soc.* **2007**, *129*, 10084-10085; (b) Kojima, S.; Ohkawa, H.; Hirano, T.; Maki, S.; Niwa, H.; Ohashi, M.; Inouye, S.; Tsuji, F. I. *Tetrahedron Lett.* **1998**, *39*, 5239-5242.

[17] Simeonov, A.; Jadhav, A.; Thomas, C. J.; Wang, Y.; Huang, R.; Southall, N. T.; Shinn, P.; Smith, J.; Austin, C. P.; Auld, D. S.; Inglese, J. *J. Med. Chem.* **2008**, *51*, 2363-2371.

[18] Inglese, J.; Shamu, C. E.; Guy, R. K. *Nat. Chem. Biol.* **2007**, *3*, 438-441.

[19] (a) O'Connor, N. A.; Stevens, N.; Samaroo, D.; Solomon, M. R.; Marti, A. A.; Dyer, J.; Vishwasrao, H.; Akins, D. L.; Kandel, E. R.; Turro, N. J. *Chem. Commun.* **2009**, 2640-2642; (b) Li, Q.; Kim, Y.; Namm, J.; Kulkarni, A.; Rosania, G. R.; Ahn, Y. H.; Chang, Y. T. *Chem. Biol.* **2006**, *13*, 615-623; (c) Lee, J. W.; Jung, M.; Rosania, G. R.; Chang, Y. T. *Chem. Commun.* **2003**, 1852-1853.

[20] (a) Kragh-Hansen, U.; Chuang, V. T.; Otagiri, M. *Biol. Pharm. Bull.* **2002**, *25*, 695-704; (b) Min, J.; Lee, J. W.; Ahn, Y. H.; Chang, Y. T. *J. Comb. Chem.* **2007**, *9*, 1079-1083.

[21] Baldridge, A.; Samanta, S. R.; Jayaraj, N.; Ramamurthy, V.; Tolbert, L. M. *J. Am. Chem. Soc*. ***2011,*** *133, 712-715.*

CHAPTER 7

ACTING AS A FLUORESCENT PROBE AND A LIGAND: THE INTERACTION OF AMI CHROMOPHORES AND NUCLEAR RECEPTORS

The research highlighted within in this chapter represents collaboration between the Tolbert lab and the Doyle/Azizi lab. Throughout the entire collaboration, the synthesis and design of the chromophores was completed within the Tolbert lab and the work with nuclear receptors was completed within the Doyle/Azizi lab. Data analysis and manuscript preparation was equally shared between the two collaborating labs.

Introduction to the Estrogen Receptor

Nuclear receptors (NR) are a superfamily of ligand-activated transcription factors that play crucial roles in a number of important biological and physiological processes.[2,3] Their role in the regulation of gene expression via small molecule ligands makes their function critical to many developmental processes. Structurally, they share a common organization that consists of a highly conserved DNA binding domain (DBD) and a ligand–binding domain (LBD), connected by a flexible hinge region. The C- terminal helix (helix 12) of the LBD plays a critical role in its function, serving as a main region for interaction with coactivator proteins in the activation mechanism.[4,5] Following binding, ligand activating receptors position the helix 12 in an active conformation, providing an interaction surface for co-activator proteins and eventually recruiting transcriptional machinery.

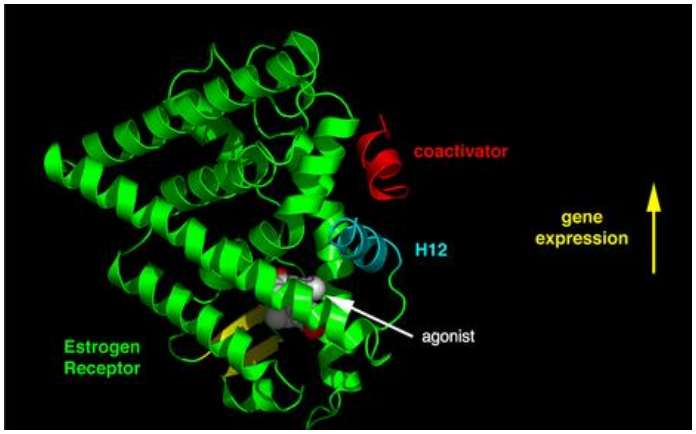

Figure7.1. Depiction of mechanism of nuclear receptor actions upon binding of agonist in ligand binding domain.

The estrogen receptor α (ERα) is a member of the NR superfamily and represents one of the first NRs to be discovered. Endogenous estrogens, i.e., 17β-estradiol and its derivatives, are natural ligands of ERα.[6] The wide distribution of ERα in various human tissues, including bone, uterus, breast and brain, along with their significant role in gene expression, implicates this receptor in a number of diseases, including breast cancer, osteoporosis and cardiovascular diseases.[7] Tamoxifen, the most widely used drug to treat breast cancer, is, in fact, an ERα antagonist.[8] A keen interest lies in developing novel ligands for ERα as well as other NRs that could serve as potential drugs for a number of NR-related diseases. Furthermore, some highly successful drugs, like tamoxifen, which are used in the treatment of the ER- positive breast cancer, face the issue of cells developing resistance as noted in 40% of patients.[9] Thus identification of a novel class of small molecules as potential agonists or antagonists is a key step in developing drugs that will enhance therapy for ER related diseases.

In recent years, the discovery of fluorescent probes has helped visualize NRs inside cells, enhancing and increasing knowledge about the localization and trafficking of these receptors. In particular, the use of the green fluorescent protein (GFP) from

Aequorea victoria fused to specific nuclear receptors has provided a powerful method for detecting both function and mobility of NRs *in vivo*.[10]

A disadvantage to using fusion proteins is the potential interference with the natural function of receptors, since nuclear receptors undergo a conformational change upon ligand binding, the presence of a bulky protein such as GFP could affect the normal conformational change of these proteins. The use of potentially fluorescent small molecule ligands would provide additional diagnostic capabilities, while allowing the receptor to act in its natural state, thus providing additional insight into various NR mechanisms.

Recent studies have described various ERα ligand/fluorescent dye conjugates for the detection and expression of ERα. In most cases the fluorescent conjugates are attached to well-known ERα ligands such as 17-β-estradiol (E2) or tamoxifen (Figure 7.2).[11]

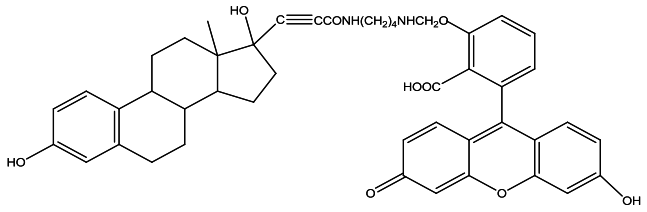

E2(4)cF

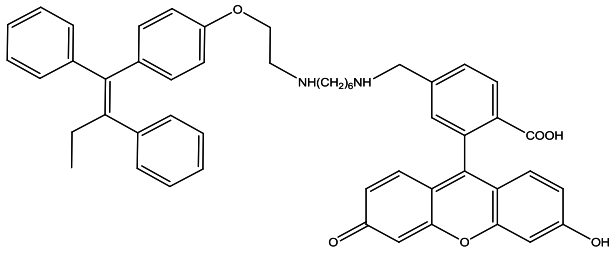

OHT-6C

Figure 7.2. Selected structures of fluorescent ligands for ERα.

However, the bulky conjugates of these ligands decrease their affinity for the receptor.[12] This manuscript focuses on the development of new ER ligands with unique visualization properties, derivatives of fluorescent protein chromophores containing the arylmethyleneimidazolidinone (AMI) fluorophore, which mimic non-steroidal ERα ligands. Based on the AMI core structure, a variety of chromophore analogs were designed that could activate the estrogen receptor without the exhibition of fluorescence or bind the receptor thus mimicking the restrictive β-barrel of GFP providing chromophore emission upon binding to the receptor's ligand binding domain (LBD). It should be noted that unlike GFP, these molecules are virtually devoid of fluorescence in solution.

Experimental Protocols for Nuclear Receptors with AMI Chromophores

Synthesis of Ligands

Synthesis of the ligands was carried out as highlighted in Chapter 2. For compounds 1-3 and 5 the Schiff base was obtained by reacting the aromatic aldehyde (1eq), the primary amine (1eq) and sodium hydroxide (1.1eq) in 40.0 mL of MeOH at reflux for 4hr, followed by removal of solvent under reduced pressure to yield product. For 4 and 6-9 the aldehyde (1eq) and primary amine (1eq) were allowed to stir 12 h, yielding pure product. The imidate was prepared as previously described.[13] Imidazolindinones ligands were synthesized by combining the corresponding Schiff base with the imidate and ~0.5mL of MeOH with stirring for 12 h which resulted in precipitate formation for 4 and 6-9. Solvent removal from compounds 1-3 and 5 under reduced pressure provided solid products as nearly pure materials. All products were further washed with cold Et_2O to yield the desired products as light yellow crystalline materials. Characterization of these compounds is found in Appendix A.

In Silico Docking Studies

Modeling of ligand–protein complexes was carried out with AutoDock Vina®[14] using the estradiol–ERα ligand binding domain (pdb: 1ERE) crystal structure under standard parameters. The estrogen receptor was prepared for docking via UCSF CHIMERA, an interactive molecular graphics program, by removing the ligand and water molecules, adding polar hydrogens, and assigning Kollman united atom charges.[15] Ligands were created using ChemBioDraw Ultra 11.0 / ChemBio3D Ultra 11.0 (Cambridge Soft, USA) and were minimized using MMFF94 force field. Ligands were modified with the AutoDockTools by adding Gasteiger charges to set the partial charge of each atom.[16] The best docked ligand/receptor complexes were subjected to further studies.

Liquid Quantification Assay in Yeast

Variants were tested in liquid quantification assays in 96-well plates with media lacking histidine, leucine, and tryptophan (SC-HLW), 0.1 mM 3AT, and with or without chromophores or 17β-estradiol at varying concentrations. Media and cells were added in a 4:1 ratio into 96-well plates. Plates were incubated at 30°C, with shaking at 170 rpm. Optical density (OD) readings at 630 nm were recorded at 0, 24, and 48 hours to measure growth density.

Cell culture

HEK293T cells (ATCC, USA) were transfected with the plasmid pCMXwthERαLBD. This plasmid contains the Gal4DBD (GBD) fused to the wild-type ERα ligand binding domain LBD (GBD:LBD fusion under the control of a cytomegalovirus (CMV) promoter). The reporter plasmid, p17*4TATAluc, contained the *Renilla* luciferase gene under the control of four Gal4 response elements located upstream from a minimal thymidine kinase promoter. The pCMXβgal, a plasmid containing the β-galactosidase gene under the control of the mammalian CMV promoter, was also used as an internal standard. Lipofectamine 2000 (Invitrogen, USA) was used as the cationic lipid and transfection experimental details are described in Taylor et al.[17] Ligands were added to the wells at various concentrations. Cells were harvested and analyzed for luciferase and

β-galactosidase activity. All data points represent the average of triplicate experiments normalized against β-galactosidase activity.

Fluorescence Microscopy

Transfection of NIH3T3 cells was performed in a single plate with PolyFect (Qiagen, USA) transfection reagent according to the manufacturer's protocol. Plasmids pCMXwthERαLBD expressing Gal4DBD:ERαLBD fusion protein and mCherry-nuc as control were co-transfected into NIH3T3 cells. After 8 hours of transfection at 37˚C in humidified air with 5% CO_2, the media in the wells was removed and ligand (10mM) was added with the media to the wells. Cells were then subjected to microscopy after 30 hours of incubation. Samples were washed with 1X PBS and confocal imaging was performed using a Zeiss LSM 510 NLO w/META MPE confocal microscope (Carl Zeiss MicroImaging GmbH, Germany).

Results of ERα with AMI Chromophores

Fluorescent protein chromophore design.

The ERα selective FP chromophores were rationally designed using the arylmethyleneimidazolidinone (AMI) core, to resemble the ABCD ring system of steroids (Figure 7.3).

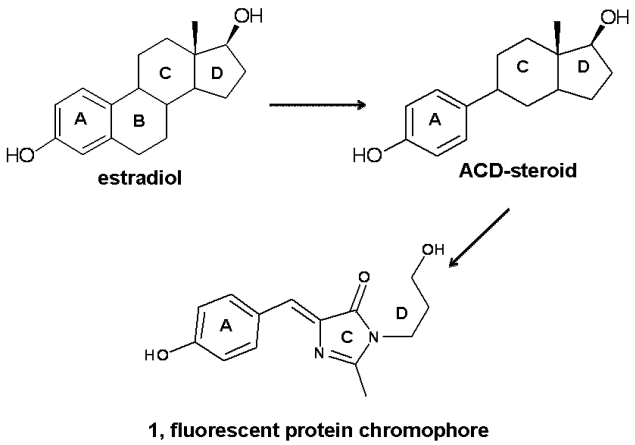

Figure 7.3. Rational design of AMI based on ABCD steroid ring system (common ligands for ER α).

Substituents were not incorporated at the B ring, by analogy to known estrogen receptor agonists incorporating only the A-CD ring system.[18] In analyzing the AMI core, a phenolic aryl group was retained to play a role analogous to the functionalized ring A of the steroid molecule. The imidazolindinone group in the AMI structure was designed to mimic the C ring of a steroid molecule, and alkyl substituents around the heterocycle (R4) were employed to compensate for the absent steroidal D ring. A series of such derivatives was designed based on the core structure, with the addition of substituents to create potential ligands for ERα.

The ability of the designed chromophores to mimic the overall interaction of the heterocyclic core of various ERα ligands was determined via molecular modeling. AMI **4** was docked into the crystal structure of the ERα ligand binding domain (1ERE) using AutoDock Vina[14] and showed binding to ERα with favorable superimposition with estradiol. In addition, modeling showed the phenolic group superimposed on the A ring of estradiol (E2), created a potential hydrogen bond with glutamate E353 and arginine R394 (Figure 7.3A), analogous to estradiol. However, the same calculations failed to

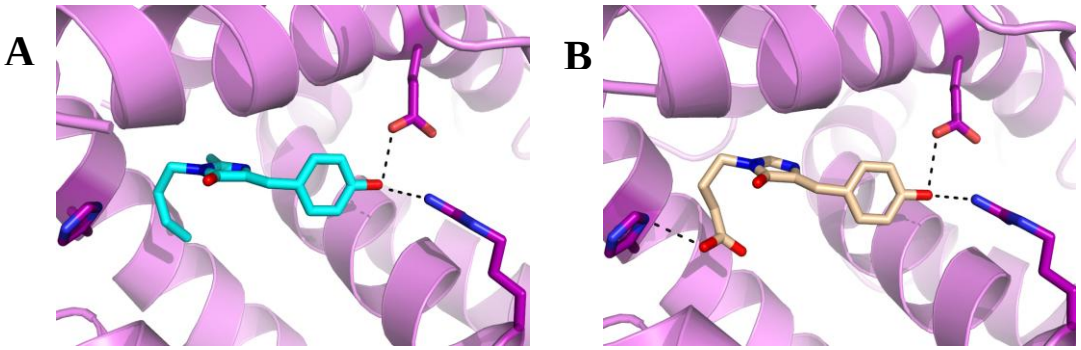

Figure 7.4. Docking resulting of structures of the AMIs ligands docked into the crystal of ERα (pdb:1ERE) using the software Autodock Vina with compound 4 (A) and compound 1 (B).

overlay the imidazolindinone ring of the AMI compound with the C ring of estradiol. This is probably due to the free rotation between the phenyl and the imidazolindinone ring, which is crucial for the fluorescence of these AMIs, as

previously reported.[19]

Based on the docking results and examination of known structures with ERα agonists, additional compounds were designed with potential hydrogen bonding between the ligand and H524. Histidine H524 is known to form a hydrogen bond with the 17-β hydroxyl group on the D-ring of E2 (Figure 7.3B).[20] From this, adding a polar group such as the hydroxyl group as in compound **3** or with the addition of the carboxyl group in compound **1,** could provide the additional hydrogen bond, based on the *in silico* modeling results providing increased probability of ligand binding and activation.

Despite the advantages of molecular modeling as a tool for visualizing protein-ligand interactions, such calculations are limited in providing information about the importance of specific substituents. Therefore, additional AMI molecules with various substituents were designed, synthesized, and tested. The various activation profiles could help in determining a correlation between the structures of moieties and ligand binding with ERα (Table 7.1).

Table 7.1. Substitution patterns AMI used in the ER α nuclear receptor study.

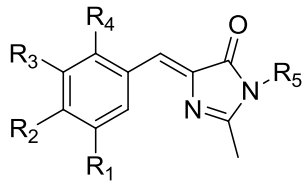

Compound	R_1	R_2	R_3	R_4	R_5
1	H	OH	H	H	$C_3H_6CO_2H$
2	H	OH	H	H	$C_5H_{10}CO_2H$
3	H	OH	H	H	C_3H_6OH
4	H	OH	H	H	C_3H_7
5	H	H	H	H	$C_3H_6CO_2H$
6	H	CH_3	H	H	CH_3
7	H	H	H	H	CH_3
8	CH_3	OH	CH_3	H	CH_3
9	H	$N(Me)_2$	H	H	CH_3
10	H	$N(Me)_2$	H	OH	C_5H_{11}

Chemical Complementation: evaluating fluorescence ER chromophore interaction with the receptor in yeast.

Chemical complementation is a semi high-throughput selection, where the survival of the yeast (*Saccharomyces cerevisiae*) strain, PJ69-4A, is linked to the ability of a small molecule ligand to activate a nuclear receptor.[21] PJ69-4A contains Gal4 response elements (Gal4RE) controlling expression of the genetic selection genes, *HIS3* and *ADE2,* involved in the histidine and adenine biosynthetic pathway, respectively. Two fusion proteins consisting of the Gal4 DNA binding domain (GBD) fused to the ERα LBD (GBD: ERα LBD) is transformed into yeast along with the fusion protein of the NR coactivator fused to Gal4 activation domain (GAD). Upon ligand binding to the ERα LBD, the GBD: ERα LBD fusion binds to Gal4RE, recruiting the coactivator, the GAD fusion protein. Thus the GAD serves to recruit the yeast transcriptional machinery required to initiate transcription of the selection gene (*ADE2* or *HIS3*).[21b] Activation of the selection gene, such as the *HIS3* gene, enables the yeast strain to grow on media lacking histidine in the presence of the ligand (Figure 7.5).

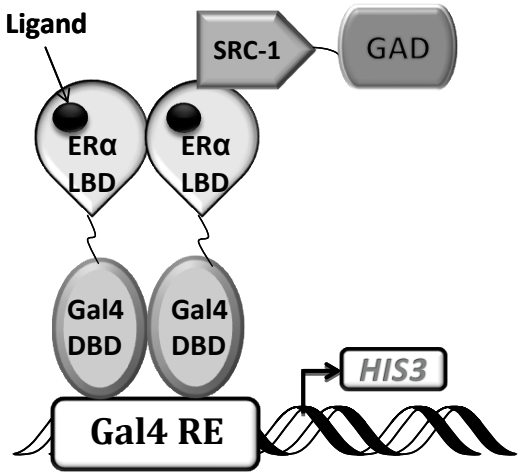

Figure 7.5. Chemical complementation in yeast scheme of chemical complementation assay.

Thus, the survival of the yeast depends on the presence of the small ligand molecules. Chemical complementation has successfully been used as a versatile quick and efficient system for detecting new ligands capable of activating various nuclear receptors.[21a]

Ten synthetic AMI ligands were tested in chemical complementation. The growth of the yeast strain PJ69-4A expressing fusion proteins GBD: ERαLBD and SRC-1: GAD was observed in histidine selective media at (SC-HLW with 0.1 mM 3AT), containing concentrations of chromophores ranging from 0.01 μM -10 μM. To reduce leakiness of the *HIS3* gene, 3-amino-1,2,4-triazole (3AT) was added.[22] Chromophores **1** and **2** showed slight activation (two-fold) and low sensitivity (EC_{50} >10μM) with ERα, as shown in Figure 7.7. However, most of the tested ligands did not induce growth in yeast, indicating that the ligand was unable to bind and activate the receptor, allowing the yeast to survive.

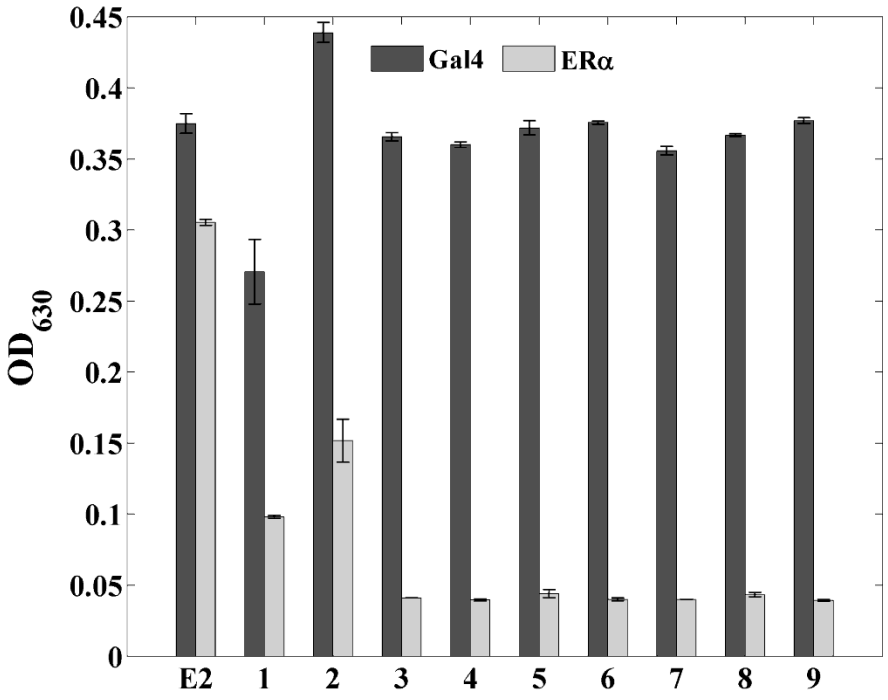

Figure 7.6. Results of chemical complementation in histidine selective media (-HLW) with 1mM 3-AT. The ligand concentration of 10 μM was used. Gal4 is a ligand independent transcription factor and is used as a positive control. ERα with estradiol (E2) is also used as a positive control.

Estrogen Receptor Activation by Fluorescent ER Chromophores in mammalian cells.

To determine whether a similar trend in activation seen in yeast is observed in mammalian cells, the chromophores were analyzed for activation and fluorescence in human embryonic kidney 293T cells (HEK293T). The Gal4 DNA binding domain fused to the ERα ligand binding domain (GBD: ERαLBD) was cloned into a mammalian expression vector (pCMX) containing a cytomegalovirus (CMV) promoter. Using a luciferase reporter gene assay, HEK293T cells were co-transfected with a reporter plasmid containing the *Renilla luciferase* gene under the control of Gal4 response elements. Cells were transfected with the two plasmids and various chromophores were added and tested for activation at concentration of 10 μM.

The ten synthetic AMI chromophores were tested with ERα at a concentration of 10μM or absence of ligand. The highest activation was observed with chromophores **1**-**4**, **8** and **9** displaying an approximately 10–14 fold activation as shown in Figure 7.7, in comparison to the 21- fold activation observed with estradiol.

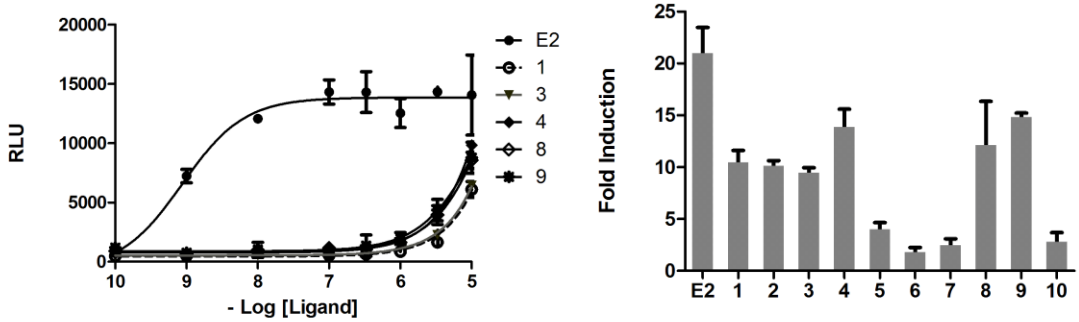

Figure 7.7. Activation profile of chromophores in mammalian cells (HEK293T), A) Relative inductions of ERα in the presence of 10μM of each ligand B) Dose response curves for the activation of ERα (Gal4DBD: ERαLBD) in response to various concentrations of **1**, **3**, **4**, **8**, **9**. Activity is measured in relative light units (RLU) derived from the measurement of luciferase activity and normalization against a β-galactosidase internal standard.

To determine the EC_{50} values of these compounds, a dose response curve was generated for each compound. As seen in Figure 7.7, compounds **4**, **8** and **9** showed the highest sensitivity with an EC_{50} of 3 μM whereas compounds **2**, **3** and **4** displayed $EC_{50} > 3$ μM. Compounds **5**, **6** and **7** showed no activation. Despite the fact that these compounds have a higher EC_{50} value and lower activation in comparison to ERα and estradiol (873 pM), compounds **4**, **8** and **9** show promise as starting points for a potentially a new class of ERα agonists.

Visualization of ERα in mammalian cells using Fluorescent ER Chromophores

As mentioned previously, a goal of developing AMIs as novel ligands was to determine if fluorescence would be observed upon binding to the NRs. The chromophores were tested for fluorescence in the presence of ERα in NIH3T3 mammalian cells. Confocal microscopy was used to monitor cellular uptake and localization of the chromophores in the cell. The cells were transfected with the mammalian expression vector pCMXGhERLBD expressing Gal4DBD:ERαLBD fusion protein and incubated in media in each of the ten chromophores. To determine the amount of background fluorescence observed with cells and the compounds, a series of negative controls were employed. First, the NIH3T3 cells transfected with ERα were exposed either to no ligands or to estradiol alone, addressing the basal fluorescence observed due to the cells and in the presence of ERα. Cells lacking the ERα were also exposed to the AMI compounds, addressing the potential fluorescence due to non specific binding of the fluorophore to endogenous proteins.

As shown in Figure 7.8, slight basal fluorescence was observed in the case of one of the controls, cells lacking ERα and incubated with compound **10**. In the presence of ERα, 6 out of the 10 of the chromophores that showed activation yet displayed no fluorescence. However in case of compound **10,** fluorescence was observed in the

cytoplasm of the NIH3T3 cells. This finding was surprising, since compound **10** did not

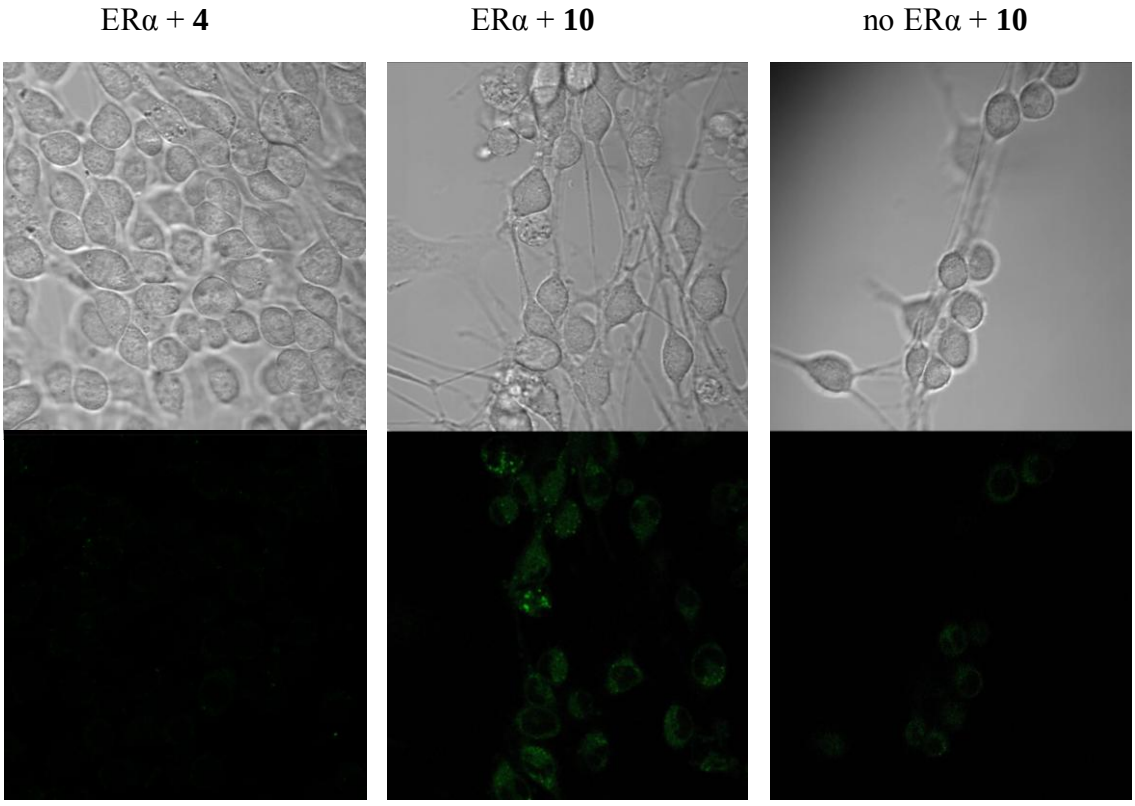

Figure 7.8. Imaging of NIH 3T3 cells with the fluorescent chromophores. Mammalian cells expressing ERα (Gal4DBD: ERαLBD) were incubated with **4** and **10**. As a negative control cells lacking ERα were incubated with **10**.

activate the ERα,

but also suggests that activation and fluorescence can be independent of each other. In other words, these chromophores could serve as agonists that bind, activate and display fluorescence. Conversely, in other instances these compounds can bind and fluoresce but not activate, similar to a traditional antagonist. The localization of the observed fluorescence in the cytoplasm of the cell was also unexpected due to the fact that previous research and findings have shown ERα localizes to the nucleus in the presence of agonist or an antagonist.[23] However, Rickert et al have recently shown that OHT-derived conjugates display fluorescence in cytoplasm.[11c]

Discussion of ERα with AMI Chromophores

The wide interest in nuclear receptor ligands as potential drug targets and therapeutics for diseases, including cancer, makes these receptors compelling pharmaceutical objectives, particularly in the case of ER. Novel agonists and antagonists for ERα, as well as selective estrogen receptor modulators (SERMs) and selective estrogen receptor down-regulators (SERDs) have expanded the possibilities of ERα related drugs, serving as drugs for several NR based diseases.[24] Due to the build-up of resistance with current ER ligands, developing a new class of ligands as potential drugs will enhance therapy for these diseases. Furthermore, in addition to drug development, designing ligands with visualization features would prove extremely useful in the determination of expression and trafficking of nuclear receptors, such as ERα in specific tissues.[11] In recent years, ER ligands with fluorescent conjugates have been developed for applications in ER mobility, but have been limited in their binding affinity to these receptors.[10,11] An additional approach, using a fusion of GFP to the estrogen receptor, has been useful but interference from the bulky GFP is hypothesized since nuclear receptors undergo severe structural changes as a consequence of their function. This fusion may limit the full scope of the NR binding and activation.

A novel class of arylmethylene-imidazolidinone (AMI) chromophores, based on the steroid ring system of estradiol to mimic A-CD rings were designed and *in silico* studies of these novel ligands indicated that AMI derivatives would bind to binding pocket similar to that observed with ERα and estradiol (Figure 7.4). These were tested with ERα. Of the ten compounds tested via chemical complementation in yeast, compounds **1** and **2** displayed slight activation (Figure 7.7) in comparison to estradiol. However, when tested in HEK293T mammalian cells, the activation profile for these compounds with ERα differed from that in yeast. Most of these compounds displayed similar activation with the highest sensitivity (1μM) and the highest activation observed with **4**, **8** and **9**.

These results confirm our initial hypothesis, based on molecular modeling, that a key moiety for binding of ERα LBD is the hydroxyl group of the phenyl ring of AMI, which could potentially form a hydrogen bond with E353 and R394. Compounds **5**, **6** and **7** lack a hydroxyl group at that position and as expected, these compounds did not display activation of the estrogen receptor. The importance of creating polar contacts with H524 has also been taken into account. Thus, the key moiety of chromophores is thought to be the substituent R_5 on the imidazolindinone ring. Hydrogen-bonding moieties on the alkyl group can potentially lead to an interaction with H524. However, such polar groups do not seem essential for activation. This is evident with **8,** lacking this group, which displays the same sensitivity as **1** containing a carboxyl group at this position. This substitution activity is noted for **3** with a hydroxyl group and **1** and **2** with carboxyl groups, which show the same degree of activation. A main feature of chromophore design is that the length of the alkyl group has little influence on sensitivity. Chromophore **1**, which lacks two carbons in the alkyl chain compared to **2,** has only slightly higher activation than **2.** Another factor that might contribute to increased sensitivity to ERα is the presence of substituents in positions R_3 and R_5. On the other hand, **9,** with methyl groups in these positions, shows higher sensitivity, similar to that of **1**. These groups can possibly play a role in hydrophobic interactions with non-polar residues in the binding pocket. In addition, substitutions at these positions may reduce the flexibility between the phenyl and imidazolindinone rings that can lead to a more planar conformation of the chromophore, similar to the enforced conformation of estradiol and similar to the conditions found within the restrictive β-barrel of GFP.

The absence of fluorescence in ligands which activate ERα presents a conundrum. As observed with compound **10**, no activation is observed with ERα, but fluorescence is seen in the presence of the receptor and ligand. This suggests that the chromophore is able to bind ERα and fluoresce without activation. This lack of activation may be due to the presence of a dimethylamine group rather than the hydroxyl at R_2. The hydroxyl

group in this position, creating a hydrogen bond with Glu353 and Arg394, may be essential for activation. Further work involving the design of AMIs that will both fluoresce *and* activate ERα, serving as an agonist by improving the affinity to the receptor. Such binding may produce an agonistic effect, depending upon the conformation produced. Similarly, fluorescence will depend upon the geometry of the chromophore upon bonding. Thus the production of fluorescence and/or activation upon binding creates a new tool for investigating the stereochemistry of ligand/receptor interactions.

Finally, the fluorescence of compound **10** was located in the cytoplasm. Our findings indicate that uptake of this ligand appears to be mediated by ERα, and the mechanism of compound uptake and apparent exclusion from the nucleus is not clear. Further studies of this localization are in progress.

Introduction to the Pregnane X Receptor

The pregnane X receptor (PXR; NR1I2) is a member of the nuclear receptor superfamily, expressed in liver and intestine.[25] PXR regulates a number of enzymes involved in xenobiotic metabolism, including cytochrome P450, UDP-glucuronosyltransferases, sulfotransferases and drug transporters that metabolize and excrete endogenous and exogenous potentially toxic chemicals.[26] By its nature, PXR is activated by structurally diverse ligands such as androstanes, bile acids, hormones, dietary vitamins and a broad range of prescription and herbal drugs such as rifampicin, tamoxifen, paclitaxel and St John's Wort.[27] The diversity of ligands able to bind and activate this receptor, make PXR a promiscuous receptor, which is evident through the structure.

The identification of new PXR ligands, both agonists and antagonists, could lead to the discovery of potential drugs, since this receptor has been shown to play a role in lipid homeostasis and inflammation.[28] Although exact diseases have yet to be

identified, the discovery a new class of ligands will aid in the further understand of the mechanism of this receptor in vivo. However, further studies are necessary for finding interaction in which PXR is involved in the cell. Thus cellular localization of PXR in cells will be important. Currently, there is no consensus about localization of PXR.[29] Some groups have indicated that PXR is only localized in the nucleus; however others have determined that PXR is traslocated from cytoplasm to nucleus upon ligand binding.[30] From this, the motivation to study the localization and trafficking of PXR, fusion of nuclear receptor with green fluorescent protein (GFP) from *Aequorea victoria* is currently used. While this has provided valuable information toward the understanding of the overall actions of this nuclear receptor, this system is not ideal for studying trafficking and function due to the bulky protein GFP that can affect the conformational change and recruitment other protein by nuclear receptor. Noting this, the Tolbert group has proposed novel ligands capable of visualization properties, designed based on the arylmethyleneimidazolidinone (AMI) chromophore of GFP.

Based on the findings of the ERα a library of AMI chromophores were identified and designed as novel PXR agonists based on novel AMI core. These novel ligands are specific PXR agonists and do not activate ERα. This new class of PXR ligands does not only introduce novel agonists but also enhanced fluorescence upon ligand binding. These novel small molecules could be potential novel therapeutic drugs to treat PXR related diseases.

Results and Discussion of Pregnane X Receptor with AMI Chromophores

Based on the known promiscuity of PXR and the knowledge that some ER ligands are activated by PXR, the entire library of AMIs highlighted in Chapter 2 was checked for agonistic activity with PXR. Human embryonic kidney 293T cells (HEK293T) were transfected with a mammalian expression vector expressing the Gal4 DNA binding domain fused to the PXR ligand binding domain (GBD:PXRLBD).

Transfected cells were incubated with various fluophores at concentration of 10 μM and tested for activation. The activity of PXR was determined using a luciferase report gene under the control of Gal4 response elements. Analysis of activation have shown that AMIs that activated ERα, do not activate PXR. However, ligand **13** displayed fluorescence upon binding, but do not show agonistic activity with ERα, activates the PXR as shown in Figure 7.9. These results suggested that ligands based on the AMIs core could be potential agonists for PXR.

Table 7.2. Substitution pattern and AMI used in PXR nuclear receptor studies.

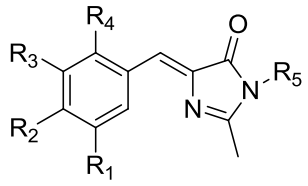

Compound	R_1	R_2	R_3	R_4	R_5
11	H	$N(Et)_2$	H	OH	CH_3
12	H	$N(Et)_2$	H	OH	C_3H_7
13	H	$N(Et)_2$	H	OH	C_5H_{11}
14	H	$N(Et)_2$	H	OH	C_6H_{13}
15	H	$N(Et)_2$	H	OH	C_7H_{15}
16	H	$N(Et)_2$	H	OH	C_8H_{17}
17	H	$N(Et)_2$	H	OH	$C_{10}H_{21}$
18	H	$N(Et)_2$	H	OH	$C_3H_6CO_2H$
19	H	H	H	CH_3	CH_3

Noting the structure of these compounds, it was hypothesized that the activation observed by **13** could be due to the presence of a diethylamino group at R_2 position. The importance of this substitution is evident when the RLU response of **13** is compared to **19**, which lacks this functional group at R_2 position and does not display activation.

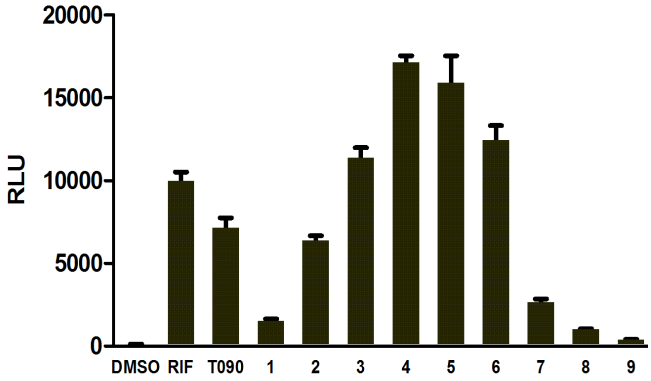

Figure 7.9. Activation profile of AMI chromophores in mammalian cells.

The importance of creating and maintaining key hydrophobic contacts in the binding pocket was taken into account for the rational design of new AMIs through the employment of different lengths of alkyl groups in the R_5 position. Following this motivation, chromophores **11 – 17** with increasing alkyl chain length were synthesized. The highest fold activation was observed in case of compound **14** that exhibited a two-fold higher activation than rifampicin, the known "industry standard" PXR activator shown in Figure 7.9. Slightly lower fold activation compared to **14** displays **15** and **16** that differ by 1 and 2 carbons in the alkyl group, respectively. However, **12** displays less than half the fold activation noted by **14**. These fold activation results suggest that the optimal length of alkyl chain for activation is six carbons, while more than eight carbons in this position result in a drastic decrease in the activation. Methyl group in this position in compound **11** as expected did not display activation. On the other hand, **18**, which has carboxyl group on the same length of the alkyl group as **12** shows significant lower activation. These findings suggest that not only alkyl chain length is crucial for achieving the high activation but also the AMIs overall hydrophobicity measured by log P values.

These results confirm our initial hypothesis, that a key moiety for binding of PXR

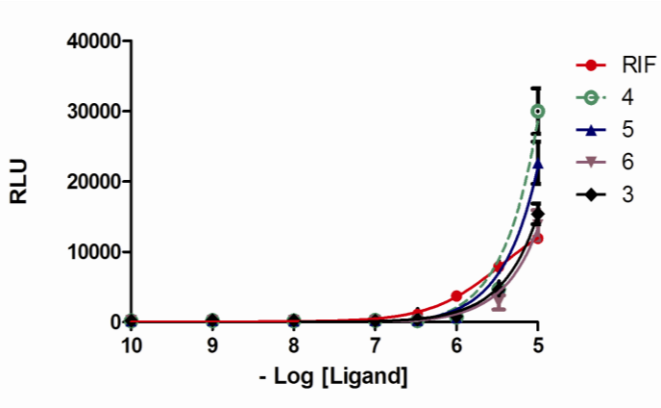

Figure 7.10. Dose response curves for activation of PXR in response to various AMI concentrations.

is not only dimethylamine but also alkyl group that can possibly play a role in hydrophobic interactions with non-polar residues in the binding pocket. Thus, the length of the alkylic chain is the crucial for getting optimal these interactions. To determine the EC_{50} values of these compounds, a dose response curve was generated for each compound. As shown in Figure 7.10, all synthesized compounds showed the highest sensitivity with an EC_{50} of 1μM in comparison to the 10 μM of rifampicin. However new compounds showed significantly higher fold activation in comparison to known PXR activators such as rifampicin and T090.

Conclusions

From the data presented in this chapter it is shown that a series of fluorescent protein chromophores can be used as ligands, especially agonists, which can be used to activate the estrogen receptor α as well as the pregnane X receptor. These novel fluorescent ligands provide for a new class of ligands toward the development of new fluorescent probes for ERα that do not involve fluorescent conjugates attached to a known ERα ligand core. This provides great advantages as a non-invasive approach to monitor nuclear receptor mechanisms through the fluorescence generated by these small molecules compared to bulky fluorescent proteins that are commonly employed. This

chapter highlights work completed to the date of this dissertation but it should be noted and is highlighted in the future work section that additional ligands that interact with other nuclear receptors are currently underway. Additionally through the employment of rational design, a variety of different AMI chromophores are proposed to both increase the sensitivity and emission quantum yield enhancement upon binding to nuclear receptors.

References

[1] Duraj-Thatte, A. M.; Baldridge, A.; Azizi, B.; Tolbert, L. M. *J. Med. Chem.* Submitted.

[2] Novac, N.; Heinzel, T. *Curr Drug Targets Inflamm Allergy* **2004,** 3, 335-46.

[3] Gronemeyer, H.; Gustafsson, J. A.; Laudet, V. *Nat Rev Drug Discov* **2004,** 3, 950-64.

[4] Wurtz, J. M.; Bourguet, W.; Renaud, J. P.; Vivat, V.; Chambon, P.; Moras, D.; Gronemeyer, H. *Nat Struct Biol* **1996,** 3, 206.

[5] Greschik, H.; Moras, D. *Curr Top Med Chem* **2003,** 3, 1573-99.

[6] Katzenellenbogen, J. A.; Katzenellenbogen, B. S. *Chem Biol* **1996,** 3, 529-36.

[7] (a) Khan, S. A.; Rogers, M. A.; Obando, J. A.; Tamsen, A. *Cancer Res* **1994,** 54, 993-7. (b) Yager, J. D. *J Natl Cancer Inst Monogr* **2000**, 67-73. (c) Lonard, D. M.; Lanz, R. B.; O'Malley, B. W. *Endocr Rev* **2007,** 28, 575-87. (d)Mendelsohn, M. E. *Climacteric* **2009,** 12 Suppl 1, 18-21.

[8] (a)Crosignani, P. G.; Kenemans, P.; Paoletti, R.; Soma, M. R.; Woodford, F. P. *Eur J Obstet Gynecol Reprod Biol* **1997,** 74, 67-72. (b)Jordan, V. C. *Br J Pharmacol* **2006,** 147 Suppl 1, S269-76.

[9] Ring, A.; Dowsett, M. *Endocr Relat Cancer* **2004,** 11, 643-58.

[10] Htun, H.; Holth, L. T.; Walker, D.; Davie, J. R.; Hager, G. L. *Mol Biol Cell* **1999,** 10, 471-86. (b) Zhao, H.; Hart, L. L.; Keller, U.; Holth, L. T.; Davie, J. R. *J Cell Biochem* **2002,** 86, 365-75.

[11] (a) Adamczyk, M.; Reddy, R. E.; Yu, Z. *Bioorg Med Chem Lett* **2002,** 12, 1283-5. (b) Asai, D.; Tokunaga, T.; Kondo, K.; Kawaguchi, T.; Takayanagi, S.; Shinmyozu, T.; Nakai, M.; Yakabe, Y.; Shimohigashi, Y. *J Biochem* **2008,** 143, 781-92. (c) Rickert, E. L.; Oriana, S.; Hartman-Frey, C.; Long, X.; Webb, T. T.; Nephew, K. P.; Weatherman, R. V. *Bioconjug Chem* **2010,** 21, 903-10.

[12] Silke, C. F.-J., MA. *Biopolymers (Biospectroscopy)* **2003,** 72, 256-263.

[13] (a) Lerestif, J. M.; Perrocheau, J.; Tonnard, F.; Bazureau, J. P.; Hamelin, J. *Tetrahedron* **1995,** 51, 6757-6774. (b) Baldridge, A.; Kowalik, J.; Tolbert, L. M. *Synthesis-Stuttgart* **2010**, 2424-2436.

[14] Trott, O.; Olson, A. J. *J Comput Chem* **2010,** 31, 455-61.

[15] Pettersen, E. F.; Goddard, T. D.; Huang, C. C.; Couch, G. S.; Greenblatt, D. M.; Meng, E. C.; Ferrin, T. E. *J. Comput. Chem.* **2004,** 25, 1605-1612.

[16] Sanner, M. F. Python: *J. Mol. Graph.* **1999,** 17, 57-61.

[17] Taylor, J. L.; Rohatgi, P.; Spencer, H. T.; Doyle, D. F.; Azizi, B. *BMC Biotechnol* **2010,** 10, 15.

[18] Asim, M.; El-Salfiti, M.; Qian, Y.; Choueiri, C.; Salari, S.; Cheng, J.; Shadnia, H.; Bal, M.; Christine Pratt, M. A.; Carlson, K. E.; Katzenellenbogen, J. A.; Wright, J. S.; Durst, T. *Bioorg Med Chem Lett* **2009,** 19, 1250-3.

[19] (a) Enoki, S.; Saeki, K.; Maki, K.; Kuwajima, K. *Biochemistry* **2004,** 43, 14238-48. 23. (b) Martin, M. E.; Negri, F.; Olivucci, M. *J Am Chem Soc.* **2004,** 126, 5452-64.

[20] Brzozowski, A. M.; Pike, A. C.; Dauter, Z.; Hubbard, R. E.; Bonn, T.; Engstrom, O.; Ohman, L.; Greene, G. L.; Gustafsson, J. A.; Carlquist, M. *Nature* **1997,** 389, 753-8.

[21] (a)Azizi, B.; Chang, E. I.; Doyle, D. F. *Biochem Biophys Res Commun* **2003,** 306, 774-80. (b) Schwimmer, L. J.; Rohatgi, P.; Azizi, B.; Seley, K. L.; Doyle, D. F. *Proc Natl Acad Sci U S A* **2004,** 101, 14707-12. (c) Baker, K.; Bleczinski, C.; Lin, H.; Salazar-Jimenez, G.; Sengupta, D.; Krane, S.; Cornish, V. W. *Proc Natl Acad Sci U S A* **2002,** 99, 16537-42.

[22] Struhl, K.; Davis, R. W. *Proc Natl Acad Sci U S A* **1977,** 74, 5255-9.

[23] (a) Miksicek, R. J. *J Histochem Cytochem* **1993,** 41, 801-10. (b) Dull, A.; Goncharova, E.; Hager, G.; McMahon, J. B. *J Steroid Biochem Mol Biol* **2010,** 122, 341-51.

[24] (a) Riggs, B. L.; Hartmann, L. C. *N Engl J Med* **2003,** 348, 618-29. (b) Kieser, K. J.; Kim, D. W.; Carlson, K. E.; Katzenellenbogen, B. S.; Katzenellenbogen, J. A. *J Med Chem* **2010,** 53, 3320-9. (c) McDonnell, D. P.; Wardell, S. E. *Curr. Opin. Pharmacol* **2010**.

[25] Kliewer, S. A., Moore, J. T., Wade, L., Staudinger, J. L., Watson, M. A., Jones, S. A., McKee, D. D., Oliver, B. B., Willson, T. M., Zetterstrom, R. H., Perlmann, T., and Lehmann, J. M. *Cell* **1998,** *92*, 73-82.

[26] (a) Xie, W., Uppal, H., Saini, S. P., Mu, Y., Little, J. M., Radominska-Pandya, A., and Zemaitis, M. A. *Drug Discov Today* **2004**, *9*, 442-449. (b) Sonoda, J., Rosenfeld, J. M., Xu, L., Evans, R. M., and Xie, W. *Curr Drug Metab* **2003**, *4*, 59-72.

[27] Zhang, B., Xie, W., and Krasowski, M. D. *Pharmacogenomics* **2008**, *9*, 1695-1709.

[28] (a) Zheng, C., Han, L., Yap, C. W., Xie, B., and Chen, Y. *Drug Discov Today* **2006**, *11*, 412-420. (b) Watkins, R. E., Wisely, G. B., Moore, L. B., Collins, J. L., Lambert, M. H., Williams, S. P., Willson, T. M., Kliewer, S. A., and Redinbo, M. R. *Science* **2001**, *292*, 2329-2333.

[29] Squires, E. J., Sueyoshi, T., and Negishi, M. *J Biol Chem* **2004**, *279*, 49307-49314.

[30] Kawana, K., Ikuta, T., Kobayashi, Y., Gotoh, O., Takeda, K., and Kawajiri, K. *Mol Pharmacol* **2003**, *63*, 524-531.

CHAPTER 8

RECAPTURE OF FLUORESCENCE IN A PROTEIN HOST: PROBE DEVELOPMENT USING GFP CHROMOPHORES

Introduction

The green fluorescent protein (GFP) and its derivatives have revolutionized molecular biology by providing a fluorescent tag which can be attached to other proteins using gene expression techniques. The marker itself, a 238-amino acid protein which maintains the chromophore within a restrictive β–barrel,[2] serves primarily as a probe without providing direct functional information. Moreover, the size of this 29kD protein limits a number of applications, which has driven us to examine the use not of the protein, but only of its chromophore, derivatives of which, however, are invariably weakly fluorescent, an observation we have been able to attribute to the intervention of additional vibrational modes in the unbound state.[3]

Mimicking the effects of the β–barrel and restoring the fluorescence by rigidifying the otherwise conformationally flexible chromophore has been the subject of several studies. For instance, we showed that encapsulation within an octa acid cavitand results in a 15-fold fluorescence enhancement.[4] Could we obtain similar results using a protein host? If so, such a chromophore could act as a high-sensitivity "turn on" probe for proteins. Unlike other probes, e.g., aminonaphthalenesulfonate (ANS), which respond to hydrophobic vs. hydrophilic sites, such a probe would be a *topological* one, responding to the conformational rigidity of a host site.

Using an unbiased high-throughput screening process, a variety of GFP chromophore analogs were tested against selected protein analytes, and those with 4-$N(Et)_2$ substituents showed selective emission quantum yield (EQY) enhancement for

human serum albumin (HSA).[5] Using this lead, we now report an HSA probe with dramatically improved sensitivity and proof of concept that proteins can act to turn on fluorescence in benzylideneimidazolidinones (BDIs) when the guest is rigidified in a binding site.

HSA, the major protein component of blood plasma, is marked by an exceptional affinity that allows binding a myriad of ligands.[6] In fact, its twelve binding sites are probably a reason that albumin would be selected in a broad spectrum assay.

Although HSA is not a primary target for disease screening, microalbuminuria (MA), referring to a urinary albumin content of 30-300mg/24hr, has become an important diagnostic and is linked to various diseases.[7] Thus a sensitive and selective determination of albumin concentration over this range is of medical significance. Moreover, such a protein serves as a test case for the use of BDIs in protein binding.

Currently, Albumin 580 (AB580) is commercially used as a fluorescent probe, given its selectivity for albumin over other proteins, its low susceptibility to environmental factors, and its favorable spectroscopic characteristics (λ_{abs} = 580 nm, λ_{em} = 610 nm).[8] Other assays used for HSA detection include immunoassays[9], electrochemical assays[10], and spectrophotometric assays.[11]

Experimental

General Experimental Section

All reagents were purchased from commercial sources and used without further purification. NMR spectra were recorded using a Varian Mercury spectrometer (300MHz) and processed using MestRe-C 2.3a. Absorbance spectroscopy was completed using a Perkin-Elmer Lambda 19 Spectrometer and fluorescence spectroscopy was completed using a Horiba Jobin Yvon Flurolog Spectrophotometer. Mass spectroscopy data was completed by the Georgia Tech Mass Spectroscopy Center.

Synthesis

Synthesis of the 13 compounds was carried out by a 2+3 cycloaddition of the corresponding aromatic Schiff base with the imine ester highlighted in Chapter 2. Schiff bases (imines) were prepared by the reaction of 4-diethylaminobenzaldehyde or 2-hydroxy-4-diethylaminobenzaldehyde with the corresponding primary alkyl amine in quantitative yields. The imine ester was prepared as highlighted in Chapter 2 by the reaction of glycine methyl ester and ethyl acetimidate with potassium carbonate in a water/diethyl ether solution.

Emission On/Off Ratio Studies

For each chromophore, 10 mL of a ~$5x10^{-5}$ M of each chromophore was prepared with absorbance and fluorescence spectra taken of each, which would act as the baseline for each. The absorbance for all solutions was approximately 0.5. Following this, 5.0 mg of HSA was added to give an albumin concentration of 0.5 mg/L in each case. Absorbance and fluorescence spectra were immediately taken of each. Using these maximum values, the F/Fo value was calculated by taking the ratio of the maximum emission intensity of the HSA:Chromophore solution and the baseline of the chromophore.

Titration Studies

A $3.00x10^{-5}$ M solution of chromophore was prepared and titrated with a HSA solution in increments of 10 mg/L albumin. Following each addition, spectroscopy was immediately completed. Titration continued until no change (increase) in fluorescence intensity was noted.

Competition Studies

Ibuprofen and Warfarin titrations: 5.0 mL of $3.00x10^{-5}$ M solution of chromophore was prepared and to this was added 1eq of HSA. Following, an Ibuprofen (0.1071 M) and separately a Warfarin ($5.64 x10^{-2}$ M) solution was titrated using pre-determined equivalents (1, 5, 10, 30, 50, 75, 100, and 200) of each. After each addition, absorbance and fluorescence spectra were immediately taken of each. Following the

separate titrations, a titration of warfarin to 100 eq. followed by ibuprofen to 100 eq. was done to determine if all chromophore could be competitively expelled.

AB580: AB580 was purchased from Sigma-Aldrich as a 0.1% 2-propanol solution. For this, equimolar concentrations of AB580 and chromophore were prepared and titrated with HSA in increments of 10 mg/L. Following each addition, an absorbance and fluorescence spectrum was immediately taken. (Spectra provided in paper)

Fluorescence Quantum Yield Studies

Fluorescence quantum yields were determined using the integrated emission area for the known standard Rhodamine 6G when excited at 488 nm (Φ = 0.95). Quantum yields were calculated using the below equation, where Q represents the quantum yield, n is reflective index of the solvent, I is integrated intensity, and OD is optical density. In each case the subscript r represents the values of the standard.

$$Q = Q_r\left(\frac{I}{I_r}\right)\left(\frac{OD_r}{OD}\right)\left(\frac{n^2}{n_r^2}\right)$$

Interference Studies

For each protein/macromolecule, 2.0 mL of 8.35×10^{-5} M ligand stock solution were combined with 2.0 mL of 1.0 mg/L solution of each protein/macromolecule and mixed to give a final concentration of 4.18×10^{-5} M ligand and 0.5 mg/L protein/macromolecule. Absorbance and fluorescence spectra were immediately taken. For the F/Fo ratio, a 4.18×10^{-5} M ligand solution (giving an absorbance of approximately 0.5) was prepared to act as the baseline.

Fitting data to one-site and two-site binding models

The relative fluorescence quantum yields F/Fo were fit to a one-site and a two-site binding model according to the equation: $v(x) = \frac{K_1 x}{1+K_1 x}$ for a one-site binding model and $v(x) = \frac{K_1 x + 2K_1 K_2 x^2}{1+K_1 x+K_1 K_2 x^2}$ for the two-site binding model. The results are shown in Figure 8.1, with the one-site model in green and the two-site model in red. The dissociation

constants were 3.33×10^{-6} in the first case and 4.26×10^{-6} and 2.23×10^{-6} in the second, with Fsat = 138 in the first case and 113 in the second.

Results

From an initial EQY screening showing enhancement for R_2 = Me, n-Pr or pentyl, a number of 4-$N(Et)_2$-FP analogs were combinatorially synthesized using techniques highlighted elsewhere[12] to determine the maximum EQY achievable with a given substitution. These results are summarized below in Table 8.1.

Table 8.1. FP Analogs and EQY Enhancements of compounds 1-13 with HSA. [a] Intensity(bound)/Intensity(unbound) at λ_{em} for 7.5 μM (0.5 mg/mL) HSA solutions.

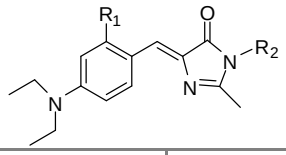

#	R_1	R_2	F/F_o [a]	#	R_1	R_2	F/F_o [a]
1	H	Me	3	**8**	OH	Pentyl	36
2	H	n-Pr	11	**9**	OH	Hexyl	67
3	H	Pentyl	24	**10**	OH	Heptyl	72
4	H	Hexyl	20	**11**	OH	Octyl	52
5	H	$C_3H_6CO_2H$	6	**12**	OH	Undecyl	7
6	OH	Me	30	**13**	OH	$C_3H_6CO_2H$	28
7	OH	n-Pr	48				

Increasing turn-on ratios with increasing alkyl chain length substitution are readily rationalized by the increasing hydrophobicity of the chromophores coupled with the known hydrophobicity of the binding pockets,[13] which reach a limit, respective of alkyl chain length, with the heptyl group. Additionally, we speculated that substitution of an *ortho*- hydroxyl would provide additional sensitivity due to a cluster of polar residues located in each site.[14]

From the preliminary screening, **10** was chosen for more extensive studies to determine its application to albumin sensing in aqueous solution. For all experiments, phosphate buffered saline (PBS) at pH = 7.4 was used. Within PBS, **10** showed favorable spectral characteristics (λ_{abs} = 470nm, λ_{em} = 510nm), which shows some

differences compared to the Green Fluorescent Protein (λ_{abs} = 398nm, λ_{em} = 508nm).[15] A Langmuir calibration curve for **10** required a two-site cooperative binding model[16] and showed a sensing range of 0.15 μM to 15 μM (10 mg/L to ~1000 mg/L) with two dissociation constants (K_d) of 0.24 μM and 0.45 μM, offering a higher sensitivity and greater sensing range than AB580 (Figure 8.1).

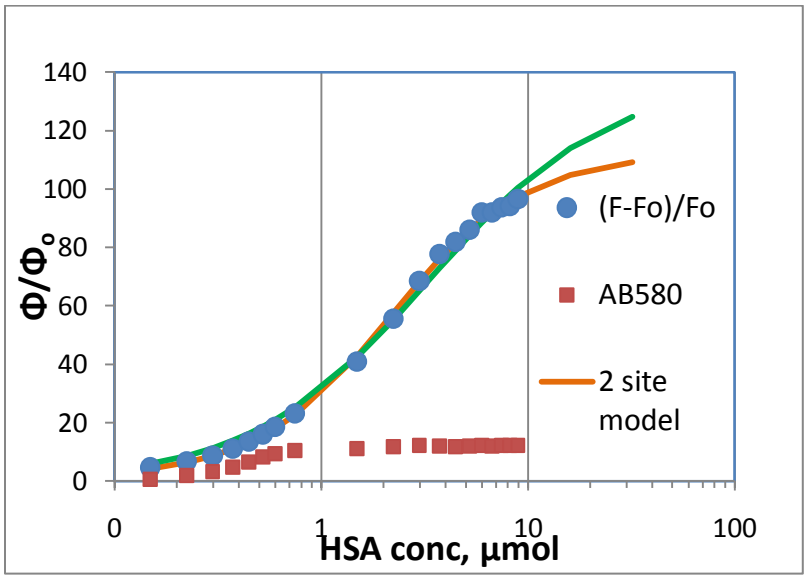

Figure 8.1. Emission response Plot of one-site and two-site binding model vs. F/Fo data.

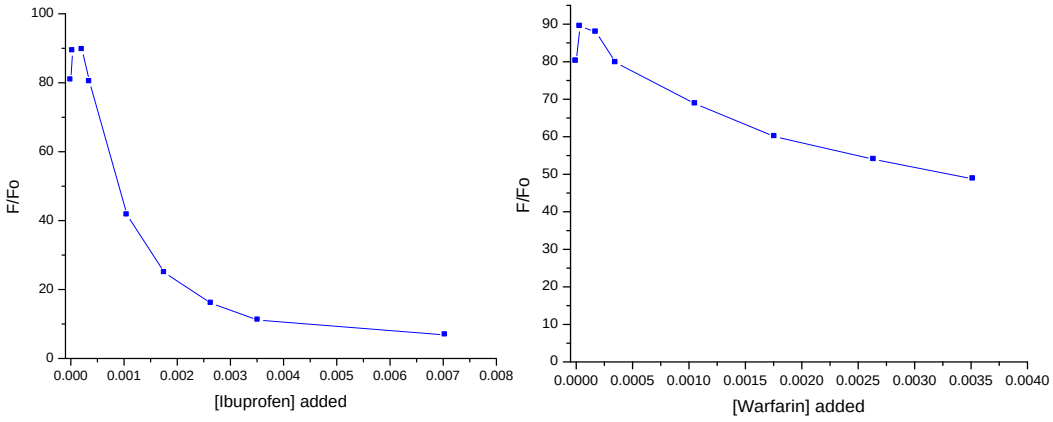

Figure 8.2. Competition titration of **10**:HSA complex with Ibuprofen (left) and Warfarin (right).

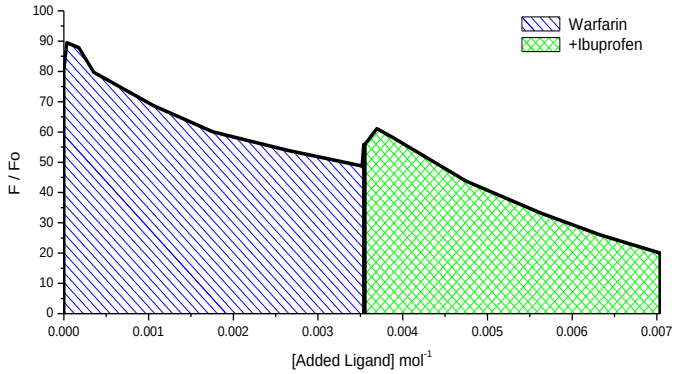

Figure 8.4. Competitive binding study with ibuprofen and Warfarin.

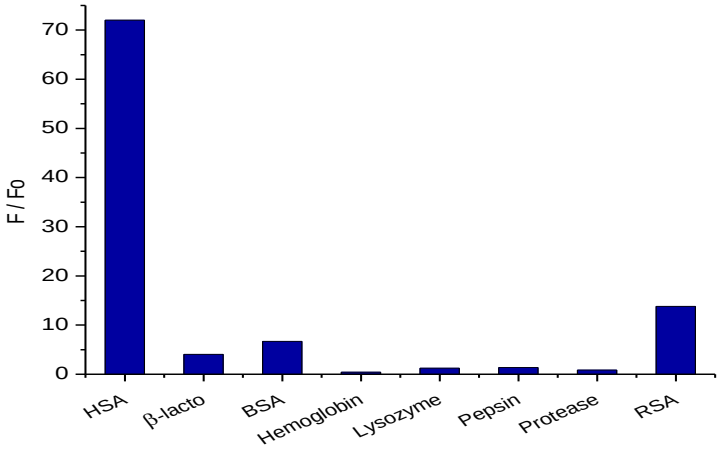

Figure 8.3. Emission response of 10 with proteins and macromolecules 7.5 μM (0.5 mg/mL) in PBS buffer.

Given the relative fluorescence yield of 72, which we obtain at saturation with the heptyl analog **10**, we also subjected the bound protein to competitive binding studies against **10** using warfarin and ibuprofen, which selectively bind Sudlow's Sites I and II.[17] As noted from Figure 8.2, binding of **10** to HSA occurs at both binding pockets, each of which is displaced by one of the secondary binders. We attribute the initial increase in fluorescence to allosteric effects, a conclusion consistent with the two-site binding model. These results, mentioned earlier, are not surprising since secondary binding of ligands to HSA sites is common and well established.[18] Apparently, binding of one ligand, either Warfarin, ibuprofen, or HSA itself, leads to tighter binding of the secondary site and an increased fluorescence.

HSA probes find application in the medical community as methods of quantification of albumin within biological samples. For these purposes, probes must be both selective and sensitive to quantify HSA as well to operate within an aqueous environment. To explore the selectivity of **10**, buffered solutions of proteins representative of those found in biological fluids were prepared with equimolar amounts of the probe. Additionally, the selectivity of **10** was explored by testing other albumins. The results of these interference studies are summarized in Figure 8.3.

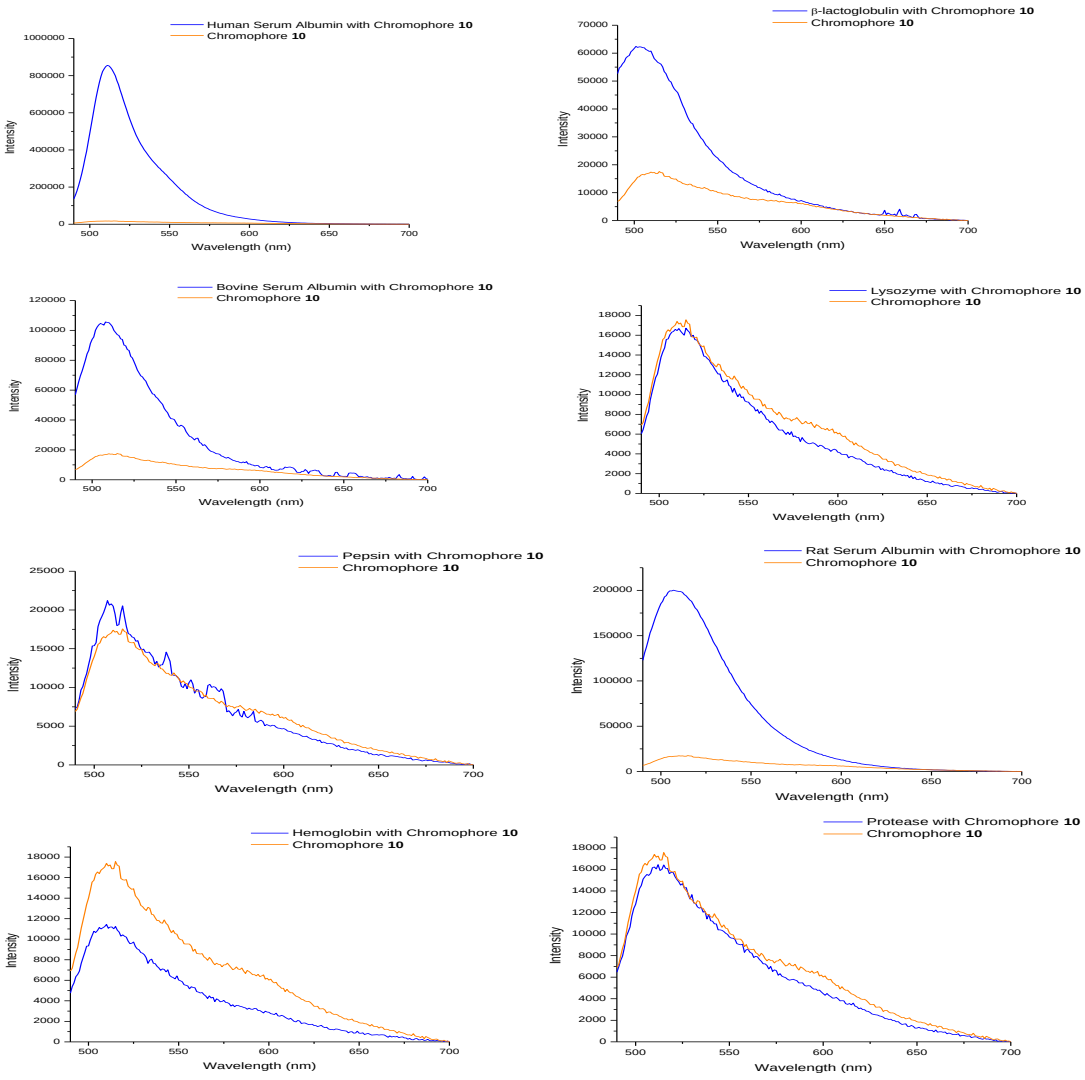

Figure 8.5. Emission spectra of compound 10 with various biological analytes.

The data from Figure 8.4 shows the selectivity of **10** to HSA compared to other analytes. One remarkable quality is the selectivity over albumins from other species. In PBS buffer, **10** showed a ~70-fold enhancement at 5 μmol HSA (for general reference, Φ = 0.25) compared to a 5-fold and a 13-fold enhancement for Bovine Serum Albumin (BSA) and Rat Serum Albumin (RSA), respectively.

The similar responses of RSA and BSA were anticipated, due to the high degree of structural homology shared by HSA, BSA, and RSA.[19] Other proteins did not show such enhancements, and in one case exhibited emission quenching, providing a very robust probe that experiences little interference.

Conclusions and Outlook

Mentioned earlier, AB580 has gained significant application as a fluorescent probe for the detection of albumin in biological samples.[20] To test the competitiveness of **10** against AB580, equimolar probe solutions were prepared and tested in PBS buffer. In Figure 8.1, **10** exhibits significantly higher fluorescence enhancement ratios compared to AB580 as well as a wider operation range for sensing providing for its use as a candidate for a small molecule probe for HSA. AB580 is generally used to accurately detect albumin from 0.15 μM to 3.0 μM (10 mg/L to 200 mg/L). In both cases, the probes exhibit weak unbound fluorescence followed by 10 to 100-foldstrong enhancements with binding to HSA. Given the few synthetic iterations completed to attain an optimization on the initial hit, we anticipate that further enhancements using combinatorial synthesis will produce even better probes with relative ease.[21]

The efficient fluorescence of the chromophore in GFP has been ascribed to the uniqueness of the β-barrel. We have shown that such chromophores can be activated by a non-barrel protein and can accommodate an aqueous environment. This study represents one of the first cases utilizing a FP chromophore as a probe, with the exclusion of metal sensing,[22] and provides motivation for this class of compounds to be considered for general sensing applications. We note that other probes for HSA exist and are

documented in the literature[23], however unlike probes which depend upon changes in environmental (solvent) polarity, this is a topological probe, depending instead upon conformational freezing for its efficacy and signalling mechanism.

References

[1] Baldridge, A.; Feng, S.; Tolbert, L.M.; Chang, Y-T. *ACS Comb. Chem.*

[2] Enoki, S.; Saeki, K.; Maki, K.; Kuwajima, K. *Biochemistry* **2004**, *43*, 14238-14248.

[3] Stavrov, S. S.; Solntsev, K. M.; Tolbert, L. M.; Huppert, D. *J. Am. Chem. Soc.* 2006, *128*, 1540-1546.

[4] Baldridge, A.; Samanta, S. R.; Jayaraj, N; Ramamurthy, V.; Tolbert, L. M. *J. Am. Chem. Soc.* 2010, *132*(5), 1498-1499.

[5] Baldridge, A.; Feng, S.; Chang, Y.-T., Tolbert, L. M. *ACS Comb. Sci.* **2011**,*11*, 32-38.

[6] Peters, T. *All about Albumin: Biochemistry, Genetics, and Medical Applications*, Academic Press: San Diego, **1995**.

[7] Ward, K.M. *Anal. Chem.* **1995**, *65*, 383R-391R

[8] Kessler, M.A.; Meinitzer, A.; Wolfbeis, O.S. *Anal Biochem* **1997**, *248*, 180-182.

[9] Doumas, B.T.; Peters Jr., T. *Clin. Chim Acta* **1997**, *258*, 3-20.

[10] Zhang, H.M.; Zhu, Z.W.; Li, N.Q. *J. Anal. Chem.* **1999**, *363*, 408.

[11] Tugirimana, P.L; Delanghe, J.R. *Nep. Dial Trans.* **2008**, 1-5.

[12] Baldridge, A; Kowalik, J.; Tolbert, L.M. *Synthesis* **2010**, *14*, 2424-2437.

[13] Fasano, M., Curry, S., Terreno, E., Galliano, M., Fanali,G., Narciso, P., Notari, S., Ascenzi, P. *IUBMB Life* **2005**, *57(12)*, 787-796.

[14] Ghuman, J., Zunszain, P.A., Petitpas, I., Bhattacharya, A.A., Otagiri, M., Curry, S. *J. Mol. Biol.* **2005**, *353*, 38-52.

[15] Zimmer, M. *Chem. Rev.* **2002**, *102*, 759-781.

[16] Dill, K.; Bromberg, S. *Molecular Driving Forces: Statistical Thermodynamics in Biology, Chemistry, Physics, and Nanoscience*. Garland Science: New York, 2011.

[17] Sudlow, G., Birkett, D.J., Wade, D.N. *Mol. Pharm*. **1975**, *11*, 824-832.

[18] Baroni, S.; Mattu, M.; Vannini, A.; Cipollone, R.; Aime, S.; Ascenzi, P.; Fasano, M. *Eur. J. Biochem*. **2001**, *268*, 6214-6220.

[19] (a) He, X.M.; Carter, D.C. *Nature* **1992**, *358*, 209-215. (b) Ahn, Y.H.; Lee, J.S.; Chang, Y.T. *J. Comb. Chem* **2008**, *10*, 376-380. (c) Wagner, B. K.; Carrinski, H. A.; Ahn, Y. H.; Kim, Y. K.; Gilbert, T. J.; Fomina, Dina A.; Schreiber, S. L.; Chang, Y. T.; Clemons, P. A. *J. Am Chem. Soc* **2008**, *130(13)*, 4208-4209. (d) Min, J.i; Lee, J. W.; Ahn, Y.H; Chang, Y.T. *J. Comb. Chem*. **2007**, *9(6)*, 1079-1083.

[20] In addition, AB580 suffers from some instability and must be provided in an 2-isopropanol solution.

[21] (a) Choi, S.; Choi, E.Y.; Kim, D.J.; Kim, J.H.; Kim, T.S.; Oh, S.W. *Clin. Chim. Acta* **2004**, *339*, 147-156. (b) Ikariyama, Y; Suzuki, S. *Anal. Chim. Acta* **1984**, 156, 245-252. (c) Hou, Z.; Tong, X; Dong, W.; Dong, C.; Shuang, S. *Spect. Acta Part A* **2007**, *66*, 552-556.

[22] Baldridge, A.; Solntsev, K.M.; Song, C.; Tanioka, T.; Kowalik, J.; Tolbert, L.M. *Chem. Commun*. **2010**, *46*, 5686.

[23] (a) Liu, B.; Xue, C.; Wang, J.; Yang, C.; Zhao, F.; Lv, Y. *J. of Luminescence* **2010**, *130*, 1999-2003. (b) Lee, S.H.; Suh, J.K.; Li, M. *Bull. Korean Chem. Soc.* **2003**, *24*, 45. (c) Phillipou, G.; James, S.K.; Seaborn, C.J.; Phillips, P.J. *Clin. Chem*. **1989**, *35*, 456-458. (d) Kessler, M.A.; Hubmann, M.R.; Dremel, B.A.; Wofbeis, O.S. *Clin Chem.* **1992**, *38*, 2089-2092. (e) Hou, X.; Tong, X.; Dong, W.; Dong, C.; Shuang, S. *Spectrochimica Acta A*, **2007**, *66*, 552-556.

CHAPTER 9

AMI CHROMOPHORES AS LIQUID CRYSTALS

Work highlighted in this chapter was carried out in collaboration with the laboratory of Dr. Mohan Srinivasarao. The synthesis of the compounds tested was completed within the Tolbert lab while the solid-state optical spectroscopy and testing of liquid crystal properties was completed within Dr. Srinivasarao's laboratory. Additional studies were completed at Argonne National Lab, APS MUCAT (Sector 6).

Introduction

Liquid crystals have found wide application in optical displays and other devices.[1] Extensive literature exits on the physics of the organization and orientation of liquid crystals as well as how external effects including temperature, pressure and composition cause significant changes in the properties, both physical and optical of liquid crystals.[2] This chapter is by no means designed to provide an overview of this widely important class of molecules but rather provides motivation for use of AMI chromophores as possible candidates for liquid crystalline molecules. Compounds termed as mesogens are commonly cited as having liquid crystalline properties. These compounds are characterized as being both rod-like and disk-like in their appearance.[3] In the case of rod-like mesogens, the compounds are characterized by a number of different properties but a specific class that is widely used contains an aliphatic/aromatic hydrocarbon moiety that provides rigidity, a flexible aliphatic chain and an electron-withdrawing group.[4] From their structure, arylmethyleneimidazolidinones (AMIs) possess a similar scaffold with a hydrophobic phenyl moiety that can readily be substituted with various functionalities to become increasingly hydrophobic, while the imidazolindinone ring provides the electron-withdrawing group.

A class of rod-like mesogens that have gained significant application are the 4-n-alkyl-4'-cyanobiphenyls.[5] Within devices, two of these mesogens include 4-n-octyl-4-cyanobiphenyl (8CB) and 4-n-pentyl-4-cyanobiphenyl (5CB), whose wide application

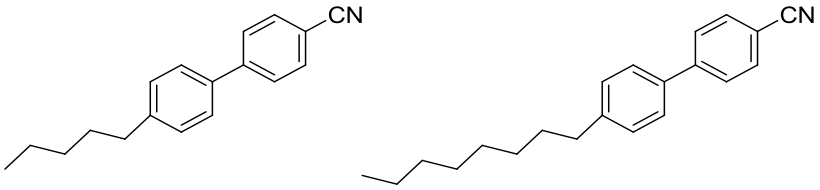

Figure 9.1. Structures of 5CB (left) and 8CB (right) mesogens.

results from their large, complimenting operating ranges, with respect to temperature, as well as their general synthetic ease for manufacturing.[6] Using these compounds as motivation, it was envisioned that replacement of the cyano group with the imidazolindinone ring should provide compounds with liquid crystal properties. Additional to this motivation are continuing studies on the solid state behavior of AMI chromophores where the fluorescent properties of these compounds upon solid-liquid transitions could provide insight into the interaction of AMI's within the solid state as highlighted in Chapter 4.

Experimental

Synthesis

Synthesis of the compounds was carried out as highlighted in Chapter 2 following the synthesis of the aldehyde. Synthesis of the aldehyde is accomplished by adding 0.02 mol of 4-alkyl-4'-cyanobiphenyl with 50 mL of 75% formic acid and 4g of Raney Ni that is refluxed for 2 hrs. Following this, 3g of Raney Ni is added to the mixture and allowed to reflux an additional hrs. The solution is cooled and diluted with 50 mL of H_2O. The organic layer is extracted with 40 mL of Et_2O with the remaining reaction slurry filtered and washed with an additional 10 mL of Et_2O. The organic extracts were combined and solvent removed in vacuo to afford pure aldehyde product in good yield (~60%).[7]

The Schiff base was obtained by stirring the biphenylbenzaldehyde (1eq) with the primary amine (1eq) in 5.0 mL of MeOH overnight, followed by removal of solvent under reduced pressure to yield product. The aminoimidate was prepared as previously described.[8] Imidazolindinones (liquid crystal candidates) were synthesized by combining the corresponding Schiff base (1eq) with the imidate (1.1 eq) and ~0.5mL of MeOH, which with stirring for 12 h resulted in the formation of bright yellow precipitate. Filtering of the precipitate followed by washing with cold Et_2O yielded the desired products as bright yellow powdered materials. Characterization of these compounds is found in Appendix A.

Differential Scanning Calorimetry (DSC)

DSC measurements on the imidazolinones were completed by preparing a 3.00 mg of sample of each in a seal aluminum pan and completing a heat/cool/heat scan with the following sequence:

1: Equilibrate at -20.00 °C	2: Ramp 20.00 °C/min to 100.00 °C
3: Mark end of cycle	4: Isothermal for 2.00 min
5: Ramp 5.00 °C/min to -30.00 °C	6: Isothermal for 2.00 min
7: Mark end of cycle 0	8: Ramp 5.00 °C/min to 300.00 °C
9: Isothermal for 2.00 min	10: Mark end of cycle 0

Results

Results of DSC measurements show similar phase transitions as the parent compounds. The transitions for the 5-CB and 8-CB parent compounds are well documented. For the 8CB mesogen the following transitions are noted. <20 C degree, crystalline; 20-34 C degree, Smectic-A; 34-41 C degree, Nematic; >41 C degree, isotropic.[9] As a control, the DSC of both the synthesized molecule and the commercially available 8CB are shown (Figure 9.2).

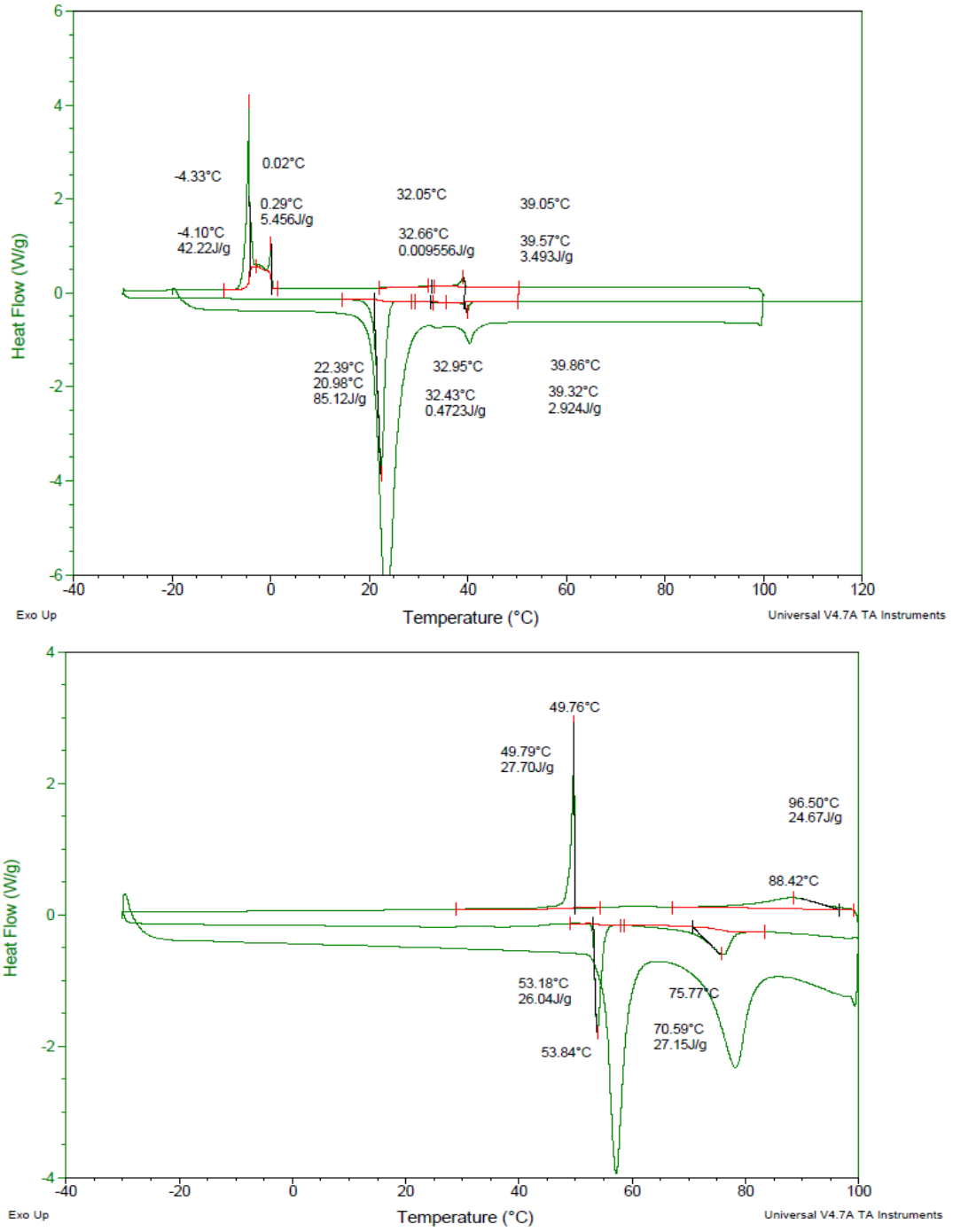

Figure 9.2. DSC measurements of 8CB (top) and AMI C8 (bottom).

From these DSC results, the 3 major transitions noted for the 8CB can be compared to AMI C8 and are summaried in Table 9.1. Additional studies on AMI C8 were completed using a much slower heating and cooling rate.

Table 9.1. Transitions of AMI C8 as noted from DSC measurements.

AMI C8	Transition #1/^{o}C	Transition #2/^{o}C	Transition #3/^{o}C
DSC +5 ^{o}C/min	58	70	94
DSC -5 ^{o}C/min	34	45	94
DSC +0.4 ^{o}C/min	52.5	73	94
DSC -0.4 ^{o}C/min	44	57	94
DSC +0.4 ^{o}C/min	50	84	98
DSC -0.4 ^{o}C/min	48	80	92

Additional XRD studies completed at Aragon National Lab, show the compounds reach an isotropic phase, which is a phase where the compound exhibits properties of a conventional liquid. XRD shows that the imidazolinone samples are crystalline below isotropic. Further characterization of these molecules using a polarizing microscope

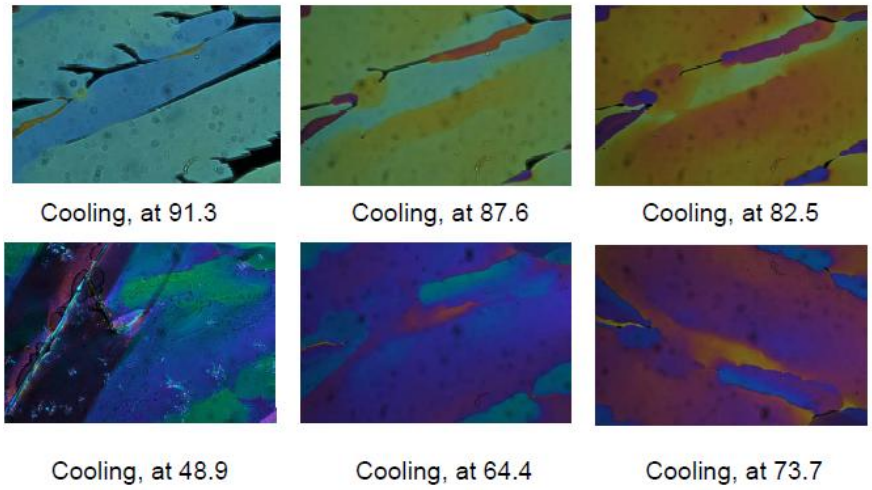

Figure 9.3. Polarized microscope images at transitions temperatures of AMI C8 showing Semitic B phase characteristics.

reveals a Smectic B phase of the molecule upon heating and cooling as indicated by the mosaic appearance of the crystals.

Following the completion of DSC measurements the emission spectra of the compounds reveals a high emission quantum yield in the solid state most likely attributed to the tight, ordered organization of the molecules hindering the conformational freedom that provides the main emission deactivation for these compounds. Following heating to 58^{o}C, the first transition, a marked difference in the EQY is observed with a quenching of the fluorescence upon the transition from solid to liquid phase (Figure 9.3). A similar EQY vs. temperature profile was noted upon cooling but did not result in full restoration of the EQY observed in the initial solid. This observation could be attributed to the different reorganization of the solid upon cooling possibly resulting in a bending of these molecules thus extinguishing the solid state fluorescence due to loss of planarity.

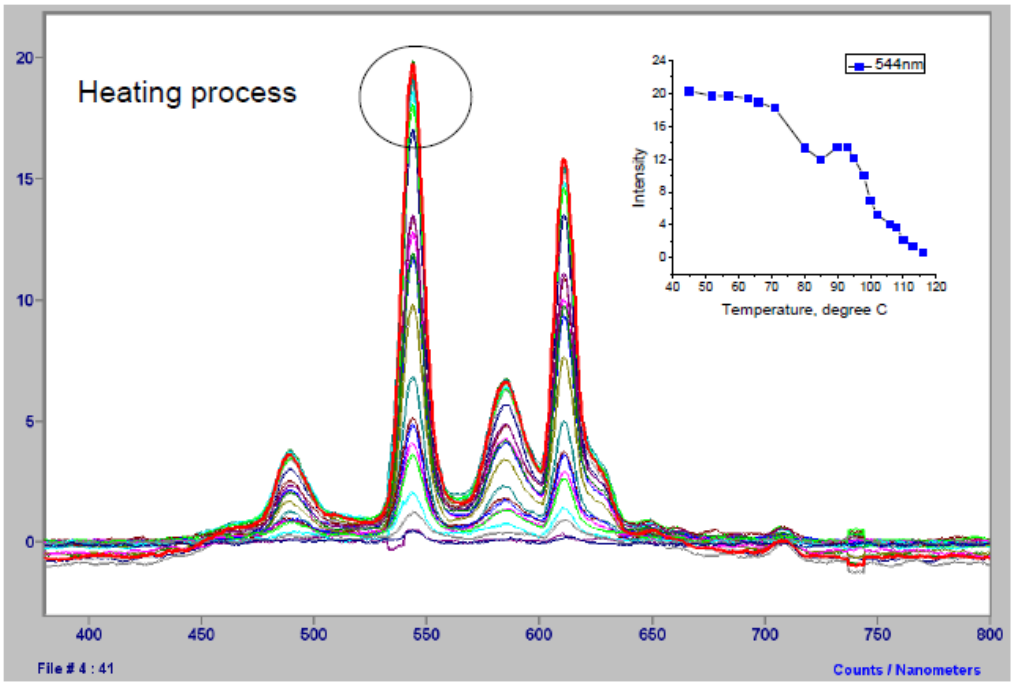

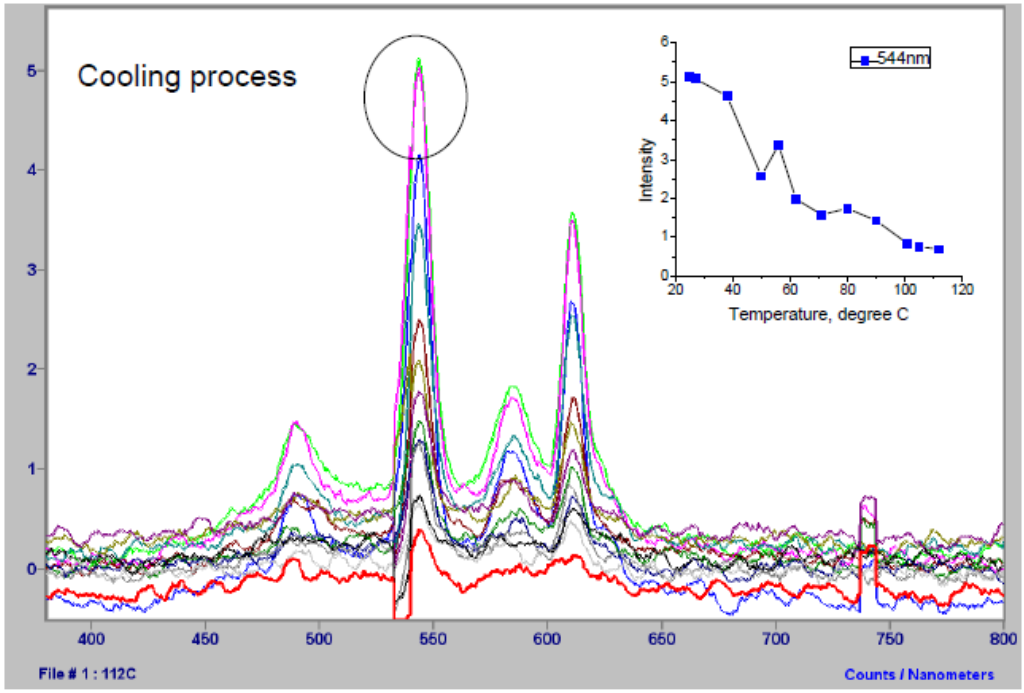

Figure 9.4. Emission spectra of AMI C8 with incremental heating (top) and cooling (bottom) coupled with respective EQY inserts.

Discussion and Conclusions

From the data, it is initially shown that substitution of the cyano group with the imidazolinone group provides a molecule with similar but significantly contrasting characteristics compared to the parent 4-alkyl-4-cyanobiphenyl compounds. XRD results show that only a crystalline structure is observed below the isotropic phase both for AMI C8. Characterization using a polarized microscope reveals a Semitic B is observed with these compounds. Following these initial studies it is also noted that upon heating and cooling a significant change in the EQY is noted for both temperature cycles. The melting of the solid provides a quenching of the fluorescence while cooling restores a portion of the EQY but does not provide a restoration to the initial EQY level. This study can be used to support the hypothesis that the solid state does provide an inhibition of the torsional motions of AMI chromophores as evident from the high initial EQY and the resulting restoration of EQY upon cooling and recrystallization. Additional studies to continue the characterization of these compounds and explore their liquid crystalline

properties are currently underway in collaboration with Dr. Mohan Srinivasarao. Studies involving the doping of these compounds with the parent 4-alkyl-4-cyanobiphenyl compounds are also underway.

References

[1] Pandey, M. B.; Dhar, R.; Wadhawan, V. K. *Phase Transitions* **2009**, *82(12)*, 831-849.

[2] Sluckin, T. J. *Contemporary Physics* **2000**, *41(1)*, 37-56.

[3] Marin, L.; Ciocilteu, S. *Materiale Plastice* **2006**, *43(4)*, 288-291.

[4] Mahlstedt, S.; Janietz, D.; Stracke, A.; Wendorff, J. H. *Chem. Comm.* **2000**, *1*, 15-16.

[5] Byron, D. J.; Gray, G. W.; Wilson, R. C. *J. Chem. Soc. C* **1966**, *9*, 840-5. (b) Gray, G. W.; Lydon, J. E. *Nature* **1974**, *252*, 221-222.

[6] Gray, G.W.; Harrison, K. J.; Nash, J A. *Electronics Letters* **1973** *9 (6)*: 130–131. (b) searching "5CB, display" and/or "8CB, display" yields thousands of results.

[7] Ruoliene, J.; Adomenas, P.; Surutkaitis, R. A.; Denis, G. I. *Zhurnal Organicheskoi Khimii* **1984**, *20(6)*, 1305-10.

[8] (a) Lerestif, J. M.; Perrocheau, J.; Tonnard, F.; Bazureau, J. P.; Hamelin, J. *Tetrahedron* **1995,** 51, 6757-6774. (b) Baldridge, A.; Kowalik, J.; Tolbert, L. M. *Synthesis* **2010**, 2424-2436.

[9] Sharma, Dipti; MacDonald, John C.; Iannacchione, Germano S. *J. Phys. Chem. B* **2006**, *110(33)*, 16679-16684.

CHAPTER 10

CONCLUSIONS AND FUTURE WORK

Conclusions

Since its discovery in the 1960's and subsequent isolation, the Green Fluorescent Protein has revolutionized molecular biology by providing a highly fluorescent marker in a myriad of environments. Responsible for the remarkable fluorescence within this 11-stranded β-barrel protein is a chromophore protectively housed from the surrounding environment resulting from an autocatalytic cyclization and autoxidation of the Ser-65, Tyr-66, and Ser-67 residues.[1] The resulting p-hydroxybenzylideneimidazolidinone chromophore along with multiple analogs have been successfully synthesized[2] and continue to be the subject of numerous studies. [3]

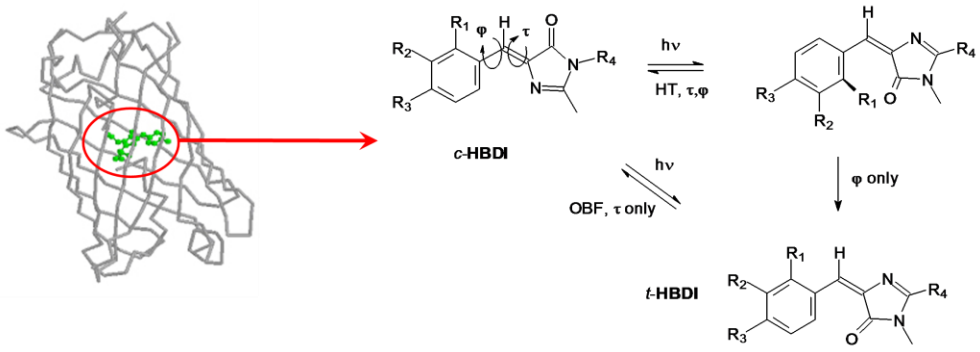

Figure 10.1. Encapsulated chromophore within the 11-stranded β-barrel and torsional motions that result following removal from the restrictive β-barrel.

A number of these studies revolve around the observation that upon denaturation, the chromophore no longer exhibits the same photophysical characteristics as when encapsulated owing to excited state torsional motions that provide for rapid internal conversion resulting in a four order of magnitude emission quantum yield decrease. It is believed that this observation is the result of cis/trans isomerization about the benzylidene

double bond but has also been attributed to other mechanisms including triplet formation,[4] proton transfer,[5] a hula twist,[6] or phenyl rotation.[7]

From the interesting photophysical properties noted in both the protein and the denatured chromophore, the necessity to develop synthetic protocols to study this interesting class of molecules is readily noted. Prior to the work in this dissertation, synthesis of GFP chromophore analogs in the literature has commonly been carried out using Tonge's modification[8] of the Niwa synthesis,[9] often referred to as the Erlenmeyer azalactone synthesis. This synthesis involves somewhat harsh conditions and is not amiable to a number of functionalities. Additionally, this synthesis requires multiple purification steps leading to poor and fair yields. To overcome this obstacle and to fully study the properties of FP chromophores, a combinatorial synthesis utilizing a 2+3 cycloaddition highlighted within Chapter 2 is proposed and shows great promise and results as a way to readily synthesize AMI chromophores in good to excellent yields with minimal purification and overall excellent synthetic tolerance. Further research has shown that functionalization on all branches of the AMI chromophore is realized through synthetic modifications as well as post-synthetic modifications of the AMI chromophores. As noted throughout this work, this cycloaddition has provided avenues to a myriad of products that in subsequent studies have significantly added to the understanding of these AMI chromophores as well as providing new uses for this class of compounds. Chapters 3-9 highlight a number of completed research projects that were made possible through the efficient synthetic protocols developed within this dissertation.

Following the successful synthesis of a number of compounds, studies highlighted in Chapters 3 and 5 show the importance of conformational freedom within AMI chromophores whereby inhibition of certain torsional motions restore some of the emission quantum yield. Chapter 5 adds a significant result in that the inhibition of free rotation about the formal single aryl bond leads to a portion of the internal conversion noted within the free AMI chromophores in solution. This is verified in both the octa

acid cavitands and the cholate salt aggregates in that irradiation of the encapsulated chromophores still exhibit cis/trans isomerization as verified through complete emission quantum yield quenching as well as NMR experiments showing formation of the trans product. This result has not been reported within the literature extensively prior to the works of this dissertation. Most significant to note is the notion that inhibition of different paths and inclusion within a restrictive environment provide for an emission "turn-on" mechanism. This finding was exploited within the works highlighted in Chapters 4 and 5-8.

Noting the discoveries concerning the photophysics of inclusion within supramolecular environments, it follows that these AMI chromophores can act as probes for various analytes. To test this hypothesis, collaboration with Dr. Young-Tae Chang provided for an efficient screening mechanism to determine possible interactions between AMI chromophores synthesized using the 2+3 cycloaddition and various analytes including biologically relevant analytes. These results highlighted in Chapter 6 show the emission quantum enhancement of AMI chromophores in the presence of a variety of chromophores. Additionally, this screening method, by experimental design, allows for the development of AMI chromophores that can act as selective probes for a number of analytes. These results coupled with the combinatorial synthesis allow for a rational design of probes. This idea was realized in Chapter 8 where the development of a human serum albumin probe proved successful by selectively sensing HSA compared to other homologous albumins and competitive binding in the presence of known ligands. In an additional collaboration, the use of AMI chromophores as ligands for nuclear receptors is also realized as highlighted in Chapter 7 working off the principles of rational synthetic design coupled with emission quantum yield enhancement upon inclusion. Results show that AMI can act as ligands for both the ER(α) nuclear receptor as well as ligands for the pregnane X receptor. In the case of the latter, binding of AMIs is shown to be greater than the leading ligands found within the literature.

Work within this dissertation shows a building principle based upon the discovery of an efficient synthesis whose products can be used in a variety of studies. Coupling the observation that inclusion within supramolecular environments leads to an emission quantum yield enhancement with the noted synthetic versatility, the application of these chromophores as small molecule probes that upon inclusion (the sensing mechanism) go from effectively non-fluorescent to fluorescent provides the basis and evidence for the use of AMI chromophores as a new class of probes.

Future Work

While this dissertation highlights a wide body of work completed on the synthesis, photophysics, and application of AMI chromophores, a considerable amount of work remains. Expansion of the combinatorial synthesis and building of the AMI compound library will provide additional substitution patterns that may provide applications to different environments than currently tested and may provide for the discovery of new photophysical data. Expansion of the library could focus on the production of bathochromically shifted chromophores using the SeO_2 oxidation or exploitation of specific functional groups as highlighted in Chapter 2. These red-shifted

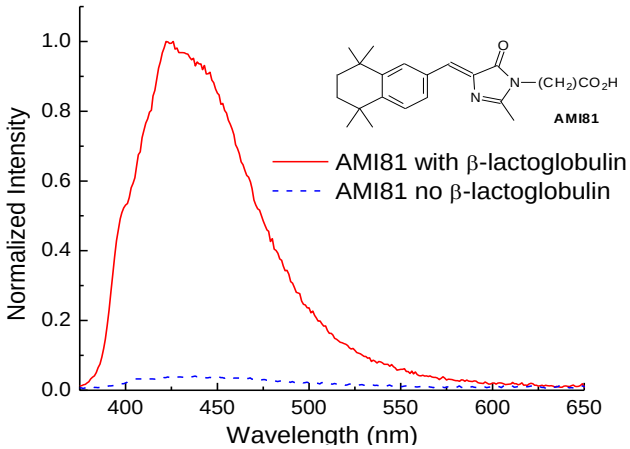

Figure 10.2. Emission enhancement spectra of a tetramethyl-AMI derivative in the presecene of β-lactoglobulin.

chromophores could provide favorable spectral characteristics that are advantageous to a number of different applications.

Following the expansion of the AMI compound library, additional screening studies expanding the analytes tested is motivated to expand this class of compounds as small molecule probes. Interactions with different analytes may provide new discoveries into the photophysical nature of these chromophores while at the same time adding to the rational design protocols currently developed.

The notion of using specific AMI chromophores as small molecule probes has provided interesting results especially in the case of HSA as highlighted in this work. Preliminary work with β-lactoglobulin, the main protein found in mammalian milk, shows that the rational design of an AMI chromophore provides an order of magnitude EQY enhancement (Figure 10.2). Continuing studies using the combinatorial synthesis coupled with these initial results are motivated from these initial findings.

The findings of the interaction of AMI chromophores with nuclear receptors warrants the synthetic design of chromophores for other NR's expanding beyond the initial two highlighted in Chapter 7. At the time of publication, new collaborations are being developed to expand chromophore design to sense the androgen receptor, the retinoic X receptor, and the retinoic acid receptor. Preliminary results (not provided) show promise but extended rational design and additional synthetic analogs are needed.

Finally, work toward the inhibition of cis/trans isomerization upon inclusion of AMI chromophores within supramolecular environments is motivated from the multiple studies highlighted within this dissertation. While the enhancements in EQY are notable upon inclusion, isomerization still remains a main deactivation pathway for use of these chromophores. Synthetic modifications to freeze the rotational path have allowed for some advancements on this front such as the bidentate ligands highlighted in Chapter 3, but additional work is warranted within this area.

References

[1] (a) Tsien, R. Y. The Green Fluorescent Protein. *Annu. Rev. Biochem.* **1998**, *67*, 509-544. (b) Cubitt, A. B.; Heim, R.; Adams, S. R.; Boyd, A. E.; Gross, L. A.; Tsien, R. Y. *Trends Biochem. Sci.* **1995**, *20*, 448-455.

[2] Litvinenko, K. L.; Webber, N. M.; Meech, S. R. *J. Phys. Chem. A* **2003**, *107*, 2616-2623.

[3] Stübner, M.; Schellenberg, P. *J. Phys. Chem. A* **2003**, *107*, 1246-1252.

[4] (a) Habuchi, S.; Ando, R.; Dedecker, P.; Verheijen, W.; Mizuno, H.; Miyawaki, A.; Hofkens, J. *Proc. Natl. Acad. Sci. USA* **2005**, *102*, 9511-9516. (b) Jimenez-Banzo, A.; Nonell, S.; Hofkens, J.; Flors, C. *Biophys. J.* **2008**, *94*, 168-172.

[5] (a) Haupts, U.; Maiti, S.; Schwille, P.; Webb, W. W. *Proc. Natl. Acad. Sci. USA* **1998**, *95*, 13573-13578. (b) Liu, Y.; Kim, H. –R.; Heikal, A. A. *J. Phys. Chem. B* **2006**, *110*, 24138-24146.

[6] Liu, R. S. H. *Acc. Chem. Res.* **2001**, *34*, 555-562.

[7] Martin, M. E.; Negri, F.; Olivucci, M. *J. Am. Chem. Soc.* **2004**, *126*, 5452-5464.

[8] He, X.; Bell, A. F.; Tonge, P. J. *FEBS Lett.* **2003**, *549*, 35-38.

[9] Kojima, S.; Ohkawa, H.; Hirano, T.; Maki, S.; Niwa, H.; Ohashi, M.; Inouye, S.; Tsuji, F. I. *Tetrahedron Lett.* **1998**, *39*, 5239-5242.

APPENDIX A

CHARACTERIZATION OF AMI COMPOUNDS SYNTHESIZED

	Analysis / AMI		^{1}H NMR (ppm)	^{13}C NMR (ppm)	Mass Spec M^{+} (intensity)
#	R1	R2			
1	4-Me	Me	in $CDCl_3$: 2.35 (s, 3H); 2.37 (s, 3H); 3.16 (s, 3H); 7.08 (s, 1H); 7.21 (d, J_{HH} = 8.2 Hz, 2H); 8.01 (d, J_{HH} = 7.7 Hz, 2H)	in $CDCl_3$: 15.87, 21.89, 26.81, 127.77, 129.73, 131.68, 132.38, 138.40, 140.89, 162.17, 171.00	214.1 (45); 55.6 (100)
2	3-OMe	Me	in $CDCl_3$: 2.36 (s, 3H); 3.16 (s, 3H); 3.84 (s, 3H); 6.92 (dd, J_{HH} = 8.2, 1.2 Hz, 1H); 7.06 (s, 1H); 7.31 (t, J_{HH} = 7.8 Hz, 1H); 7.63 (d, J_{HH} = 7.5 Hz, 1H); 7.31 (t, J_{HH} = 1.6 Hz, 1H)	in $CDCl_3$: 15.99, 26.84, 55.51, 116.63, 116.78, 125.17, 127.41, 129.82, 135.63, 139.11, 159.85, 162.86, 170.96	230.1 (40); 149.0 (12); 68.8 (27); 55.6 (100)
3	3-OH	Me	in DMSO-d_6: 2.33 (s, 3H); 3.07 (s, 3H); 6.79 (dd, J_{HH} = 7.8, 2.0 Hz 1H); 6.84 (s, 1H); 7.21 (t, J_{HH} = 7.6 Hz, 1H); 7.50 (d, J_{HH} = 7.8 Hz, 1H); 7.72 (t, J_{HH} = 2.1 Hz, 1H); 9.58 (s, 1H)	in DMSO-d_6: 16.07, 26.93, 118.08, 118.59, 124.02, 125.63, 130.20, 135.84, 139.47, 158.04, 164.97, 170.56	216.1 (45); 55.6 (100)
4	2,3-OMe	Me	in $CDCl_3$: 2.37 (s, 3H); 3.18 (s, 3H); 3.87 (s, 3H); 3.88 (s, 3H) 6.94 (dd, J_{HH} = 7.8, 1.8 Hz, 1H); 7.12 (t, J_{HH} = 8.1 Hz 1H); 7.57 (s, 1H); 8.31 (dd, J_{HH} = 8.1, 1.3 Hz, 1H)	in $CDCl_3$: 15.96, 26.84, 56.05, 62.03, 114.32, 121.62, 124.41, 124.46, 139.43, 145.50, 149.77, 152.83, 162.80, 170.90	260.1 (30); 229.1 (95); 55.6 (100)
5	4-NO_2	Me	in $CDCl_3$: 2.41 (s,	in $CDCl_3$:	245.1 (100);

			3H); 3.20 (s, 3H); 7.04 (s, 3H); 8.24 (m, 4H)	16.08, 26.95, 123.52, 123.94, 132.69, 140.63, 141.61, 147.91, 165.65, 170.55	215.2 (75); 199.2 (14); 55.1 (97)
6	2,5-OMe	Me	in $CDCl_3$: 2.35 (s, 3H); 3.17 (s, 3H); 3.82 (s, 3H); 3.83 (s, 3H); 6.82 (s, 1H); 6.88 (d, J_{HH} = 3.3 Hz, 2H); 7.62 (s, 1H); 8.41 (d, J_{HH} = 2.7 Hz, 1H)	in $CDCl_3$: 15.70, 26.53, 55.71, 56.12, 111.74, 116.90, 117.83, 121.12, 123.65, 138.30, 153.80, 161.90, 170.64	260.1 (100); 229.1 (99); 188.1 (49); 160.1 (47); 137.0 (31); 55.1 (95)
7	3,5-t-Bu 4-OH	Me	in $CDCl_3$: 1.47 (s, 18H); 2.35 (s, 3H); 3.18 (s, 3H); 5.59 (m, 2H); 7.08 (s, 1H); 8.06 (s, 2H)	in $CDCl_3$: 15.77, 26.55, 30.16, 34.34, 125.91, 129.00, 130.07, 136.19, 156.21, 160.38, 170.88	328.1 (100); 313.1 (46); 257.0 (43); 55.9 (47)
8	4-CO_2H	Me	in DMSO-d_6: 2.36 (s, 3H); 3.10 (s, 3H); 6.95 (s, 1H); 7.88 (d, J_{HH} = 8.2 Hz, 2H); 8.10 (d, J_{HH} = 8.2 Hz, 2H)	in DMSO-d_6: 15.32, 26.20, 122.90, 124.71, 129.07, 130.91, 134.03, 138.60, 164.22, 169.83	244.1 (16); 111.8 (17); 55.1 (100)
9	4-$N(Me)_2$	Me	in $CDCl_3$: 2.35 (s, 3H); 3.04 (s, 6H); 3.17 (s, 3H); 6.69 (d, J_{HH} = 9.3 Hz, 2H); 7.08 (s, 1H); 8.04 (d, J_{HH} = 9.0 Hz, 2H)	in $CDCl_3$: 15.70, 26.58, 55.78, 61.77, 114.06, 121.36, 124.15, 124.20, 139.17, 145.24, 149.51, 152.57, 162.54, 170.53	243.1 (94); 159.1 (10); 134.1 (11); 56.0 (100)
10	2-F	Me	in $CDCl_3$: 2.37 (s, 3H); 3.18 (s, 3H); 7.04 (s, 1H); 7.08 (AA' of a AA'XX' spin system, 2H); 8.12 (XX' of a AA'XX' spin system, 2H)	in $CDCl_3$: 15.65, 26.56, 115.82 (J_{CF} = 21.8 Hz), 122.16, 125.85, 130.44, 134.13 (J_{CF} = 8.0 Hz), 138.24, 162.64, 163.57 (J_{CF} = 252.4 Hz), 170.59	218.1 (92); 199.1 (45); 134.0 (12); 107.0 (16); 56.0 (100)
11	4-OBz	Me	in $CDCl_3$: 2.35 (s,	in $CDCl_3$:	306.1 (84);

			3H); 3.17 (s, 3H); 5.11 (s, 2H); 7.00 (d, J_{HH} = 8.7 Hz, 2H); 7.39 (m, 5H); 8.10 (d, J_{HH} = 9.0 Hz, 2H)	15.64, 26.56, 69.98, 115.13, 122.18, 127.30, 127.45, 128.09, 128.62, 134.00, 136.43, 136.95, 160.35, 161.28, 170.73	215.1 (58); 91.0 (100); 65.0 (17); 56.0 (87)
12	2,4,5-OMe	Me	in $CDCl_3$: 2.34 (s, 3H); 3.17 (s, 3H); 3.87 (s, 3H); 3.92 (s, 3H); 3.93 (s, 3H); 6.46 (s, 1H); 7.62 (s, 1H); 8.54 (s, 1H)	in $CDCl_3$: 15.71, 26.52, 55.89, 56.22, 56.38, 95.90, 114.70, 115.20, 121.39, 136.07, 143.15, 152.26, 155.33, 160.15, 170.67	290.1 (94); 259.1 (87); 181.1 (20); 154.1 (32); 137.1 (28); 56.0 (100)
13	2-pyridyl-4-OH	Me	in DMSO-d_6: 2.33 (s, 3H); 3.08 (s, 3H); 6.83 (s, 1H); 7.03 (dd, J_{HH} = 5.6, 0.6 Hz, 1H); 8.05 (dd, J_{HH} = 2.3, 0.6 Hz, 1H); 8.61 (dd, J_{HH} = 8.2, 0.6 Hz, 1H)	in DMSO-d_6: 15.25, 26.14, 122.36, 126.15, 128.59, 136.30, 140.23, 140.64, 158.95, 162.69, 169.78	
14	4-OH	Me	in DMSO-d_6: 2.31 (s, 3H); 3.07 (s, 3H); 6.82 (d, J_{HH} = 8.8 Hz, 2H); 6.88 (s, 1H); 8.07 (d, J_{HH} = 8.8 Hz, 2H); 10.11 (s, 1H)	in DMSO-d_6: 15.20, 26.12, 115.67, 125.29, 125.41, 134.03, 136.20, 159.50, 162.20, 169.75	216.1 (48); 82.5 (14); 68.4 (16); 55.2 (100)
15	2-Me	Me	in $CDCl_3$: 2.37 (s, 3H); 2.48 (s, 3H); 3.19 (s, 2H); 7.21 (m, 1H); 7.25 (t, J_{HH} = 2.1 Hz 1H); 7.28 (s, 1H); 7.39 (s, 1H); 8.59 (dd, J_{HH} = 5.1, 3.0 Hz, 1H)	in $CDCl_3$: 15.70, 20.09, 26.59, 124.4, 126.32, 129.96, 130.40, 131.95, 132.59, 138.65, 139.29, 162.75, 170.70	214.1 (83); 199.1 (19); 142.0 (31); 131.1 (44); 115.0 (17); 56.0 (100)
16	4-CN	Me	in $CDCl_3$: 2.39 (s, 3H); 3.18 (s, 3H); 6.99 (s, 1H); 7.65 (d, J_{HH} = 9.0 Hz, 1H); 8.19 (d, J_{HH} = 8.1 Hz, 1H)	in $CDCl_3$: 15.76, 26.65, 112.47, 118.70, 123.88, 132.11, 132.14, 138.44, 140.94, 164.88, 170.29	225.1 (22); 58.0 (100); 56.0 (41)
17	4-$N(Et)_2$	Me	in $CDCl_3$: 1.17 (t, J_{HH}	in $CDCl_3$:	271.2 (87);

			= 7.2 Hz, 6H); 2.33 (s, 3H); 3.15 (s, 3H); 3.39 (q, J_{HH} = 7.2 Hz, 4H); 6.64 (d, J_{HH} = 8.7 Hz, 2H); 7.05 (s, 1H); 8.01 (d, J_{HH} = 9.0 Hz, 2H)	12.55, 15.52, 26.47, 44.45, 111.16, 121.36, 128.89, 134.21, 134.39, 149.09, 158.48, 170.65	256.1 (100); 227.1 (29); 143.1 (18); 56.0 (79)
18	4-OH	n-Pr	in $CDCl_3$: 0.94 (t, J_{HH} = 7.8 Hz, 3H); 1.65 (m, 2H); 2.36 (s, 3H); 3.56 (t, J_{HH} = 7.2 Hz, 2H); 6.82 (d, J_{HH} = 8.1 Hz, 2H); 7.09 (s, 1H); 7.94 (d, J_{HH} = 9.0 Hz, 2H)	in $CDCl_3$: 11.18, 15.42, 22.58, 42.26, 116.10, 126.07, 128.85, 134.33, 135.59, 158.95, 161.24, 170.85	244.1 (100); 225.1 (24); 185.1 (24); 159.1 (21); 130.1 (20); 84.1 (34); 55.0(17)
19	4-OH	n-Pn	in $CDCl_3$: 0.88 (t, J_{HH} = 7.0 Hz, 3H); 1.32 (m, 4H); 1.60 (m, 2H); 2.36 (s, 3H); 3.58 (t, J_{HH} = 7.0 Hz, 2H); 6.83 (d, J_{HH} = 8.7 Hz, 2H) 7.08 (s, 1H); 7.94 (d, J_{HH} = 8.7 Hz, 2H)	in $CDCl_3$: 13.88, 15.47, 22.26, 28.82, 29.01, 40.70, 116.06, 126.13, 128.59, 134.30, 135.75, 158.92, 161.19, 170.78	272.1 (100); 255.1 (81); 216.1 (31); 161.0 (32); 146.1 (23); 132.0 (25); 71.1 (26); 55.0 (37)
20	4-OH	n-Bu	in $CDCl_3$: 0.94 (t, J_{HH} = 7.2 Hz, 3H); 1.36 (m, 2H); 1.60 (m, 2H); 2.38 (s, 3H); 3.60 (t, J_{HH} = 7.2 Hz, 2H); 6.82 (d, J_{HH} = 8.7 Hz, 2H); 7.09 (s, 1H); 7.95 (d, J_{HH} = 8.7 Hz, 2H)	in $CDCl_3$: 13.65, 15.41, 19.97, 31.36, 40.51, 116.08, 126.11, 128.82, 134.32, 135.62, 158.89, 161.28, 170.82	258.1 (100); 241.1 (88); 216.1 (58); 161.1 (58); 133.1 (40); 57.1 (62)
21	4-Me	n-Pr	in $CDCl_3$: 0.95 (t, J_{HH} = 7.2 Hz, 3H); 1.65 (m, 2H); 2.37 (s, 6H); 3.55 (t, J_{HH} = 7.0 Hz, 2H); 7.07 (s, 1H); 7.21 (d, J_{HH} = 7.8 Hz, 2H); 8.01 (d, J_{HH} = 8.4 Hz, 2H)	in $CDCl_3$: 11.15, 15.71, 21.61, 22.57, 42.09, 122.15, 127.31, 129.44, 131.45, 132.04, 137.86, 140.52, 161.90, 170.76	242.1 (100); 235.1 (20); 185.1 (21); 159.1 (19); 130.1 (18); 84.1 (32); 55.0 (17)
22	4-$N(Me)_2$	n-Pr	in $CDCl_3$: 0.95 (t, J_{HH} = 7.2 Hz, 3H); 1.65 (m, 2H); 2.36 (s, 3H); 3.04 (s, 6H); 3.55 (t, J_{HH} = 7.5 Hz, 2H); 6.70 (d, J_{HH} = 8.7 Hz, 2H); 7.06 (s, 1H); 8.05 (d, J_{HH} = 9.3 Hz, 2H)	in $CDCl_3$: 11.20, 15.65, 22.64, 40.01, 42.03, 111.69, 122.16, 122.24, 128.62, 134.04, 151.38, 159.01, 170.71	271.2 (100); 254.2 (13); 229.1 (15); 159.1 (35); 143.1 (15); 134.1 (13); 84.1 (38)

23	4-OH	C_3CO_2H	in DMSO-d_6: 1.67 (m, 2H); 1.91 (t, J_{HH} = 7.0 Hz, 2H); 2.34 (s, 3H); 3.53 (t, J_{HH} = 7.6 Hz, 2H); 6.77 (d, J_{HH} = 8.5 Hz, 2H); 6.83 (s, 1H); 8.01 (d, J_{HH} = 8.8 Hz, 2H)	in DMSO-d_6: 15.19, 25.75, 34.24, 116.25, 123.81, 126.02, 134.12, 135.18, 161.10, 162.01, 169.77, 175.99	288.2 (10); 274.1 (100); 146.1 (18); 132.1 (15); 114.1 (23); 86.1 (65); 55.1 (25)
24	4-OH	C_5CO_2H	in DMSO-d_6: 1.25 (m, 2H); 1.49 (m, 4H); 1.94 (t, J_{HH} = 7.0 Hz, 2H); 2.32 (s, 3H); 3.50 (t, J_{HH} = 7.9 Hz, 2H); 6.74 (d, J_{HH} = 8.5 Hz, 2H); 6.83 (s, 1H); 7.98 (d, J_{HH} = 8.8 Hz, 2H)	in DMSO-d_6: 14.88, 15.14, 25.73, 26.41, 28.69, 37.52, 116.58, 116.94, 122.89, 126.45, 134.21, 134.46, 160.16, 169.62, 176.90	316.3 (27); 194.1 (18); 111.0 (25); 69.0 (47); 55.1 (100)
25	1-naphthyl	Me	in $CDCl_3$: 2.40 (s, 3H); 3.23 (s, 3H); 7.56 (m, 3H); 7.87 (m, 2H); 7.98 (s, 1H); 8.31 (d, J_{HH} = 8.4 Hz, 1H); 8.79 (d, J_{HH} = 7.2 Hz, 1H)	in $CDCl_3$: 15.65, 26.56, 122.89, 123.15, 125.69, 125.88, 126.83, 128.80, 129.90, 130.55, 131.19, 132.40, 133.54, 139.38, 163.22, 170.48	250.1 (93); 167.1 (21); 139.1 (11); 56.0 (100)
26	4-Et	Me	in $CDCl_3$: 1.24 (t, J_{HH} = 7.6 Hz, 3H); 2.37 (s, 3H); 2.67 (q, J_{HH} = 7.8 Hz, 3H); 3.18 (s, 3H); 7.10 (s, 1H); 7.25 (d, J_{HH} = 9.0 Hz, 2H); 8.04 (d, J_{HH} = 7.5 Hz, 2H)	in $CDCl_3$: 15.27, 15.62, 26.52, 28.89, 127.51, 128.24, 131.60, 132.14, 137.95, 146.84, 161.88, 170.56	228.1 (100); 213.1 (21); 199.1 (14); 58.0 (95); 56.0 (97)
27	3-Me	Me	in $CDCl_3$: 2.38 (s, 3H); 2.39 (s, 3H); 3.18 (s, 3H); 7.08 (s, 1H); 7.18 (d, J_{HH} = 7.7 Hz, 1H); 7.30 (t, J_{HH} = 7.7 Hz, 1H); 7.93 (d, J_{HH} = 9.4 Hz, 2H)	in $CDCl_3$: 15.67, 21.40, 26.58, 127.65, 128.57, 129.33, 131.00, 132.60, 134.03, 138.27, 138.47, 162.38, 170.74	214.1 (100); 199.1 (21); 130.1 (13); 115.1 (22); 103.0 (20); 77.1 (21); 56.0 (97)
28	2,4-Me	Me	in $CDCl_3$: 2.36 (s, 3H); 2.37 (s, 3H); 2.43 (s,3H); 3.18 (s, 3H); 7.07 (s, 2H); 7.36 (s,	in $CDCl_3$: 15.65, 19.62, 21.12, 26.55, 122.15, 124.68,	228.1 (91); 213.1 (36); 156.1 (68); 145.1 (67);

			1H); 8.40 (s, 1H)	130.28, 130.94, 132.21, 132.33, 135.65, 136.38, 138.36, 170.96	129.1 (14); 115.0 (19); 56.0 (100)
29	2-quinoline	Me	in $CDCl_3$: 2.40 (s, 3H); 3.18 (s, 3H); 7.42 (s, 1H); 7.54 (d, J_{HH} = 8.2 Hz, 1H); 7.70 (t of d, J_{HH} = 8.2, 1.1 Hz, 1H); 7.79 (d, J_{HH} = 8.2 Hz, 1H); 8.10 (d, J_{HH} = 8.8 Hz, 1H); 8.17 (d, J_{HH} = 8.8 Hz, 1H); 8.85 (d, J_{HH} = 8.8 Hz, 1H)	in $CDCl_3$: 15.82, 26.61, 123.95, 127.15, 127.40, 127.51, 129.64, 129.76, 135.96, 141.79, 154.03, 164.79, 170.50	251.1 (52); 223.1 (12); 168.1 (12); 140.1 (10); 56.0 (100)
30	2,5-Me	Me	in $CDCl_3$: 2.32 (s, 3H); 2.36 (s, 3H); 2.45 (s,3H); 3.18 (s, 3H); 7.02 (s, 1H); 7.08 (d, J_{HH} = 8.2 Hz, 1H); 7.37 (s, 1H); 8.53 (d, J_{HH} = 7.7 Hz, 1H)	in $CDCl_3$: 15.64, 19.97, 21.47, 26.55, 124.52, 127.19, 129.83, 131.20, 131.96, 137.93, 139.33, 140.41, 162.50, 170.73	228.1 (60); 213.1 (11); 156.1 (34); 145.1 (28); 56.0 (100)
31	1-naphthyl	Et	in $CDCl_3$: 1.27 (t, J_{HH} = 7.1 Hz 3H); 2.40 (s, 3H); 3.68 (q, d, J_{HH} = 7.1 Hz, 2H); 7.55 (m, 3H); 7.86 (m, 2H); 7.97 (s, 1H); 8.31 (d, J_{HH} = 8.2 Hz, 1H); 8.80 (d, J_{HH} = 8.2 Hz, 1H)	in $CDCl_3$: 14.62, 15.64, 35.36, 122.74, 123.18, 125.69, 125.88, 126.81, 128.82, 129.96, 130.52, 131.16, 132.43, 133.56, 139.41, 163.01, 170.33	264.1 (100); 235.1 (15); 166.1 (39); 141.1 (20); 139.1 (25); 70.1 (81); 51.0 (16)
32	4-*i*-Pr	n-Pr	in $CDCl_3$: 1.12 (t, J_{HH} = 7.1 Hz, 3H); 1.41 (s, 3H); 1.43 (s, 3H); 1.82 (m, 2H); 2.54 (s, 3H); 3.09 (m, 1H); 3.72 (t, J_{HH} = 7.1 Hz, 2H); 7.44 (d, J_{HH} = 8.2 Hz, 2H); 8.22 (d, J_{HH} = 8.2 Hz, 2H)	in $CDCl_3$: 11.11, 15.64, 22.51, 23.62, 34.07, 42.03, 126.75, 127.27, 131.76, 132.08, 137.89, 151.26, 161.88, 170.71	270.2 (100); 255.1 (82); 185.1 (32); 144.1 (21); 84.1 (49); 55.0 (23)
33	4-$N(Me)_2$	n-Bu	in $CDCl_3$: 0.93 (t, J_{HH} = 7.3 Hz, 3H); 1.36 (m, 2H); 1.56 (m, 2H); 2.35 (s, 3H); 3.03 (s,	in $CDCl_3$: 13.66, 15.61, 19.95, 31.44, 39.98, 111.64,	Analysis not completed

			6H); 3.58 (t, J_{HH} = 7.3 Hz, 2H); 6.68 (d, J_{HH} = 9.1 Hz, 2H); 7.05 (s, 1H); 8.04 (d, J_{HH} = 9.1 Hz, 2H)	122.17, 128.60, 129.30, 134.02, 151.36, 158.96, 160.64, 170.65	
34	2-CF_3	Me	in $CDCl_3$: 2.36 (s, 3H); 3.17 (s, 3H); 7.42 (m, 2H); 7.60 (t, J_{HH} = 7.7 Hz, 1H); 7.68 (d, J_{HH} = 7.7 Hz, 1H); 8.69 (d, J_{HH} = 8.2 Hz, 1H)	in $CDCl_3$: 15.68, 26.58, 121.37, 121.40, 122.16, 125.78, 125.85, 129.03, 131.73, 133.44, 140.44, 164.76, 170.15	Analysis not completed
35	2-naphthyl	Me	in $CDCl_3$: 2.40 (s, 3H); 3.19 (s, 3H); 7.50 (m, 2H); 7.85 (m, 3H); 8.42 (s, 1H); 8.43 (d, d, J_{HH} = 7.7 Hz, 1H)	in $CDCl_3$: 15.71, 26.59, 126.32, 127.37, 127.65, 128.10, 128.30, 128.88, 131.92, 133.12, 133.21, 133.89, 138.82, 162.48, 170.71	250.1 (82); 141.1 (10); 56.0 (100)
36	4-$N(Et)_2$	*i*-Pr	in $CDCl_3$: 1.17 (t, J_{HH} = 7.1 Hz, 6H); 1.44 (s, 3H); 1.46 (s, 3H); 2.38 (s, 3H); 3.39 (q, J_{HH} = 7.1 Hz, 4H); 4.26 (m, 1H); 6.65 (d, J_{HH} = 8.8 Hz, 2H); 6.99 (s, 1H); 8.00 (d, J_{HH} = 8.8 Hz, 2H)	in $CDCl_3$: 12.55, 16.96, 20.61, 44.42, 44.92, 111.16, 121.51, 122.13, 128.28, 134.27, 149.00, 158.54, 170.74	299.2 (88); 284.2 (100); 242.1 (11); 187.1 (12); 172.1 (11); 143.1 (18)
37	4-OH	EtOH	in DMSO-d_6: 2.36 (s, 3H); 3.52 (d, J_{HH} = 5.0 Hz, 3.60 (d, J_{HH} = 5.0 Hz, 2H); 6.83 (d, J_{HH} = 8.8 Hz, 2H); 6.88 (s, 1H); 8.08 (d, J_{HH} = 8.8 Hz, 2H)	Analysis not completed	Analysis not completed
38	4-OH	$CH_2(CF_2)_7CF_3$	in acetone-d_6: 2.46 (d, J_{HF} = 0.6 Hz, 3 H), 4.59 (tt, J_{HF} = 16.5 Hz, 2 H), 6.93 (AA′ part of AA′BB′ spin system, 2 H), 7.02 (s, 1 H), 8.18 (BB′ part of AA′BB′ spin system, 2	Analysis not completed	584.1 (98), 565.1 (18), 424.0 (100), 132.1 (9), 69.0 (12)

			H), 9.06 (br s, 1 H)		
39	4-Et	n-Pr	in $CDCl_3$: 0.93 (t, J_{HH} = 7.1 Hz, 3H); 1.22 (t, J_{HH} = 7.1 Hz, 3H); 1.64 (m, 2H); 2.36 (s, 3H); 2.65 (q, J_{HH} = 7.7 Hz, 2H); 3.54 (t, J_{HH} = 7.1 Hz, 2H); 7.07 (s, 1H); 7.22 (d, J_{HH} = 8.2 Hz, 2H); 8.03 (d, J_{HH} = 8.2 Hz, 2H)	in $CDCl_3$: 11.11, 15.23, 15.65, 22.51, 28.84, 42.03, 127.28, 128.19, 131.61, 132.08, 137.84, 146.75, 161.90, 170.71	256.1 (100); 239.2 (15); 185.2 (23); 130.1 (12); 83.9 (27); 54.6 (12)
40	2-Et	Me	in $CDCl_3$: 1.23 (m, 6H); 2.38 (s, 3H); 2.83 (q, J_{HH} = 7.1 Hz, 2H), 3.66 (q, J_{HH} = 7.1 Hz, 2H); 7.21 (m, 1H); 7.28 (m, 2H); 7.40 (s, 1H); 8.57 (m, 1H)	in $CDCl_3$: 14.60, 15.61, 16.02, 26.61, 35.30, 124.00, 126.22, 128.85, 130.05, 132.16, 138.72, 145.41, 162.41, 170.45	228.1 (84); 213.1 (53); 199.2 (23); 156.1 (37); 145.2 (42); 128.1 (21); 115.0 (20); 55.6 (100)
41	2-Me	n-Pr	in $CDCl_3$: 0.97 (t, J_{HH} = 7.1 Hz, 3H); 1.23 (t, J_{HH} = 7.7 Hz, 3H); 1.67 (m, 2H); 2.38 (s, 3H); 2.84 (q, J_{HH} = 7.7 Hz, 2H); 3.57 (t, J_{HH} = 7.1 Hz, 2H); 7.21 (m, 1H); 7.28 (m, 2H); 7.41 (s, 1H); 8.58 (m, 1H)	in $CDCl_3$: 11.11, 15.65, 19.97, 22.49, 42.05, 124.06, 126.20, 129.82, 130.29, 131.83, 132.52, 138.46, 139.17, 162.72, 170.65	242.1 (100); 199.2 (28); 142.1 (25); 131.1 (34); 115.0 (24); 103.0 (19); 83.9 (78)
42	2-Me	CH_2CF_3	in $CDCl_3$: 2.34 (s, 3H); 2.49 (s, 3H); 3.79 (s, 2H); 7.19-7.31 (m, 3H); 7.43 (s, 1H); 8.57-8.65 (m, 1H)	Analysis not completed	Analysis not completed
43	4-OH	PrOH	in DMSO-d_6: 1.69 (pentet, J_{HH} = 6.7 Hz, 2H); 2.35 (s, 3H); 3.41 (t, J_{HH} = 6.2 Hz, 2H); 3.60 (t, J_{HH} = 7.0 Hz, 2H); 6.80 (d, J_{HH} = 8.5 Hz, 2H); 6.86 (s, 1H); 8.05 (d, J_{HH} = 8.5 Hz, 2H)	in DMSO-d_6: 15.14, 31.55, 37.24, 57.83, 116.02, 124.47, 125.79, 134.14, 135.50, 160.92, 161.39, 169.81	260.2 (100); 216.2 (49); 58.9 (38)
44	2-Et	n-Pr	in $CDCl_3$: 0.97 (t, J_{HH} = 7.7 Hz, 3H); 1.23 (t, J_{HH} = 7.7 Hz, 3H);1.67	in $CDCl_3$: 11.17, 15.71, 16.05, 22.54,	256.0 (100); 241.0 (35); 213.0 (27);

			(m, 2H); 2.38 (s, 3H); 2.84 (q, J_{HH} = 7.7 Hz, 2H); 3.57 (t, J_{HH} = 7.1 Hz, 2H); 7.22 (m, 1H); 7.28 (m, 2H); 7.41 (s, 1H); 8.58 (m, 1H)	26.59, 42.11, 123.97, 126.20, 128.83, 130.03, 131.73, 132.16, 138.65, 145.41, 162.66, 170.71	156.0 (29); 145.1 (31); 83.9 (68); 57.6 (30)
45	3-NO_2	Me	in $CDCl_3$: 2.37 (s, 3H); 3.19 (s, 3H); 7.49 (s, 2H); 7.66 (t, J_{HH} = 7.7 Hz, 1H); 7.99 (d, J_{HH} = 8.2 Hz, 1H); 8.46 (d, J_{HH} = 7.7 Hz, 1H)	in $CDCl_3$: 15.74, 26.65, 120.85, 124.61, 128.74, 129.68, 132.89, 133.62, 133.62, 141.25, 141.75, 165.21, 169.86	245.0 (28); 215.0 (21); 199.0 (24); 119.0 (85); 91.9 (78); 55.5 (100)
46	4-$N(Et)_2$	n-Pr	in $CDCl_3$: 0.94 (t, J_{HH} = 7.1 Hz, 3H); 1.18 (t, J_{HH} = 7.1 Hz, 6H); 1.64 (m, 2H); 2.35 (s, 3H); 3.40 (q, J_{HH} = 6.6 Hz, 4H); 3.55 (t, J_{HH} = 7.7 Hz, 2H); 6.65 (d, J_{HH} = 9.3 Hz, 2H); 7.04 (s, 1H); 8.01 (d, J_{HH} = 8.8 Hz, 2H)	in $CDCl_3$: 11.17, 12.55, 15.59, 22.61, 41.97, 44.43, 111.16, 121.52, 128.73, 134.17, 134.35, 149.06, 158.50, 170.67	299.1 (72); 284.0 (100); 162.1 (32); 143.0 (12); 83.9 (12); 68.7 (15); 54.5 (27)
47	2,6-Me	Me	in $CDCl_3$: 2.26 (s, 6H); 2.30 (s, 3H); 3.18 (s, 3H); 7.05 (d, J_{HH} = 7.7 Hz, 2H); 7.13 (t, J_{HH} = 8.2 Hz, 1H); 7.32 (s, 1H)	in $CDCl_3$: 15.61, 20.88, 26.55, 127.60, 128.19, 128.42, 132.54, 136.72, 140.49, 162.63, 169.50	228.0 (98); 213.0 (48); 156.0 (92); 145.1 (85); 128.0 (36); 115.0 (34); 55.5 (100)
48	4-*i*-Pr	Me	in $CDCl_3$: 1.23 (s, 3H); 1.25 (s, 3H); 2.35 (s, 3H); 3.16 (s, 3H); 7.09 (s, 1H); 7.26 (d, J_{HH} = 8.3 Hz, 2H); 8.04 (d, J_{HH} = 8.3 Hz, 2H)	Analysis not completed	Analysis not completed
49	4-*t*-Bu	Me	in $CDCl_3$: 1.32 (s, 9H); 2.36 (s, 3H); 3.16 (s, 3H); 7.10 (s, 1H); 7.43 (d, J_{HH} = 8.2 Hz, 2H); 8.04 (d, J_{HH} = 8.8 Hz, 2H)	in $CDCl_3$: 15.62, 26.52, 31.05, 34.86, 122.13, 125.66, 127.36, 131.35, 131.84, 138.12, 153.53, 161.90	256.0 (82); 241.0 (100); 55.5 (95)

50	3-indole	Me	in DMSO-d_6: 2.34 (s, 3H); 3.10 (s, 3H); 7.17 (m, 2H); 7.30 (s, 1H); 7.47 (dd, J_{HH} = 7.1, 1.1 Hz, 1H); 8.20 (d, J_{HH} = 7.1 Hz, 1H); 8.39 (s, 1H); 11.93 (s, 1H)	in DMSO-d_6: 15.23, 26.12, 111.01, 112.07, 119.38, 120.64, 122.43, 126.61, 132.65, 133.89, 136.28, 159.28, 169.10	239.0 (88); 155.0 (12); 130.0 (10); 55.5 (100)
51	2-F	n-Pr	in $CDCl_3$: 0.96 (t, J_{HH} = 7.1 Hz, 3H); 1.67 (m, 2H); 2.38 (s, 3H); 3.57 (t, J_{HH} = 7.7 Hz, 3H); 7.41 (s, 1H); 7.43 (t, J_{HH} = 7.7 Hz, 1H); 7.61 (t, J_{HH} = 7.7 Hz, 1H); 7.69 (d, J_{HH} = 7.7 Hz, 1H); 8.73 (d, J_{HH} = 7.7 Hz, 1H)	in $CDCl_3$: 11.15, 15.77, 22.51, 42.21, 121.07, 122.18, 125.79, 125.87, 129.00, 131.73, 133.45, 140.38, 164.77, 170.24	296.0 (86); 257.0 (18); 227.0 (100); 185.0 (67); 178.0 (21); 165.0 (19); 54.5 (37)
52	4-$N(Me)_2$	*i*-Pr	in $CDCl_3$: 1.45 (s, 3H); 1.47 (s, 3H); 2.39 (s, 3H); 3.03 (s, 6H); 3.08 (s, 3H); 4.26 (m, 1H); 6.69 (dd, J_{HH} = 6.6, 2.2 Hz, 2H); 7.01 (s, 1H); 8.03 (d, J_{HH} = 8.8 Hz, 2H)	in $CDCl_3$: 17.02, 20.64, 40.03, 45.01, 110.95, 111.71, 122.33, 128.22, 133.98, 151.35, 159.07, 170.80	271.0 (100); 229.0 (14); 159.1 (36); 143.0 (11); 134.1 (12); 83.9 (17)
53	4-tetralin	Me	in $CDCl_3$: 1.28 (s, 6H); 1.30 (s, 6H); 1.68 (s, 4H); 2.36 (s, 3H); 3.17 (s, 3H); 7.09 (s, 1H); 7.35 (d, J_{HH} = 8.2 Hz, 1H); 7.91 (d, J_{HH} = 1.7 Hz, 1H); 8.03 (dd, J_{HH} = 8.2, 1.7 Hz, 1H)	in $CDCl_3$: 15.68, 26.53, 31.56, 31.76, 34.46, 34.83, 34.89, 127.04, 128.00, 128.92, 131.04, 131.43, 137.96, 147.60, 161.58, 170.80	310.1 (77); 295.1 (100); 253.0 (21); 55.6 (78)
54	2-Me	Et	in $CDCl_3$: 1.26 (t, J_{HH} = 7.1 Hz, 3H); 2.39 (s, 3H); 2.48 (s, 3H); 3.67 (q, J_{HH} = 7.1 Hz, 2H); 7.21 (m, 1H); 7.26 (m, 2H); 7.38 (s, 1H); 8.60 (m, 1H)	in $CDCl_3$: 14,65, 15.65, 20.07, 35.35, 124.20, 126.31, 129.91, 130.38, 130.61, 131.92, 132.62, 139.27, 162.52, 170.48	228.0 (98); 199.0 (31); 142.0 (37); 131.0 (51); 115.0 (29); 102.9 (24); 69.7 (100)
55	4-$N(Et)_2$	n-Pn	in $CDCl_3$: 0.89 (t, J_{HH} = 7.0 Hz, 3H); 1.18 (t, J_{HH} = 7.0 Hz, 6H);	in $CDCl_3$: 12.60, 13.91, 15.64, 22.31,	327.2 (100); 312.1 (88); 162.1 (45);

			1.33 (m, 4H); 1.61 (m, 2H); 2.35 (s, 3H); 3.40 (q, J_{HH} = 7.0 Hz, 4H); 3.57 (t, J_{HH} = 7.3 Hz, 2H); 6.65 (d, J_{HH} = 9.1 Hz, 2H); 7.05 (s, 1H); 8.02 (d, J_{HH} = 9.1 Hz, 2H)	28.85, 29.10, 40.48, 44.48, 111.20, 121.47, 128.78, 134.21, 134.39, 149.10, 158.52, 170.66	57.6 (25)
56	Benzyl	Me	in $CDCl_3$: 2.36 (s, 3H); 3.16 (s, 3H); 7.09 (s, 1H); 7.39 (m, 3H); 8.11 (dd, J_{HH} = 8.2, 2.2 Hz, 2H)	in $CDCl_3$: 15.67, 26.56, 127.24, 128.63, 130.00, 132.05, 134.10, 138.66, 162.57, 170.68	200.0 (100); 116.0 (14); 101.9 (12); 88.9 (18); 55.6 (97)
57	2-OH 3-OEt	Me	in $CDCl_3$: 1.49 (t, J_{HH} = 6.6 Hz, 3H); 2.34 (s, 3H); 3.18 (s, 3H); 4.08 (q, J_{HH} = 7.1 Hz, 2H); 6.78 (t, J_{HH} = 7.7 Hz, 1H); 6.91 (d, J_{HH} = 6.0 Hz, 1H); 6.92 (d, J_{HH} = 7.1Hz, 1H); 7.14 (s, 1H)	in $CDCl_3$: 14.86, 14.95, 26.68, 64.36, 116.26, 118.70, 119.79, 127.74, 130.06, 132.74, 148.83, 149.03, 157.34, 167.79	260.0 (95); 245.0 (54); 231.0 (56); 203.0 (80); 174.0 (27); 55.6 (100)
58	4-F	Me	in $CDCl_3$: 2.35 (s, 3 H), 3.16 (s, 3 H), 7.03 (s, 1 H), 7.08 (AA′ of a AA′BB′X spin system, 2 H), 8.12 (BB′ of a AA′BB′X spin system, 2 H)	in $CDCl_3$: 15.01, 26.53, 115.79 (J_{CF} = 21.8 Hz), 125.81, 130.43, 134.10 (J_{CF} = 9.2 Hz), 162.64, 163.54 (J_{CF} = 252.4 Hz), 170.56	218.0 (93), 148.8 (10), 58.0 (17), 56.1 (100)
59	2-OH 4-$N(Et)_2$	Me	in $CDCl_3$: 1.19 (t, J_{HH} = 7.1 Hz, 6H); 2.33 (s, 3H); 3.20 (s, 3H); 3.38 (q, J_{HH} = 6.6 Hz, 4H); 6.16 (s, 1H); 6.22 (dd, J_{HH} = 8.8, 2.7 Hz, 1H); 7.12 (s, 1H); 7.11 (d, J_{HH} = 8.8 Hz, 1H)	in $CDCl_3$: 12.70, 14.85, 26.61, 44.52, 99.15, 104.50, 109.34, 122.13, 127.56, 131.35, 138.57, 152.89, 160.82, 167.72	287.2 (100); 272.1 (83); 232.1 (72); 217.0 (32); 56.1 (73)
60	2-imidazole	Me	in DMSO-d_6: 2.33 (s, 3H); 3.07 (s, 3H); 6.91 (s, 1H); 7.77 (s, 1H); 7.80 (s, 1H)		Analysis not completed
61	2-Et	Et	in $CDCl_3$: 1.24 (m,	in $CDCl_3$:	242.1 (100);

			6H); 2.38 (s, 3H); 2.83 (q, J_{HH} = 7.1 Hz, 2H); 3.66 (q, J_{HH} = 7.1 Hz, 2H); 7.21 (m, 1H); 7.28 (m, 2H); 7.40 (s, 1H); 8.57 (m, 1H)	14.60, 16.61, 16.06, 26.61, 35.30, 124.00, 126.22, 128.85, 130.05, 131.72, 132.16, 138.73, 145.41, 162.41, 170.45	227.1 (29); 213.0 (31); 155.9 (23); 144.9 (27); 70.0 (67)
62	3-Me	n-Pr	in DMSO-d_6: 0.85 (t, J_{HH} = 7.7 Hz, 3H); 1.56 (m, 2H); 2.32 (s, 3H); 2.37 (s, 3H); 3.52 (t, J_{HH} = 7.2 Hz, 2H); 6.91 (s, 1H); 7.22 (d, J_{HH} = 7.2 Hz, 1H); 7.33 (t, J_{HH} = 7.2 Hz, 1H); 7.98 (s, 1H); 8.04 (d, J_{HH} = 7.7 Hz, 1H)	in DMSO-d_6: 10.96, 15.35, 20.93, 21.81, 41.36, 124.82, 128.34, 128.48, 129.03, 130.62, 132.24, 133.92, 137.64, 163.92, 169.88	242.1 (100); 225.0 (53); 158.9 (47); 143.9 (40); 130.9 (52); 83.9 (63); 55.1 (19)
63	2-Me	n-Bu	in $CDCl_3$: 0.96 (t, J_{HH} = 7.3 Hz, 3H); 1.38 (sextet, J_{HH} = 7.6 Hz, 2H); 1.61 (pentet, J_{HH} = 7.3 Hz, 2H); 2.38 (s, 3H); 2.48 (s, 3H); 3.60 (t, J_{HH} = 7.3 Hz, 2H); 7.17-7.31(m, 3H); 7.37 (s, 1H); 8.60 (dd, J_{HH} = 6.5, 2.9 Hz, 1H)	in $CDCl_3$: 13.68, 15.76, 19.98, 20.08, 31.41, 40.39, 124.22, 126.30, 129.92, 130.39, 131.91, 132.61, 138.56, 139.28, 162.78, 170.74	Analysis not completed
64	2-Me	n-Pn	in $CDCl_3$: 0.90 (t, J_{HH} = 6.7 Hz, 3H); 1.33 (sextet, J_{HH} = 7.3 Hz, 4H); 1.62 (pentet, J_{HH} = 7.3 Hz, 2H); 2.39 (s, 6H); 3.59 (t, J_{HH} = 7.3 Hz, 2H); 7.07 (s, 1H); 7.18 (d, J_{HH} = 7.3 Hz, 1H); 7.31 (t, J_{HH} = 7.6 Hz, 1H); 7.92 (s, 1H); 7.94 (d, J_{HH} = 8.8 Hz, 1H)	in $CDCl_3$: 13.90, 15.77, 21.40, 22.28, 28.82, 29.01, 40.61, 127.43, 128.56, 129.29, 130.94, 132.54, 134.08, 138.25, 138.40, 162.42, 170.74	Analysis not completed
65	2-Me	*i*-Pr	in $CDCl_3$: 1.48 (s, 3H); 1.50 (s, 3H); 2.41 (s, 3H); 2.47 (s, 3H); 7.17-7.29 (m, 3H); 7.32 (s, 1H); 8.57-8.61 (m, 1H)	Analysis not completed	Analysis not completed

66	3-OMe 4-OH	C_3CO_2H	in DMSO-d_6: 1.70 (m, 2H); 1.98 (t, J_{HH} = 7.1 Hz, 2H); 2.34 (s, 3H); 3.54 (t, J_{HH} = 7.7 Hz, 2H); 6.80 (d, J_{HH} = 8.8 Hz, 1H); 6.84 (s, 1H); 7.54 (dd, J_{HH} = 8.2, 1.7 Hz, 1H); 7.91 (s, 1H)	in DMSO-d_6: 15.33, 18.52, 25.65, 34.02, 55.34, 115.20, 116.10, 123.60, 126.46, 127.54, 134.83, 144.10, 148.16, 160.61, 169.71, 175.89	318.0 (100); 246.0 (14); 137.0 (23); 86.9 (63); 54.8 (22)
67	4-Me	Et	in $CDCl_3$: 1.24 (t, J_{HH} = 7.1 Hz, 3H); 2.37 (s, 3H); 2.38 (s, 3H); 3.65 (q, J_{HH} = 7.1 Hz, 2H); 7.07 (s, 1H); 7.21 (d, J_{HH} = 7.7 Hz, 2H); 8.01 (d, J_{HH} = 8.2 Hz, 2H)	in $CDCl_3$: 16.62, 15.59, 21.61, 35.27, 127.28, 129.44, 131.42, 132.05, 137.93, 140.53, 161.64, 170.48	Analysis not completed
68	2,3-OMe	C_3CO_2H	in DMSO-d_6: 1.69 (m, 2H); 1.92 (t, J_{HH} = 6.7 Hz, 2H); 2.39 (s, 3H); 3.55 (t, J_{HH} = 7.3 Hz, 3H); 3.79 (s, 3H); 3.82 (s, 3H); 7.11 (s, 1H); 7.12 (d, J_{HH} = 6.7 Hz, 1H); 7.19 (s, 1H); 8.32 (dd, J_{HH} = 7.0, 2.3 Hz, 1H)	in DMSO-d_6: 15.36, 25.79, 34.56, 55.71, 61.07, 114.60, 117.60, 123.49, 123.99, 127.52, 139.22, 148.55, 152.22, 164.58, 169.93, 176.17	332.0 (58); 301.0 (100); 215.0 (47); 151.0 (32); 136.0 (30); 96.9 (54); 54.9 (42)
69	4-$N(Et)_2$	C_3CO_2H	in DMSO-d_6: 1.10 (t, J_{HH} = 6.4 Hz, 6H); 1.68 (m, 2H); 1.92 (t, J_{HH} = 6.4 Hz, 2H); 2.34 (s, 3H); 3.53 (t, J_{HH} = 7.0 Hz, 2H); 3.39 (q, J_{HH} = 6.7 Hz, 4H); 6.69 (d, J_{HH} = 8.8 Hz, 2H); 6.82 (s, 1H); 8.02 (d, J_{HH} = 8.5 Hz, 2H)	in DMSO-d_6: 12.21, 12.41, 15.14, 25.95, 34.58, 43.70, 110.49, 110.97, 120.82, 123.90, 126.30, 134.05, 134.14, 148.68, 151.83, 159.75, 169.61, 176.33	Analysis not completed
70	4-Cl	Me	in $CDCl_3$: 2.36 (s, 3H); 3.16 (s, 3H); 7.01 (s, 1H); 7.36 (d, J_{HH} = 8.5 Hz, 2H); 8.05 (d, J_{HH} = 8.8 Hz, 2H)	in $CDCl_3$: 15.64, 26.55, 125.53, 128.86, 132.58, 133.16, 135.88, 138.91, 162.97, 170.46	234.1 (72); 55.2 (100)
71	3-CF_3	n-Pr	in $CDCl_3$: 0.96 (t, J_{HH} = 7.6 Hz, 3H); 1.67	in $CDCl_3$: 11.13, 15.79,	Analysis not

			(sextet, J_{HH} = 7.3 Hz, 2H); 2.40 (s, 3H); 3.57 (t, J_{HH} = 7.6 Hz, 2H); 7.06 (s, 1H); 7.47-7.66 (m, 2H); 8.28 (d, J_{HH} = 7.6 Hz, 1H); 8.44 (s, 1H)	22.52, 42.19, 124.66, 126.11 (J_{CF} = 4.4 Hz), 128.45 (J_{CF} = 3.3 Hz), 129.04, 130.80, 134.88, 139.83, 163.93, 170.50	completed
72	4-CF_3	Me	in $CDCl_3$: 2.36 (s, 3H); 3.17 (s, 3H); 7.42 (m, 2H); 7.60 (t, J_{HH} = 7.7 Hz, 1H); 7.68 (d, J_{HH} = 7.7 Hz, 1H); 8.69 (d, J_{HH} = 8.2 Hz, 1H)	in $CDCl_3$: 15.74, 26.63, 124.79, 125.36 (J_{CF} = 4.4 Hz), 125.47 (J_{CF} = 4.4 Hz), 131.98, 137.42, 140.30, 144.50, 164.16, 170.46	268.1 (79); 249.1 (10); 55.2 (100)
73	4-OH	$C_3N(Me)_2$	in DMSO-d_6: 1.67 (m, 2H); 2.11 (s, 6H); 2.19 (t, J_{HH} = 6.7 Hz, 2H); 2.35 (s, 3H); 3.56 (t, J_{HH} = 7.6 Hz, 2H); 6.82 (d, J_{HH} = 8.8 Hz, 2H); 6.87 (s, 1H); 8.07 (d, J_{HH} = 8.8 Hz, 2H)	in DMSO-d_6: 15.13, 26.32, 38.08, 44.99, 55.95, 115.73, 125.10, 125.48, 134.05, 135.88, 159.77, 161.77, 169.80	Analysis not completed
74	3-CF_3	Me	in $CDCl_3$: 2.38 (s, 3H); 3.17 (s, 3H); 7.05 (s, 1H); 7.48-7.60 (m, 2H); 8.26 (d, J_{HH} = 7.6 Hz, 1H); 8.42 (s, 1H)	in $CDCl_3$: 15.73, 26.61, 122.11, 124.85, 126.15, 128.50 (J_{CF} = 4.4 Hz), 129.08 (J_{CF} = 4.4 Hz), 131.26, 134.88, 134.94, 139.96, 163.91, 170.47	Analysis not completed
75	2,4-OH	C_3CO_2H	in DMSO-d_6: 1.72 (m, 2H); 1.99 (t, J_{HH} = 5.8 Hz, 2H); 2.35 (s, 3H); 3.56 (t, J_{HH} = 5.8 Hz, 2H); 6.25 (s (broad), 2H); 7.13 (s, 1H); 7.80 (d, J_{HH} = 7.3 Hz, 1H)	in DMSO-d_6: 14.87, 25.53, 33.96, 48.51, 103.44, 108.87, 111.48, 125.32, 130.68, 136.05, 157.39, 160.70, 164.88, 168.16, 175.79	
76	3,4-OH	C_3CO_2H	in DMSO-d_6: 1.72 (m, 2H); 1.99 (t, J_{HH} =	Analysis not completed	Analysis not

			5.8 Hz, 2H); 2.35 (s, 3H); 3.56 (t, J_{HH} = 5.8 Hz, 2H); 6.68 (d, J_{HH} = 8.2 Hz, 1H); 6.76 (s, 1H); 7.33 (d, J_{HH} = 7.9 Hz, 1H); 7.77 (s, 1H)		completed
77	2-Cl	Me	in $CDCl_3$: 2.38 (s, 3H); 3.19 (s, 3H); 7.26 (t of d, J_{HH} = 2.1, 7.6 Hz, 1H); 7.33 (t of d, J_{HH} = 1.5, 7.6 Hz, 1H); 7.41 (dd, J_{HH} = 1.5, 7.9 Hz, 1H); 7.56 (s, 1H); 8.74 (dd, J_{HH} = 1.8, 7.6 Hz, 1H)	in $CDCl_3$: 15.73, 26.61, 122.23, 126.92, 129.68, 130.70, 132.03, 133.23, 136.11, 139.82, 163.84, 170.38	Analysis not completed
78	2-Cl	n-Pr	in $CDCl_3$: 0.97 (t, J_{HH} = 7.6 Hz, 3H); 1.67 (m, 2H); 2.39 (s, 3H); 3.57 (t, J_{HH} = 7.6 Hz, 2H); 7.27 (t of d, J_{HH} = 1.8, 7.6 Hz, 1H); 7.41 (dd, J_{HH} = 1.8, 7.6 Hz, 1H); 7.33 (t of d, J_{HH} = 1.5, 7.3 Hz, 1H); 7.55 (s, 1H); 8.76 (dd, J_{HH} = 1.8, 7.6 Hz, 1H)	in $CDCl_3$: 11.20, 15.83, 22.57, 42.21, 122.03, 126.93, 129.70, 130.67, 133.20, 136.14, 137.27, 163.88, 170.47	Analysis not completed
79	4-CF_3	n-Pr	in $CDCl_3$: 0.96 (t, J_{HH} = 7.3 Hz, 3H); 1.66 (m, 2H); 2.40 (s, 3H); 3.60 (t, J_{HH} = 7.3 Hz, 2H); 7.05 (s, 1H); 7.64 (d, J_{HH} = 7.9 Hz, 2H); 8.22 (d, J_{HH} = 8.2 Hz, 2H)	in $CDCl_3$: 11.15, 15.80, 22.54, 42.22, 124.59, 125.44, 130.71, 131.95, 137.49, 140.24, 164.22, 170.53	296.1 (100); 279.1 (14); 185.0 (42); 198.1 (15); 54.2 (18)
80	3,5-Me	Me	in $CDCl_3$: 2.35 (s, 6H); 2.38 (s, 3H); 3.17 (s, 3H); 7.01 (s, 1H); 7.05 (s, 1H); 7.74 (s, 2H)	in $CDCl_3$: 15.64, 21.25, 26.54, 127.87, 129.88, 132.09, 133.95, 138.12, 162.15, 170.74	Analysis not completed
81	4-tetralin	C_3CO_2H	in DMSO-d_6: 1.24 (s, 12H); 1.64 (m, 2H); 1.65 (s, 4H); 1.92 (t, J_{HH} = 6.2 Hz, 2H); 2.38 (s, 3H); 3.55 (t, J_{HH} = 7.9 Hz, 2H);	in DMSO-d_6: 15.47, 25.82, 31.25, 31.49, 31.59, 31.68, 33.85, 34.08, 34.34, 34.49,	Analysis not completed

			6.92 (s, 1H); 7.38 (d, J_{HH} = 8.2 Hz, 1H); 8.04 (d, J_{HH} = 7.9 Hz, 1H); 8.09 (s, 1H)	125.08, 126.68, 128.78, 130.64, 131.43, 138.06, 144.58, 146.67, 163.46, 169.87, 175.99	
82	Benzyl	C_3CO_2H	in DMSO-d_6: 1.70 (m, 2H); 1.92 (t, J_{HH} = 6.7 Hz, 2H); 2.40 (s, 3H); 3.56 (t, J_{HH} = 8.8 Hz, 2H); 6.95 (s, 1H); 7.42 (m, 3H); 8.19 (d, J_{HH} = 8.5 Hz, 2H)	in DMSO-d_6: 15.36, 25.81, 34.53, 41.12, 124.44, 128.56, 129.79, 131.78, 131.94, 134.06, 138.08, 138.81, 164.45, 169.84, 176.12	Analysis not completed
83	2-OH 4-N(Et)$_2$	C_3CO_2H	in DMSO-d_6: 1.07 (t, J_{HH} = 6.7 Hz, 3H); 1.09 (t, J_{HH} = 6.7 Hz, 3H); 1.72 (m, 2H); 1.95 (t, J_{HH} = 5.9 Hz, 2H); 2.35 (s, 3H); 3.33 (q, J_{HH} = 7.3 Hz, 4H); 3.56 (t, J_{HH} = 7.0 Hz, 2H); 6.13 (s, 1H); 6.23 (dd, J_{HH} = 6.7, 2.6 Hz, 1H); 7.02 (d, J_{HH} = 8.8 Hz, 1H); 8.10 (s, 1H)	in DMSO-d_6: 12.61, 14.85, 25.79, 27.86, 34.37, 43.70, 52.37, 55.38, 97.70, 102.47, 104.13, 107.72, 109.05, 133.14, 151.26, 162.96, 167.53, 168.74, 176.21	Analysis not completed
84	4-N(Me)$_2$	C_3CO_2H	in DMSO-d_6: 1.67 (m, 2H); 1.90 (t, J_{HH} = 6.7 Hz, 2H); 2.35(s, 3H); 2.99 (s, 6H); 3.53 (t, J_{HH} = 7.0 Hz, 2H); 6.73 (d, J_{HH} = 8.8 Hz, 2H); 6.84 (s, 1H); 8.05 (d, J_{HH} = 8.8 Hz, 2H)	in DMSO-d_6: 15.20, 26.01, 34.67, 48.52, 111.00, 111.57, 121.57, 126.20, 133.70, 134.56, 151.14, 160.28, 169.64, 176.07	Analysis not completed
85	4-OC_6H_{13}	Me	in $CDCl_3$: 0.90 (t, J_{HH} = 7.0 Hz, 3H); 1.34 (m, 4H); 1.46 (m, 2H); 1.79 (m, 2H); 2.37 (s, 3H); 3.18 (s, 3H); 3.99 (t, J_{HH} = 6.4 Hz, 2H); 6.92 (d, J_{HH} = 9.1 Hz, 2H); 7.07 (s, 1H); 8.08 (d J_{HH} = 8.8 Hz, 2H)	in $CDCl_3$: 13.99, 15.60, 22.54, 25.62, 26.52, 29.06, 31.50, 68.04, 114.04, 126.80, 127.49, 133.99, 136.69, 160.82, 161.03, 170.71	Analysis not completed
86	2,6-Me 4-OH	Me	in DMSO-d_6: 2.14 (s, 6H); 2.24 (s, 3H); 3.07	in DMSO-d_6: 15.19, 20.84,	244.2 (72); 172.0 (64);

			(s, 3H); 6.49 (s, 2H); 7.04 (s, 1H); 9.44 (s (broad), 1H)	26.14, 114.35, 123.72, 125.83, 138.31, 139.67, 157.35, 162.99, 168.86	161.0 (42); 73.1 (58); 56.1 (100)
87	3,5-*t*-Bu 4-OH	Benzyl	in $CDCl_3$: 1.47 (s, 18H); 2.22 (s, 3H); 4.82 (s, 2H); 7.16-7.35 (m, 6H); 8.08 (s, 2H)	in $CDCl_3$: 16.12, 30.13, 34.33, 43.73, 125.82, 126.93, 127.74, 128.82, 129.57, 130.11, 135.95, 136.26, 156.34, 160.34, 170.76	404.4 (100); 399.4 (31); 91.0 (49); 57.1 (13)
88	4-OH	Benzyl	in DMSO-d_6: 2.34 (s, 3H); 4.82 (s, 2H); 6.85 (d, J_{HH} = 8.5 Hz, 2H); 6.99 (s, 1H); 7.28 (m, 5H); 8.10 (d, J_{HH} = 8.5 Hz, 2H)	in DMSO-d_6: 15.45, 42.82, 115.76, 125.11, 126.39, 126.76, 127.41, 127.77, 128.22, 128.72, 129.65, 134.22, 135.62, 136.85, 159.81, 161.32, 169.74	292.2 (100); 132.0 (16); 91.0 (81)
89	3,5-Me 4-OH	Me	in DMSO-d_6: 2.18 (s, 6H); 2.32 (s, 3H); 3.07 (s, 3H); 6.80 (s, 1H); 7.81 (s, 2H)	in DMSO-d_6: 15.22, 16.58, 26.10, 124.27, 125.22, 125.72, 132.67, 136.14, 155.71, 161.95, 169.77	244.2 (78); 56.1 (100)
90	3-F	Me	in $CDCl_3$: 2.37 (d, J_{HH} = 0.6 Hz, 3 H), 3.17 (s, 3 H), 7.02 (s, 1 H), 7.00-7.10 (m, 1 H), 7.30-7.4 (m, 1 H), 7.70-7.75 (m, 1 H), 8.00-8.08 (m, 1 H)	in $CDCl_3$: 15.67, 26.58, 116.75 (J_{CF} = 22.0 Hz), 118.25 (J_{CF} = 22.0 Hz), 125.45, 127.97, 130.01 (J_{CF} = 7.7 Hz), 136.20, 139.51, 162.69 (J_{CF} = 245.5 Hz), 163.4, 170.50	218.1 (64), 56.1 (100)
91	3-OH	C_3CO_2H	in DMSO-d_6: 1.71 (pentet, J_{HH} = 7.3 Hz,	in DMSO-d_6: 15.33, 25.63,	Analysis not

			2H); 1.99 (t, J_{HH} = 6.7 Hz, 2H); 2.37 (s, 3H); 3.55 (t, J_{HH} = 7.3 Hz, 2H); 6.83 (s, 1H); 6.85 (d, J_{HH} = 7.9 Hz, 1H); 7.19 (t, J_{HH} = 7.9 Hz, 1H); 7.51 (d, J_{HH} = 7.9 Hz, 1H); 7.69 (s, 1H)	34.21, 52.50, 117.59, 118.20, 122.80, 125.13, 129.36, 135.01, 138.49, 157.91, 163.95, 169.93, 176.15	completed
92	4-$OC_{12}H_{25}$	Me	in $CDCl_3$: 0.88 (t, J_{HH} = 6.7 Hz, 3H); 1.18-1.39 (m, 18H); 1.45 (sextet, J_{HH} = 7.9 Hz, 2H); 1.79 (pentet, J_{HH} = 7.9 Hz, 2H); 2.36 (s, 3H); 3.18 (s, 3H); 3.99 (t, J_{HH} = 6.5 Hz, 2H); 6.92 (d, J_{HH} = 8.8 Hz, 2H); 7.07 (s, 1H); 8.09 (d, J_{HH} = 8.8 Hz, 2H)	in $CDCl_3$: 14.10, 15.62, 22.67, 25.97, 26.57, 29.12, 29.34, 29.36, 29.54, 29.57, 29.61, 31.90, 68.09, 114.75, 126.83, 127.55, 134.02, 136.70, 160.86, 161.04, 170.75	Analysis not completed
93	4-OMe	Me	in $CDCl_3$: 2.63 (s, 3H); 3.17 (s, 3H); 3.84 (s, 3H); 6.93 (d, J_{HH} = 9.1 Hz, 2H); 7.07 (s, 1H); 8.10 (d, J_{HH} = 9.1 Hz, 2H)	in $CDCl_3$: 15.63, 26.55, 55.32, 114.22, 127.08, 127.37, 133.99, 136.86, 161.20, 170.72	Analysis not completed
94	2-OMe	Me	in $CDCl_3$: 2.34 (s, 3H); 3.15 (s, 3H); 3.86 (s, 3H); 6.86 (d, J_{HH} = 8.2 Hz 1H); 7.00 (t, J_{HH} = 7.6 Hz, 1H); 7.32 (t, J_{HH} = 7.00 Hz, 1H); 7.66 (s, 1H); 8.70 (dd, J_{HH} = 7.9, 1.8 Hz, 1H)	in $CDCl_3$: 15.60, 26.48, 55.43, 110.47, 120.74, 121.26, 123.02, 131.54, 132.69, 138.08, 158.92, 161.92, 170.60	230.2 (48); 199.1 (42); 130.0 (19); 56.1 (100)
95	4-OMe	n-Pr	in $CDCl_3$: 0.95 (t, J_{HH} = 7.6 Hz, 3H); 1.65 (m, 2H); 2.37 (s, 3H); 3.55 (t, J_{HH} = 7.6 Hz, 2H); 3.84 (s, 3H); 6.93 (d, J_{HH} = 9.1 Hz, 2H); 7.06 (s, 1H); 8.10 (d, J_{HH} = 8.8 Hz, 2H)	in $CDCl_3$: 11.17, 15.70, 22.58, 42.08, 55.29, 113.87, 114.20, 127.12, 129.45, 133.93, 136.80, 161.22, 170.74	258.2 (100); 175.0 (21); 146.0 (21); 84.0 (26); 55.1 (19)
96	4-Cl	n-Pr	in $CDCl_3$: 0.96 (t, J_{HH} = 7.3 Hz, 3H); 1.66 (sextet, J_{HH} = 7.3 Hz,	in $CDCl_3$: 11.20, 15.78, 22.61, 42.19,	246.2 (100); 229.2 (29); 163.0 (37);

			2H); 2.38 (s, 3H); 3.56 (t, J_{HH} = 7.3 Hz, 2H); 7.04 (s, 1H); 7.10 (AA′ of a AA′BB′X spin system, 2 H), 8.14 (BB′ of a AA′BB′X spin system, 2 H)	115.86 (J_{CF} = 21.0 Hz), 125.74, 130.57, 134.12 (J_{CF} = 8.8 Hz), 162.72, 163.59 (J_{CF} = 253.2 Hz), 170.70	135.0 (35); 84.1 (29); 55.1 (27)
97	4-Br	Me	in $CDCl_3$: 2.36 (s, 3H); 3.17 (s, 3H); 6.99 (s, 1H); 7.51 (d, J_{HH} = 8.8 Hz, 2H); 7.98 (d, J_{HH} = 8.5 Hz, 2H)	in $CDCl_3$: 15.69, 26.58, 124.49, 125.58, 131.85, 133.02, 133.38, 139.09, 163.06, 170.49	Analysis not completed
98	2-OMe	n-Pr	in $CDCl_3$: 0.94 (t, J_{HH} = 7.3 Hz, 3H); 1.64 (m, 2H); 2.36 (s, 3H); 3.55 (t, J_{HH} = 7.6 Hz, 2H); 3.86 (s, 3H); 6.87 (d, J_{HH} = 8.2 Hz, 1H); 7.01 (t, J_{HH} = 6.7 Hz, 1H); 7.32 (t, J_{HH} = 6.7 Hz, 1H); 7.66 (s, 1H); 8.70 (d, J_{HH} = 7.9 Hz, 1H)	in $CDCl_3$: 11.30, 15.70, 22.54, 42.03, 55.45, 110.48, 120.75, 121.12, 123.11, 131.49, 132.66, 138.03, 158.93, 158.93, 161.92, 170.65	Analysis not completed
99	2-Br	Me	in $CDCl_3$: 2.36 (s, 3H); 3.18 (s, 3H); 7.17 (t, J_{HH} = 7.9 Hz, 1H); 7.36 (t, J_{HH} = 7.9 Hz, 1H); 7.50 (s, 1H); 7.60 (d, J_{HH} = 7.9 Hz, 1H); 8.70 (d, J_{HH} = 7.9 Hz, 1H)	in $CDCl_3$: 15.71, 26.58, 124.87, 126.71, 127.50, 130.78, 133.01, 133.36, 133.64, 139.83, 163.90, 170.30	Analysis not completed
100	4-PhC_8H_{17}	Me	in $CDCl_3$: 0.89 (t, J_{HH} = 7.0 Hz, 3H); 1.19-1.42 (m, 10H); 1.60-1.70 (m, 2H); 2.40 (s, 3H); 2.65 (t, J_{HH} = 7.9 Hz, 2H); 3.20 (s, 3H); 7.15 (s, 1H); 7.28 (d, J_{HH} = 6.4 Hz, 4H); 7.47-7.60 (m, 4H); 7.66 (d, J_{HH} = 8.2 Hz, 2H); 8.20 (d, J_{HH} = 8.2 Hz, 2H)	in $CDCl_3$: 14.10, 15.71, 22.66, 26.61, 29.25, 29.35, 29.47, 31.47, 31.87, 35.63, 126.86, 126.89, 127.03, 127.09, 128.92, 132.54, 132.88, 137.55, 142.57, 142.82, 163.03, 170.69	Analysis not completed
101	4-Br	n-Pr	in $CDCl_3$: 0.95 (t, J_{HH}	in $CDCl_3$:	

			= 7.3 Hz, 3H); 1.66 (sextet, J_{HH} = 7.3 Hz, 2H); 2.37 (s, 3H); 3.55 (t, J_{HH} = 7.3 Hz, 2H); 6.99 (s, 1H); 7.53 (d, J_{HH} = 8.5 Hz, 2H); 8.00 (d, J_{HH} = 8.5 Hz, 2H)	11.22, 15.83, 22.60, 42.22, 124.48, 125.46, 131.91, 133.12, 133.37, 139.05, 163.15, 170.60	
102	2-Br	n-Pr	in $CDCl_3$: 0.96 (t, J_{HH} = 7.3 Hz, 3H); 1.67 (sextet, J_{HH} = 7.3 Hz, 2H); 2.38 (s, 3H); 3.57 (t, J_{HH} = 7.3 Hz, 2H); 7.18 (t of d, J_{HH} = 7.9, 1.8 Hz, 1H); 7.37 (t of d, J_{HH} = 7.9, 1.5 Hz, 1H); 7.61 (dd, J_{HH} = 8.2, 1.2 Hz, 1H); 7.50 (s, 1H); 8.72 (dd, J_{HH} = 8.2, 1.5 Hz, 1H)	in $CDCl_3$: 11.22, 15.84, 22.58, 42.23, 124.75, 126.80, 127.53, 130.81, 133.08, 133.37, 133.74, 139.80, 163.97, 170.42	Analysis not completed
103	3-F	n-Pr	in $CDCl_3$: 0.96 (t, J_{HH} = 7.3 Hz, 3H); 1.67 (sextet, J_{HH} = 7.3 Hz, 2H); 2.39 (s, 3H); 3.56 (t, J_{HH} = 7.3 Hz, 2H); 7.02 (s, 1H); 7.05 (t of d, J_{HH} = 8.2, 2.6 Hz, 1H); 7.36 (d of t, J_{HH} = 6.1 Hz, 1H); 7.73 (d, J_{HH} = 7.9 Hz, 1H); 8.05 (ddd, J_{HH} = 10.6, 2.6, 1.5 Hz, 1H)	in $CDCl_3$: 11.16, 15.77, 22.55, 42.18, 116.86 (J_{CF} = 21.0 Hz), 118.23, 125.32, 127.94, 129.96 (J_{CF} = 8.8 Hz), 136.29, 139.47, 162.72 (J_{CF} = 245.5 Hz), 163.46, 170.59	Analysis not completed
104	3-Cl	Me	in $CDCl_3$: 2.37 (s, 3H); 3.16 (s, 3H); 6.98 (s, 1H); 7.29-7.35 (m, 2H); 7.87-7.94 (m, 1H); 8.20 (s, 1H)	in $CDCl_3$: 15.66, 26.55, 125.13, 129.77, 130.12, 131.44, 134.49, 135.82, 139.57, 163.50, 170.43	Analysis not completed
105	3-OMe	n-Pr	in $CDCl_3$: 0.95 (t, J_{HH} = 7.6 Hz, 3H); 1.66 (sextet, J_{HH} = 7.3 Hz, 2H); 2.38 (s, 3H); 3.56 (t, J_{HH} = 7.6 Hz, 2H); 3.85 (s, 3H); 6.93 (dd, J_{HH} = 8.2, 2.3 Hz, 1H);	in $CDCl_3$: 11.17, 15.80, 22.57, 42.14, 55.24, 116.36, 116.43, 124.90, 126.95, 129.54, 135.41, 138.78,	Analysis not completed

			7.05 (s, 1H); 7.32 (t, J_{HH} = 7.9 Hz, 1H); 7.64 (d, J_{HH} = 7.6 Hz, 1H); 7.81 (s, 1H)	159.59, 162.64, 170.74	
106	Benzyl	n-Pr	in $CDCl_3$: 0.95 (t, J_{HH} = 7.6 Hz, 3H); 1.66 (sextet, J_{HH} = 7.6 Hz, 2H); 2.38 (s, 3H); 3.56 (t, J_{HH} = 7.6 Hz, 2H); 7.09 (s, 1H); 7.32-7.44 (m, 3H); 8.12 (d, J_{HH} = 6.2 Hz, 2H)	in $CDCl_3$: 11.16, 15.74, 22.55, 42.12, 127.06, 128.63, 129.95, 132.00, 134.14, 138.56, 162.59, 170.72	Analysis not completed
107	3-OH	C_3CO_2H	in DMSO-d_6: 1.15-1.29 (m, 2H); 1.39-1.57 (m, 4H); 1.93 (t, J_{HH} = 7.3 Hz, 2H); 2.36 (s, 3H); 3.51 (t, J_{HH} = 7.6 Hz, 2H); 6.83 (s, 1H); 6.85 (d, J_{HH} = 8.2 Hz, 1H); 7.19 (t, J_{HH} = 7.9 Hz, 1H); 7.51 (d, J_{HH} = 7.9 Hz, 1H); 7.68 (s, 1H)	in DMSO-d_6: 15.60, 26.13, 26.73, 28.88, 38.06, 52.74, 117.91, 118.52, 122.90, 125.55, 129.57, 135.19, 138.59, 158.33, 163.90, 170.12, 177.34	Analysis not completed
108	Benzyl	C_3CO_2H	in DMSO-d_6: 1.23 (pentet, J_{HH} = 7.0 Hz, 2H); 1.41-1.57 (m, 4H); 1.87 (t, J_{HH} = 7.3 Hz, 2H); 2.38 (s, 3H); 3.53 (t, J_{HH} = 7.0 Hz, 2H); 6.96 (s, 1H); 7.17-7.46 (m, 3H); 8.20 (d, J_{HH} = 6.4 Hz, 2H)	in DMSO-d_6: 15.36, 25.91, 26.48, 28.62, 37.90, 48.49, 124.62, 128.56, 129.82, 131.78, 134.02, 138.66, 164.12, 169.78, 176.87	Analysis not completed
109	4-PhC_5H_{11}	Me	in $CDCl_3$: 0.91 (t, J_{HH} = 6.5 Hz, 3H); 1.30-1.41 (m, 4H); 1.66 (pentet, J_{HH} = 7.6 Hz, 2H); 2.39 (s, 3H); 2.65 (t, J_{HH} = 7.9 Hz, 2H); 3.19 (s, 3H); 7.14 (s, 1H); 7.27 (d, J_{HH} = 6.2 Hz, 2H); 7.56 (d, J_{HH} = 8.2 Hz, 2H); 7.65 (d, J_{HH} = 8.5 Hz, 2H); 8.19 (d, J_{HH} = 8.5 Hz, 2H)	in $CDCl_3$: 14.02, 15.69, 22.52, 26.60, 31.12, 31.50, 35.57, 126.87, 127.00, 127.08, 128.92, 132.54, 132.88, 137.55, 138.49, 142.56, 142.81, 162.30, 170.68	346.2 (100); 289.2 (45); 55.8 (86)

110	4-*i*-Pr	Me	in $CDCl_3$: 0.89 (s, 3H); 0.91 (s, 3H); 1.88 (septet, J_{HH} = 6.7 Hz, 1H); 2.37 (s, 3H); 2.50 (d, J_{HH} = 7.0 Hz, 2H); 3.18 (s, 3H); 7.10 (s, 1H); 7.20 (d, J_{HH} = 8.2 Hz, 2H); 8.04 (d, J_{HH} = 8.2 Hz, 2H)	in $CDCl_3$: 15.66, 22.32, 26.57, 30.17, 45.43, 127.62, 129.54, 131.69, 131.95, 137.96, 144.48, 161.89, 170.74	Analysis not completed
111	3,4-Me	Me	in $CDCl_3$: 2.29 (s, 3H); 2.30 (s, 3H); 2.37 (s, 3H); 3.17 (s, 3H); 7.07 (s, 1H); 7.18 (d, J_{HH} = 8.5 Hz, 1H); 7.87 (s, 1H); 7.89 (d, J_{HH} = 6.2 Hz, 1H)	in $CDCl_3$: 15.64, 19.76, 19.93, 26.54, 127.82, 129.82, 130.04, 131.79, 133.16, 136.89, 137.78, 139.50, 161.68, 170.74	Analysis not completed
112	2-OH 4-$N(Et)_2$	n-Pn	in $CDCl_3$: 0.89 (t, J_{HH} = 7.0 Hz, 3H); 1.18 (t, J_{HH} = 7.0 Hz, 4H); 1.32 (m, 4H); 1.62 (m, 2H); 2.33 (s, 3H); 3.37 (q, J_{HH} = 7.0 Hz, 4H); 3.59 (t, J_{HH} = 7.3 Hz, 2H); 6.15 (d, J_{HH} = 2.6 Hz, 1H); 6.21 (dd, J_{HH} = 8.8, 2.3 Hz, 1H); 7.09 (s, 1H); 7.11 (d, J_{HH} = 7.0 Hz, 1H)	in $CDCl_3$: 12.71, 13.87, 14.94, 22.25, 28.79, 40.66, 44.51, 99.18, 104.47, 109.37, 127.62, 131.27, 138.57, 152.30, 152.85, 160.81, 167.69	343.3 (100); 328.2 (64); 232.2 (64); 211.2 (35); 112.1 (34); 71.0 (45); 54.8 (21)
113	2-OH 4-$N(Et)_2$	n-heptyl	in $CDCl_3$: 0.86 (t, J_{HH} = 6.2 Hz, 3H); 1.18 (t, J_{HH} = 7.0 Hz, 6H); 1.27 (m, 8H); 1.60 (m, 2H); 2.32 (s, 3H); 3.37 (q, J_{HH} = 7.0 Hz, 4H); 3.59 (t, J_{HH} = 7.3 Hz, 2H); 6.15 (s, 1H); 6.20 (d, J_{HH} = 9.1 Hz, 1H); 7.09 (s, 1H); 7.10 (d, J_{HH} = 7.3 Hz, 1H)	in $CDCl_3$: 12.70, 13.97, 14.92, 22.47, 26.65, 28.81, 29.29, 31.58, 40.69, 44.51, 99.18, 104.47, 109.37, 122.13, 131.28, 138.57, 152.30, 152.87, 160.81, 167.69	Analysis not completed
114	2-OH 4-$N(Et)_2$	n-Pr	in $CDCl_3$: 0.95 (t, J_{HH} = 7.3 Hz, 3H); 1.19 (t, J_{HH} = 7.0 Hz, 6H); 1.66 (m, 2H); 2.33 (s, 3H); 3.38 (q, J_{HH} = 7.0 Hz, 4H); 3.58 (t, J_{HH} =	in $CDCl_3$: 11.17, 12.74, 14.95, 22.57, 42.21, 44.54, 99.21, 104.49, 109.40, 127.63,	Analysis not completed

			7.6 Hz, 2H); 6.15 (d, J_{HH} = 2.3 Hz, 1H); 6.21 (dd, J_{HH} = 9.1, 2.6 Hz, 1H); 7.10 (s, 1H); 7.11 (d, J_{HH} = 8.8 Hz, 1H)	131.34, 138.62, 152.34, 152.90, 160.84, 167.76	
115	4-N(Et)$_2$	n-hexyl	in $CDCl_3$: 0.88 (t, J_{HH} = 6.7 Hz, 3H); 1.19 (t, J_{HH} = 7.3 Hz, 6H); 1.30 (m, 6H); 1.60 (m, 2H); 2.35 (s, 3H); 3.40 (q, J_{HH} = 7.0 Hz, 4H); 3.57 (t, J_{HH} = 7.6 Hz, 2H); 6.65 (d, J_{HH} = 9.1 Hz, 2H); 7.05 (s, 1H); 8.02 (d, J_{HH} = 8.8 Hz, 2H)	in $CDCl_3$: 12.60, 13.99, 15.66, 22.48, 26.44, 29.41, 31.41, 40.52, 44.48, 111.22, 121.50, 128.73, 134.27, 134.37, 149.09, 158.54, 170.66	Analysis not completed
116	2-OH 4-N(Et)$_2$	n-hexyl	in $CDCl_3$: 0.86 (t, J_{HH} = 6.2 Hz, 3H); 1.17 (t, J_{HH} = 7.3 Hz, 4H); 1.29 (m, 8H); 1.60 (m, 2H); 2.32 (s, 3H); 3.36 (q, J_{HH} = 7.0 Hz, 4H); 3.58 (t, J_{HH} = 7.3 Hz, 2H); 6.14 (s, 1H); 6.20 (dd, J_{HH} = 8.8, 2.1 Hz, 1H); 7.08 (s, 1H); 7.10 (d,, J_{HH} = 7.6 Hz, 1H)	in $CDCl_3$: 12.68, 13.90, 14.89, 22.39, 26.33, 29.23, 31.30, 40.66, 44.49, 99.16, 104.45, 109.36, 127.61, 131.22, 138.55, 152.30, 152.84, 160.79, 167.66	Analysis not completed
117	2-OH	n-Pr	in $CDCl_3$: 0.96 (t, J_{HH} = 7.3 Hz, 3H); 1.68 (sextet, J_{HH} = 7.3 Hz, 2H); 2.39 (s, 3H); 3.60 (t, J_{HH} = 7.6 Hz, 2H); 6.85 (t, J_{HH} = 7.9 Hz, 1H); 6.95 (d, J_{HH} = 8.2 Hz, 1H); 7.15 (s, 1H); 7.27-7.37 (m, 2H)	in $CDCl_3$: 11.19, 15.26, 22.52, 42.42, 119.17, 119.46, 119.66, 130.09, 132.79, 134.05, 136.35, 157.46, 165.88, 168.04	Analysis not completed
118	3-Cl	n-Pr	in $CDCl_3$: 0.96 (t, J_{HH} = 7.6 Hz, 3H); 1.66 (sextet, J_{HH} = 7.3 Hz, 2H); 2.39 (s, 3H); 3.56 (t, J_{HH} = 7.3 Hz, 2H); 6.99 (s, 1H); 7.30-7.36 (m, 2H); 7.89-7.95 (m, 1H); 8.22 (s, 1H)	in $CDCl_3$: 11.17, 15.79, 22.55, 42.19, 125.04, 129.79, 130.11, 131.46, 134.53, 135.91, 139.51, 163.56, 170.55	Analysis not completed
119	2-OH	Dodecyl	in $CDCl_3$: 0.87 (t, J_{HH}	in $CDCl_3$:	

	4-$N(Et)_2$		= 6.7 Hz, 3H); 1.19 (t, J_{HH} = 7.0 Hz, 6H); 1.24 (m, 18H); 1.61 (m, 2H); 2.34 (s, 3H); 3.38 (q, J_{HH} = 7.0 Hz, 4H); 3.60 (t, J_{HH} = 7.3 Hz, 2H); 6.16 (s, 1H); 6.22 (dd, J_{HH} = 8.8, 2.1 Hz, 1H); 7.11 (s, 1H); 7.12 (d, J_{HH} = 7.0 Hz, 1H)	12.76, 14.09, 14.98, 22.66, 26.76, 29.22, 29.31, 29.36, 29.44, 29.51, 29.57, 31.87, 40.74, 44.57, 99.24, 104.51, 109.43, 127.69, 131.34, 138.63, 152.33, 152.91, 160.86, 167.75	
120	2-OH 4-$N(Et)_2$	Octyl	in $CDCl_3$: 0.86 (t, J_{HH} = 6.7 Hz, 3H); 1.18 (t, J_{HH} = 7.0 Hz, 6H); 1.27 (m, 10H); 1.61 (m, 2H); 2.33 (s, 3H); 3.37 (q, J_{HH} = 7.0 Hz, 4H); 3.59 (t, J_{HH} = 7.6 Hz, 2H); 6.15 (s, 1H); 6.21 (dd, J_{HH} = 8.8, 2.1 Hz, 1H); 7.10 (s, 1H); 7.11 (d, J_{HH} = 7.3 Hz, 1H)	in $CDCl_3$: 12.73, 14.00, 14.94, 22.54, 26.71, 29.07, 29.13, 29.32, 31.68, 40.70, 44.52, 99.21, 104.48, 109.40, 127.65, 131.28, 138.60, 152.31, 152.88, 160.82, 167.69	Analysis not completed
121	4-*i*-Bu	C_3CO_2H	in CD_3OD: 0.90 (s, 3H); 0.92 (s, 3H); 1.82-1.96 (m, 3H); 2.20 (t, J_{HH} = 7.3 Hz, 2H); 2.44 (s, 3H); 2.51 (d, J_{HH} = 7.3 Hz, 2H); 3.67 (t, J_{HH} = 7.6 Hz, 2H); 7.03 (s, 1H); 7.22 (d, J_{HH} = 8.2 Hz, 2H); 8.01 (d, J_{HH} = 7.9 Hz, 2H)	in CD_3OD: 15.54, 22.76, 27.06, 31.47, 35.85, 41.59, 46.43, 128.37, 130.56, 133.07, 133.21, 139.10, 145.94, 165.04, 172.35, 181.18	Analysis not completed
122	4-*i*-Bu	n-heptyl	in $CDCl_3$: 0.74-1.01 (m, 9H); 1.14-1.41 (m, 8H); 1.52-1.69 (m, 2H); 1.87 (septet, J_{HH} = 6.7 Hz, 1H); 2.37 (s, 3H); 2.49 (d, J_{HH} = 7.0 Hz, 2H); 3.57 (t, J_{HH} = 7.0 Hz, 2H); 7.08 (s, 1H); 7.19 (d, J_{HH} = 7.6 Hz, 2H); 8.03 (d, J_{HH} = 7.6 Hz,	in $CDCl_3$: 13.99, 15.73, 22.29, 22.50, 26.65, 28.82, 29.32, 30.13, 31.61, 40.58, 45.39, 127.34, 129.49, 131.71, 131.88, 137.89, 144.33, 161.92, 170.68	Analysis not completed

			2H)		
123	3,4-Me	C_3CO_2H	in CD_3OD: 1.89 (pentet, J_{HH} = 7.3 Hz, 2H); 2.21 (t, J_{HH} = 7.3 Hz, 2H); 2.29 (s, 6H); 2.43 (s, 3H); 3.66 (t, J_{HH} = 7.3 Hz, 2H); 6.98 (s, 1H); 7.17 (d, J_{HH} = 7.6 Hz, 1H); 7.80 (d, J_{HH} = 7.9 Hz, 1H); 7.85 (s, 1H)	in CD_3OD: 15.50, 19.77, 20.01, 26.99, 35.68, 41.55, 128.79, 131.02, 131.12, 133.08, 134.24, 138.12, 138.76, 140.98, 164.74, 172.33, 181.03	Analysis not completed
124	3-pyridyl	Me	in $CDCl_3$: 2.36 (s, 3H); 3.16 (s, 3H); 7.02 (s, 1H); 7.32 (dd, J_{HH} = 7.9, 4.7 Hz, 8.53 (dd, J_{HH} = 5.0, 1.5 Hz, 1H); 8.66 (d of t, J_{HH} = 8.2, 1.8 Hz, 1H); 9.01 (dd, J_{HH} = 2.3 Hz, 1H)	in $CDCl_3$: 15.67, 26.58, 122.92, 123.55, 130.26, 138.31, 140.42, 150.13, 152.74, 163.81, 170.12	Analysis not completed
125	3-Br	n-Pr	in $CDCl_3$: 0.95 (t, J_{HH} = 7.3 Hz, 3H); 1.66 (sextet, J_{HH} = 7.3 Hz, 2H); 2.39 (s, 3H); 3.56 (t, J_{HH} = 7.6 Hz, 2H); 6.97 (s, 1H); 7.27 (t, J_{HH} = 7.9 Hz, 1H); 7.48 (d, J_{HH} = 7.9 Hz, 1H); 7.99 (d, J_{HH} = 7.6 Hz, 1H); 8.35 (s, 1H)	in $CDCl_3$: 11.17, 15.80, 22.55, 42.19, 122.70, 124.92, 130.07, 130.52, 132.66, 134.37, 136.20, 139.51, 139.51, 163.60, 170.53	Analysis not completed
126	2,4-Cl	Me	in $CDCl_3$: 2.36 (s, 3H); 3.17 (s, 3H); 7.28 (d, J_{HH} = 8.5 Hz, 1H); 7.41 (s, 1H); 7.43 (s, 1H); 8.75 (d, J_{HH} = 8.5 Hz, 1H)	in $CDCl_3$: 15.71, 26.60, 120.62, 127.33, 129.44, 130.62, 133.96, 135.86, 136.57, 140.02, 164.19, 170.19	Analysis not completed
127	2-OH	Me	in $CDCl_3$: 2.36 (s, 3H); 3.11 (s, 3H); 6.86 (t, J_{HH} = 7.0 Hz, 1H); 6.87 (d, J_{HH} = 8.5 Hz, 1H); 7.24 (s, 1H); 7.27 (t of d, J_{HH} = 7.0, 1.8 Hz, 1H); 8.17 (dd, J_{HH} = 7.9, 1.8 Hz, 1H)	in $CDCl_3$: 15.17, 26.30, 116.81, 119.21, 120.27, 122.35, 132.44, 133.81, 135.62, 157.55, 162.11, 168.67	Analysis not completed
128	3-Br	Me	in $CDCl_3$: 2.38 (s, 3H); 3.18 (s, 3H); 6.98	in $CDCl_3$: 15.73, 26.62,	Analysis not

			(s, 1H); 7.27 (t, J_{HH} = 7.9 Hz, 1H); 7.48 (d, J_{HH} = 7.9 Hz, 1H); 7.98 (d, J_{HH} = 7.9 Hz, 1H); 8.35 (s, 1H)	122.72, 125.13, 130.08, 130.59, 132.73, 134.44, 136.17, 139.61, 163.56, 170.48	completed
129	4-PhC_3H_7	Me	in $CDCl_3$: 0.98 (t, J_{HH} = 7.3 Hz, 3H); 1.69 (sextet, J_{HH} = 7.6 Hz, 2H); 2.39 (s, 3H); 2.64 (t, J_{HH} = 7.9 Hz, 2H); 3.19 (s, 3H); 7.15 (s, 1H); 7.28 (d, J_{HH} = 8.2 Hz, 1H); 7.56 (d, J_{HH} = 8.2 Hz, 1H); 7.65 (d, J_{HH} = 8.5 Hz, 1H); 8.19 (d, J_{HH} = 8.5 Hz, 1H)	in $CDCl_3$: 13.84, 15.69, 24.50, 26.58, 37.67, 126.86, 126.99, 127.06, 128.97, 132.53, 132.88, 137.58, 138.47, 142.54, 162.30	Analysis not completed
130	3,5-t-Bu 4-OH	n-Pr	in $CDCl_3$: 0.94 (t, J_{HH} = 7.3 Hz, 3H); 1.46 (s, 18H); 1.65 (sextet, J_{HH} = 7.6 Hz, 2H); 2.35 (s, 3H); 3.55 (t, J_{HH} = 7.3 Hz, 2H); 7.06 (s, 1H); 8.05 (s, 2H)	in $CDCl_3$: 11.13, 15.82, 22.58, 30.11, 34.29, 42.03, 125.86, 128.84, 129.96, 136.16, 136.20, 156.15, 160.45, 170.84	Analysis not completed
131	3,5-t-Bu 4-OH	n-Pn	in $CDCl_3$: 0.89 (t, J_{HH} = 6.7 Hz, 3H); 1.25-1.38 (m, 4H); 1.46 (s, 18H); 1.61 (pentet, J_{HH} = 7.0 Hz, 2H); 2.36 (s, 3H); 3.58 (t, J_{HH} = 7.3 Hz, 2H); 7.06 (s, 1H); 8.06 (s, 2H)	in $CDCl_3$: 13.91, 15.88, 22.31, 28.84, 29.09, 30.16, 34.33, 40.51, 125.94, 129.73, 129.96, 136.17, 136.30, 156.13, 160.44, 170.81	Analysis not completed
132	3,5-t-Bu 4-OH	n-hexyl	in $CDCl_3$: 0.87 (t, J_{HH} = 7.0 Hz, 3H); 1.22-1.35 (m, 6H); 1.46 (s, 18H); 1.54-1.65 (m, 2H); 2.35 (s, 3H); 3.57 (t, J_{HH} = 7.3 Hz, 2H); 7.06 (s, 1H); 8.05 (s, 2H)	in $CDCl_3$: 13.96, 15.85, 22.47, 26.39, 29.35, 30.01, 30.13, 31.37, 34.31, 40.54, 125.88, 128.82, 129.96, 136.16, 136.23, 156.15, 160.47, 170.81	Analysis not completed
133	4-OMe	EtOH	in $CDCl_3$: 2.36 (s, 3H); 3.72 (d, J_{HH} = 4.7	in $CDCl_3$: 15.79, 43.57,	Analysis not

			Hz, 2H); 3.79 (d, J_{HH} = 5.3 Hz, 2H); 3.85 (s, 3H); 6.94 (d, J_{HH} = 9.1 Hz, 2H); 7.02 (s, 1H); 8.08 (d, J_{HH} = 8.8 Hz, 2H)	55.33, 60.78, 114.23, 126.93, 127.87, 134.14, 136.32, 161.32, 171.22	completed
134	3,4-OMe	n-Pr	in $CDCl_3$: 0.94 (t, J_{HH} = 7.3 Hz, 3H); 1.64 (sextet, J_{HH} = 7.6 Hz, 2H); 2.36 (s, 3H); 3.55 (t, J_{HH} = 7.6 Hz, 2H); 3.91 (s, 3H); 3.94 (s, 3H); 6.88 (d, J_{HH} = 8.5 Hz, 1H); 7.03 (s, 1H); 7.52 (dd, J_{HH} = 8.2, 1.8 Hz, 1H); 8.03 (s, 1H)	in $CDCl_3$: 11.13, 15.77, 22.55, 42.06, 55.78, 55.81, 110.72, 113.93, 126.70, 127.24, 127.40, 136.90, 148.87, 150.89, 161.22, 170.66	Analysis not completed
135	2-OH 3-OEt	2-phenol	in $CDCl_3$: 1.45 (t, J_{HH} = 7.0 Hz, 3H); 2.22 (s, 3H); 4.09 (q, J_{HH} = 7.0 Hz, 2H); 6.78 (t, J_{HH} = 7.9 Hz, 1H); 6.90 (dd, J_{HH} = 8.2, 1.2 Hz, 1H); 6.94-7.04 (m, 3H); 7.13 (dd, J_{HH} = 8.2, 1.2 Hz, 1H); 7.16 (s, 1H); 7.28 (t of d, J_{HH} = 8.2, 1.5 Hz, 1H)	in $CDCl_3$: 14.83, 15.46, 64.48, 116.60, 118.64, 119.03, 119.75, 121.22, 127.95, 128.50, 130.96, 131.50, 132.27, 148.91, 149.06, 152.16, 157.38, 162.98, 168.08	Analysis not completed
136	4-OH	$C_2N(Me)_2$	in DMSO-d_6: 2.17 (s, 6H); 2.36 (s, 3H); 2.38 (t, J_{HH} = 6.4 Hz, 2H); 3.63 (t, J_{HH} = 6.4 Hz, 2H); 6.83 (d, J_{HH} = 8.8 Hz, 2H); 6.87 (s, 1H0; 8.06 (d, J_{HH} = 8.8 Hz, 2H)	in DMSO-d_6: 15.30, 37.95, 45.25, 57.50, 115.73, 125.09, 125.57, 134.03, 135.84, 159.79, 161.84, 169.71	Analysis not completed
137	3-OH	$C_2N(Me)_2$	in DMSO-d_6: 2.17 (s, 6H); 2.39 (s, 3H); 3.64 (t, J_{HH} = 6.2 Hz, 4H); 6.82 (dd, J_{HH} = 8.2, 1.8 Hz, 1H); 6.85 (s, 1H); 7.23 (t, J_{HH} = 7.6 Hz, 1H); 7.53 (d, J_{HH} = 7.9 Hz, 1H); 7.72 (s, 1H)	in DMSO-d_6: 15.42, 38.02, 45.24, 57.43, 117.37, 117.85, 123.25, 125.01, 129.45, 135.04, 138.46, 157.28, 163.97, 169.80	Analysis not completed
138	2-OH	Me	in $CDCl_3$: 2.34 (s,	in $CDCl_3$:	Analysis

			3H); 2.76 (s, 3H); 3.20 (s, 3H); 6.97 (t, J_{HH} = 7.9 Hz, 1H); 7.03 (d, J_{HH} = 8.2 Hz, 1H); 7.32 (t, J_{HH} = 8.2 Hz, 1H); 7.45 (d, J_{HH} = 8.2 Hz, 1H)	15.20, 19.26, 26.60, 120.36, 120.59, 127.68, 130.07, 131.79, 132.98, 144.77, 154.52, 157.96, 167.24	not completed
139	4-N(Et)$_2$	C_2-sym	in $CDCl_3$: 1.19 (t, J_{HH} = 7.3 Hz, 6H); 2.19 (s, 3H); 3.41 (q, J_{HH} = 7.0 Hz, 4H); 3.87 (s, 2H); 6.67 (d, J_{HH} = 9.1 Hz, 2H); 7.08 (s, 1H); 8.03 (d, J_{HH} = 9.1 Hz, 2H)	in $CDCl_3$: 12.58, 15.07, 39.22, 44.52, 111.22, 121.19, 129.74, 133.36, 134.74, 149.37, 157.45, 170.74	Analysis not completed
140	Benzyl	C_2N(Me)$_2$	in $CDCl_3$: 2.27 (s, 6H); 2.41 (s, 3H); 2.49 (t, J_{HH} = 6.7 Hz, 2H); 3.68 (t, J_{HH} = 6.7 Hz, 2H); 7.08 (s, 1H); 7.31-7.46 (m, 3H); 8.10 (d, J_{HH} = 7.6 Hz, 2H)	in $CDCl_3$: 15.80, 38.91, 45.65, 57.97, 127.12, 128.63, 129.35, 129.96, 132.03, 134.12, 162.77, 170.66	Analysis not completed
141	3,5-t-Bu 4-OH	EtOH	in $CDCl_3$: 1.47 (s, 18H); 2.38 (s, 3H); 3.72-3.82 (m, 4H); 7.07 (s, 1H); 8.05 (s, 2H)	in $CDCl_3$: 15.96, 30.16, 34.34, 43.66, 61.13, 125.77, 129.58, 130.18, 135.85, 136.23, 160.56, 171.48	Analysis not completed
142	2-OH 4-OMe	n-Pr	in $CDCl_3$: 0.96 (t, J_{HH} = 7.3 Hz, 3H); 1.67 (sextet, J_{HH} = 7.6 Hz, 2H); 2.37 (s, 3H); 3.59 (t, J_{HH} = 7.6 Hz, 2H); 3.82 (s, 3H); 6.42-6.49 (m, 2H); 7.12 (s, 1H); 7.20 (d, J_{HH} = 9.3 Hz, 1H)	in $CDCl_3$: 11.17, 15.11, 22.52, 42.34, 55.40, 102.71, 107.50, 113.46, 130.33, 137.89, 155.40, 160.79, 164.92, 167.85	Analysis not completed
143	2,4-Cl	n-Pr	in $CDCl_3$: 0.96 (t, J_{HH} = 7.3 Hz, 3H); 1.66 (sextet, J_{HH} = 7.3 Hz, 2H); 2.38 (s, 3H); 3.57 (t, J_{HH} = 7.3 Hz, 2H); 7.30 (d, J_{HH} = 7.9 Hz, 1H); 7.43 (s, 1H); 7.45 (s, 1H); 8.78 (d, J_{HH} =	in $CDCl_3$: 11.19, 15.83, 22.55, 42.24, 120.50, 127.36, 129.49, 130.72, 133.96, 135.88, 136.61, 139.99, 164.25, 170.33	Analysis not completed

			8.5 Hz, 1H)		
144	4-$N(Et)_2$	C_4-sym	in $CDCl_3$: 1.19 (t, J_{HH} = 7.0 Hz, 3H); 1.60-1.72 (m, 2H); 2.35 (s, 3H); 3.40 (q, J_{HH} = 7.0 Hz, 2H); 3.61-3.74 (m, 2H); 6.67 (d, J_{HH} = 9.1 Hz, 2H); 7.05 (s, 1H); 8.02 (d, J_{HH} = 9.1 Hz, 2H)	in $CDCl_3$: 12.60, 15.64, 26.60, 39.79, 44.49, 111.22, 121.42, 129.08, 134.49, 149.19, 158.14, 170.75	Analysis not completed
145	2-OH 4-OMe	Me	in $CDCl_3$: 2.35 (s, 3H); 3.20 (s, 3H); 3.82 (s, 3H); 6.41-6.47 (m, 2H), 7.13 (s, 1H); 7.20 (d, J_{HH} = 9.4 Hz, 1H)	in $CDCl_3$: 15.03, 26.70, 55.39, 102.68, 107.48, 113.38, 130.45, 137.92, 155.46, 160.81, 164.95, 167.79	Analysis not completed
146	Piperonal	Me	in $CDCl_3$: 2.35 (s, 3H); 3.17 (s, 3H); 6.00 (s, 2H); 6.83 (d, J_{HH} = 8.2 Hz, 1H); 7.01 (s, 1H); 7.41 (dd, J_{HH} = 8.2, 1.8 Hz, 1H); 7.98 (d, J_{HH} = 1.8 Hz, 1H)	in $CDCl_3$: 15.60, 26.54, 101.43, 108.43, 111.14, 127.22, 128.29, 137.12, 148.02, 149.38, 161.41, 170.63	Analysis not completed
147	2-CF_3	n-Pr	in $CDCl_3$: 0.96 (t, J_{HH} = 7.3 Hz, 3H); 1.67 (sextet, J_{HH} = 7.6 Hz, 2H); 2.38 (s, 3H); 3.57 (t, J_{HH} = 7.6 Hz, 2H); 7.40-7.47 (m, 2H); 7.61 (t, J_{HH} = 8.2 Hz, 1H); 7.70 (d, J_{HH} = 7.9 Hz, 1H); 8.75 (t, J_{HH} = 7.9 Hz, 1H)	in $CDCl_3$: 11.20, 15.59, 22.55, 42.26, 121.16 (J_{CF} = 4.4 Hz), 122.33, 125.88 (J_{CF} = 5.5 Hz), 129.04, 129.30, 131.78, 132.08, 133.47, 140.40, 164.79, 170.28	Analysis not completed
148	4-OH	Allyl	in $CDCl_3$: 2.32 (s, 3H); 4.32 (d, J_{HH} = 5.3 Hz, 2H); 5.12 (d, J_{HH} = 9.6 Hz, 1H); 5.20 (d, J_{HH} = 9.6 Hz, 1H); 5.73-5.88 (m, 1H); 6.83 (d, J_{HH} = 8.8 Hz, 2H); 7.10 (s, 1H); 7.65 (d, J_{HH} = 8.8 Hz, 2H)	in $CDCl_3$: 15.41, 42.44, 52.81, 116.52, 117.12, 125.32, 129.35, 131.88, 134.56, 135.07, 160.44, 170.37	Analysis not completed
149	2,5-OMe	n-Pr	in $CDCl_3$: 0.94 (t, J_{HH} = 7.6 Hz, 3H); 1.65	in $CDCl_3$: 11.15, 15.77,	Analysis not

			(sextet, J_{HH} = 7.3 Hz, 2H); 2.35 (s, 3H); 3.55 (t, J_{HH} = 7.3 Hz, 2H); 3.82 (s, 3H); 3.83 (s, 3H); 6.82 (s, 1H); 6.88 (d, J_{HH} = 2.9 Hz, 1H); 7.61 (s, 1H); 8.42 (d, J_{HH} = 3.2 Hz, 1H)	22.55, 42.05, 55.68, 56.68, 111.74, 116.77, 117.84, 120.87, 123.68, 138.22, 153.37, 153.79, 161.92, 170.63	completed
150	4-N(Me)$_2$	PrOH	in $CDCl_3$: 1.77 (pentet, J_{HH} = 7.6 Hz, 2H); 2.35 (s, 3H); 3.03 (s, 6H); 3.55 (t, J_{HH} = 5.6 Hz, 2H); 3.75 (t, J_{HH} = 6.2 Hz, 2H); 6.68 (d, J_{HH} = 8.8 Hz, 2H); 7.09 (s, 1H); 8.05 (d, J_{HH} = 9.1 Hz, 2H)	in $CDCl_3$: 15.29, 31.69, 36.39, 39.94, 57.81, 111.61, 121.83, 130.01, 133.89, 134.36, 151.62, 158.16, 171.73	Analysis not completed
151	3-OH 4-Br	Me	in $CDCl_3$: 2.38 (s, 3H); 3.11 (s, 3H); 6.76 (dd, J_{HH} = 8.5, 2.9 Hz, 1H); 7.10 (s, 1H); 7.49 (d, J_{HH} = 8.5 Hz, 1H); 8.29 (d, J_{HH} = 3.2 Hz, 1H); 9.92 (broad, 1H)	Analysis not completed	Analysis not completed
152	4-OH	2-heptyl	in $CDCl_3$: 0.88 (t, J_{HH} = 6.7 Hz, 3H); 0.92 (d, J_{HH} = 7.3 Hz, 3H); 1.19-1.38 (m, 8H); 1.68 (sextet, J_{HH} = 6.2 Hz, 1H); 2.37 (s, 3H); 3.49 (d, J_{HH} = 7.3 Hz, 2H); 6.84 (d, J_{HH} = 8.8 Hz, 2H); 7.09 (s, 1H); 7.98 (d, J_{HH} = 8.8 Hz, 2H)	in $CDCl_3$: 10.57, 14.03, 15.74, 22.96, 23.77, 28.60, 30.45, 39.22, 44.67, 116.06, 126.36, 128.54, 134.31, 135.81, 158.67, 161.60, 171.17	Analysis not completed
153	4-Ph	Me	in $CDCl_3$: 2.40 (s, 3H); 3.20 (s, 3H); 7.15 (s, 1H); 7.39 (d, J_{HH} = 7.3 Hz, 1H); 7.46 (t, J_{HH} = 7.6 Hz, 2H); 7.65 (t, J_{HH} = 7.0 Hz, 4H); 8.20 (d, J_{HH} = 8.2 Hz, 2H)	in $CDCl_3$: 15.70, 26.60, 126.83, 127.05, 127.30, 127.77, 128.84, 132.54, 133.20, 138.66, 140.29, 142.54, 162.46, 170.66	Analysis not completed
154	4-OMe	Allyl	in $CDCl_3$: 2.33 (s, 3H); 3.84 (s, 3H); 4.23 (d, J_{HH} = 4.7 Hz, 2H);	in $CDCl_3$: 15.67, 42.34, 55.30, 114.22,	Analysis not completed

			5.09-5.22 (m, 2H); 5.74-5.92 (m, 1H); 6.94 (d, J_{HH} = 8.5 Hz, 2H); 7.09 (s, 1H); 8.11 (d, J_{HH} = 8.5 Hz, 2H)	116.96, 127.03, 127.53, 129.61, 132.13, 134.01, 136.57, 161.22, 170.24	
155	2-OH 4-OMe	PrOH	in $CDCl_3$: 1.82 (pentet, J_{HH} = 5.3 Hz, 2H); 2.38 (s, 3H); 3.58 (t, J_{HH} = 5.6 Hz, 2H); 3.79 (d, J_{HH} = 5.9 Hz, 2H); 3.82 (s, 3H); 6.42-6.46 (m, 2H); 7.15 (s, 1H); 7.19 (d, J_{HH} = 9.4 Hz, 1H)	in $CDCl_3$: 14.85, 31.47, 36.99, 55.42, 58.03, 102.66, 107.67, 113.31, 129.90, 131.44, 138.12, 154.93, 161.04, 165.24, 168.79	Analysis not completed
156	4-$N(Me)_2$	2-heptyl	in $CDCl_3$: 0.80-0.92 (m, 6H); 1.17-1.37 (m, 8H); 1.67 (sextet, J_{HH} = 6.2 Hz, 1H); 2.35 (s, 3H); 3.02 (s, 6H); 3.46 (d, J_{HH} = 8.8 Hz, 3H); 6.69 (d, J_{HH} = 9.1 Hz, 2H); 7.05 (s, 1H); 8.05 (d, J_{HH} = 8.8 Hz, 2H)	in $CDCl_3$: 10.55, 13.99, 15.85, 22.92, 23.73, 28.62, 30.42, 39.22, 39.95, 44.41, 111.64, 122.23, 128.54, 133.99, 134.58, 151.33, 159.28, 170.93	Analysis not completed
157	4-OC_4H_9	Me	in $CDCl_3$: 0.97 (t, J_{HH} = 7.3 Hz, 3H); 1.49 (sextet, J_{HH} = 7.6 Hz, 2H); 1.77 (pentet, J_{HH} = 7.9 Hz, 2H); 2.36 (s, 3H); 3.17 (s, 3H); 4.00 (t, J_{HH} = 6.4 Hz, 2H); 6.92 (d, J_{HH} = 9.1 Hz, 2H); 7.07 (s, 1H); 8.08 (d, J_{HH} = 8.8 Hz, 2H)	in $CDCl_3$: 13.80, 15.61, 19.16, 26.54, 31.14, 67.74, 114.73, 126.83, 127.49, 134.01, 136.71, 160.84, 161.04, 170.74	Analysis not completed
158	4-$N(Me)_2$	$C_2N(Me)_2$	in $CDCl_3$: 2.26 (s, 6H); 2.37 (s, 3H); 2.47 (t, J_{HH} = 6.7 Hz, 2H); 3.02 (s, 6H); 3.66 (t, J_{HH} = 7.0 Hz, 2H); 6.68 (d, J_{HH} = 9.1 Hz, 2H); 7.04 (s, 1H); 8.03 (d, J_{HH} = 9.1 Hz, 2H)	in $CDCl_3$: 15.63, 38.80, 39.94, 45.65, 58.05, 111.61, 122.16, 128.56, 134.01, 151.33, 159.05, 170.53	Analysis not completed
159	4-$N(Me)_2$	C_2CN	in $CDCl_3$: 2.45 (s, 3H); 2.76 (t, J_{HH} = 6.4 Hz, 2H); 3.06 (s, 6H); 3.88 (t, J_{HH} = 6.4 Hz,	in $CDCl_3$: 15.51, 17.62, 36.79, 40.01, 111.69, 117.32,	Analysis not completed

			2H); 6.70 (d, J_{HH} = 9.1 Hz, 2H); 7.09 (s, 1H); 8.07 (d, J_{HH} = 8.8 Hz, 2H)	121.82, 130.13, 133.49, 134.49, 151.74, 156.72, 170.27	
160	2-OH 4-N(Et)$_2$	C2-sym	in $CDCl_3$: 1.20 (t, J_{HH} = 7.0 Hz, 3H); 2.20 (s, 3H); 3.40 (q, J_{HH} = 7.0 Hz, 2H); 3.93 (s, 2H); 6.16 (s, 1H); 6.23 (dd, J_{HH} = 8.8 Hz, 1H); 7.12 (d, J_{HH} = 9.1 Hz, 1H); 7.14 (s, 1H)	Analysis not completed	Analysis not completed
161	4-Me	C_2H_4CN	in $CDCl_3$: 2.38 (s, 3H); 2.47 (s, 3H); 2.76 (t, J_{HH} = 6.4 Hz, 2H); 3.88 (t, J_{HH} = 6.4 Hz, 2H); 7.11 (s, 1H); 7.23 (d, J_{HH} = 8.2 Hz, 2H); 8.03 (d, J_{HH} = 8.2 Hz, 2H)	in $CDCl_3$: 15.58, 17.56, 21.65, 36.79, 117.15, 128.81, 129.54, 131.03, 132.34, 136.86, 141.21, 159.87, 170.40	Analysis not completed
162	2-Indole	n-Pn	in $CDCl_3$: 0.86 (t, J_{HH} = 7.3 Hz, 3H); 1.17-1.35 (m, 4H); 1.54 (pentet, J_{HH} = 7.0 Hz, 2H); 2.35 (s, 3H); 3.54 (t, J_{HH} = 7.3 Hz, 2H); 7.15 (t, J_{HH} = 7.0 Hz, 1H); 7.21 (t, J_{HH} = 7.0 Hz, 1H); 7.32 (s, 1H); 7.48 (d, J_{HH} = 7.0 Hz, 1H); 8.21 (d, J_{HH} = 8.2 Hz, 1H); 8.41 (s, 1H)	in $CDCl_3$: 13.80, 15.23, 21.70, 28.31, 28.40, 39.62, 111.06, 112.10, 119.48, 119.55, 120.63, 122.43, 126.65, 132.69, 133.68, 136.30, 158.74, 169.11	Analysis not completed
163	3-OH	2-heptyl	in $CDCl_3$: 0.85 -0.93 (m, 6H); 1.19-1.37 (m, 8H); 1.67 (sextet, J_{HH} = 6.0 Hz, 1H); 2.34 (s, 3H); 3.47 (d, J_{HH} = 7.9 Hz, 2H); 6.85 (dd, J_{HH} = 8.2, 2.6 Hz, 1H); 7.10 (s, 1H); 7.23 (t, J_{HH} = 7.9 Hz, 1H); 7.45 (d, J_{HH} = 7.6 Hz, 1H); 7.78 (s, 1H)	in $CDCl_3$: 10.49, 13.99, 15.71, 22.92, 23.71, 28.53, 30.39, 39.16, 44.64, 117.85, 118.03, 124.43, 128.00, 129.88, 135.04, 137.89, 156.40, 163.56, 170.79	Analysis not completed
164	3-OH	3-Pn	in $CDCl_3$: 0.87 (t, J_{HH} = 7.3 Hz, 6H); 1.58-1.66 (m, 1H); 1.69-	in $CDCl_3$: 11.04, 11.19, 16.74, 25.56,	Analysis not completed

			1.82 (m, 2H); 1.92-2.11 (m, 2H); 2.34 (s, 3H); 6.85 (d, J_{HH} = 8.2 Hz, 1H); 7.03 (s, 1H); 7.22 (t, J_{HH} = 7.6 Hz, 1H); 7.48 (d, J_{HH} = 7.9 Hz, 1H); 7.72 (s, 1H)	28.57, 65.86, 75.19, 118.03, 124.30, 127.59, 129.82, 135.09, 137.94, 156.44, 164.04, 170.87	
165	2-Indole	$C_3N(Me)_2$	in $CDCl_3$: 1.82 (pentet, J_{HH} = 7.3 Hz, 2H); 2.22 (s, 6H); 2.32 (t, J_{HH} = 7.3 Hz, 2H); 2.36 (s, 3H); 3.66 (t, J_{HH} = 7.0 Hz, 2H); 7.21-7.25 (m, 2H); 7.39 (dd, J_{HH} = 5.9, 3.2 Hz, 1H); 7.55 (s, 1H); 7.94 (dd, J_{HH} = 6.7, 2.6 Hz, 1H); 8.45 (s, 1H)	in $CDCl_3$: 15.50, 27.24, 38.62, 45.31, 56.34, 111.58, 112.20, 119.11, 120.77, 121.35, 123.05, 127.40, 131.34, 134.58, 135.98, 158.76, 170.12	Analysis not completed
166	4-$N(Me)_2$	EtOH	in $CDCl_3$: 2.32 (s, 3H); 3.03 (s, 6H); 3.69 (d, J_{HH} = 5.0 Hz, 2H); 3.75 (d, J_{HH} = 4.4 Hz, 2H); 6.68 (d, J_{HH} = 9.1 Hz, 2H); 7.01 (s, 1H); 8.01 (d, J_{HH} = 8.8 Hz, 2H)	in $CDCl_3$: 15.64, 39.97, 43.60, 60.79, 111.61, 121.95, 129.35, 133.99, 134.24, 151.51, 159.25, 171.12	Analysis not completed
167	4-$N(Et)_2$	C_6-sym	in $CDCl_3$: 1.18 (t, J_{HH} = 7.0 Hz, 3H); 1.32-1.42 (m, 2H); 1.57-.71 (m. 2H); 2.34 (s, 3H); 3.40 (t, J_{HH} = 7.0 Hz, 2H); 3.57 (t, J_{HH} = 7.3 Hz, 2H); 6.65 (d, J_{HH} = 9.1 Hz, 2H); 7.04 (s, 1H); 8.02 (d, J_{HH} = 9.1 Hz, 2H)	in $CDCl_3$: 12.58, 15.63, 26.30, 29.22, 40.26, 44.46, 111.19, 121.42, 128.79, 134.14, 134.37, 149.09, 158.36, 170.63	Analysis not completed
168	2-Indole	n-Pr	in $CDCl_3$: 0.96 (t, J_{HH} = 7.6 Hz, 3H); 1.67 (sextet, J_{HH} = 7.3 Hz, 2H); 2.36 (s, 3H); 3.57 (t, J_{HH} = 7.3 Hz, 2H); 7.21-7.25 (m, 2H); 7.39 (dd, J_{HH} = 7.6, 2.3 Hz, 1H); 7.56 (s, 1H); 7.94 (dd, J_{HH} =	in $CDCl_3$: 11.22, 15.61, 22.67, 42.14, 111.58, 112.24, 119.14, 120.77, 121.38, 123.09, 127.36, 131.21, 134.68, 135.92, 158.81, 170.12	Analysis not completed

			6.7, 3.2 Hz, 1H); 8.45 (s, 1H)		
169	3-OH	2-heptyl	Analysis not completed	Analysis not completed	Analysis not completed
170	4-CN	PrOH	in $CDCl_3$: 1.83 (pentet, J_{HH} = 5.3 Hz, 2H); 2.43 (s, 3H); 3.61 (t, J_{HH} = 5.8 Hz, 2H); 3.79 (t, J_{HH} = 6.4 Hz, 2H); 7.03 (s, 1H); 7.68 (d, J_{HH} = 8.5 Hz, 2H); 8.22 (d, J_{HH} = 8.2 Hz, 2H)	in $CDCl_3$: 15.68, 31.53, 37.02, 58.27, 112.77, 118.67, 124.73, 126.74, 132.24, 138.26, 140.61, 164.55, 171.38	Analysis not completed

APPENDIX B

CRYSTALLOGRAPHIC INFORMATION ON SELECT AMI CHROMOPHORES

2,3-OMe/Me AMI Chromophore

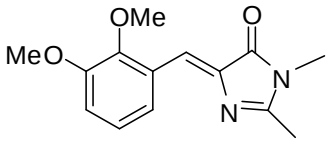

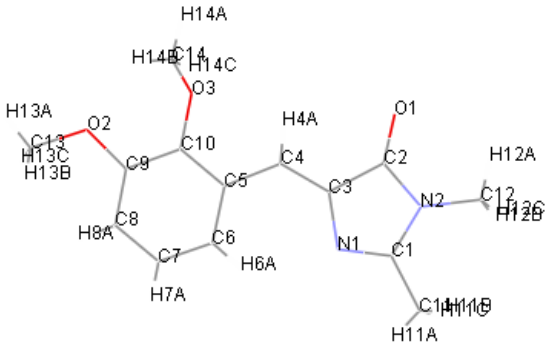

data_ab_3_3bs	
symmetry_cell_setting	monoclinic
symmetry_space_group_name_H-M	'P 21/c'

cell_length_a	7.173(4)
cell_length_b	7.902(3)
cell_length_c	22.746(9)
cell_angle_alpha	90.00
cell_angle_beta	96.44(3)
cell_angle_gamma	90.00
cell_volume	1281.13

Spatial Coordinates of 2,3-OMe/Me

C1	C	0.70223(18)	0.38143(17)	0.04495(5)
C2	C	0.46737(18)	0.46825(16)	0.09518(5)
C3	C	0.62756(17)	0.59036(16)	0.09871(5)
C4	C	0.62572(17)	0.73869(16)	0.12816(5)
H4A	H	0.5153	0.7618	0.1462

C5	C	0.77205(17)	0.86844(16)	0.13582(5)
C6	C	0.95567(18)	0.84070(17)	0.12127(6)
H6A	H	0.9877	0.7351	0.1052
C7	C	1.08863(18)	0.96676(17)	0.13036(6)
H7A	H	1.2126	0.9453	0.1214
C8	C	1.04561(17)	1.12474(17)	0.15240(5)
H8A	H	1.1383	1.2110	0.1572
C9	C	0.86583(17)	1.15502(16)	0.16725(5)
C10	C	0.72992(17)	1.02594(16)	0.16002(5)
C11	C	0.8052(2)	0.26679(19)	0.00827(6)
H11A	H	0.9272	0.3167	0.0028
H11B	H	0.7322	0.2508	-0.0304
H11C	H	0.8244	0.1571	0.0282
C12	C	0.4113(2)	0.19228(17)	0.04154(6)
H12A	H	0.2920	0.1983	0.0586
H12B	H	0.4789	0.0896	0.0555
H12C	H	0.3868	0.1894	-0.0017
C13	C	0.95038(19)	1.42981(17)	0.20406(6)
H13A	H	0.8937	1.5316	0.2191
H13B	H	1.0106	1.4587	0.1688
H13C	H	1.0444	1.3844	0.2346
C14	C	0.5370(2)	1.0677(2)	0.23624(6)
H14A	H	0.4063	1.0890	0.2428
H14B	H	0.6160	1.1608	0.2530
H14C	H	0.5793	0.9613	0.2555
N1	N	0.76716(15)	0.52530(14)	0.06632(5)
N2	N	0.52462(15)	0.34052(14)	0.05963(5)
O1	O	0.31945(13)	0.47427(13)	0.11679(4)
O2	O	0.80757(12)	1.30513(11)	0.18904(4)
O3	O	0.55066(12)	1.05584(12)	0.17407(4)

Bond Angles of 2,3-OMe/Me

Number	Atom1	Atom2	Atom3	Angle
1	C11	C1	N1	124.3(1)
2	C11	C1	N2	121.4(1)
3	N1	C1	N2	114.3(1)
4	C3	C2	N2	103.0(1)
5	C3	C2	O1	130.6(1)
6	N2	C2	O1	126.3(1)
7	C2	C3	C4	122.4(1)
8	C2	C3	N1	108.9(1)
9	C4	C3	N1	128.6(1)
10	C3	C4	H4A	115.9(1)
11	C3	C4	C5	128.3(1)
12	H4A	C4	C5	115.8(1)
13	C4	C5	C6	122.6(1)

14	C4	C5	C10	118.9(1)
15	C6	C5	C10	118.4(1)
16	C5	C6	H6A	120.0(1)
17	C5	C6	C7	120.1(1)
18	H6A	C6	C7	120.0(1)
19	C6	C7	H7A	119.2(1)
20	C6	C7	C8	121.6(1)
21	H7A	C7	C8	119.2(1)
22	C7	C8	H8A	120.3(1)
23	C7	C8	C9	119.4(1)
24	H8A	C8	C9	120.3(1)
25	C8	C9	C10	119.7(1)
26	C8	C9	O2	124.5(1)
27	C10	C9	O2	115.8(1)
28	C5	C10	C9	120.7(1)
29	C5	C10	O3	119.3(1)
30	C9	C10	O3	120.0(1)
31	C1	C11	H11A	109.5(1)
32	C1	C11	H11B	109.5(1)
33	C1	C11	H11C	109.4(1)
34	H11A	C11	H11B	109.4(1)
35	H11A	C11	H11C	109.5(1)
36	H11B	C11	H11C	109.5(1)
37	H12A	C12	H12B	109.5(1)
38	H12A	C12	H12C	109.4(1)
39	H12A	C12	N2	109.5(1)
40	H12B	C12	H12C	109.4(1)
41	H12B	C12	N2	109.5(1)
42	H12C	C12	N2	109.5(1)
43	H13A	C13	H13B	109.4(1)
44	H13A	C13	H13C	109.4(1)
45	H13A	C13	O2	109.5(1)
46	H13B	C13	H13C	109.5(1)
47	H13B	C13	O2	109.5(1)
48	H13C	C13	O2	109.5(1)
49	H14A	C14	H14B	109.5(1)
50	H14A	C14	H14C	109.4(1)
51	H14A	C14	O3	109.5(1)
52	H14B	C14	H14C	109.5(1)
53	H14B	C14	O3	109.4(1)
54	H14C	C14	O3	109.5(1)
55	C1	N1	C3	105.6(1)
56	C1	N2	C2	108.1(1)
57	C1	N2	C12	128.0(1)
58	C2	N2	C12	123.9(1)
59	C9	O2	C13	116.3(1)

60	C10	O3	C14	114.1(1)

Bond Lengths of 2,3-OMe/Me

Number	Atom1	Atom2	Type	Length
1	C1	C11	Unknown	1.483(2)
2	C1	N1	Unknown	1.302(2)
3	C1	N2	Unknown	1.391(2)
4	C2	C3	Unknown	1.496(2)
5	C2	N2	Unknown	1.384(2)
6	C2	O1	Unknown	1.219(2)
7	C3	C4	Unknown	1.351(2)
8	C3	N1	Unknown	1.405(2)
9	C4	H4A	Unknown	0.950(1)
10	C4	C5	Unknown	1.464(2)
11	C5	C6	Unknown	1.411(2)
12	C5	C10	Unknown	1.407(2)
13	C6	H6A	Unknown	0.949(1)
14	C6	C7	Unknown	1.379(2)
15	C7	H7A	Unknown	0.950(1)
16	C7	C8	Unknown	1.393(2)
17	C8	H8A	Unknown	0.950(1)
18	C8	C9	Unknown	1.390(2)
19	C9	C10	Unknown	1.408(2)
20	C9	O2	Unknown	1.369(2)
21	C10	O3	Unknown	1.380(2)
22	C11	H11A	Unknown	0.980(2)
23	C11	H11B	Unknown	0.980(1)
24	C11	H11C	Unknown	0.981(1)
25	C12	H12A	Unknown	0.980(2)
26	C12	H12B	Unknown	0.980(1)
27	C12	H12C	Unknown	0.980(1)
28	C12	N2	Unknown	1.458(2)
29	C13	H13A	Unknown	0.980(1)
30	C13	H13B	Unknown	0.980(1)
31	C13	H13C	Unknown	0.980(1)
32	C13	O2	Unknown	1.435(2)
33	C14	H14A	Unknown	0.980(2)
34	C14	H14B	Unknown	0.979(2)
35	C14	H14C	Unknown	0.980(2)
36	C14	O3	Unknown	1.432(2)

2,4-Me/Me AMI Chromophore

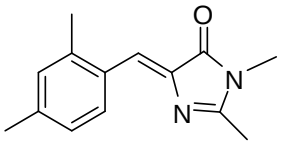

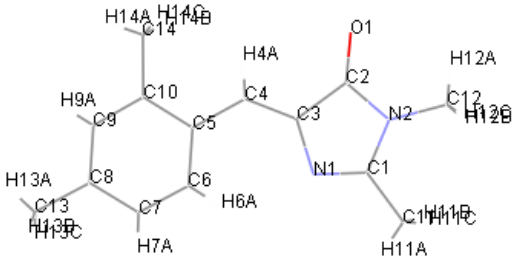

cell_length_a	27.8365(7)
cell_length_b	27.8365(7)
cell_length_c	8.2402(5)
cell_angle_alpha	90.00
cell_angle_beta	90.00
cell_angle_gamma	120.00
cell_volume	5529.6(4)
cell_formula_units_Z	18
cell_measurement_temperature	173(2)
cell_measurement_reflns_used	4505
cell_measurement_theta_min	3.18
cell_measurement_theta_max	65.54

exptl_crystal_description	rod
exptl_crystal_colour	colorless
exptl_crystal_size_max	0.41
exptl_crystal_size_mid	0.15
exptl_crystal_size_min	0.14
exptl_crystal_density_meas	?
exptl_crystal_density_diffrn	1.234
exptl_crystal_density_method	'not measured'
exptl_crystal_F_000	2196
exptl_absorpt_coefficient_mu	0.625
exptl_absorpt_correction_type	multi-scan
exptl_absorpt_correction_T_min	0.7838
exptl_absorpt_correction_T_max	0.9176
exptl_absorpt_process_details	SADABS

Spatial Coordinates of 2,3-OMe/Me

C1	C	0.70223(18)	0.38143(17)	0.04495(5)
C2	C	0.46737(18)	0.46825(16)	0.09518(5)
C3	C	0.62756(17)	0.59036(16)	0.09871(5)
C4	C	0.62572(17)	0.73869(16)	0.12816(5)
H4A	H	0.5153	0.7618	0.1462
C5	C	0.77205(17)	0.86844(16)	0.13582(5)
C6	C	0.95567(18)	0.84070(17)	0.12127(6)
H6A	H	0.9877	0.7351	0.1052
C7	C	1.08863(18)	0.96676(17)	0.13036(6)
H7A	H	1.2126	0.9453	0.1214
C8	C	1.04561(17)	1.12474(17)	0.15240(5)
H8A	H	1.1383	1.2110	0.1572
C9	C	0.86583(17)	1.15502(16)	0.16725(5)
C10	C	0.72992(17)	1.02594(16)	0.16002(5)
C11	C	0.8052(2)	0.26679(19)	0.00827(6)
H11A	H	0.9272	0.3167	0.0028
H11B	H	0.7322	0.2508	-0.0304
H11C	H	0.8244	0.1571	0.0282
C12	C	0.4113(2)	0.19228(17)	0.04154(6)
H12A	H	0.2920	0.1983	0.0586
H12B	H	0.4789	0.0896	0.0555
H12C	H	0.3868	0.1894	-0.0017
C13	C	0.95038(19)	1.42981(17)	0.20406(6)
H13A	H	0.8937	1.5316	0.2191
H13B	H	1.0106	1.4587	0.1688
H13C	H	1.0444	1.3844	0.2346
C14	C	0.5370(2)	1.0677(2)	0.23624(6)
H14A	H	0.4063	1.0890	0.2428
H14B	H	0.6160	1.1608	0.2530
H14C	H	0.5793	0.9613	0.2555
N1	N	0.76716(15)	0.52530(14)	0.06632(5)
N2	N	0.52462(15)	0.34052(14)	0.05963(5)
O1	O	0.31945(13)	0.47427(13)	0.11679(4)
O2	O	0.80757(12)	1.30513(11)	0.18904(4)
O3	O	0.55066(12)	1.05584(12)	0.17407(4)

Bond Angles of 2,3-OMe/Me

Number	Atom1	Atom2	Atom3	Angle
1	C11	C1	N1	124.3(1)
2	C11	C1	N2	121.4(1)
3	N1	C1	N2	114.3(1)
4	C3	C2	N2	103.0(1)
5	C3	C2	O1	130.6(1)

6	N2	C2	O1	126.3(1)
7	C2	C3	C4	122.4(1)
8	C2	C3	N1	108.9(1)
9	C4	C3	N1	128.6(1)
10	C3	C4	H4A	115.9(1)
11	C3	C4	C5	128.3(1)
12	H4A	C4	C5	115.8(1)
13	C4	C5	C6	122.6(1)
14	C4	C5	C10	118.9(1)
15	C6	C5	C10	118.4(1)
16	C5	C6	H6A	120.0(1)
17	C5	C6	C7	120.1(1)
18	H6A	C6	C7	120.0(1)
19	C6	C7	H7A	119.2(1)
20	C6	C7	C8	121.6(1)
21	H7A	C7	C8	119.2(1)
22	C7	C8	H8A	120.3(1)
23	C7	C8	C9	119.4(1)
24	H8A	C8	C9	120.3(1)
25	C8	C9	C10	119.7(1)
26	C8	C9	O2	124.5(1)
27	C10	C9	O2	115.8(1)
28	C5	C10	C9	120.7(1)
29	C5	C10	O3	119.3(1)
30	C9	C10	O3	120.0(1)
31	C1	C11	H11A	109.5(1)
32	C1	C11	H11B	109.5(1)
33	C1	C11	H11C	109.4(1)
34	H11A	C11	H11B	109.4(1)
35	H11A	C11	H11C	109.5(1)
36	H11B	C11	H11C	109.5(1)
37	H12A	C12	H12B	109.5(1)
38	H12A	C12	H12C	109.4(1)
39	H12A	C12	N2	109.5(1)
40	H12B	C12	H12C	109.4(1)
41	H12B	C12	N2	109.5(1)
42	H12C	C12	N2	109.5(1)
43	H13A	C13	H13B	109.4(1)
44	H13A	C13	H13C	109.4(1)
45	H13A	C13	O2	109.5(1)
46	H13B	C13	H13C	109.5(1)
47	H13B	C13	O2	109.5(1)
48	H13C	C13	O2	109.5(1)
49	H14A	C14	H14B	109.5(1)
50	H14A	C14	H14C	109.4(1)
51	H14A	C14	O3	109.5(1)

52	H14B	C14	H14C	109.5(1)
53	H14B	C14	O3	109.4(1)
54	H14C	C14	O3	109.5(1)
55	C1	N1	C3	105.6(1)
56	C1	N2	C2	108.1(1)
57	C1	N2	C12	128.0(1)
58	C2	N2	C12	123.9(1)
59	C9	O2	C13	116.3(1)
60	C10	O3	C14	114.1(1)

Bond Lengths of 2,3-OMe/Me

Number	Atom1	Atom2	Type	Length
1	C1	C11	Unknown	1.483(2)
2	C1	N1	Unknown	1.302(2)
3	C1	N2	Unknown	1.391(2)
4	C2	C3	Unknown	1.496(2)
5	C2	N2	Unknown	1.384(2)
6	C2	O1	Unknown	1.219(2)
7	C3	C4	Unknown	1.351(2)
8	C3	N1	Unknown	1.405(2)
9	C4	H4A	Unknown	0.950(1)
10	C4	C5	Unknown	1.464(2)
11	C5	C6	Unknown	1.411(2)
12	C5	C10	Unknown	1.407(2)
13	C6	H6A	Unknown	0.949(1)
14	C6	C7	Unknown	1.379(2)
15	C7	H7A	Unknown	0.950(1)
16	C7	C8	Unknown	1.393(2)
17	C8	H8A	Unknown	0.950(1)
18	C8	C9	Unknown	1.390(2)
19	C9	C10	Unknown	1.408(2)
20	C9	O2	Unknown	1.369(2)
21	C10	O3	Unknown	1.380(2)

2,5-Me/Me AMI Chromophore

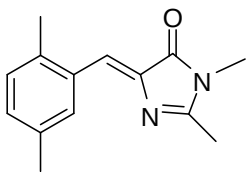

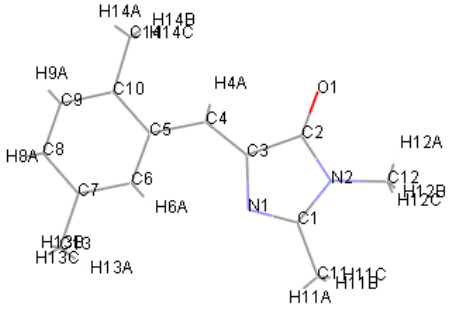

cell_length_a	7.4859(7)
cell_length_b	21.6997(17)
cell_length_c	8.0387(7)
cell_angle_alpha	90.00
cell_angle_beta	110.755(5)
cell_angle_gamma	90.00
cell_volume	1221.08(18)
cell_formula_units_Z	4
cell_measurement_temperature	173(2)
cell_measurement_reflns_used	3594
cell_measurement_theta_min	4.07
cell_measurement_theta_max	65.33

exptl_crystal_description	plate
exptl_crystal_colour	colourless
exptl_crystal_size_max	0.31
exptl_crystal_size_mid	0.26
exptl_crystal_size_min	0.15
exptl_crystal_density_meas	?
exptl_crystal_density_diffrn	1.242
exptl_crystal_density_method	'not measured'
exptl_crystal_F_000	488
exptl_absorpt_coefficient_mu	0.629
exptl_absorpt_correction_type	multi-scan
exptl_absorpt_correction_T_min	0.8290
exptl_absorpt_correction_T_max	0.9116

exptl_absorpt_process_details SADABS

diffrn_ambient_temperature 173(2)
diffrn_radiation_wavelength 1.54178
diffrn_radiation_type CuK\a
diffrn_radiation_source 'fine-focus sealed tube'
diffrn_radiation_monochromator graphite
diffrn_measurement_device_type 'CCD area detector'
diffrn_measurement_method 'phi and omega scans'
diffrn_detector_area_resol_mean ?
diffrn_reflns_number 9487
diffrn_reflns_av_R_equivalents 0.0344
diffrn_reflns_av_sigmaI/netI 0.0265
diffrn_reflns_limit_h_min -8
diffrn_reflns_limit_h_max 8
diffrn_reflns_limit_k_min -25
diffrn_reflns_limit_k_max 24
diffrn_reflns_limit_l_min -9
diffrn_reflns_limit_l_max 9
diffrn_reflns_theta_min 4.07
diffrn_reflns_theta_max 65.76
reflns_number_total 2000
reflns_number_gt 1718
reflns_threshold_expression >2sigma(I)

Spatial Coordinates of 2,5-Me/Me

C1	C	0.3109(3)	0.46573(9)	0.2565(3)
C2	C	0.6310(3)	0.45991(9)	0.3567(3)
C3	C	0.5555(3)	0.51468(9)	0.2399(2)
C4	C	0.6749(3)	0.55591(9)	0.2084(2)
H4A	H	0.8070	0.5467	0.2623
C5	C	0.6307(3)	0.61272(8)	0.1035(2)
C6	C	0.4432(3)	0.62977(9)	0.0040(3)
H6A	H	0.3414	0.6040	0.0062
C7	C	0.4003(3)	0.68335(9)	-0.0983(3)
C8	C	0.5503(3)	0.72121(9)	-0.0963(3)
H8A	H	0.5246	0.7585	-0.1623
C9	C	0.7377(3)	0.70505(9)	0.0012(3)
H9A	H	0.8380	0.7316	-0.0005
C10	C	0.7831(3)	0.65125(9)	0.1013(3)
C11	C	0.1143(3)	0.44677(11)	0.2348(3)
H11A	H	0.0231	0.4760	0.1562
H11B	H	0.0996	0.4464	0.3512
H11C	H	0.0897	0.4054	0.1825
C12	C	0.4690(4)	0.37499(9)	0.4587(3)
H12A	H	0.6013	0.3621	0.5216

H12B	H	0.4011	0.3428	0.3746
H12C	H	0.4056	0.3818	0.5449
C13	C	0.1970(4)	0.69889(11)	-0.2107(4)
H13A	H	0.1113	0.6671	-0.1949
H13B	H	0.1846	0.7007	-0.3362
H13C	H	0.1630	0.7390	-0.1742
C14	C	0.9896(4)	0.63544(11)	0.2009(4)
H14A	H	1.0714	0.6678	0.1816
H14B	H	1.0199	0.5960	0.1576
H14C	H	1.0117	0.6322	0.3283
N1	N	0.3552(3)	0.51433(7)	0.1835(2)
N2	N	0.4675(3)	0.43194(7)	0.3622(2)
O1	O	0.7948(2)	0.44221(7)	0.4315(2)

Bond Lengths of 2,5-Me/Me

Number	Atom1	Atom2	Atom3	Angle
1	C1	C11	Unknown	1.478(3)
2	C1	N1	Unknown	1.306(3)
3	C1	N2	Unknown	1.388(3)
4	C2	C3	Unknown	1.496(3)
5	C2	N2	Unknown	1.381(3)
6	C2	O1	Unknown	1.221(2)
7	C3	C4	Unknown	1.351(3)
8	C3	N1	Unknown	1.404(3)
9	C4	H4A	Unknown	0.950(2)
10	C4	C5	Unknown	1.464(2)
11	C5	C6	Unknown	1.397(3)
12	C5	C10	Unknown	1.420(3)
13	C6	H6A	Unknown	0.950(2)
14	C6	C7	Unknown	1.394(3)
15	C7	C8	Unknown	1.387(3)
16	C7	C13	Unknown	1.507(3)
17	C8	H8A	Unknown	0.949(2)
18	C8	C9	Unknown	1.388(3)
19	C9	H9A	Unknown	0.950(2)
20	C9	C10	Unknown	1.390(3)
21	C10	C14	Unknown	1.507(3)
22	C11	H11A	Unknown	0.981(2)
23	C11	H11B	Unknown	0.980(3)
24	C11	H11C	Unknown	0.981(2)
25	C12	H12A	Unknown	0.980(3)
26	C12	H12B	Unknown	0.980(2)
27	C12	H12C	Unknown	0.980(3)
28	C12	N2	Unknown	1.457(3)
29	C13	H13A	Unknown	0.980(3)
30	C13	H13B	Unknown	0.981(3)

31	C13	H13C	Unknown	0.980(3)
32	C14	H14A	Unknown	0.980(3)
33	C14	H14B	Unknown	0.980(3)
34	C14	H14C	Unknown	0.980(3)

Bond Angles of 2,5-Me/Me

Number	Atom1	Atom2		Type	Length
1	C11	C1		N1	124.9(2)
2	C11	C1	N2	121.0(2)	
3	N1	C1	N2	114.1(2)	
4	C3	C2	N2	103.1(2)	
5	C3	C2	O1	130.5(2)	
6	N2	C2	O1	126.4(2)	
7	C2	C3	C4	121.1(2)	
8	C2	C3	N1	108.7(2)	
9	C4	C3	N1	130.2(2)	
10	C3	C4	H4A	115.2(2)	
11	C3	C4	C5	129.5(2)	
12	H4A	C4	C5	115.2(2)	
13	C4	C5	C6	121.9(2)	
14	C4	C5	C10	119.0(2)	
15	C6	C5	C10	119.1(2)	
16	C5	C6	H6A	118.9(2)	
17	C5	C6	C7	122.2(2)	
18	H6A	C6	C7	118.9(2)	
19	C6	C7	C8	118.1(2)	
20	C6	C7	C13	120.8(2)	
21	C8	C7	C13	121.1(2)	
22	C7	C8	H8A	119.7(2)	
23	C7	C8	C9	120.6(2)	
24	H8A	C8	C9	119.7(2)	
25	C8	C9	H9A	119.0(2)	
26	C8	C9	C10	122.0(2)	
27	H9A	C9	C10	119.0(2)	
28	C5	C10	C9	118.0(2)	
29	C5	C10	C14	122.5(2)	
30	C9	C10	C14	119.5(2)	
31	C1	C11	H11A	109.4(2)	
32	C1	C11	H11B	109.5(2)	
33	C1	C11	H11C	109.5(2)	
34	H11A	C11	H11B	109.4(2)	
35	H11A	C11	H11C	109.5(2)	
36	H11B	C11	H11C	109.5(2)	
37	H12A	C12	H12B	109.6(2)	
38	H12A	C12	H12C	109.4(2)	
39	H12A	C12	N2	109.4(2)	

40	H12B	C12	H12C	109.4(2)
41	H12B	C12	N2	109.5(2)
42	H12C	C12	N2	109.5(2)
43	C7	C13	H13A	109.4(2)
44	C7	C13	H13B	109.5(2)
45	C7	C13	H13C	109.5(2)
46	H13A	C13	H13B	109.5(3)
47	H13A	C13	H13C	109.6(3)
48	H13B	C13	H13C	109.4(3)
49	C10	C14	H14A	109.5(2)
50	C10	C14	H14B	109.4(2)
51	C10	C14	H14C	109.4(2)
52	H14A	C14	H14B	109.5(3)
53	H14A	C14	H14C	109.5(3)
54	H14B	C14H14C		109.5(3)
55	C1	N1	C3	105.8(2)
56	C1	N2	C2	108.3(2)
57	C1	N2	C12	128.3(2)
58	C2	N2	C12	123.4(2)

2-naphthyl/Me AMI Chromophore

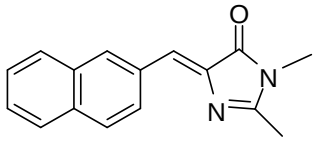

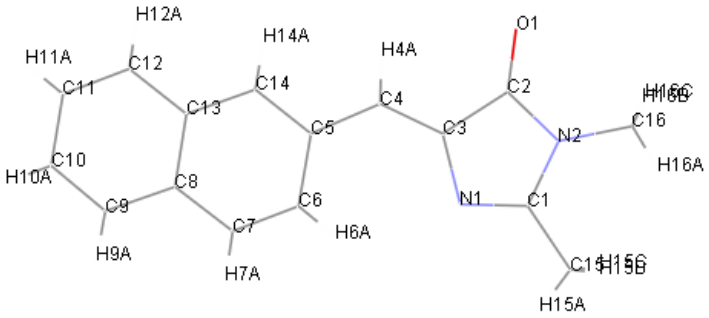

cell_length_a	7.6089(3)
cell_length_b	7.1163(3)
cell_length_c	22.9767(8)
cell_angle_alpha	90.00
cell_angle_beta	98.190(2)
cell_angle_gamma	90.00
cell_volume	1231.44(8)
cell_formula_units_Z	4
cell_measurement_temperature	173(2)
cell_measurement_reflns_used	2443
cell_measurement_theta_min	5.92
cell_measurement_theta_max	65.36

exptl_crystal_description	rod
exptl_crystal_colour	colourless
exptl_crystal_size_max	0.24
exptl_crystal_size_mid	0.11
exptl_crystal_size_min	0.09
exptl_crystal_density_meas	?
exptl_crystal_density_diffrn	1.350
exptl_crystal_density_method	'not measured'
exptl_crystal_F_000	528
exptl_absorpt_coefficient_mu	0.681
exptl_absorpt_correction_type	multi-scan
exptl_absorpt_correction_T_min	0.8536
exptl_absorpt_correction_T_max	0.9412

exptl_absorpt_process_details SADABS

diffrn_ambient_temperature 173(2)
diffrn_radiation_wavelength 1.54178
diffrn_radiation_type CuK\a
diffrn_radiation_source 'fine-focus sealed tube'
diffrn_radiation_monochromator graphite
diffrn_measurement_device_type 'CCD area detector'
diffrn_measurement_method 'phi and omega scans'
diffrn_detector_area_resol_mean ?
diffrn_standards_number ?
diffrn_standards_interval_count ?
diffrn_standards_interval_time ?
diffrn_standards_decay_% ?
diffrn_reflns_number 8270
diffrn_reflns_av_R_equivalents 0.0448
diffrn_reflns_av_sigmaI/netI 0.0861
diffrn_reflns_limit_h_min -8
diffrn_reflns_limit_h_max 9
diffrn_reflns_limit_k_min -6
diffrn_reflns_limit_k_max 8
diffrn_reflns_limit_l_min -27
diffrn_reflns_limit_l_max 27
diffrn_reflns_theta_min 3.89
diffrn_reflns_theta_max 66.28
reflns_number_total 2069
reflns_number_gt 1524
reflns_threshold_expression >2sigma(I)

Spatial Coordinates of 2-naphthyl/Me

C1	C	0.6086(3)	0.8372(3)	1.09078(9)
C2	C	0.6902(3)	0.5570(3)	1.12979(9)
C3	C	0.7069(3)	0.5690(3)	1.06587(9)
C4	C	0.7665(3)	0.4244(3)	1.03695(9)
H4A	H	0.7963	0.3159	1.0604
C5	C	0.7934(3)	0.4047(3)	0.97562(9)
C6	C	0.7646(3)	0.5537(3)	0.93418(10)
H6A	H	0.7237	0.6720	0.9460.
C7	C	0.7953(3)	0.5284(4)	0.87775(10)
H7A	H	0.7745	0.6297	0.8507
C8	C	0.8570(3)	0.3561(4)	0.85843(9)
C9	C	0.8934(3)	0.3251(4)	0.79993(10)
H9A	H	0.8763	0.4245	0.7721
C10	C	0.9523(3)	0.1546(4)	0.78340(10)
H10A	H	0.9766	0.1369	0.7443

C11	C	0.9772(3)	0.0056(4)	0.82366(11)
H11A	H	1.0175	-0.1127	0.8117
C12	C	0.9438(3)	0.0300(4)	0.88029(10)
H12A	H	0.9609	-0.0720	0.9072
C13	C	0.8843(3)	0.2043(4)	0.89907(10)
C14	C	0.8503(3)	0.2344(3)	0.95732(9)
H14A	H	0.8674	0.1335	0.9846. .
C15	C	0.5399(3)	1.0323(3)	1.09047(10)
H15A	H	0.5334	1.0850	1.0508
H15B	H	0.6197	1.1091	1.1181
H15C	H	0.4211	1.0317	1.1023
C16	C	0.5948(3)	0.7918(4)	1.20005(10)
H16A	H	0.5520	0.9219	1.1978
H16B	H	0.7050	0.7841	1.2278
H16C	H	0.5048	0.7103	1.2135
N1	N	0.6531(2)	0.7494(3)	1.04531(8)
N2	N	0.6283(2)	0.7310(3)	1.14215(8)
O1	O	0.7219(2)	0.4263(2)	1.16457(6)

Bond Angles of 2-naphthyl/Me

Number	Atom1	Atom2	Atom3	Angle
1	C15	C1	N1	125.2(2)
2	C15	C1	N2	120.5(2)
3	N1	C1	N2	114.3(2)
4	C3	C2	N2	103.4(2)
5	C3	C2	O1	130.3(2)
6	N2	C2	O1	126.3(2)
7	C2	C3	C4	121.7(2)
8	C2	C3	N1	108.7(2)
9	C4	C3	N1	129.6(2)
10	C3	C4	H4A	114.4(2)
11	C3	C4	C5	131.1(2)
12	H4A	C4	C5	114.5(2)
13	C4	C5	C6	123.1(2)
14	C4	C5	C14	118.3(2)
15	C6	C5	C14	118.6(2)
16	C5	C6	H6A	119.7(2)
17	C5	C6	C7	120.6(2)
18	H6A	C6	C7	119.8(2)
19	C6	C7	H7A	119.2(2)
20	C6	C7	C8	121.7(2)
21	H7A	C7	C8	119.1(2)
22	C7	C8	C9	123.4(2)
23	C7	C8	C13	118.6(2)
24	C9	C8	C13	118.1(2)
25	C8	C9	H9A	119.5(2)

26	C8	C9	C10	121.0(2)
27	H9A	C9	C10	119.5(2)
28	C9	C10	H10A	119.7(2)
29	C9	C10	C11	120.5(2)
30	H10A	C10	C11	119.8(2)
31	C10	C11	H11A	119.9(2)
32	C10	C11	C12	120.3(2)
33	H11A	C11	C12	119.8(2)
34	C11	C12	H12A	119.6(2)
35	C11	C12	C13	120.9(2)
36	H12A	C12	C13	119.6(2)
37	C8	C13	C12	119.4(2)
38	C8	C13	C14	118.4(2)
39	C12	C13	C14	122.2(2)
40	C5	C14	C13	122.1(2)
41	C5	C14	H14A	119.0(2)
42	C13	C14	H14A	118.9(2)
43	C1	C15	H15A	109.5(2)
44	C1	C15	H15B	109.5(2)
45	C1	C15	H15C	109.4(2)
46	H15A	C15	H15B	109.5(2)
47	H15A	C15	H15C	109.5(2)
48	H15B	C15	H15C	109.5(2)
49	H16A	C16	H16B	109.5(2)
50	H16A	C16	H16C	109.5(2)
51	H16A	C16	N2	109.4(2)
52	H16B	C16	H16C	109.5(2)
53	H16B	C16	N2	109.5(2)
54	H16C	C16	N2	109.5(2)
55	C1	N1	C3	105.3(2)
56	C1	N2	C2	108.3(2)
57	C1	N2	C16	127.0(2)
58	C2	N2	C16	124.7(2)

Bond Lengths of 2,3-OMe/Me

Number	Atom1	Atom2	Type	Length
1	C1	C15	Unknown	1.483(3)
2	C1	N1	Unknown	1.303(3)
3	C1	N2	Unknown	1.392(3)
4	C2	C3	Unknown	1.495(3)
5	C2	N2	Unknown	1.369(3)
6	C2	O1	Unknown	1.228(3)
7	C3	C4	Unknown	1.339(3)
8	C3	N1	Unknown	1.408(3)
9	C4	H4A	Unknown	0.950(2)
10	C4	C5	Unknown	1.459(3)

11	C5	C6	Unknown	1.421(3)
12	C5	C14	Unknown	1.373(3)
13	C6	H6A	Unknown	0.950(2)
14	C6	C7	Unknown	1.362(3)
15	C7	H7A	Unknown	0.950(3)
16	C7	C8	Unknown	1.407(4)
17	C8	C9	Unknown	1.428(3)
18	C8	C13	Unknown	1.424(4)
19	C9	H9A	Unknown	0.950(3)
20	C9	C10	Unknown	1.366(4)
21	C10	H10A	Unknown	0.951(2)
22	C10	C11	Unknown	1.402(4)
23	C11	H11A	Unknown	0.950(3)
24	C11	C12	Unknown	1.372(4)
25	C12	H12A	Unknown	0.950(3)
26	C12	C13	Unknown	1.409(4)
27	C13	C14	Unknown	1.415(3)
28	C14	H14A	Unknown	0.950(2)
29	C15	H15A	Unknown	0.980(2)
30	C15	H15B	Unknown	0.980(2)
31	C15	H15C	Unknown	0.980(2)
32	C16	H16A	Unknown	0.980(3)
33	C16	H16B	Unknown	0.980(2)
34	C16	H16C	Unknown	0.980(3)
35	C16	N2	Unknown	1.456(3)

2-pyridyl/Me AMI Chromophore

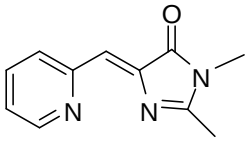

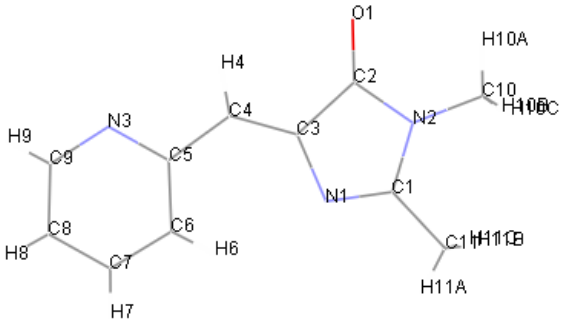

cell_length_a	16.109(4)
cell_length_b	17.406(5)
cell_length_c	7.1321(19)
cell_angle_alpha	90.00
cell_angle_beta	90.00
cell_angle_gamma	90.00
cell_volume	1999.8(9)
cell_formula_units_Z	8
cell_measurement_temperature	172(2)
cell_measurement_reflns_used	6737
cell_measurement_theta_min	2.34
cell_measurement_theta_max	29.15

exptl_crystal_description	needle
exptl_crystal_colour	yellow
exptl_crystal_size_max	0.37
exptl_crystal_size_mid	0.14
exptl_crystal_size_min	0.12
exptl_crystal_density_meas	?
exptl_crystal_density_diffrn	1.337
exptl_crystal_density_method	'not measured'
exptl_crystal_F_000	848
exptl_absorpt_coefficient_mu	0.090
exptl_absorpt_correction_type	multi-scan
exptl_absorpt_correction_T_min	0.9675
exptl_absorpt_correction_T_max	0.9893
exptl_absorpt_process_details	SADABS

diffrn_ambient_temperature 172(2)
diffrn_radiation_wavelength 0.71073
diffrn_radiation_type MoK\a
diffrn_radiation_source 'fine-focus sealed tube'
diffrn_radiation_monochromator graphite
diffrn_measurement_device_type 'CCD area detector'
diffrn_measurement_method 'phi and omega scans'
diffrn_detector_area_resol_mean ?
diffrn_reflns_number 35200
diffrn_reflns_av_R_equivalents 0.0490
diffrn_reflns_av_sigmaI/netI 0.0257
diffrn_reflns_limit_h_min -22
diffrn_reflns_limit_h_max 23
diffrn_reflns_limit_k_min -23
diffrn_reflns_limit_k_max 23
diffrn_reflns_limit_l_min -9
diffrn_reflns_limit_l_max 9
diffrn_reflns_theta_min 1.72
diffrn_reflns_theta_max 30.55
reflns_number_total 2959
reflns_number_gt 2221
reflns_threshold_expression >2sigma(I)

Spatial Coordinates of 2-pyridyl/Me

C1	C	-0.01029(7) 0.32163(7) 0.61845(17)
C2	C	-0.07978(7) 0.21371(7) 0.68824(18)
C3	C	0.00561(7) 0.19872(6) 0.61530(16)
C4	C	0.03445(7) 0.12693(7) 0.58573(17)
H4	H	-0.0035 0.0865 0.6120.
C5	C	0.11619(7) 0.10308(6) 0.51871(17).
C6	C	0.18355(8) 0.15341(7) 0.50145(18).
H6	H	0.1770 0.2066 0.5273
C7	C	0.25997(8) 0.12449(7) 0.4460(2).
H7	H	0.3070 0.1572 0.4362
C8	C	0.26630(8) 0.04704(7) 0.40531(19).
H8	H	0.3178 0.0255 0.3670.
C9	C	0.19630(7) 0.00137(7) 0.42143(19).
H9	H	0.2010 -0.0514 0.3896
C10	C	-0.15946(9) 0.33647(8) 0.7319(2). .
H10A	H	-0.2027 0.3013 0.7764
H10B	H	-0.1792 0.3636 0.6201.
H10C	H	-0.1465 0.3738 0.8304.
C11	C	0.00107(8) 0.40579(7) 0.5925(2).
H11A	H	0.0570 0.4159 0.5442.
H11B	H	-0.0061 0.4319 0.7131.
H11C	H	-0.0402 0.4250 0.5030.

N1	N	0.04459(6) 0.26938(5) 0.57851(15)
N2	N	-0.08510(6) 0.29293(6) 0.68555(16)
N3	N	0.12247(6) 0.02737(6) 0.47928(16).
O1	O	-0.13382(5) 0.16958(5) 0.74147(14)

Bond Lengths of 2-pyridyl/Me

Number	Atom1	Atom2	Atom3	Angle
1	C1	C11	Unknown	1.488(2)
2	C1	N1	Unknown	1.300(2)
3	C1	N2	Unknown	1.390(2)
4	C2	C3	Unknown	1.494(2)
5	C2	N2	Unknown	1.382(2)
6	C2	O1	Unknown	1.221(1)
7	C3	C4	Unknown	1.350(2)
8	C3	N1	Unknown	1.406(1)
9	C4	H4	Unknown	0.951(1)
10	C4	C5	Unknown	1.461(2)
11	C5	C6	Unknown	1.400(2)
12	C5	N3	Unknown	1.351(2)
13	C6	H6	Unknown	0.950(1)
14	C6	C7	Unknown	1.388(2)
15	C7	H7	Unknown	0.950(1)
16	C7	C8	Unknown	1.383(2)
17	C8	H8	Unknown	0.951(1)
18	C8	C9	Unknown	1.384(2)
19	C9	H9	Unknown	0.949(1)
20	C9	N3	Unknown	1.338(2)
21	C10	H10A	Unknown	0.980(1)
22	C10	H10B	Unknown	0.980(1)
23	C10	H10C	Unknown	0.979(1)
24	C10	N2	Unknown	1.456(2)
25	C11	H11A	Unknown	0.981(1)
26	C11	H11B	Unknown	0.980(1)
27	C11	H11C	Unknown	0.980(1)

Bond Angles of 2-pyridyl/Me

Number	Atom1	Atom2	Type	Length
1	C11	C1	N1	125.3(1)
2	C11	C1	N2	120.2(1)
3	N1	C1	N2	114.4(1)
4	C3	C2	N2	103.1(1)
5	C3	C2	O1	130.9(1)
6	N2	C2	O1	126.0(1)
7	C2	C3	C4	122.2(1)
8	C2	C3	N1	108.88(9)

9	C4	C3	N1	128.8(1)
10	C3	C4	H4	115.7(1)
11	C3	C4	C5	128.6(1)
12	H4	C4	C5	115.7(1)
13	C4	C5	C6	123.3(1)
14	C4	C5	N3	114.4(1)
15	C6	C5	N3	122.3(1)
16	C5	C6	H6	120.4(1)
17	C5	C6	C7	119.1(1)
18	H6	C6	C7	120.5(1)
19	C6	C7	H7	120.7(1)
20	C6	C7	C8	118.6(1)
21	H7	C7	C8	120.7(1)
22	C7	C8	H8	120.6(1)
23	C7	C8	C9	118.8(1)
24	H8	C8	C9	120.5(1)
25	C8	C9	H9	118.1(1)
26	C8	C9	N3	123.7(1)
27	H9	C9	N3	118.2(1)
28	H10A	C10	H10B	109.5(1)
29	H10A	C10	H10C	109.5(1)
30	H10A	C10	N2	109.5(1)
31	H10B	C10	H10C	109.5(1)
32	H10B	C10	N2	109.5(1)
33	H10C	C10	N2	109.4(1)
34	C1	C11	H11A	109.5(1)
35	C1	C11	H11B	109.5(1)
36	C1	C11	H11C	109.5(1)
37	H11A	C11	H11B	109.5(1)
38	H11A	C11	H11C	109.5(1)
39	H11B	C11	H11C	109.5(1)
40	C1	N1	C3	105.5(1)
41	C1	N2	C2	108.0(1)
42	C1	N2	C10	127.2(1)
43	C2	N2	C10	124.6(1)
44	C5	N3	C9	117.4(1)

3,4,5-OMe/Me AMI Chromophore

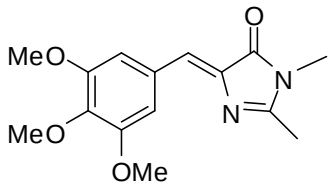

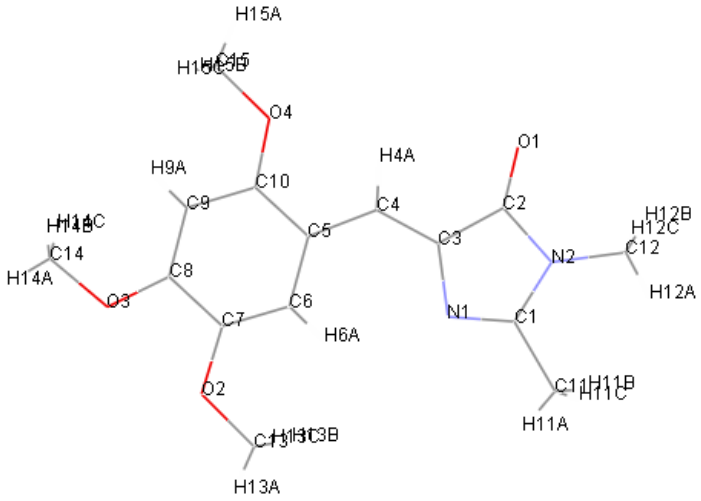

cell_length_a	7.6811(13)
cell_length_b	8.0170(12)
cell_length_c	23.929(4)
cell_angle_alpha	90.00
cell_angle_beta	90.00
cell_angle_gamma	90.00
cell_volume	1473.5(4)
cell_formula_units_Z	4
cell_measurement_temperature	173(2)
cell_measurement_reflns_used	821
cell_measurement_theta_min	3.69
cell_measurement_theta_max	44.87

exptl_crystal_description	rod
exptl_crystal_colour	yellow
exptl_crystal_size_max	0.31
exptl_crystal_size_mid	0.07
exptl_crystal_size_min	0.06
exptl_crystal_density_meas	?
exptl_crystal_density_diffrn	1.309
exptl_crystal_density_method	'not measured'
exptl_crystal_F_000	616

exptl_absorpt_coefficient_mu 0.793
exptl_absorpt_correction_type multi-scan
exptl_absorpt_correction_T_min 0.7911
exptl_absorpt_correction_T_max 0.9517
exptl_absorpt_process_details ?

diffrn_ambient_temperature 173(2)
diffrn_radiation_wavelength 1.54178
diffrn_radiation_type CuK\a
diffrn_radiation_source 'fine-focus sealed tube'
diffrn_radiation_monochromator graphite
diffrn_measurement_device_type 'CCD area detector'
diffrn_measurement_method 'phi and omega scans'
diffrn_detector_area_resol_mean ?
diffrn_reflns_number 6727
diffrn_reflns_av_R_equivalents 0.1040
diffrn_reflns_av_sigmaI/netI 0.1439
diffrn_reflns_limit_h_min -8
diffrn_reflns_limit_h_max 6
diffrn_reflns_limit_k_min -9
diffrn_reflns_limit_k_max 7
diffrn_reflns_limit_l_min -28
diffrn_reflns_limit_l_max 25
diffrn_reflns_theta_min 3.69
diffrn_reflns_theta_max 67.53
reflns_number_total 2077
reflns_number_gt 869
reflns_threshold_expression >2sigma(I)

Spatial Coordinates of 3,4,5-OMe/Me

C1	C	1.078(2) 0.2955(15) 0.0778(6)
C2	C	1.0355(18) 0.2198(15) 0.1661(7)
C3	C	0.8955(17) 0.3211(14) 0.1432(5).
C4	C	0.7563(18) 0.3694(15) 0.1739(5)
H4A	H	0.7568 0.3322 0.2116
C5	C	0.6083(18) 0.4678(14) 0.1583(5).
C6	C	0.5832(18) 0.5511(14) 0.1071(4)
H6A	H	0.6699 0.5422 0.0790.
C7	C	0.4379(19) 0.6443(14) 0.0968(5)
C8	C	0.2966(19) 0.6483(16) 0.1349(5).
C9	C	0.3215(17) 0.5703(14) 0.1859(4)
H9A	H	0.2334 0.5781 0.2137
C10	C	0.474(2) 0.4797(15) 0.1976(5)
C11	C	1.1809(16) 0.3044(16) 0.0216(4)
H11A	H	1.1146 0.3706 -0.0055.
H11B	H	1.1980 0.1915 0.0069

H11C	H	1.2943 0.3569 0.0280.
C12	C	1.3210(16) 0.1216(14) 0.1248(5)
H12A	H	1.3801 0.1277 0.0886
H12B	H	1.3022 0.0044 0.1348
H12C	H	1.3932 0.1752 0.1534
C13	C	0.5498(15) 0.7289(18) 0.0070(5)
H13A	H	0.5145 0.7912 -0.0263.
H13B	H	0.5789 0.6140 -0.0034
H13C	H	0.6519 0.7823 0.0238 0.137.
C14	C	0.0233(16) 0.7646(15) 0.1560(4)
H14A	H	-0.0667 0.8359 0.1396 0.119
H14B	H	0.0672 0.8162 0.1904 0.119
H14C	H	-0.0265 0.6551 0.1648
C15	C	0.3421(17) 0.4006(15) 0.2879(5)
H15A	H	0.3771 0.3417 0.3220
H15B	H	0.2433 0.3428 0.2707
H15C	H	0.3082 0.5151 0.2973
N1	N	0.9316(16) 0.3700(12) 0.0865(4)
N2	N	1.1523(14) 0.2076(12) 0.1212(5)
O1	O	1.0578(11) 0.1555(10) 0.2117(4)
O2	O	0.4080(11) 0.7276(10) 0.0471(3)
O3	O	0.1662(11) 0.7444(10) 0.1163(3)
O4	O	0.4887(12) 0.4039(10) 0.2485(3).

Bond Angles of 3,4,5-OMe/Me

Number	Atom1	Atom2	Atom3	Angle
1	C11	C1	N1	124(1)
2	C11	C1	N2	118(1)
3	N1	C1	N2	118(1)
4	C3	C2	N2	103(1)
5	C3	C2	O1	133(1)
6	N2	C2	O1	124(1)
7	C2	C3	C4	123(1)
8	C2	C3	N1	111(1)
9	C4	C3	N1	126(1)
10	C3	C4	H4A	115(1)
11	C3	C4	C5	130(1)
12	H4A	C4	C5	115(1)
13	C4	C5	C6	127(1)
14	C4	C5	C10	117(1)
15	C6	C5	C10	117(1)
16	C5	C6	H6A	119(1)
17	C5	C6	C7	122(1)
18	H6A	C6	C7	119(1)
19	C6	C7	C8	121(1)
20	C6	C7	O2	124(1)

21	C8	C7	O2	115(1)
22	C7	C8	C9	117(1)
23	C7	C8	O3	112(1)
24	C9	C8	O3	131(1)
25	C8	C9	H9A	119(1)
26	C8	C9	C10	122(1)
27	H9A	C9	C10	119(1)
28	C5	C10	C9	121(1)
29	C5	C10	O4	121(1)
30	C9	C10	O4	118(1)
31	C1	C11	H11A	109(1)
32	C1	C11	H11B	110(1)
33	C1	C11	H11C	110(1)
34	H11A	C11	H11B	109(1)
35	H11A	C11	H11C	109(1)
36	H11B	C11	H11C	110(1)
37	H12A	C12	H12B	109(1)
38	H12A	C12	H12C	109(1)
39	H12A	C12	N2	109(1)
40	H12B	C12	H12C	109(1)
41	H12B	C12	N2	110(1)
42	H12C	C12	N2	110(1)
43	H13A	C13	H13B	110(1)
44	H13A	C13	H13C	109(1)
45	H13A	C13	O2	110(1)
46	H13B	C13	H13C	109(1)
47	H13B	C13	O2	109(1)
48	H13C	C13	O2	109(1)
49	H14A	C14	H14B	109(1)
50	H14A	C14	H14C	109(1)
51	H14A	C14	O3	110(1)
52	H14B	C14	H14C	109(1)
53	H14B	C14	O3	110(1)
54	H14C	C14	O3	109(1)
55	H15A	C15	H15B	110(1)
56	H15A	C15	H15C	109(1)
57	H15A	C15	O4	109(1)
58	H15B	C15	H15C	109(1)
59	H15B	C15	O4	109(1)
60	H15C	C15	O4	110(1)
61	C1	N1	C3	101(1)
62	C1	N2	C2	106(1)
63	C1	N2	C12	130(1)
64	C2	N2	C12	123(1)
65	C7	O2	C13	116.6(9)
66	C8	O3	C14	114.2(9)

67	C10	O4	C15	121.1(9)

Bond Lengths of 3,4,5-OMe/Me

Number	Atom1	Atom2	Type	Length
1	C1	C11	Unknown	1.56(2)
2	C1	N1	Unknown	1.29(2)
3	C1	N2	Unknown	1.38(2)
4	C2	C3	Unknown	1.45(2)
5	C2	N2	Unknown	1.40(2)
6	C2	O1	Unknown	1.22(2)
7	C3	C4	Unknown	1.35(2)
8	C3	N1	Unknown	1.44(2)
9	C4	H4A	Unknown	0.95(1)
10	C4	C5	Unknown	1.43(2)
11	C5	C6	Unknown	1.41(2)
12	C5	C10	Unknown	1.40(2)
13	C6	H6A	Unknown	0.95(1)
14	C6	C7	Unknown	1.37(2)
15	C7	C8	Unknown	1.42(2)
16	C7	O2	Unknown	1.38(1)
17	C8	C9	Unknown	1.38(2)
18	C8	O3	Unknown	1.34(2)
19	C9	H9A	Unknown	0.95(1)
20	C9	C10	Unknown	1.41(2)
21	C10	O4	Unknown	1.37(1)
22	C11	H11A	Unknown	0.98(1)
23	C11	H11B	Unknown	0.98(1)
24	C11	H11C	Unknown	0.98(1)
25	C12	H12A	Unknown	0.98(1)
26	C12	H12B	Unknown	0.98(1)
27	C12	H12C	Unknown	0.98(1)
28	C12	N2	Unknown	1.47(2)
29	C13	H13A	Unknown	0.98(1)
30	C13	H13B	Unknown	0.98(1)
31	C13	H13C	Unknown	0.98(1)
32	C13	O2	Unknown	1.45(1)
33	C14	H14A	Unknown	0.98(1)
34	C14	H14B	Unknown	0.98(1)
35	C14	H14C	Unknown	0.98(1)
36	C14	O3	Unknown	1.46(1)
37	C15	H15A	Unknown	0.98(1)
38	C15	H15B	Unknown	0.98(1)

39	C15	H15C	Unknown	0.98(1)
40	C15	O4	Unknown	1.47(2)

4-(Et)$_2$/Me AMI Chromophore

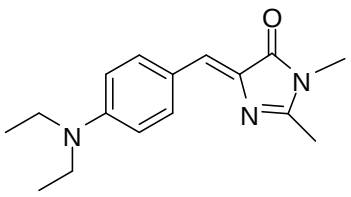

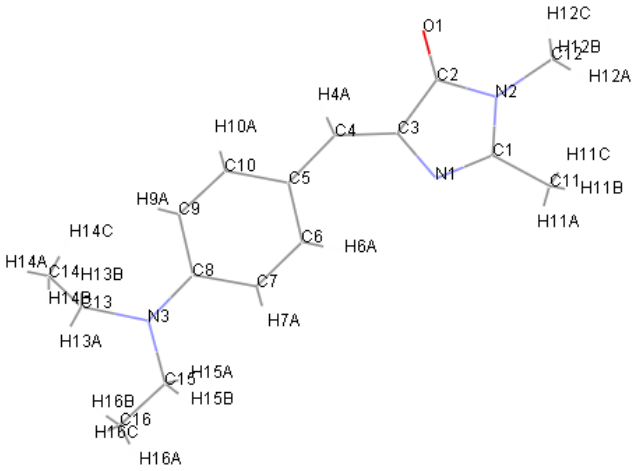

cell_length_a	13.4980(7)
cell_length_b	11.2673(7)
cell_length_c	9.8819(6)
cell_angle_alpha	90.00
cell_angle_beta	102.138(3)
cell_angle_gamma	90.00
cell_volume	1469.30(15)
cell_formula_units_Z	4
cell_measurement_temperature	173(2)
cell_measurement_reflns_used	4815
cell_measurement_theta_min	3.35
cell_measurement_theta_max	65.80

exptl_crystal_description	irreg
exptl_crystal_colour	orange
exptl_crystal_size_max	0.32
exptl_crystal_size_mid	0.29
exptl_crystal_size_min	0.24
exptl_crystal_density_meas	?
exptl_crystal_density_diffrn	1.227
exptl_crystal_density_method	'not measured'

exptl_crystal_F_000 584
exptl_absorpt_coefficient_mu 0.619
exptl_absorpt_correction_type multi-scan
exptl_absorpt_correction_T_min 0.8264
exptl_absorpt_correction_T_max 0.8656
exptl_absorpt_process_details SADABS

diffrn_ambient_temperature 173(2)
diffrn_radiation_wavelength 1.54178
diffrn_radiation_type CuK\a
diffrn_radiation_source 'fine-focus sealed tube'
diffrn_radiation_monochromator graphite
diffrn_measurement_device_type 'CCD area detector'
diffrn_measurement_method 'phi and omega scans'
diffrn_detector_area_resol_mean ?
diffrn_standards_number ?
diffrn_standards_interval_count ?
diffrn_standards_interval_time ?
diffrn_standards_decay_% ?
diffrn_reflns_number 10750
diffrn_reflns_av_R_equivalents 0.0161
diffrn_reflns_av_sigmaI/netI 0.0118
diffrn_reflns_limit_h_min -16
diffrn_reflns_limit_h_max 15
diffrn_reflns_limit_k_min -10
diffrn_reflns_limit_k_max 12
diffrn_reflns_limit_l_min -11
diffrn_reflns_limit_l_max 11
diffrn_reflns_theta_min 3.35
diffrn_reflns_theta_max 66.27
reflns_number_total 2372
reflns_number_gt 2138
reflns_threshold_expression >2sigma(I)

Spatial Coordinates of 4-(Et)$_2$/Me

C1	C	0.0568(2) 0.9485(3) -0.1516(3)
C2	C	0.0106(2) 0.8047(3) -0.0209(3)
C3	C	0.1168(2) 0.8409(3) 0.0281(3)
C4	C	0.1774(2) 0.7916(3) 0.1406(3)
H4A	H	0.1460 0.7307 0.1831
C5	C	0.2809(2) 0.8149(3) 0.2071(3). .
C6	C	0.3407(3) 0.9051(3) 0.1671(4)
H6A	H	0.3133 0.9524 0.0885.
C7	C	0.4375(3) 0.9266(3) 0.2388(4)
H7A	H	0.4757 0.9883 0.2087
C8	C	0.4819(3) 0.8589(4) 0.3567(4)

C9	C	0.4233(3) 0.7642(4) 0.3921(4)
H9A	H	0.4518 0.7129 0.4665
C10	C	0.3262(3) 0.7454(3) 0.3208(4)
H10A	H	0.2880 0.6829 0.3495
C11	C	0.0446(3) 1.0345(3) -0.2677(4)
H11A	H	0.1084 1.0771 -0.2636
H11B	H	-0.0090 1.0914 -0.2603
H11C	H	0.0261 0.9919 -0.3559
C12	C	-0.1257(3) 0.8755(4) -0.2165(4)
H12A	H	-0.1316 0.9343 -0.2908
H12B	H	-0.1735 0.8950 -0.1576
H12C	H	-0.1412 0.7965 -0.2567
C13	C	0.6192(4) 0.8121(5) 0.5607(6)
H13A	H	0.6701 0.8591 0.6257
H13B	H	0.5645 0.7894 0.6086
C14	C	0.6660(4) 0.7067(5) 0.5189(8)
H14A	H	0.6947 0.6592 0.6008
H14B	H	0.7199 0.7297 0.4715
H14C	H	0.6149 0.6598 0.4560
C15	C	0.6345(4) 0.9853(5) 0.3925(8)
H15A	H	0.6289 0.9795 0.2912
H15B	H	0.5999 1.0596 0.4095
C16	C	0.7344(4) 0.9989(6) 0.4507(9)
H16A	H	0.7616 1.0665 0.4077
H16B	H	0.7712 0.9267 0.4361
H16C	H	0.7423 1.0134 0.5502
N1	N	0.1399(2) 0.9310(2) -0.0603(3)
N2	N	-0.0230(2) 0.8766(3) -0.1337(3)
N3	N	0.5756(3) 0.8857(4) 0.4334(4)
O1	O	-0.04115(18) 0.7300(2) 0.0234(2)

Bond Angles of 4-$(Et)_2$/Me

Number	Atom1	Atom2	Atom3	Angle
1	C11	C1	N1	125.1(3)
2	C11	C1	N2	121.1(3)
3	N1	C1	N2	113.8(3)
4	C3	C2	N2	103.6(3)
5	C3	C2	O1	131.2(3)
6	N2	C2	O1	125.1(3)
7	C2	C3	C4	122.4(3)
8	C2	C3	N1	108.8(3)
9	C4	C3	N1	128.9(3)
10	C3	C4	H4A	114.3(3)
11	C3	C4	C5	131.5(3)
12	H4A	C4	C5	114.3(3)
13	C4	C5	C6	124.3(3)

14	C4	C5	C10	118.9(3)
15	C6	C5	C10	116.8(3)
16	C5	C6	H6A	119.2(4)
17	C5	C6	C7	121.6(3)
18	H6A	C6	C7	119.2(4)
19	C6	C7	H7A	119.3(4)
20	C6	C7	C8	121.5(4)
21	H7A	C7	C8	119.2(4)
22	C7	C8	C9	116.6(4)
23	C7	C8	N3	121.4(4)
24	C9	C8	N3	122.0(4)
25	C8	C9	H9A	119.6(4)
26	C8	C9	C10	120.9(4)
27	H9A	C9	C10	119.5(4)
28	C5	C10	C9	122.4(3)
29	C5	C10	H10A	118.7(4)
30	C9	C10	H10A	118.8(4)
31	C1	C11	H11A	109.5(3)
32	C1	C11	H11B	109.4(3)
33	C1	C11	H11C	109.5(3)
34	H11A	C11	H11B	109.4(4)
35	H11A	C11	H11C	109.5(4)
36	H11B	C11	H11C	109.4(4)
37	H12A	C12	H12B	109.5(4)
38	H12A	C12	H12C	109.5(4)
39	H12A	C12	N2	109.5(4)
40	H12B	C12	H12C	109.5(4)
41	H12B	C12	N2	109.4(4)
42	H12C	C12	N2	109.5(4)
43	H13A	C13	H13B	108.3(5)
44	H13A	C13	C14	109.9(5)
45	H13A	C13	N3	109.9(5)
46	H13B	C13	C14	109.8(5)
47	H13B	C13	N3	109.8(5)
48	C14	C13	N3	109.2(5)
49	C13	C14	H14A	109.5(6)
50	C13	C14	H14B	109.4(6)
51	C13	C14	H14C	109.4(6)
52	H14A	C14	H14B	109.6(6)
53	H14A	C14	H14C	109.4(6)
54	H14B	C14	H14C	109.5(6)
55	H15A	C15	H15B	106.8(6)
56	H15A	C15	C16	107.1(6)
57	H15A	C15	N3	107.2(5)
58	H15B	C15	C16	107.1(6)
59	H15B	C15	N3	107.2(5)

60	C16	C15	N3	120.8(6)
61	C15	C16	H16A	109.4(6)
62	C15	C16	H16B	109.4(6)
63	C15	C16	H16C	109.4(6)
64	H16A	C16	H16B	109.5(7)
65	H16A	C16	H16C	109.5(7)
66	H16B	C16	H16C	109.5(7)
67	C1	N1	C3	105.5(3)
68	C1	N2	C2	108.3(3)
69	C1	N2	C12	127.3(3)
70	C2	N2	C12	124.3(3)
71	C8	N3	C13	119.5(4)
72	C8	N3	C15	120.3(4)
73	C13	N3	C15	120.2(4)

Bond Lengths of 4-$(Et)_2$/Me

Number	Atom1	Atom2	Type	Length
1	C1	C11	Unknown	1.484(5)
2	C1	N1	Unknown	1.298(4)
3	C1	N2	Unknown	1.389(4)
4	C2	C3	Unknown	1.471(4)
5	C2	N2	Unknown	1.375(4)
6	C2	O1	Unknown	1.231(4)
7	C3	C4	Unknown	1.353(4)
8	C3	N1	Unknown	1.416(4)
9	C4	H4A	Unknown	0.950(3)
10	C4	C5	Unknown	1.438(4)
11	C5	C6	Unknown	1.405(5)
12	C5	C10	Unknown	1.400(5)
13	C6	H6A	Unknown	0.950(4)
14	C6	C7	Unknown	1.371(5)
15	C7	H7A	Unknown	0.950(4)
16	C7	C8	Unknown	1.416(5)
17	C8	C9	Unknown	1.415(6)
18	C8	N3	Unknown	1.365(5)
19	C9	H9A	Unknown	0.951(4)
20	C9	C10	Unknown	1.368(5)
21	C10	H10A	Unknown	0.951(4)
22	C11	H11A	Unknown	0.979(4)
23	C11	H11B	Unknown	0.981(4)
24	C11	H11C	Unknown	0.980(4)
25	C12	H12A	Unknown	0.980(4)
26	C12	H12B	Unknown	0.980(4)
27	C12	H12C	Unknown	0.979(4)
28	C12	N2	Unknown	1.454(4)
29	C13	H13A	Unknown	0.990(5)

30	C13	H13B	Unknown	0.991(6)
31	C13	C14	Unknown	1.446(8)
32	C13	N3	Unknown	1.518(7)
33	C14	H14A	Unknown	0.980(7)
34	C14	H14B	Unknown	0.979(7)
35	C14	H14C	Unknown	0.980(6)
36	C15	H15A	Unknown	0.990(8)
37	C15	H15B	Unknown	0.990(6)
38	C15	C16	Unknown	1.359(7)
39	C15	N3	Unknown	1.480(8)
40	C16	H16A	Unknown	0.980(7)
41	C16	H16B	Unknown	0.980(7)
42	C16	H16C	Unknown	0.980(9)

4-N(Me)$_2$/Me AMI Chromophore

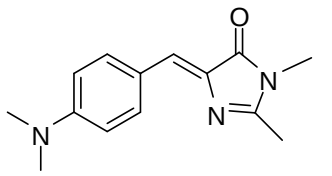

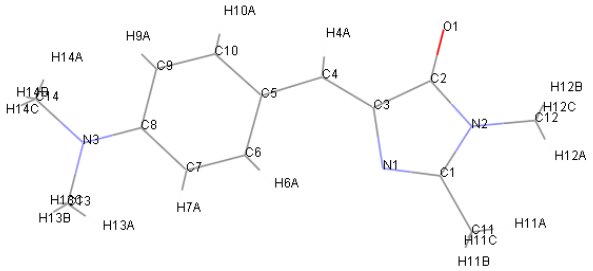

cell_length_a	7.0520(12)
cell_length_b	12.411(3)
cell_length_c	14.761(4)
cell_angle_alpha	90.00
cell_angle_beta	97.434(12)
cell_angle_gamma	90.00
cell_volume	1281.0(5)
cell_formula_units_Z	4
cell_measurement_temperature	173(2)
cell_measurement_reflns_used	183
cell_measurement_theta_min	6.65
cell_measurement_theta_max	41.64

exptl_crystal_description	rod
exptl_crystal_colour	yellow
exptl_crystal_size_max	0.21
exptl_crystal_size_mid	0.08
exptl_crystal_size_min	0.06
exptl_crystal_density_meas	?
exptl_crystal_density_diffrn	1.262
exptl_crystal_density_method	'not measured'
exptl_crystal_F_000	520
exptl_absorpt_coefficient_mu	0.653
exptl_absorpt_correction_type	multi-scan
exptl_absorpt_correction_T_min	0.8750

exptl_absorpt_correction_T_max 0.9618
exptl_absorpt_process_details ?

diffrn_ambient_temperature 173(2)
diffrn_radiation_wavelength 1.54178
diffrn_radiation_type CuK\a
diffrn_radiation_source 'fine-focus sealed tube'
diffrn_radiation_monochromator graphite
diffrn_measurement_device_type 'CCD area detector'
diffrn_measurement_method 'phi and omega scans'
diffrn_detector_area_resol_mean ?
diffrn_reflns_number 7921
diffrn_reflns_av_R_equivalents 0.1907
diffrn_reflns_av_sigmaI/netI 0.1938
diffrn_reflns_limit_h_min -8
diffrn_reflns_limit_h_max 7
diffrn_reflns_limit_k_min -12
diffrn_reflns_limit_k_max 12
diffrn_reflns_limit_l_min -16
diffrn_reflns_limit_l_max 16
diffrn_reflns_theta_min 4.67
diffrn_reflns_theta_max 62.38
reflns_number_total 1854
reflns_number_gt 725
reflns_threshold_expression >2sigma(I)

Spatial Coordinates of 4-N(Me)$_2$/Me

C1	C	0.6254(10) 0.6435(7) 0.6066(7)
C2	C	0.6306(10) 0.8221(9) 0.6058(6)
C3	C	0.6290(10) 0.7780(8) 0.5148(6)
C4	C	0.6272(10) 0.8402(7) 0.4402(6)
H4A	H	0.6243 0.9154 0.4519
C5	C	0.6288(10) 0.8125(7) 0.3453(6)
C6	C	0.6429(10) 0.7055(7) 0.3134(6)
H6A	H	0.6555 0.6479 0.3561
C7	C	0.6388(10) 0.6832(7) 0.2216(6)
H7A	H	0.6449 0.6104 0.2023
C8	C	0.6258(10) 0.7654(8) 0.1566(6)
C9	C	0.6156(10) 0.8717(8) 0.1868(6)
H9A	H	0.6087 0.9294 0.1441
C10	C	0.6155(10) 0.8930(7) 0.2784(6)
H10A	H	0.6059 0.9659 0.2970
C11	C	0.6185(11) 0.5345(7) 0.6467(5)
H11A	H	0.6146 0.5406 0.7126
H11B	H	0.7325 0.4939 0.6356

H11C	H	0.5038 0.4969 0.6183
C12	C	0.6305(11) 0.7369(7) 0.7605(5)
H12A	H	0.6280 0.6634 0.7847
H12B	H	0.5180 0.7765 0.7750
H12C	H	0.7468 0.7735 0.7882
C13	C	0.6244(12) 0.6318(7) 0.0334(5)
H13A	H	0.6311 0.5826 0.0856
H13B	H	0.7356 0.6204 0.0010
H13C	H	0.5070 0.6179 -0.0082
C14	C	0.6149(12) 0.8287(7) -0.0024(5)
H14A	H	0.6144 0.8989 0.0280
H14B	H	0.4978 0.8209 -0.0456
H14C	H	0.7265 0.8238 -0.0355
N1	N	0.6270(9) 0.6638(6) 0.5203(5)
N2	N	0.6286(8) 0.7327(7) 0.6621(4)
N3	N	0.6238(10) 0.7431(6) 0.0658(5)
O1	O	0.6333(8) 0.9164(5) 0.6334(4)

Bond Angles of 4-N(Me)$_2$/Me

Number	Atom1	Atom2	Atom3	Angle
1	C11	C1	N1	125.0(8)
2	C11	C1	N2	119.8(7)
3	N1	C1	N2	115.2(8)
4	C3	C2	N2	104.7(7)
5	C3	C2	O1	131.3(8)
6	N2	C2	O1	124.0(8)
7	C2	C3	C4	122.7(8)
8	C2	C3	N1	108.8(7)
9	C4	C3	N1	128.4(8)
10	C3	C4	H4A	114.4(8)
11	C3	C4	C5	131.1(8)
12	H4A	C4	C5	114.4(8)
13	C4	C5	C6	123.7(7)
14	C4	C5	C10	120.4(7)
15	C6	C5	C10	115.8(7)
16	C5	C6	H6A	119.3(8)
17	C5	C6	C7	121.4(8)
18	H6A	C6	C7	119.3(8)
19	C6	C7	H7A	119.3(8)
20	C6	C7	C8	121.3(8)
21	H7A	C7	C8	119.4(8)
22	C7	C8	C9	118.2(8)
23	C7	C8	N3	121.2(8)
24	C9	C8	N3	120.6(8)
25	C8	C9	H9A	120.0(8)

26	C8	C9	C10	120.1(8)
27	H9A	C9	C10	120.0(8)
28	C5	C10	C9	123.2(8)
29	C5	C10	H10A	118.5(8)
30	C9	C10	H10A	118.4(8)
31	C1	C11	H11A	109.5(7)
32	C1	C11	H11B	109.4(7)
33	C1	C11	H11C	109.4(7)
34	H11A	C11	H11B	109.6(8)
35	H11A	C11	H11C	109.5(8)
36	H11B	C11	H11C	109.5(8)
37	H12A	C12	H12B	109.5(8)
38	H12A	C12	H12C	109.4(8)
39	H12A	C12	N2	109.4(7)
40	H12B	C12	H12C	109.5(8)
41	H12B	C12	N2	109.5(7)
42	H12C	C12	N2	109.5(7)
43	H13A	C13	H13B	109.5(8)
44	H13A	C13	H13C	109.5(8)
45	H13A	C13	N3	109.5(7)
46	H13B	C13	H13C	109.5(8)
47	H13B	C13	N3	109.4(7)
48	H13C	C13	N3	109.5(7)
49	H14A	C14	H14B	109.4(8)
50	H14A	C14	H14C	109.5(8)
51	H14A	C14	N3	109.5(7)
52	H14B	C14	H14C	109.4(8)
53	H14B	C14	N3	109.5(7)
54	H14C	C14	N3	109.4(7)
55	C1	N1	C3	104.5(7)
56	C1	N2	C2	106.7(7)
57	C1	N2	C12	128.5(7)
58	C2	N2	C12	124.8(7)
59	C8	N3	C13	120.8(7)
60	C8	N3	C14	121.5(7)
61	C13	N3	C14	117.6(7)

Bond Lengths of 4-N(Me)$_2$/Me

Number	Atom1	Atom2	Type	Length
1	C1	C11	Unknown	1.48(1)
2	C1	N1	Unknown	1.30(1)
3	C1	N2	Unknown	1.38(1)
4	C2	C3	Unknown	1.45(1)
5	C2	N2	Unknown	1.39(1)
6	C2	O1	Unknown	1.24(1)
7	C3	C4	Unknown	1.34(1)

8	C3	N1	Unknown	1.42(1)
9	C4	H4A	Unknown	0.950(9)
10	C4	C5	Unknown	1.44(1)
11	C5	C6	Unknown	1.42(1)
12	C5	C10	Unknown	1.40(1)
13	C6	H6A	Unknown	0.950(9)
14	C6	C7	Unknown	1.38(1)n
15	C7	H7A	Unknown	0.950(9)
16	C7	C8	Unknown	1.40(1)
17	C8	C9	Unknown	1.40(1)
18	C8	N3	Unknown	1.37(1)
19	C9	H9A	Unknown	0.951(9)
20	C9	C10	Unknown	1.38(1)
21	C10	H10A	Unknown	0.950(9)
22	C11	H11A	Unknown	0.980(7)
23	C11	H11B	Unknown	0.980(8)
24	C11	H11C	Unknown	0.980(8)
25	C12	H12A	Unknown	0.981(9)
26	C12	H12B	Unknown	0.980(8)
27	C12	H12C	Unknown	0.979(8)
28	C12	N2	Unknown	1.45(1)
29	C13	H13A	Unknown	0.979(8)
30	C13	H13B	Unknown	0.980(9)
31	C13	H13C	Unknown	0.980(8)
32	C13	N3	Unknown	1.46(1)
33	C14	H14A	Unknown	0.980(8)
34	C14	H14B	Unknown	0.981(8)
35	C14	H14C	Unknown	0.980(9)
36	C14	N3	Unknown	1.46(1)

3-OH/Me AMI Chromophore

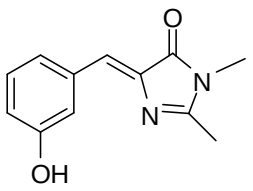

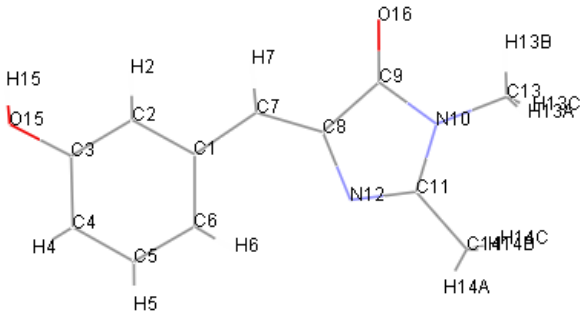

cell_length_a	7.0404(8)
cell_length_b	7.2141(7)
cell_length_c	11.4902(11)
cell_angle_alpha	74.020(6)
cell_angle_beta	80.942(6)
cell_angle_gamma	75.193(4)
cell_volume	540.02(10)
cell_formula_units_Z	2
cell_measurement_temperature	293(2)

exptl_crystal_description	'prism'
exptl_crystal_colour	'colorless'
exptl_crystal_size_max	0.310
exptl_crystal_size_mid	0.100
exptl_crystal_size_min	0.065
exptl_crystal_density_meas	?
exptl_crystal_density_diffrn	1.330
exptl_crystal_density_method	'not measured'
exptl_crystal_F_000	228
exptl_absorpt_coefficient_mu	0.092
exptl_absorpt_correction_type	'sphere'
exptl_absorpt_correction_T_min	0.9719
exptl_absorpt_correction_T_max	0.9945
exptl_absorpt_process_details	'SADABS (Sheldrick, 1996)'

diffrn_ambient_temperature	293(2)

diffrn_radiation_wavelength 0.71073
diffrn_radiation_type MoK\a
diffrn_radiation_source 'rotating anode'
diffrn_radiation_monochromator 'multilayer confocal TXS mirror'
diffrn_measurement_device_type 'Bruker SMART APEX2 diffractometer'
diffrn_measurement_method '\w scans'
diffrn_detector_area_resol_mean ?
diffrn_standards_number ?
diffrn_standards_interval_count ?
diffrn_standards_interval_time ?
diffrn_standards_decay_% ?
diffrn_reflns_number 7058
diffrn_reflns_av_R_equivalents 0.0287
diffrn_reflns_av_sigmaI/netI 0.0306
diffrn_reflns_limit_h_min -7
diffrn_reflns_limit_h_max 8
diffrn_reflns_limit_k_min -8
diffrn_reflns_limit_k_max 8
diffrn_reflns_limit_l_min -13
diffrn_reflns_limit_l_max 13
diffrn_reflns_theta_min 1.85
diffrn_reflns_theta_max 25.00
reflns_number_total 1905
reflns_number_gt 1250
reflns_threshold_expression >2sigma(I)

Spatial Coordinates of 3-OH/Me

H7	H	0.228(4) 0.888(4) -0.050(2)
H15	H	-0.165(4) 0.788(4) 0.333(3)
C2	C	0.1352(4) 0.7605(4) 0.1804(3)
H2	H	0.0278 0.8285 0.1361
C1	C	0.3245(4) 0.7380(4) 0.1207(3)
N10	N	0.6940(4) 0.8605(4) -0.2653(2)
C7	C	0.3448(4) 0.8198(4) -0.0100(3)
O16	O	0.3608(4) 0.9895(4) -0.2786(2)
C8	C	0.5071(4) 0.8153(4) -0.0897(3)
C3	C	0.1035(5) 0.6836(4) 0.3045(3)
C6	C	0.4826(5) 0.6351(5) 0.1890(3)
H6	H	0.6108 0.6182 0.1516
C9	C	0.4995(5) 0.9045(5) -0.2199(3)
O15	O	-0.0783(4) 0.6989(4) 0.3652(2)
N12	N	0.7061(4) 0.7279(3) -0.0663(2)
C4	C	0.2624(5) 0.5822(5) 0.3693(3)
H4	H	0.2430 0.5292 0.4526
C5	C	0.4486(5) 0.5588(5) 0.3118(3)
H5	H	0.5549 0.4897 0.3568

C11	C	0.8058(4)	0.7575(5)	-0.1709(3)
C14	C	1.0221(5)	0.6868(6)	-0.1914(4)
H14A	H	1.0734	0.6102	-0.1159
H14B	H	1.0822	0.7982	-0.2229
H14C	H	1.0511	0.6062	-0.2487
C13	C	0.7601(6)	0.9168(6)	-0.3948(3)
H13A	H	0.8579	0.9933	-0.4065
H13B	H	0.6497	0.9942	-0.4392
H13C	H	0.8160	0.7998	-0.4238.

Bond Angles of 3-OH/Me

Number	Atom1	Atom2	Atom3	Angle
1	H2	C2	C1	119.4(3)
2	H2	C2	C3	119.3(3)
3	C1	C2	C3	121.3(3)
4	C2	C1	C7	117.9(3)
5	C2	C1	C6	118.2(3)
6	C7	C1	C6	123.9(3)
7	C9	N10	C11	108.7(3)
8	C9	N10	C13	123.2(3)
9	C11	N10	C13	128.1(3)
10	H7	C7	C1	118(2)
11	H7	C7	C8	111(2)
12	C1	C7	C8	130.3(3)
13	C7	C8	C9	122.8(3)
14	C7	C8	N12	128.3(3)
15	C9	C8	N12	108.9(3)
16	C2	C3	O15	123.0(3)
17	C2	C3	C4	119.1(3)
18	O15	C3	C4	117.9(3)
19	C1	C6	H6	120.1(3)
20	C1	C6	C5	119.8(3)
21	H6	C6	C5	120.1(4)
22	N10	C9	O16	126.2(3)
23	N10	C9	C8	103.0(3)
24	O16	C9	C8	130.7(3)
25	H15	O15	C3	116(2)
26	C8	N12	C11	105.2(3)
27	C3	C4	H4	119.9(3)
28	C3	C4	C5	120.2(3)
29	H4	C4	C5	119.9(4)
30	C6	C5	C4	121.4(3)
31	C6	C5	H5	119.3(3)
32	C4	C5	H5	119.3(3)
33	N10	C11	N12	114.1(3)
34	N10	C11	C14	121.4(3)

35	N12	C11	C14	124.4(3)
36	C11	C14	H14A	109.5(4)
37	C11	C14	H14B	109.5(4)
38	C11	C14	H14C	109.5(4)
39	H14A	C14	H14B	109.4(4)
40	H14A	C14	H14C	109.5(4)
41	H14B	C14	H14C	109.5(4)
42	N10	C13	H13A	109.5(3)
43	N10	C13	H13B	109.5(3)
44	N10	C13	H13C	109.5(3)
45	H13A	C13	H13B	109.4(4)
46	H13A	C13	H13C	109.5(4)
47	H13B	C13	H13C	109.4(4)

Bond Lengths of 3-OH/Me

Number	Atom1	Atom2	Type	Length
1	H7	C7	Unknown	0.96(3)
2	H15	O15	Unknown	0.81(3)
3	C2	H2	Unknown	0.930(3)
4	C2	C1	Unknown	1.391(4)
5	C2	C3	Unknown	1.385(4)
6	C1	C7	Unknown	1.453(4)
7	C1	C6	Unknown	1.392(4)
8	N10	C9	Unknown	1.376(4)
9	N10	C11	Unknown	1.369(4)
10	N10	C13	Unknown	1.463(4)
11	C7	C8	Unknown	1.347(4)
12	O16	C9	Unknown	1.208(4)
13	C8	C9	Unknown	1.460(5)
14	C8	N12	Unknown	1.417(4)
15	C3	O15	Unknown	1.351(4)
16	C3	C4	Unknown	1.373(5)
17	C6	H6	Unknown	0.930(3)
18	C6	C5	Unknown	1.373(4)
19	N12	C11	Unknown	1.285(4)
20	C4	H4	Unknown	0.930(3)
21	C4	C5	Unknown	1.363(5)
22	C5	H5	Unknown	0.930(3)
23	C11	C14	Unknown	1.480(4)
24	C14	H14A	Unknown	0.960(4)
25	C14	H14B	Unknown	0.960(4)
26	C14	H14C	Unknown	0.960(5)
27	C13	H13A	Unknown	0.960(5)
28	C13	H13B	Unknown	0.960(4)
29	C13	H13C	Unknown	0.960(4)

2-F/Me AMI Chromophore

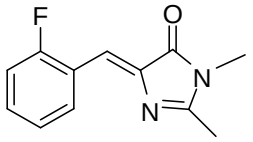

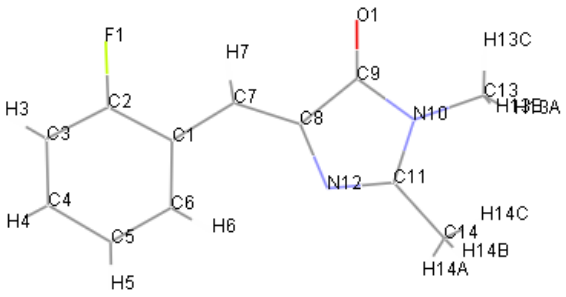

cell_length_a	7.12770(10)
cell_length_b	11.2873(2)
cell_length_c	13.6337(2)
cell_angle_alpha	90.00
cell_angle_beta	105.1860(10)
cell_angle_gamma	90.00
cell_volume	1058.56(3)
cell_formula_units_Z	4
cell_measurement_temperature	293(2)
cell_measurement_reflns_used	6195
cell_measurement_theta_min	2.38
cell_measurement_theta_max	26.83

exptl_crystal_description	'Columnar'
exptl_crystal_colour	'yellow'
exptl_crystal_size_max	0.275
exptl_crystal_size_mid	0.055
exptl_crystal_size_min	0.045
exptl_crystal_density_meas	?
exptl_crystal_density_diffrn	1.369
exptl_crystal_density_method	'not measured'
exptl_crystal_F_000	456
exptl_absorpt_coefficient_mu	0.101
exptl_absorpt_correction_type	'sphere'
exptl_absorpt_correction_T_min	?
exptl_absorpt_correction_T_max	?
exptl_absorpt_process_details	'SADABS (Sheldrick, 1996)'

Twinned structure; the ratio of one of the components
is 62.5%. Solvent: hexane

diffrn_ambient_temperature 293(2)
diffrn_radiation_wavelength 0.71073
diffrn_radiation_type MoK\a
diffrn_radiation_source 'rotating anode'
diffrn_radiation_monochromator 'multilayer confocal TXS mirror'
diffrn_measurement_device_type 'Bruker SMART APEX2 diffractometer'
diffrn_measurement_method '\w scans'
diffrn_detector_area_resol_mean ?
diffrn_standards_number ?
diffrn_standards_interval_count ?
diffrn_standards_interval_time ?
diffrn_standards_decay_% ?
diffrn_reflns_number 15287
diffrn_reflns_av_R_equivalents 0.0263
diffrn_reflns_av_sigmaI/netI 0.0205
diffrn_reflns_limit_h_min -9
diffrn_reflns_limit_h_max 9
diffrn_reflns_limit_k_min -14
diffrn_reflns_limit_k_max 14
diffrn_reflns_limit_l_min -17
diffrn_reflns_limit_l_max 17
diffrn_reflns_theta_min 1.55
diffrn_reflns_theta_max 27.50
reflns_number_total 2466
reflns_number_gt 2012
reflns_threshold_expression >2sigma(I)

Spatial Coordinates of 2-F/Me

F1	F	0.2546(3) 0.19120(13) 0.48356(12)
O1	O	0.1474(3) 0.53757(16) 0.25452(12)
N10	N	0.1714(3) 0.71227(15) 0.34443(13)
N12	N	0.2458(3) 0.64829(16) 0.50538(13)
C2	C	0.2931(4) 0.2550(2) 0.56969(18)
C3	C	0.3361(4) 0.1940(2) 0.6611(2)
H3	H	0.3382 0.1116 0.6622
C4	C	0.3751(5) 0.2568(3) 0.7487(2)
H4	H	0.4043 0.2168 0.8105
C5	C	0.3724(4) 0.3810(3) 0.74798(19)
H5	H	0.4006 0.4239 0.8083
C6	C	0.3264(4) 0.4381(2) 0.65467(17)
H6	H	0.3226 0.5205 0.6535
C1	C	0.2862(3) 0.37818(18) 0.56401(15)

C7	C	0.2389(3)	0.43420(17)	0.46444(15)
H7	H	0.2163	0.3825	0.4095
C8	C	0.2232(3)	0.55031(18)	0.44033(15)
C9	C	0.1750(4)	0.59137(19)	0.33385(16)
C11	C	0.2125(4)	0.7402(2)	0.44552(17)
C13	C	0.1276(5)	0.7916(3)	0.2572(2)
H13	C	0.0547	0.7497	0.1983
H13B	H	0.2467	0.8201	0.2454
H13A	H	0.0525	0.8575	0.2705
C14	C	0.2196(5)	0.8645(2)	0.4809(2)
H14A	H	0.2249	0.8659	0.5520
H14C	H	0.1054	0.9057	0.4434
H14B	H	0.3331	0.9026	0.4703.

Bond Angles of 2-F/Me

Number	Atom1	Atom2	Atom3	Angle
1	C11	C1	N1	124.9(2)
2	C11	C1	N2	121.0(2)
3	N1	C1	N2	114.1(2)
4	C3	C2	N2	103.1(2)
5	C3	C2	O1	130.5(2)
6	N2	C2	O1	126.4(2)
7	C2	C3	C4	121.1(2)
8	C2	C3	N1	108.7(2)
9	C4	C3	N1	130.2(2)
10	C3	C4	H4A	115.2(2)
11	C3	C4	C5	129.5(2)
12	H4A	C4	C5	115.2(2)
13	C4	C5	C6	121.9(2)
14	C4	C5	C10	119.0(2)
15	C6	C5	C10	119.1(2)
16	C5	C6	H6A	118.9(2)
17	C5	C6	C7	122.2(2)
18	H6A	C6	C7	118.9(2)
19	C6	C7	C8	118.1(2)
20	C6	C7	C13	120.8(2)
21	C8	C7	C13	121.1(2)
22	C7	C8	H8A	119.7(2)
23	C7	C8	C9	120.6(2)
24	H8A	C8	C9	119.7(2)
25	C8	C9	H9A	119.0(2)
26	C8	C9	C10	122.0(2)
27	H9A	C9	C10	119.0(2)
28	C5	C10	C9	118.0(2)
29	C5	C10	C14	122.5(2)
30	C9	C10	C14	119.5(2)

31	C1	C11	H11A	109.4(2)
32	C1	C11	H11B	109.5(2)
33	C1	C11	H11C	109.5(2)
34	H11A	C11	H11B	109.4(2)
35	H11A	C11	H11C	109.5(2)
36	H11B	C11	H11C	109.5(2)
37	H12A	C12	H12B	109.6(2)
38	H12A	C12	H12C	109.4(2)
39	H12A	C12	N2	109.4(2)
40	H12B	C12	H12C	109.4(2)
41	H12B	C12	N2	109.5(2)
42	H12C	C12	N2	109.5(2)
43	C7	C13	H13A	109.4(2)
44	C7	C13	H13B	109.5(2)
45	C7	C13	H13C	109.5(2)
46	H13A	C13	H13B	109.5(3)
47	H13A	C13	H13C	109.6(3)
48	H13B	C13	H13C	109.4(3)
49	C10	C14	H14A	109.5(2)
50	C10	C14	H14B	109.4(2)
51	C10	C14	H14C	109.4(2)
52	H14A	C14	H14B	109.5(3)
53	H14A	C14	H14C	109.5(3)
54	H14B	C14	H14C	109.5(3)
55	C1	N1	C3	105.8(2)
56	C1	N2	C2	108.3(2)
57	C1	N2	C12	128.3(2)
58	C2	N2	C12	123.4(2)

Bond Lengths of 2-F/Me

Number	Atom1	Atom2	Type	Length
1	F1	C2	Unknown	1.343(3)
2	O1	C9	Unknown	1.211(3)
3	N10	C9	Unknown	1.373(3)
4	N10	C11	Unknown	1.369(3)
5	N10	C13	Unknown	1.456(3)
6	N12	C8	Unknown	1.400(3)
7	N12	C11	Unknown	1.303(3)
8	C2	C3	Unknown	1.386(3)
9	C2	C1	Unknown	1.393(3)
10	C3	H3	Unknown	0.930(2)
11	C3	C4	Unknown	1.354(4)
12	C4	H4	Unknown	0.930(3)
13	C4	C5	Unknown	1.402(5)
14	C5	H5	Unknown	0.930(3)
15	C5	C6	Unknown	1.387(4)

16	C6	H6	Unknown	0.930(2)
17	C6	C1	Unknown	1.372(3)
18	C1	C7	Unknown	1.455(3)
19	C7	H7	Unknown	0.930(2)
20	C7	C8	Unknown	1.349(3)
21	C8	C9	Unknown	1.476(3)
22	C11	C14	Unknown	1.480(3)
23	C13	H13C	Unknown	0.959(3)
24	C13	H13B	Unknown	0.960(4)
25	C13	H13A	Unknown	0.961(4)
26	C14	H14A	Unknown	0.960(3)
27	C14	H14C	Unknown	0.960(3)
28	C14	H14B	Unknown	0.960(3)

VITA

ANTHONY BALDRIDGE

BALDRIDGE attended schools in Blue Ridge, Georgia within the Fannin County Schools system where he graduated valedictorian in 2002 from Fannin County Comprehensive High School. Following this, he attended Piedmont College in Demorest, Georgia where he received a Presidential Scholarship and earned a B.S. in Chemistry and Mathematics in 2006. While at Piedmont, he was involved in numerous activities and received the Stewart Award of Academic Excellence for being the top honor graduate. Upon earning a B.S., he applied for graduate studies at the Georgia Institute of Technology where he was awarded a Presidential Fellowship and came in Fall 2006 to pursue a doctorate degree. During his tenure at Georgia Tech, Baldridge received a TA Fellowship, a STEP Fellowship, and a COPE Fellowship. Additionally, while at Georgia Tech, he has been involved in multiple activities outside of research including serving as Graduate Student Body President in 2010-2011.